THERMODYNAMICS AND KINETICS OF ICE NUCLEATION INSIDE BIOLOGICAL CELLS DURING FREEZING: AS APPLIED TO MOUSE OOCYTES

by

MEHMET TONER

B.S. Istanbul Technical University
(1982)

S.M.M.E. Massachusetts Institute of Technology
(1985)

SUBMITTED TO THE HARVARD-MIT
DIVISION OF HEALTH SCIENCES & TECHNOLOGY
IN PARTIAL FULFILLMENT
OF THE REQUIREMENTS FOR THE
DEGREE OF

DOCTOR OF PHILOSOPHY
IN MEDICAL ENGINEERING

at the

MASSACHUSETTS INSTITUTE OF TECHNOLOGY

JANUARY 1989

Signature of Author.....
Division of Health Sciences & Technology
January 9, 1989

Certified by .....
Ernest G. Cravalho
Thesis Supervisor

Accepted by .....
Roger G. Mark
Chairman, Department Committee

THERMODYNAMICS AND KINETICS OF ICE NUCLEATION INSIDE BIOLOGICAL CELLS DURING FREEZING: AS APPLIED TO MOUSE OOCYTES

by

Mehmet Toner

Submitted to
Harvard University-Massachusetts Institute of Technology
Division of Health Sciences and Technology
on January 9, 1989 in partial fulfillment of the
requirements for the degree of Doctor of Philosophy

ABSTRACT

Experimental and theoretical models describing the kinetics of intracellular ice formation (iif) in biomaterials during freezing have been developed and applied to the case of mouse oocytes at metaphase II as the model biological system. The results suggest that there are two distinct mechanisms responsible for iif during freezing of oocytes. Both of the mechanisms are heterogeneously catalyzed, however, the active nucleators are different. Depending on the freezing conditions, the plasma membrane, i.e. 'plasma membrane catalyzed' nucleation (PMCN), and/or supramolecular structures,i.e. 'particle catalyzed' nucleation (PCN), are effective in initiating the ice nucleation within the oocytes during freezing. PMCN is characterized by the ice-plasma membrane contact angle, and PCN is characterized by the ice-particle contact angle and the radius of the particle, in addition to two parameters, Ω_o and κ_o, describing the homogeneous nucleation. The theoretical nucleation model combines PMCN and PCN mechanisms to predict the cumulative iif of oocytes. The kinetic nucleation model is also coupled with the water transport model to predict the thermodynamic state of the cell cytoplasm during a given freezing protocol. The cumulative incidence of iif for a given protocol is estimated by solving the coupled water transport and ice nucleation models.

A new cryostage with improved optical performance and 'isothermal' temperature field ($< 0.1^{o}C/10$ mm) was designed to determine the biophysical parameters describing the heterogeneous nucleation kinetics during freezing of mouse oocytes. Correlation of the theory with the experimental kinetics of the cumulative fraction of oocytes frozen internally revealed preexponentioal factors of, Ω^{I}_{o} and Ω^{II}_{o}, $3.56x10^{+9}$ and $1.84x10^{+50}$ $(1/m^2\text{-}s)$, and exponential factors of, κ^{I}_{o} and κ^{II}_{o}, $4.6x10^{+8}$ and $1.08x10^{+12}$ (K^5) for PMCN and PCN mechanisms, respectively. The contact angle for PMCN was determined to be 35^{o} in isotonic conditions increasing linearly to 47^{o} in 1,035 mosm in the case of PMCN. It is suggested that the presence of external ice alters the plasma membrane, possibly through ionic effects, to make it an energetically

favorable site for heterogeneous nucleation. For PCN, upper and lower limits for θ and R were found to be $15^{o} < \theta < 80^{o}$, and $10^{-7} < R < 4x10^{-7}$ cm, respectively.

The theoretical model was solved using the nucleation parameters determined above and was tested against four different types of experimental conditions: (1) kinetics of iif at rapid rates (120 C/min) in anisotonic conditions; (2) kinetics of iif in isotonic solutions at various cooling rates; (3) kinetics of iif at constant temperatures; and (4) kinetics of iif at rapid rates (120 C/min) with an intermediate holding temperature. The theoretical model was shown to correlate favorably with experimental observations supporting the proposed two distinct nucleation mechanisms of iif during freezing of cells.

Thesis Supervisor: Ernest G. Cravalho
Title: Edward Hood Taplin Professor of Medical Engineering
Harvard-M.I.T., Division of Health Sciences & Technology
Chief, Biomedical Engineering
Massachusetts General Hospital

To my family

ACKNOWLEDGEMENTS

During the time that I have spent at MIT there have been many people who have been of great help in various aspects of my graduate career. I am pleased to finally have the opportunity to thank them formally.

First, I would like to thank my academic and thesis adviser Prof. Ernest G. Cravalho. This work could never be achieved without his support, encouragement and guidance. His insights and direction contributed greatly to my understanding of the freezing and thawing of biological cells. I am also indebted to Prof. Cravalho for helping me out through many non-academic issues. I could not come this far without his support.

I am grateful to my thesis committee members, Emeritus Prof. David Turnbull, Prof. Marcus Karel, Prof. John D. Biggers, and Prof. Yet-Ming Chiang for their support and suggestions through the years. It was an honor for me to work with them on this research and I hope that I can create further opportunities for future interaction.

I would like to thank to my colleagues and friends at the Cryobiology Laboratory: Dr. Maury D. Cosman and Joel Kandel for developing the cryomicroscopy system and helping me in every aspects - design, experimental, theoretical and conceptual- of this work; Allison Hubel for providing scientific advice and interesting discussions, she was always ready to help out in every way; Donna Mesthene for giving me continuous moral support since my first day in the laboratory; Jim Tate for generating useful discussions on cryobiology; Dr. Edward Ingenito for his encouragement during my first and the most difficult year at MIT.

I am also grateful to Dr. Chris Körber who read this thesis at its earlier stage and offered many suggestions for its improvement. I would like to thank to Dr. Kenneth R. Diller for providing many of his unpublished data during my years at MIT.

In the course of this research and other topics I have benefited from the experience and knowledge of many scientists. I would like to express my sincere thanks to: Drs. Eric W. Overström, Karl Ebert, Tom Ducibella, and David Albertini of Tufts University, Drs. Randy Armant, Miguel D'Amien and Nongnuj Tanphaichitr of Beth Israel Hospital; Drs. Anthony P. Monaco and Takashi Maki, and Janis Porter of New England Deaconess Hospital; Dr. Ronald Tompkins of Massachusetts General Hospital. I wish to express special thanks to Kathy Jackson and Dr. Ann Kiessling of Brigham & Woman's Hospital for teaching me the necessary mouse IVF techniques. I would also like to thank Dr. Irving A. Berstein for teaching me many different aspects of biotechnology.

There are two scientists that I must thank them here. They are my undergraduate advisers from Istanbul Technical University, Profs. Abdurahman Kılıç and Aksel Öztürk. They played a major role in my early academic formation. They began my training as a scientist. They helped me discover the path that I decided to pursue.

I am also grateful to all my friends for helping me in various aspects of this work. I owe many thanks to Süreyya M. Ciliv for his brothership and support. I wish him best of luck in his life. I also thank Mehmet Aksu and Drs. Gökhan & Selen Hotamışlıgil for their continuous help and support during the last few months of this work.

Finally, I would like to thank my family to whom this work is dedicated for their support and patience. I hope one day I can deserve all they have done for me.

TABLE OF CONTENTS

LIST OF TABLES

LIST OF FIGURES

NOMENCLATURE

A	Constant in Eq.(6.89) [0.139 cP]
A_c	Surface area of the plasma membrane [m^2]
A_o	Initial surface area of the plasma membrane [m^2]
A^s, A^{s*}	Interface surface area of the ice cluster and critical cluster [m^2]
a_w^{ex}	Activity of water in the external solution
a_w^{in}	Activity of water in the cytoplasm
a, a_o	Lattice parameters for solution and ice
a'	cut-radius of the spherical cap of heterogeneous substrate
B	Cooling rate [^oC/min]
c	Concentration at the surface of the plasma membrane [mol/m^3]
c^{ex}, c^{in}	Concentrations of the extra- and intra-cellular surfaces of the plasma membrane [mol/m^3]
$[c]$	Concentration of the bulk solutions [mol/m^3]
$[c]^{ex}$, $[c]^{in}$	Concentrations of the extra- and intra-cellular bulk solutions [mol/m^3]
C	Constant in Eq.(6.64)
ΔC_p	Difference in specific heats of water & ice phases
D	Cell diameter [microns]
E	Internal energy of the system [J]
E^{α}, E^{β}, E^s	Internal energies for α, β and surface phases [J]
E_{Lp}	Activation energy for water transport [kcal/mole]

E_m	Membrane potential [Volt]
E_R	Resting membrane potential
F_d	Driving force for charged particles
F_r	Faraday constant
F	Helmholtz free energy of the system [Joule]
F^{α}, F^{β}, F^s	Helmholtz free energy of phase α, phase β and interface [Joule]
F_o	Helmholtz free energy of formation of the system in initial state [Joule]
f_o	Free energy of an homogeneous system
f_R	Friction constant
$f(\theta)$	Heterogeneous nucleation factor on a flat surface
$f(\theta_o)$	Heterogeneous nucleation factor for isotonic conditions
$f(m,x)$	Heterogeneous nucleation factor on a sphere
Δf	Free energy of activation for the transfer of molecules across the interface
Δf_i	Free energy of activation for a monomer α to join the cluster β
$(\Delta F)_{T,V}$ or ΔF	Helmholtz free energy of formation of the system
ΔF_i	Helmholtz free energy of formation of a cluster β containing i molecules
ΔF_i^*	Helmholtz free energy of formation for the critical cluster containing i^* molecules
ΔF_{BULK}	Helmholtz free energy of formation within the cluster β compared to bulk solution
ΔF_{het}	Helmholtz free energy of formation for heterogeneous nucleation

$\Delta F_{INTERFACE}$	Helmholtz free energy of formation expended in the interface between α and β phases
H_f	Latent heat of crystallization
h	Plank constant [6.6262×10^{-34} J-s]
h'	Height of the spherical cap of cluster
h_m	Apparent hydration number of solution species
h_p, h_s	Apparent hydration number of proteins and salt
ΔH	Enthalpy
ΔH_f	Enthalpy of fusion
i	No. molecules in phase β
i^*	No. molecules in critical cluster of phase β
I^s	Steady state transfer rate for homogeneous nucleation [$1/m^2$-s]
$I_{i,t}$	Net transfer rate of clusters of size i at time t
I^s_{het}	Steady state transfer rate for heterogeneous nucleation [$1/m^2$-s]
J_w	Water flux from the cell [mol/m^2-s]
k	Boltzmann constant [1.3806×10^{-23} J/K]
K_d	Parameter in diffuse interface model
k_p	Partiton coefficient
k_j	Partition coefficient for j'th ion
k_i^+	Forward reaction rate for the formation of critical cluster
k_{i+1}^-	Bacward reaction rate for the colapse of critical cluster
K, K_{het}	Pre-exponential factor in nucleation kinetics for homo- and hetero-geneous nucleations
L_1	Constant in Eq.(6.93) [36.92 J/mol-C]

L_2	Constant in Eq.(6.93) [2.826×10^{-5} J/mol]
L_p	Water permeability [μ/min-atm]
L_{pg}	Reference water permeability at T_R
$L(\Lambda)$	Langevin factor
m	Minimum number of molecules required to form a cluster of phase β
m_{DRY}	Total dry mass of the egg
mw_p	Molecular weight of proteins
mp	Total protein mass within oocytes
mw	Total water mass within oocytes
mw/mp	Mass water per mass protein
n_s^{ex}, n_s^{in}	No. moles solute in extra- and intra-cellular spaces [moles]
n_w^{ex}, n_w^{in}	No. moles water in extra- and intra-cellular spaces [moles]
n_w^B, n_w^F	No. moles bound and free water in cell [moles]
n_{ice}^{ex}	No. moles ice in the external medium [moles]
n_p	No. moles protein inside cell [moles]
n_m	No. moles fictitious species [moles]
n^α, n^β	No. moles of water and ice [moles]
n_γ	No. moles γ'th component [moles]
n_γ^α, n_γ^β, n_γ^s	No. moles γ'th component at phase α, phase β and interface [moles]
N	No. molecules present in the system
N'	No. molecules of solvent in volume or in contact with the substrate for homo- or hetero-geneous nucleation, respectively
N_o'	No. molecules of solvent in isotonic conditions in volume or in contact with the substrate for homo- or hetero-geneous nucleation, respectively

N^s	No. molecules that are in contact with the substrate in heterogeneous nucleation
N_s	No. molecules of salt in volume or in contact with the substrate for homo- or hetero-geneous nucleation, respectively
N_{AV}	Avagadro number [$6.0225 \times 10^{+23}$ /moles]
N_i	No. clusters β containing i molecules
N^{υ}	No. molecules in phase α
N_i^s	No. molecules at steady state conditions
$N_{i,t}$	No. clusters of size i present at time t
N_i^e, N_{i+1}^e	Equilibrium no. clusters of size i and i+1
N_V	No. molecules per unit volume
N_t^u	Total no. unfrozen cells at time t
N_t	Total no. frozen cells at time t
N_o	Total no. cells
[NaCl]	Molarity of the external solution [Molar]
O_i , O_i*	No. molecules that could be placed with their centers on a sphere that encloses all the molecules in the cluster containing i and i^* (critical cluster) molecules
p	upper limit for no. molecules in clusters at steady state nucleation
p^{ex}, p^{in}	Hydrostatic pressures inside and outside of cell
P	Pressure of the system
P^{α}, P^{β}	Pressures in phase α and phase β
P_o^{α}	Pressure of phase α in initial state
P_{Na^+}, P_{K^+}, P_{Cl^-}	Permeabilities of the plasma membrane to Na^+, K^+ and Cl^- [cm/s]

P_t	Probability of freezing at time t
P_T	Probability of freezing at temperature T
P^I	Probability of freezing by plasma membrane catalyzed nucleation mechanism
P^{II}	Probability of freezing by particle catalyzed nucleation mechanism
r	Radius of cluster β
r_c	Radius of pores in the plasma membrane
r_p	Radius of ions (particles)
R	Gas constant
R_c	Radius of the heteronuclei
s	Lower limit for no. molecules in clusters at steady state
S	Entropy of the system [J/K]
S^s	Surface excess entropy [J/K]
ΔS_f	Entropy of fusion
SA/V	Ratio of the surface area to volume
t	Time [minute or second]
T	Temperature [K]
T_{crt}	Critical temperature [K]
T_f	Freezing temperature [K]
T_{hom}	Homogeneous nucleation temperature [K]
T_o	Freezing temperature of the isotonic solution [-0.53°C]
T_R	Reference temperature [273.15 K]

T_{init}	Initial temperature [K]
T_c	Constant temperature in Eq.(6.89) [225 K]
ΔT	Undercooling [= T_f - T]
U_d	Potential energy of a dipole
U_j	Mobility of j'th ion
V	Volume
V_b	Inactive cell volume
V_c	Cell volume
V_o	Initial cell volume
V_m	Volume of macromolecules
V_w	Cell water volume
V	Initial cell water volume
V^{α}, V^{β}	Volume of phase α and phase β [m^3]
v	Velocity
v_s	Dissociation constant
x_w^{ex}, x_w^{in}	Water activity inside and outside of the cell
X	Any extensive thermodynamic property
X^{α}, X^{β}, X^s	Any extensive property of phase α, phase β and interface
x	Any intensive thermodynamic property
W	Reversible work to form an interface [J]
Z	Zeldovich factor
Z_v	Valence of ions

z	Lattice parameter of strained cluster

Greek Symbols

α	Liquid phase (water)
β	Solid phase (ice)
β_i	Cluster of phase β containing i molecules
β_{i^*}, β_{i^*+1}	Critical cluster of phase β containing i^* and i^*+1 molecules
β_m	Smallest cluster of phase β
ξ	Parameter [= F_r/RT]
ς	angle between dipole and the field direction
χ	Chi-square statistics
δ	Thickness of the plasma membrane
δ	Proportionality constant [10^{-8} cm]
δ	Degree of misfit between substrate and ice
ϵ	Elastic strain
Φ_j	Flux of j'th ion [mole/cm^2-s]
Φ_{Na^+}, Φ_{K^+}, Φ_{Cl^-}	Passive fluxes for Na^+, K^+ and Cl^- ions
ϕ_s	Volume fraction of solutes
ϕ_m	Volume fraction of fictitious (salt+proteins) species
γ	Pertaining to component γ
η	Viscosity [cP]
η_o	Viscosity in isotonic solution [cP]

η_w	Viscosity of pure water [cP]
θ	Contact angle of ice on substrate [degrees]
θ_o	Contact angle in isotonic conditions [degrees]
κ	Exponential factor in homogeneous nucleation equation [K^5]
κ_{het}	Exponential factor in heterogeneous nucleation equation [K^5]
κ_o^I	Exponential factor for plasma membrane catalyzed nucleation in isotonic conditions [K^5]
κ_o^{II}	Exponential factor for particle catalyzed nucleation in isotonic conditions [K^5]
Λ	Langevin factor [= $\mu_d E_m/kT$]
Λ_V	Distribution density function of volume
Λ_L	Distribution density function of permeability
Λ_E	Distribution density function of ectivation energy
Λ_S	Distribution density function of SA/V
λ	Parameter in Eq.(6.89) [-1.64]
μ_d	Dipole moment [debye]
μ_w^{ex}, μ_w^{in}	Chemical potentials of water inside and outside the cell [J/K-mole]
μ_w^{*ex}, μ_w^{*in}	Reference chemical potentials of water inside and outside the cell [J/K-mole]
μ_γ	Chemical potential of the γ'th component [J/K-mole]
μ_γ^s	Chemical potential of the surface excess of the γ'th component [J/K-mole]
μ_γ^α, μ_γ^β	Chemical potentials of γ'th component in phase α and phase β [J/K-mole]

$\mu^{\alpha}_{\gamma o}$	Chemical potential of the γ'th component in phase α at the initial state [J/K-mole]
$\Delta\mu_{\gamma}$	Difference in chemical potential of γ'th component between phase α and phase β [J/K-mole]
$\Delta\mu_{s}$	Difference in chemical potential of ice and electrolyte solution [J/K-mole]
$\Delta\mu_{b}$	Difference in chemical potential between ice and water [J/K-mole]
v_{i+}	Average jump rate of molecules in the forward direction
v_{o}	Frequency factor
v^{α}_{γ}	Specific molar volume of γ'th component in phase α [m^3/mole]
v^{β}_{γ}	Specific molar volume of γ'th component in phase β [m^3/mole]
v^{α}, v^{β}	Specific molar volume of water and ice [m^3/mole]
v_{w}	Specific molar volume of water [m^3/mole]
v^{h}_{p}, v^{h}_{s}	Hydrated molar volume of protein and salts [m^3/mole]
v^{h}_{m}	Apparent hydrated molar volume of fictitious species [m^3/mole]
π^{ex}	Osmolality of the external solution [osm/kg water]
π^{in}, π^{in}_{o}	Instantaneous and initial osmolalities of the cytoplasm [osm/kg water]
Ψ	Potential
ρ	Density [kg/m^3]
ρ_1, ρ_2	Densities at the boundaries of the diffuse interface [kg/m^3]

ρ_o	Avearge density of the liquid phase [kg/m^3]
ρ_p	Density of protein [kg/m^3]
ρ_w	Density of water [kg/m^3]
σ	Interface tension [J/m^2]
σ_o	Interfacial energy between phase α and phase β in isotonic conditions [J/m^2]
$\sigma^{\alpha S}$	Interfacial energy between phase α and substrate [J/m^2]
$\sigma^{\beta S}$	Interfacial energy between phase β and substrate [J/m^2]
$\sigma^{\alpha\beta}$	Interfacial energy between phase α and phase β [J/m^2]
σ_∞	Surface free energy of a planar interface [J/m^2]
τ	Time constant
Ω_o^I	Preexponential factor for plasma membrane catalyzed nucleation in isotonic conditions
Ω_o^{II}	Preexponential factor for particle catalyzed nucleation in isotonic conditions

CHAPTER I

INTRODUCTION

1.1. Overview of Cryobiology

The response of living tissue to subfreezing temperatures is an intriguing problem which has been of interest to the scientific and medical communities for centuries. Increased knowledge concerning the low temperature behavior of living tissue and cells can yield beneficial advancements in the fields of medicine, nutrition, and agriculture. However, the task facing the cryobiologists is an extremely challenging one. In order to successfully preserve any living material, there is a need to cool the sample to cryogenic temperatures (usually below -100°C), practically suspend the life by stopping the chemical reactions, and subsequently return to physiological conditions with full recovery of structure and complex biological functions. To appreciate the difficulties involved in going to and from such low temperatures , one has to understand the physico-chemical events occurring during freezing and thawing as well as living tissue's response to these events.

The discovery of cryoprotective properties of glycerol made by Polge et al. (1949) initiated an enormous advance in the preservation of different cell types. Since 1949, several classes of biomaterials have

been frozen successfully and a better understanding of the events occurring during a freeze-thaw cycle has emerged from these studies. It became evident that survival was increased by the use of an optimum cooling rate (Rapatz & Luyet 1965; Mazur & Schmidt 1968; Mazur et al. 1969; Mazur et al. 1972; Leibo et al. 1970). The typical dependence of survival on cooling rate is shown for several types of cells in Fig.1.1. Although the range of cooling rates for peak survival are cell-specific, the curves are qualitatively similar. They all present an inverted U-shape curve suggesting cell damage at sub- and supra-optimal cooling rates.

A quantitative interpretation of Fig.1.1 can be accommodated by the two-factor hypothesis of freezing injury originally proposed by Mazur (1963, 1965). The thermodynamic changes of state imposed by the freezing protocol is a consequence of the competing rate processes of heat transfer and water transport (Mazur 1963). For a cell suspended in a freezing medium and subjected to sub-freezing temperatures, ice preferentially forms outside the cell in the suspending medium and the solute concentration in the remaining solution increases. As a result, the thermodynamic equilibrium that exists across the cell membrane between the cell contents and the suspending medium is upset, and the cell responds by expressing water across the plasma membrane. If the temperature of the suspension is changed during the water transport, there will be a competition between the processes of heat transfer (defined by the cooling rate) and mass transfer (defined by the water permeability of the plasma membrane). Two regimes of freezing are possible: (1) slow freezing in which the cells become dehydrated during trans-membrane water transport to reach the thermodynamic equilibrium

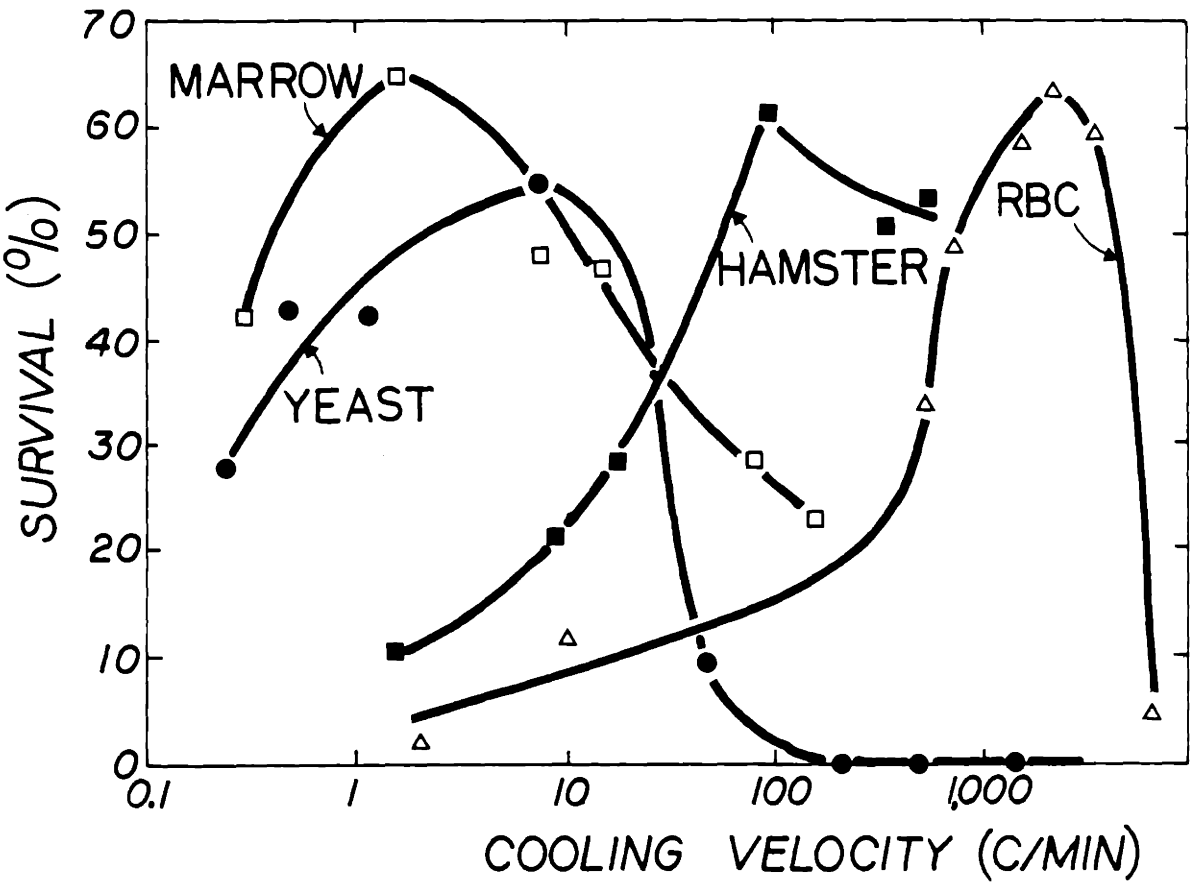

FIGURE.1.1. Dependence of survival on cooling rate for several cell types cooled to -196°C and thawed rapidly (from Mazur et al. 1970).

with the external milieu; and (2) fast freezing in which the cells become undercooled as the temperature decreases at a rate faster than the rate of trans-membrane equilibration, i.e. they exist at a temperature lower than the equilibrium freezing temperature for their chemical composition.

In the first instance the cells may be damaged by the high concentration of electrolytes that results from water loss while in the second instance damage may result from the formation of intracellular ice that forms as cells seek a stable state from the metastable (undercooled) state. From this simplified description of the thermodynamic behavior of cells during freezing, it is clear that in order to avoid, or at least minimize freezing injury, a better understanding of the damage mechanisms must be known.

Damage at Slow Cooling Rates

Lovelock (1953a,b) proposed quantitatively that the slow freezing injury occurs when extra- and intra-cellular electrolytes reach critical concentrations during freezing. According his point of view, the protective effect of permeating solutes like glycerol and dimethyl sulfoxide results from their colligative action to reduce damaging electrolyte concentration at a given subzero temperature. A quantitative thermodynamic and kinetic model developed by McGrath (1977) agreed well with Lovelock's results suggesting that exposure to high electrolyte concentrations during freezing may lead to irreversible

desorption of membrane components. Recently, Pegg & Diaper (1988) repeated and confirmed Lovelock's (1953a,b) original results. They concluded that slow freezing injury to cells is indeed due to changes in the electrolyte concentration of the solution in which they are suspended during a freeze-thaw cycle.

An alternative interpretation of slow cooling damage during freezing was proposed by Meryman (1968, 1974). Specifically, the damage occurs at slow cooling rates due to the resistance of cells to shrinkage below a certain critical volume. The protective effect of cryoprotective solutes can be explained based on their colligative action to reduce the extent of cell shrinkage at any temperature. A quantitative analysis by Steponkus & Wiest (1978) suggested that cells that have shrunk osmotically during freezing can tolerate only a certain increase in surface area during thawing. Damage results if that critical area increment is exceeded due to the inability of the cell membrane to restore its components.

Mazur and co-workers (1981, 1983, 1985) proposed a third alternative for slow freezing damage. According to their hypothesis, the damage to cells is caused by mechanical effects of the extracellular ice. During freezing the volume of liquid in the channels in which cells are sequestered decreases as water is converted into ice. The restrictions on the geometries of the channels could force the cells to become seriously deformed at subzero temperatures leading to cell damage.

It is evident from the above discussion that there are a number of

possible mechanisms of slow freezing damage. Not all mechanisms are compatible with all experimental observations, supporting the view that at suboptimal cooling rates the freeze-thaw response of cells is determined by many variables specific to the cell-type.

Damage at Rapid Cooling Rates

At higher cooling rates, the limited permeability of the plasma membrane to water prevents the cell from maintaining the chemical equilibrium with the extracellular partially frozen solution and consequently the chemical equilibrium is achieved by the formation of intracellular ice. By some mechanism, at the present time unclear, the presence of this intracellular ice results in cell damage. A brief review of intracellular ice formation studies in biological cells follows.

The study of ice formation within cells seems to begin with Goeppert's (1830,1883) observations. The first mechanistic interpretation of experimental findings was by Muller-Thurgau (1886). He proposed that ice crystals formed intracellularly at rapid cooling rates whereas ice formed only in the intercellular spaces at slow cooling rates. Molisch (1897) confirmed the earlier observations using his cold chamber. Chambers & Hale (1932) proposed that the plasma membrane of the cell acts as a barrier against internal freezing in the presence of external ice based on direct microscopic investigation. In 1936, Levitt & Scarth suggested that the ice formed intracellularly at

high cooling rates due to excessive undercooling of the cytoplasm. However, cells escaped from internal ice formation at slow rates of cooling by excessive water efflux. However, none of these studies could interpret their observations on a quantitative basis.

A quantitative interpretation of internal ice formation was not presented until 1963. Mazur (1963, 1965) suggested that external ice can grow through aqueous pores (3 to 8 Å) in the membrane if the temperature is below a critical value (usually -5 to -15°C). This is due to the depression of the freezing temperature of water in small capillaries (Jackson & Chalmers 1958). According to Mazur, above this critical temperature, external ice cannot penetrate into the cells because the plasma membrane acts as a mechanical barrier. However, the plasma membrane loses its effectiveness to prevent the external ice to grow into cells below the critical temperature (T_{crt}). The magnitude of the critical temperature corresponds to the equilibrium freezing temperature of water inside microscopic aqueous pores and is usually called 'cytoplasm ice nucleation temperature.' The 'pore' theory has been extensively used in the field.

The pore theory suggests that the damage to cells during rapid freezing is the consequence of intracellular ice formation. Specifically, Mazur (1965) proposed that the formation of ice within the cells would disturb the internal membranes and organelles and lead to injury. In the few cases examined at rapid cooling rates, a substantially higher percentage of cells often survive inferred intracellular freezing (!) when the rate of subsequent warming is high

(Sakai & Yoshida 1967; Leibo et al. 1970; Asahina et al. 1970; Mazur et al. 1972; Miller & Mazur 1976; McGann et al. 1981). These observations support the hypothesis that intracellular freezing is the consequence of cell damage. However, in most of these earlier studies, a direct microscopic correlation was not determined between internal ice formation and cell death.

In 1970, Diller & Cravalho designed a cryomicroscope system that employed an analog control system coupled with an electrically heated cold stage to study the dynamics of the freezing process which became the basis of all subsequent cryomicroscope systems. In the last decade, cryomicroscopy has emerged as a very powerful technique for quantifying and understanding cell's behavior during a freeze-thaw cycle (McGrath et al. 1975; Diller 1981; Steponkus et al. 1984a; Korber et al. 1986).

The relationship between the cooling rate and intracellular ice formation is obtained for various cell types. The critical experimental observations emerged from cryomicroscopic analysis of cells during freezing can be summarized as follows:

1- The fraction of cells containing intracellular ice is a strong function of the cooling rate (Diller et al. 1972; McGrath et al. 1975; Diller 1979; Morris & McGrath 1981; Schiewe & Korber 1983; Cosman 1983; Scwartz & Diller 1984; Callow & McGrath 1985; Schiewe & Korber 1987; Shabana & McGrath 1988). There is a very sharp demarcation zone over which the fraction of cells with internal ice increases rapidly from 0% to 100% (see Fig.1.2). This zone is cell-specific.

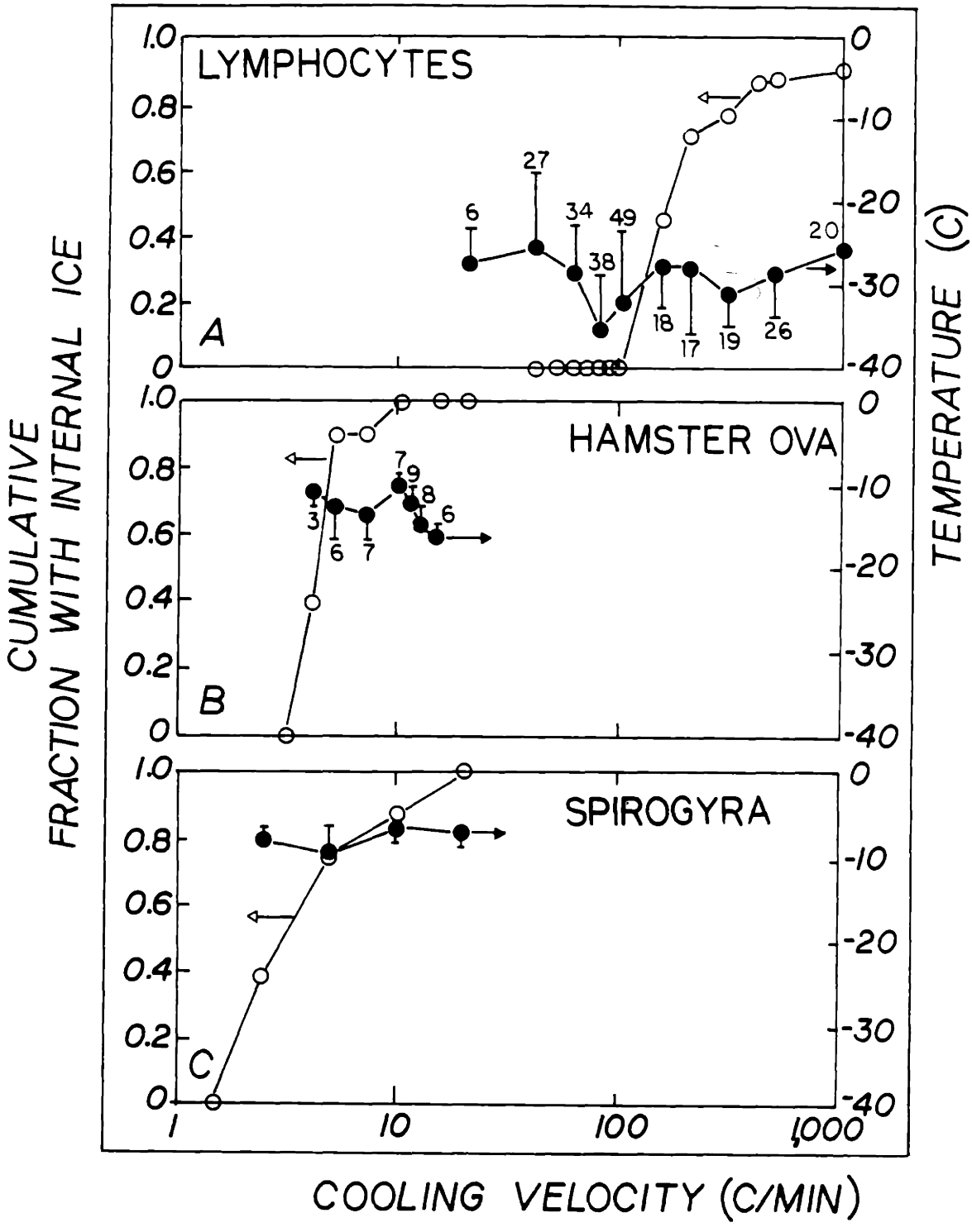

FIGURE.1.2. Filled circles: Intracellular ice formation temperatures as a function of cooling rates. Open circles: Fraction of cells exhibiting intracellular ice formation as a function of cooling rate. The cell types displayed are: (a) human lymphocytes (Scheiwe & Korber 1983); (b) hamster ova (Shabana & McGrath 1988); and (c) spirogyra (Morris & McGrath 1981).

2- The freezing temperature of the intracellular solution (T_{crt}) is independent of the cooling rate (Morris & McGrath 1981; Schiewe & Korber 1983; Callow & McGrath 1985; Schiewe & Korber 1987). Although the undercooling of the cell interior decreases drastically with decreased cooling rate, the mean freezing temperature is independent of the cooling rate (see Fig.1.2).

3- The experimental evidence supports that the cell damage at rapid rates is due to the formation of intracellular ice (see Fig.1.3). The optimum cooling rate can then be defined as the fastest possible cooling rate without internal ice formation.

Mazur (1977) modified his original theory to predict the fraction of cells with internal ice as determined from cryomicroscope observations. He assigned a value of zero to the probability of internal ice formation (P) when the degree of undercooling (ΔT) is $< 2^{o}C$ or when the ratio of the instantaneous water content to the initial water content (V_w/V_{wo}) is < 0.1 at the cytoplasm crystallization temperature (T_{crt}). P is assigned a value of 1.0 when $\Delta T > 2^{o}C$ or $(V_w/V_{wo}) > 0.1$ at T_{crt}. These assumptions are based on general experimental observations (Mazur 1977). The values for ΔT or (V_w/V_{wo}) can be determined from the thermodynamic model of water transport (Mazur 1963; Levin et al. 1979). The predicted fraction of cells with intracellular ice formation is not sensitive to the values assigned for ΔT or (V_w/V_{wo}), whereas they are very sensitive to the value assigned for T_{crt} (Mazur 1977). Using these values, Mazur (1977) was able to predict the probability of intracellular ice formation in red blood cells supporting the validity of his original

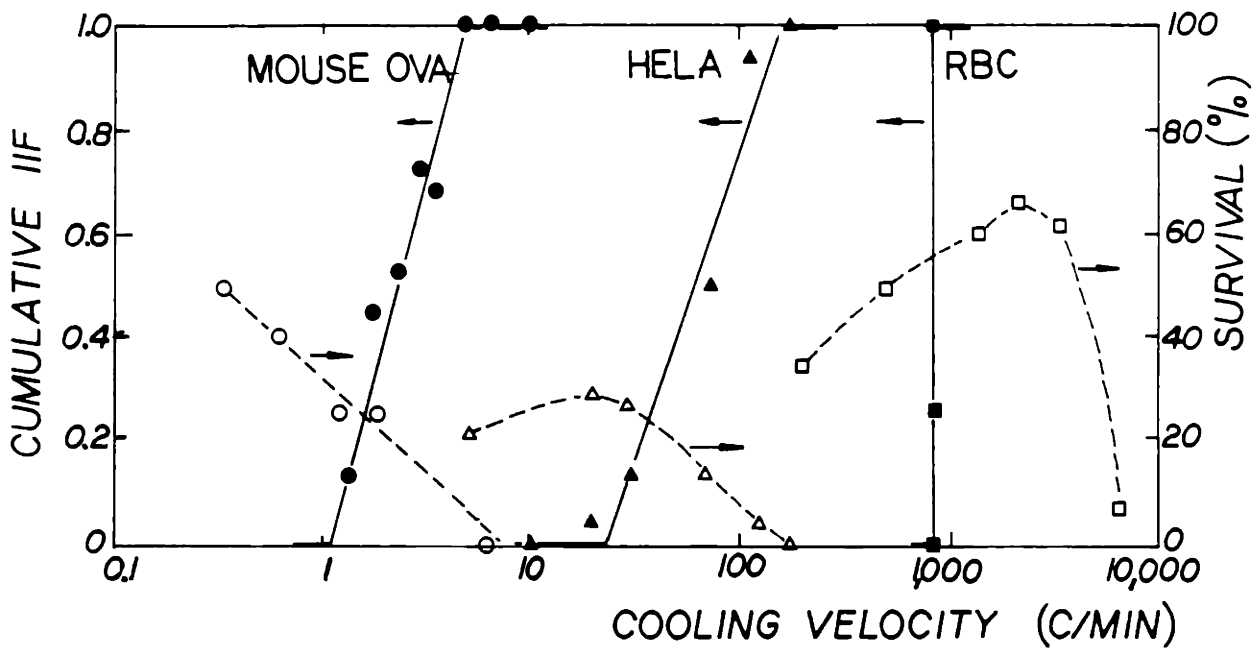

FIGURE.1.3. Intracellular ice formation and survival as a function of cooling rate (from Cosman 1983).

freezing through aqueous channels in the plasma membrane. This approach has been improved by many investigators to accommodate for specific experimental observations (Cosman et al. 1978; Cosman 1983; Mazur et al. 1984).

The general approach is to determine T_{crt} as in Fig.1.2 together with water permeability parameters from cryomicroscope observations and then use a criteria for P to predict the critical cooling rate given in Fig.1.2. Unfortunately, T_{crt} varies with different experimental conditions, such as initial temperature at which the freezing starts (Diller 1975; Mazur 1977; Cosman 1983), composition of the suspending solution used for freezing (Leibo et al. 1978), and the amount of initial dehydration prior to freezing (Schwartz & Diller 1981). It is, therefore, necessary to determine a new T_{crt} for each experimental condition in order to predict P. Since T_{crt} and P are actually determined from the same set of experiments as shown in Fig.1.2, the application of this approach remains very limited.

In contrast to the 'pore' hypothesis, Toscano et al. (1975) proposed that the internal ice formation in red blood cells between -5 to -15^{o}C can be caused by internal nucleators, namely hemoglobin, during freezing. They did not, however, rule out the possibility of external triggering. Their theory was based on heterogeneous nucleation of ice within cells. Later studies by Franks & co-workers (Franks et al. 1983; Mathias et al. 1984) showed that there are effective nucleators in yeast, erythrocytes and G. max cells, however, they are only active at

temperatures close to homogeneous nucleation temperature (usually between -30 to -40°C) of the cytoplasm. Burke et al. (1975, 1976) have investigated plant tissues and found that they do not contain heterogeneous nucleators.

Recently, some investigators have suggested that internal ice formation may be due to the membrane failure. Mechanical (Dowgert & Steponkus 1983; Scheiwe & Korber 1982b), electrical (Steponkus et al. 1984b), and thermal (Quinn 1985; Thom 1988) effects of extracellular ice may account for the membrane damage during freezing. Once the plasma membrane is damaged by one of these effects at T_{crt} then the external ice will be in direct contact with undercooled internal solution and ice can freely grow into cells. Therefore, the damage to the cell membrane is prior to the intracellular ice formation. According to the membrane failure theory, the formation of internal ice is the consequence of the cellular damage and not the cause of it as proposed by Mazur (1965). There is no quantitative theory yet to predict the probability of internal ice formation based on membrane failure hypothesis of internal ice formation.

1.2. Scope of the Present Study

This study aims to investigate the thermodynamics and kinetics of intracellular ice formation based on a heterogeneous nucleation mechanism in biological cells. A model describing the ice nucleation in cells in the presence of extracellular ice will be derived. This model

will be based on a modified heterogeneous nucleation theory. The plasma membrane and/or internal supramolecular particles will be assumed to catalyze the ice nucleation depending on the freezing conditions and the validity of these assumptions will be discussed. The effects of the external ice formation on the plasma membrane will be presented and a major emphasis will be given to ionic transients during freezing. It will be hypothesized that the formation of the external ice may influence the plasma membrane to make it a good ice nucleator leading to the nucleation of ice within the cells.

The amount of water remaining in cells, the undercooling of the internal milieu, and the viscosity of the cytoplasm are important parameters in the solution of the kinetic model for intracellular ice nucleation. These parameters will be obtained from a theoretical model for the water transport during freezing. The kinetic model for intracellular ice nucleation and the water transport will be coupled. The numerical solution of the resulting set of integro-differential equations will describe completely the thermodynamic state of the intracellular solution and its probability of ice nucleation.

The theoretical model requires the knowledge of several biophysical parameters. The kinetic model for intracellular ice formation can be solved if the values for kinetic (Ω) and thermodynamic (π) parameters appearing in the equations are known. The water transport behavior during freezing can be established if the values for the water permeability at $0^{o}C$ (L_{pg}) and its temperature dependence (E_{Lp}) are given. These parameters will be determined using cryomicroscope system

for unprotected mouse oocytes as the model system. All of the experiments will be done in normal saline because of its simplicity. For freezing experiments in saline solutions, thermodynamic states of the intra- and extra-cellular solutions can be described accurately. Mouse oocytes were chosen as the model system because it has already been shown that the freezing behavior of mouse oocytes is very similar to cells of other types (Leibo et al. 1978; Mazur et al. 1984) and their large size allows an easier visual observation of the intracellular ice formation during freezing. A special attention will be given to minimize the temperature gradients on the cryostage due to the extreme temperature sensitivity of nucleation equations. An 'isothermal' freezing stage will be designed to achieve this goal.

The overall experimental and analytical effort in this study is documented in eleven chapters. (1) An overview of the intracellular freezing studies have been discussed in Chapter I. (2) Chapter II introduces the experimental system and techniques used for mouse oocyte recovery and subsequent culture to blastocyst stage. Control experiments will be presented in this chapter. (3) In Chapter III, the cryomicroscope system and the freezing stage thermal characteristics will be described. (4) Chapter IV contains all the experimental findings for ice nucleation kinetics and water transport behavior of mouse oocytes. (5) Chapter V begins with a review of water transport in cells to establish the basic equations and assumptions. The water permeability parameters will be determined from the correlation of the theory with experimental results using non-linear regression analysis. A distributed analysis of water transport will also be included to

accommodate for cell-to-cell variations of water transport parameters. The chapter will continue with a review of ion transport during freezing from biological cells. The trans-membrane potential change will be estimated using a simple ionic transport model. One possible effect of trans-membrane hyperpolarization, namely, the orientational polarization, will be discussed. The possible role of ionic effects and orientational polarization will be outlined in the context of intracellular ice nucleation mechanism. (6) The basic theory of heterogeneous and homogeneous nucleation theories will be outlined in Chapter VI. These theories will then be expanded to biological cells. Effects of simultaneous volume, concentration and temperature changes will be incorporated to the heterogeneous nucleation equations to predict the nucleation frequency from the first principles of thermodynamics. The probability of intracellular ice nucleation within cells will be obtained from the nucleation frequency by assuming that all of the cells affects the nucleation in a similar fashion. (7) In Chapter VII, the parameters describing the nucleation kinetics (Ω_o, κ_o) will be determined from the experiments in anisotonic solutions at 120^{o}C/min. Two different ice nucleation mechanisms, i.e. plasma membrane catalyzed and supramolecular catalyzed based on the heterogeneous nucleation theory will be proposed to explain experimental observations based on the heterogeneous nucleation theory. (8) Chapter VII will be verification of the kinetic model by applying it to three different experimental conditions: (i) freezing in isotonic solutions at rates ranging from 1^{o}C/min to 120^{o}C/min; (ii) nucleation kinetics at isothermal conditions; (iii) a simple two-step freezing protocol. (9) The existing hypotheses of intracellular ice nucleation mechanisms will

be discussed in the context of experimental results from this study in Chapter IX. The weaknesses of previous interpretations of ice nucleation within cells will be outlined. (10) Chapter X will include discussion and conclusions from this thesis.

CHAPTER II

FERTILIZATION AND DEVELOPMENT IN VITRO OF MOUSE EGGS

2.1. Introduction

In 1959, Chang reported the first successful in vitro fertilization study of rabbit ova. In vitro fertilization of the eggs of the golden hamster by Yanagamachi & Chang (1963, 1964) followed the initial study on rabbit ova. The first successful mouse ova in vitro fertilization was reported by Brinster & Biggers (1965) which became the basis of all subsequent studies. For more detailed and comprehensive accounts of in vitro fertilization and subsequent culture, the reader should refer to Biggers (1971) and Mastroianni & Biggers (1981).

In an attempt to investigate the nucleation of intracellular ice during freezing of biological cells, we have decided to use mouse oocytes as a model system. There are several important reasons for this choice: (1) there are no reliable freezing methods for mouse (or other species) oocytes, although some experimental data have been accumulated (Leibo et al. 1978); (2) the oocyte's large size (80μm in diameter) allows easier observation of internal ice formation during freezing; (3) the oocyte's spherical shape allows accurate determination of its volume

during freezing; and (4) there reliable techniques to recover sufficient number of oocytes and test their viability (Jackson & Kiessling 1988).

In this chapter, the techniques used for mouse oocyte recovery and subsequent culture will be introduced and the effect of several experimental variables on fertilization and blastocyst formation rates will be investigated. The mouse in vitro fertilization system used in this study is established based on Jackson & Kiessling's (1988) procedures and protocols.

2.2. Materials and Methods

Preparation of Culture and Collection Media

The medium for in vitro fertilization and subsequent development was a slight modification of Earle's balanced salt solution (EBSS). EBSS (powder, Sigma, St. Louis, MO) was dissolved in 1 liter of freshly distilled tissue culture quality water (18 megaohm, Millipore) and then supplemented with 1.85 g/lt (22 mM) sodium bicarbonate (Mallinkrodt, NY), 0.053 g/lt (1.2 mM) calcium lactate (Calbiochem, La Jolla, CA), 3.7 ml/lt (26.4 mM) sodium lactate (Sigma), 0.035 mg/lt (0.32 mM) sodium pyruvate (Sigma), 0.08 g/lt penicillin G (Calbiochem), and 0.05 g/lt streptomycin sulfate (Calbiochem). Osmolarity of modified EBSS was adjusted to 295 to 300 milliosmols (mosm) by replacing 75 ml of the

media with distilled water. The media was filtered through a 0.22 micron filter (Nalgene, Fisher) to sterilize it. This media was kept refrigerated for one to two weeks at 4°C. Composition of the modified EBSS media is given in Table 2.1. One day prior to experiments bovine serum albumin (BSA, Sigma) was added to the culture media. The concentration of BSA used in this study was 4 mg/ml.

Dulbecco's sulfate buffered saline (PBS) solution supplemented with 4 mg/ml BSA was used for collection of oocytes. The composition of PBS is given in Table 2.1.

Superovulation

Oocytes were obtained from a hybrid-inbred strain (C57B1/6 x DBA) virgin female $B_6D_2F_1$ mice (Jackson Lab., Bar Harbor, Maine). Female mice were 4 to 10 weeks old at the time of the collection.

In order to increase the number of eggs collected from each mouse, gonadotropic hormones were used. Female mice were injected intraperitoneally with 5 IU of pregnant mare serum gonadotropin (PMSG, Sigma) in the late afternoon (5 to 7 PM). PMSG was prepared at 50 IU/ml in sterile saline or PBS and stored frozen in 1 ml aliquots. Forty eight hours later, mice were injected intraperitoneally with 5 IU of human chorionic gonadrotropin (hCG, Sigma). Following hCG injection, oocytes have arrested in the second meiotic metaphase awaiting

TABLE 2.1

Compositions of Culture and Collection Media

Component	EBSS[1] (gms/lt)	PBS[2] (gms/lt)
$CaCl_2$	0.200	0.10
NaCl	6.800	8.00
KCl	0.400	0.20
$MgSO_4$ (anhyd.)	0.098	
$NaH_2PO_4.H_2O$	0.140	
$NaHCO_3$*	1.850	
D-Glucose	1.000	
Ca Lactate*	0.053	
Na Lactate*	3.7 cc	
Na Pyruvate*	0.035	
Pen. G.*	0.080	
Strep Sulfate*	0.050	
Phenol Red	0.010	
KH_2PO_4		0.20
$MgCl_2.6H_2O$		0.10
$Na_2HPO_4.7H_2O$		2.16

[1]Modified Earle's Balanced Salt Solution used for mouse oocyte *in vitro* fertilization and subsequent culture (from Jackson & Kiessling 1988); [2] Dulbecco's Phosphate Buffered Saline used for oocyte collection; * Items that are added to EBSS by Jackson & Kiessling (1988).

ovulation. Metaphase II arrest is maintained until the oocytes are activated by sperm during *in vivo* or *in vitro* fertilization.

For control and freezing experiments, the eggs were collected at metaphase II stage about 12 to 15 hours after the hCG injection.

Oocyte Recovery and IVF Protocol

On the afternoon preceeding oocyte harvest, culture dishes containing EBSS medium were prepared. Using organ culture dishes (Falcon 3037; Fisher Scientific, Boston, MA), 4 ml of sterile water was placed in the outer ring, one ml of EBSS supplemented with BSA was placed in the center and overlayed with 1 ml of silicone oil (Aldrich Chem. Co., Milwaukee, WI; #14,615-3). The oil was treated to remove impurities by shaking it for one minute with EBSS medium (1:4 EBSS to oil) and then letting it settle overnight at ambient temperature. For each experimental condition, one plate was prepared for insemination and another for embryo development after insemination period. Sperm collection dishes were also prepared at this time by placing 0.15 ml of EBSS medium at the edge of a petri dish (Falcon 3001) and flooding the dish with silicone oil (approximately 2.5 ml) to cover the medium. The dishes were placed in a CO_2 incubator and kept overnight for equilibration under 5% CO_2 in air at 37°C.

PROTOCOL

* Sperm retrieval:

1. At 12 to 14 hours after hCG injection, a male mouse (mature $B_6D_2F_1$, 7 to 24 weeks old) were killed by cervical disl$ation.

2. Abdominal skin was wetted with 70% ethanol and then retracted in a superior-inferior direction to avoid hair contamination.

3. Using sterile instruments, the peritoneum was opened and cauda epididymus from each testis were removed.

4. Each cauda epididymus was placed in a separate sperm collection dish containing EBSS/BSA that had equilibrated in 5% CO_2 incubator for approximately 18 hours.

5. Using an insulin syringe, the cauda were perforated in 10 to 20 places to allow the sperm to swim into the media.

6. The sperm was capacitated for at least one hour in the medium before being used for insemination.

* Egg retrieval:

1. At 12 to 14 hours after hCG injection, female mice were killed by cervical dislocation.

2. Abdominal skin was wetted with 70% ethanol and then retracted in a superior-inferior direction to avoid hair contamination.

3. Using sterile instruments, the peritoneum was opened and the reproductive tract was exposed.

4. Oviducts were removed and placed into the collection dish containing a large drop of PBS/BSA.

5. The cumulus mass was released from each oviduct by holding the oviduct with forceps and pricking the bulge in the oviduct with a small gauge needle to break the wall. The empty oviduct was then discarded. This was done under a stereo dissecting microscope.

6. The cumulus masses were transferred into a drop of hyaluronidase if the cumulus was to be removed. After 5 to 10 minutes, the cumulus cells appeared as a lawn on the bottom of the drop along with free eggs. The eggs were collected with a sterile micropipet and transferred through two or three drops of EBSS medium to remove all cumulus cells. Then, the free eggs or intact cumulus masses were transferred into the insemination dishes equilibrated in 5% CO_2 incubator for approximately 18 hours. Eggs or cumulus masses from each female were pooled together and distributed evenly among each insemination dish to avoid errors due to individual animal abnormalities.

* Insemination and Culture:

1. A sample of 5 μl of collected sperm was placed in a hemocytometer. The sperm count in millions of sperm per ml was obtained by counting the number of sperm in the center grid's 4 corners and center square. In addition, the motility was calculated from the ration of the motile sperm to the total number of sperm in 5 squares.

2. Enough motile sperm was added to each dish of eggs to ensure a final concentration of 2-5 million sperm per ml. The insemination dishes were placed into the 5% CO_2 incubator for 4

to 5 hours.

3. After 4 to 5 hours, the embryos were transferred from the insemination dishes to the growth dishes that had equilibrated in the incubator. Following the transfer, the growth dishes were returned to the incubator.

Embryo Scoring

Embryos were scored for division to the 2-cell stage after 24 hours in culture to obtain the fertilization rate. The fertilization rate was calculated as the ratio of the number of the 2-cell stage embryos to the number of total embryos inseminated. Following 96 hours in culture, embryos were assessed for development to blastocyst stage. The growth or blastocyst formation rate was defined as the ratio of the number of embryos at the blastocyst stage to the number of the 2-cell embryos. It is best for proper development not to remove the embryos from the incubator frequently.

2.3. Results

In order to optimize the culture conditions, several experimental variables have been tested in the refinement of the protocol discussed in the previous section. The overall fertilization and blastocyst formation rates were found to be 90% (715/796) and 82% (583/715).

The effect of using hyaluronidase on the fertilization and the blastocyst formation rates was tested. In a series of experiments, some oocytes were denuded from the their cumulus masses by treating the eggs with hyaluronidase (120 units/ml of PBS) for 5 to 10 minutes. The oocytes were never kept in hyaluronidase for more than 10 minutes. As a control experiment, some oocytes from the same collection were immediately washed in EBSS with BSA, and placed in the insemination dishes with the cumulus intact. The fertilization and the blastocyst formation rates of oocytes without and with hyaluronidase treatments were found to be 80 and 80%, and 81 and 82%, respectively. It was concluded that the use of hyaluronidase did not effect the oocytes adversely. Fig.2.1 shows the results of hyaluronidase experiments.

In another series of experiments, the effect of using extracted oil to cover the culture media were compared to using no oil, and to using non-extracted oil. Oil was extracted as described in the previous section. The results are summarized in Fig.2.2. There was a significant effect noted when culture was carried out in medium overlayed with mineral oil to reduce ambient effects on the medium. Without mineral oil fertilization and blastocyst formation rates were 85% and 82%, respectively; the rates dropped to 74% and 51% when mineral oil was used. Extraction of the oil with EBSS to remove impurities restored the fertilization and blastocyst formation rates to 94% and 78%, respectively. Since, there was a significant difference between extracted oil and non-extracted oil on the fertilization rate ($P < 0.005$) and on the blastocyst formation rate ($P < 0.01$), it was decided to use extracted oil for the rest of this study.

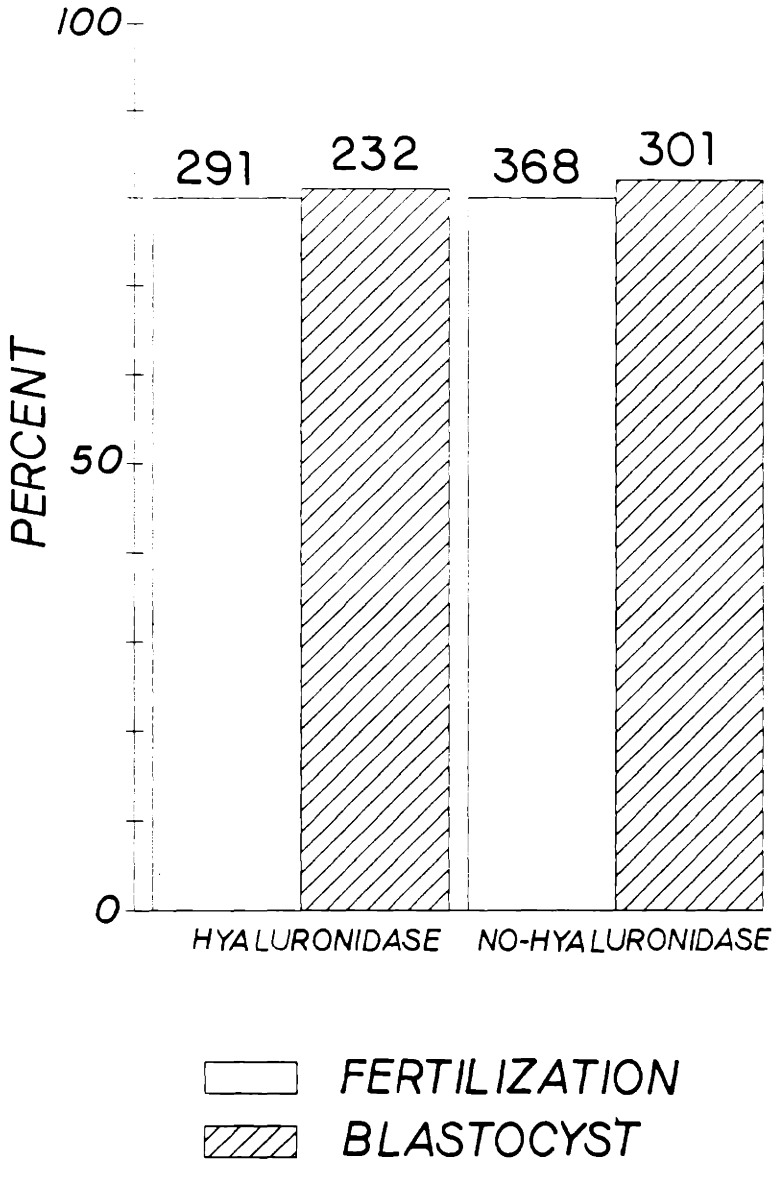

FIGURE.2.1. Effect of hyaluronidase on fertilization and subsequent blastocyst formation rate. No. ova used for each condition is shown on the figure.

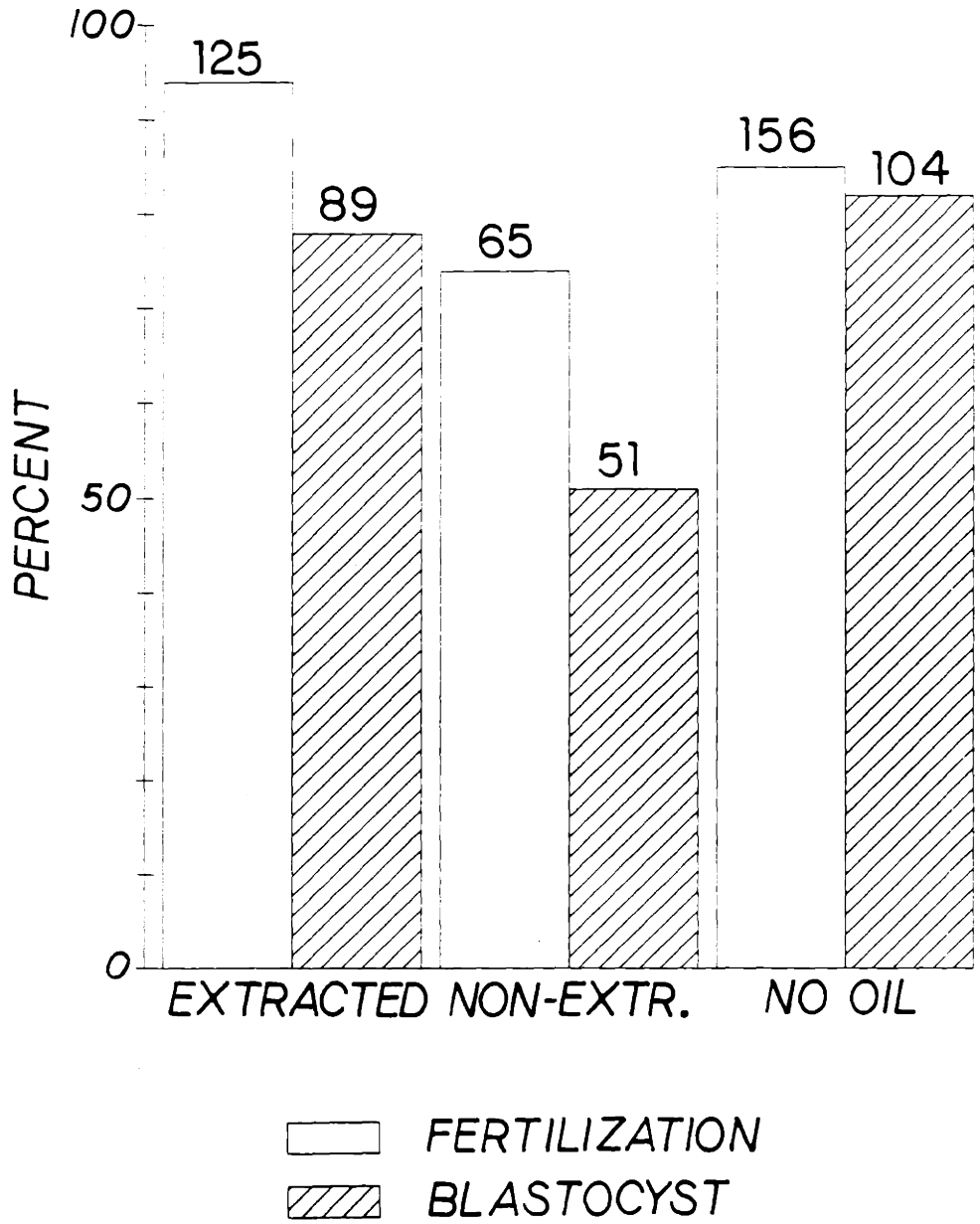

FIGURE.2.2. Effect of extracted oil, non-extracted oil, and no oil on fertilization and subsequent blastocyst formation rates. No. ova used for each condition is shown on the figure.

There was no significant difference between extracted oil and non-extracted oil.

The effect of the numbers of eggs per insemination dish on fertilization rate and subsequent blastocyst formation rate was also tested. In this series of experiments, a different number of oocytes were introduced in each insemination dish and subsequently transferred to each incubation dish. The number of oocytes per dish was varied between 1 to 90. Results are summarized in Fig.2.3. There was no significant difference in the fertilization and blastocyst formation rates between plates containing different number of oocytes. It was decided to keep the number of oocytes in the range of 10 to 30 eggs per dish to minimize the variation among experiments. Results agree with Niwa et al. (1980).

In order to test the possible positive effect of changing the culture solution every day with fresh media, EBSS media with BSA was stored in the CO_2 incubator for 4 days prior to experiments. Four day stored EBSS with BSA was then used for insemination and subsequent culture of oocytes. Fig.2.4 displays the effect of EBSS storage on the fertilization rate and the blastocyst formation rate. As can be seen from this figure, using 4-day old medium did not have any adverse effect on oocytes and it was decided to culture the embryos in the same media for 4 days.

Miralles et al. (1987) reported that the mouse oocytes obtained from white Swiss FO-1 female mice are susceptible to thermal shock. They reported that the fertilization rate dropped from approximately 30% for

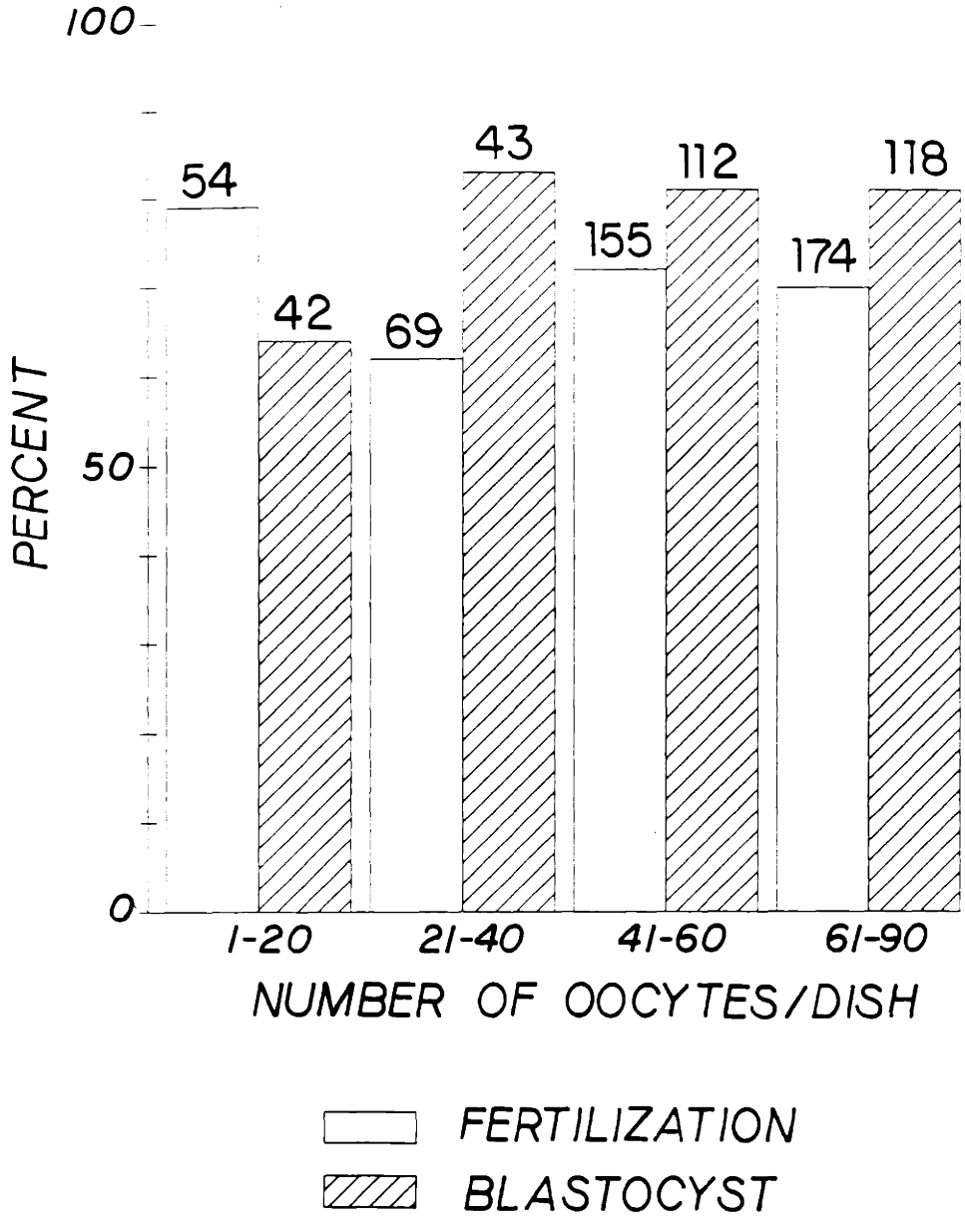

FIGURE.2.3. Effect of the number of oocytes per insemination dish on fertilization rate and the number of embryos per growth dish on blastocyst formation rate. No. ova used for each condition is shown on the figure.

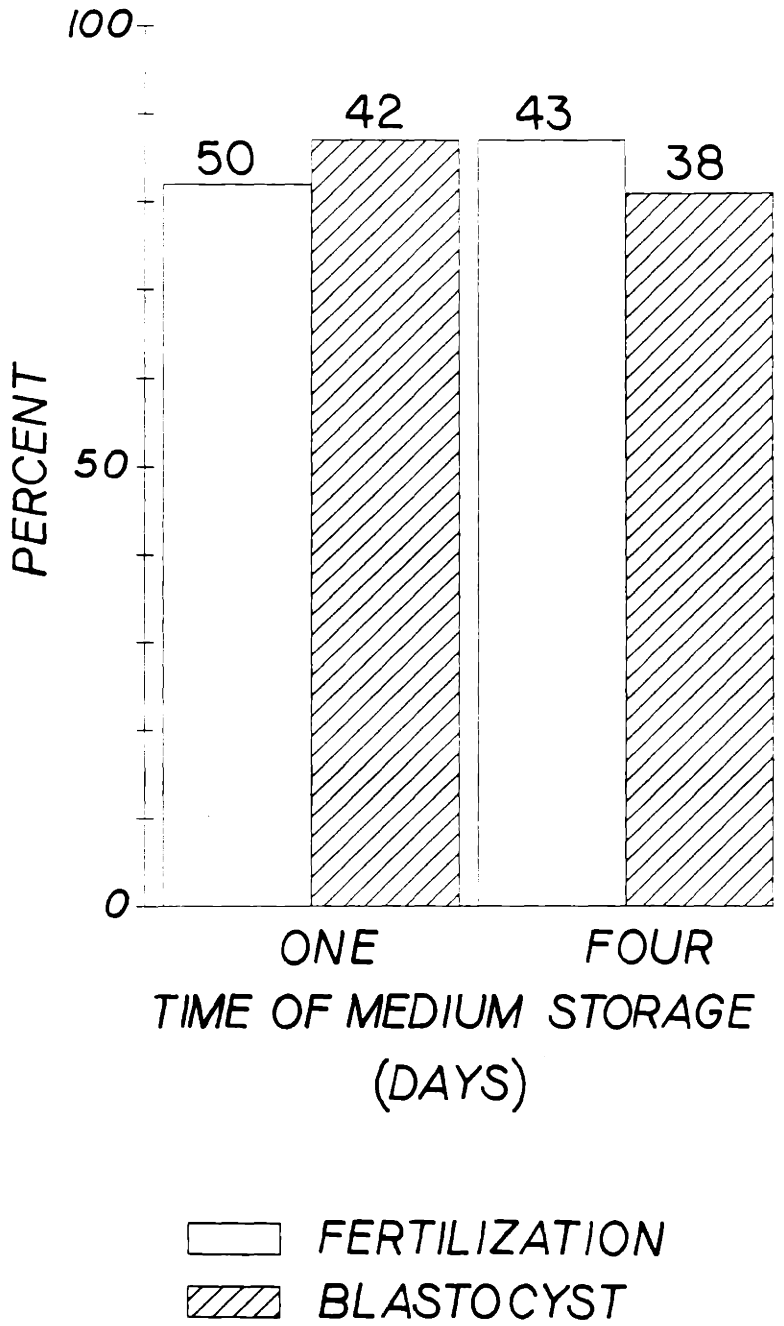

FIGURE.2.4. Effect of EBSS media storage in the 5% CO_2 incubator on fertilization rate and subsequent blastocyst formation rate. No. ova used for each condition is shown on the figure.

control oocytes without cold treatment to approximately 15% for cold treated (-1°C) oocytes. Recently, Jackson & Kiessling (1988) reported that cold treatment at 15°C does not have an effect on oocytes recovered from $B_6D_2F_1$ female mice. Since the oocytes were kept between 0 to -5°C for several minutes prior to freezing experiments, it was necessary to investigate the cold sensitivity of oocytes used in this study. Cooling oocytes to 0°C for 0, 15, 30, 60, and 150 minutes before insemination resulted in fertilization rates of 75%, 94%, 86%, 81%, and 87%, respectively; and blastocyst formation rates of 92%, 90%, 92%, 86%, and 85%, respectively. Results of culture results are depicted in Fig.2.5. When the blastocyst formed were further cultured in a complex medium (Armant et al. 1986), trophoblast differentiation and outgrowth was observed at a frequency of 77%, 63%, 74%, and 71% for the 0, 15, 30, and 60 minutes exposed groups, respectively. Fig.2.6 shows the results of outgrowth experiments. There was also no indication of parthenogenic activation due to cold shock since oocytes cooled to 0°C for 0, 60, or 150 minutes and subsequently cultured without insemination cleaved to the 2-cell stage at rates of 4%, 3% or 0%, respectively. These results indicate that oocytes are not neither damaged or parthenogenetically activated prior to freezing experiments.

Some of the freezing experiments were run in hypertonic solutions, therefore it was necessary to investigate the effect of hypertonic solutions on the viability of oocytes. Oocytes were placed in PBS+NaCl+BSA solutions of 780 and 1,265 mosm for 20 minutes at ambient temperature prior to insemination. Results shown in Fig.2.7 suggest that the hypertonic

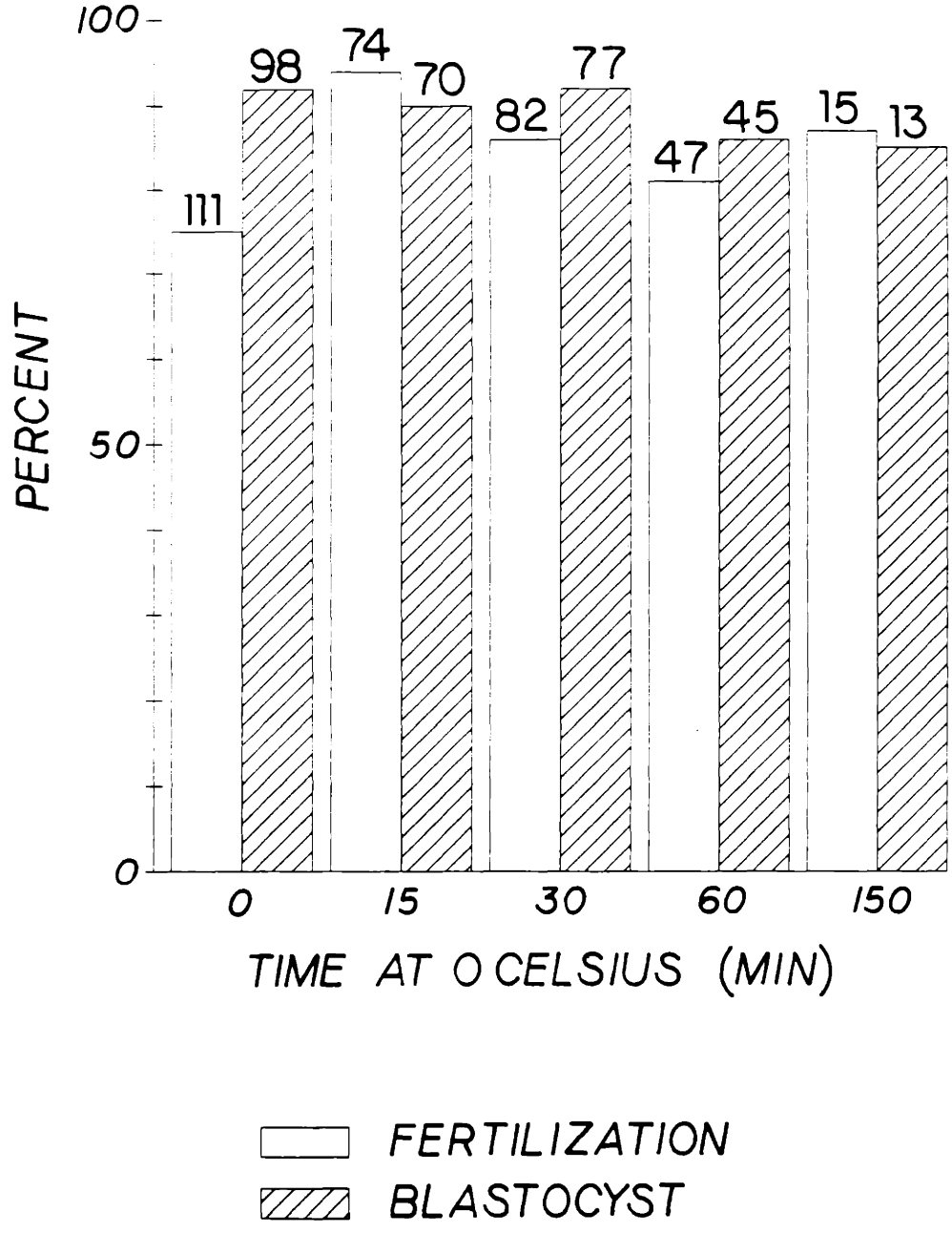

FIGURE.2.5. Effect of cooling to 0°C as a function of time at 0°C on fertilization and blastocyst formation rates. Oocytes were cooled to 0°C in 1/4 inch plastic straws in an ice bath and kept at 0°C for various amount of times. No. ova used for each condition is shown on the figure.

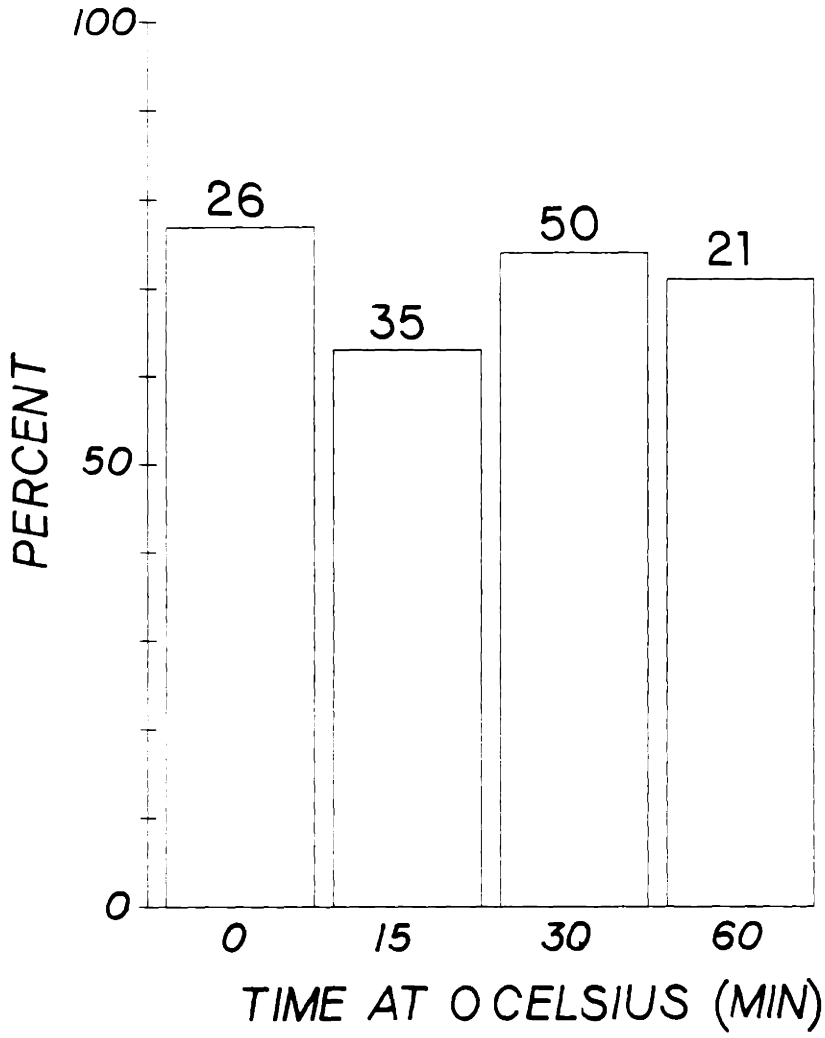

FIGURE.2.6. Effect of cooling to 0°C on outgrowth of trophoblast. Expanded oocytes from Fig.2.5 were cultured in a complex medium promoting the outgrowth of trophoblast cells. No. ova used for each condition is shown on the figure.

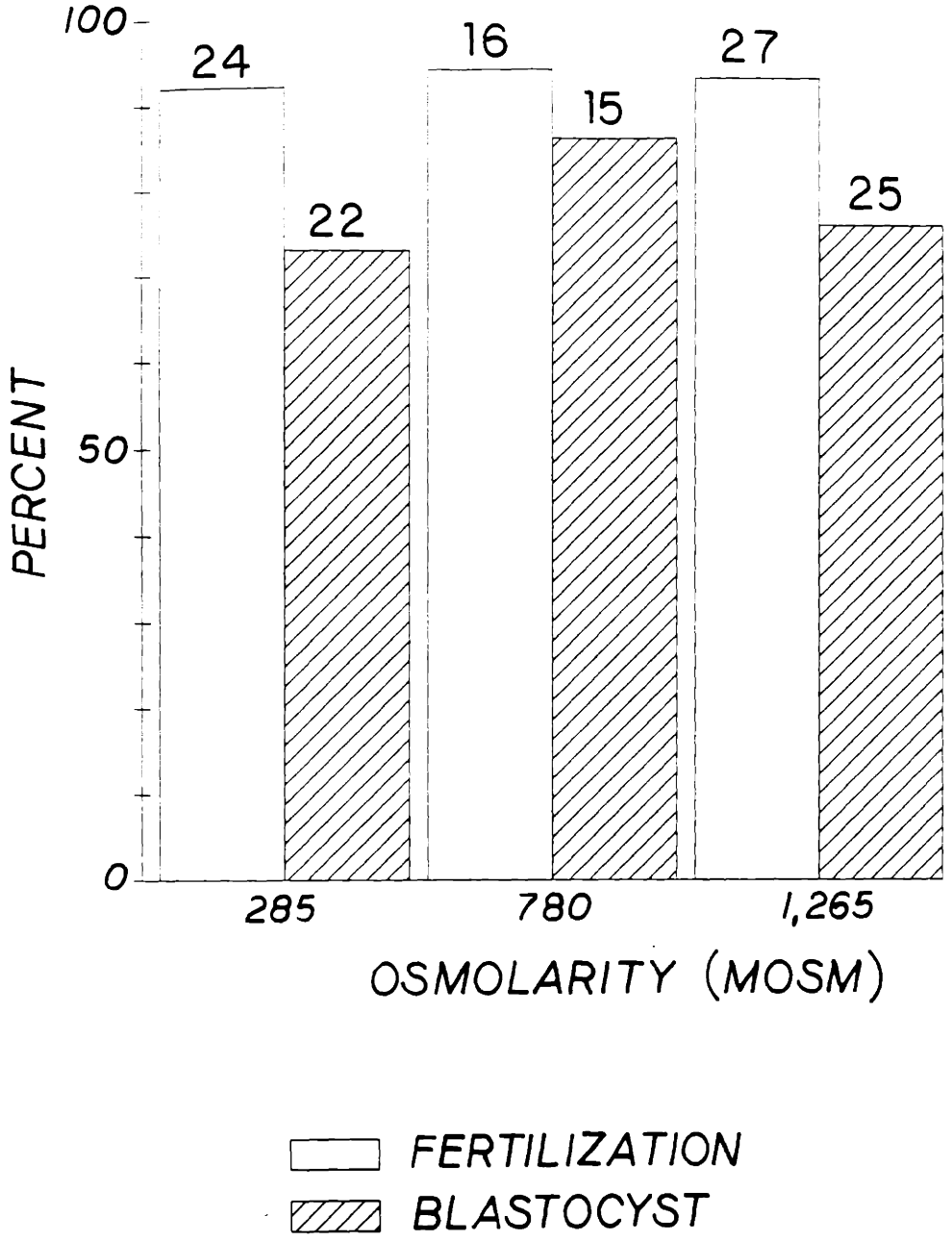

FIGURE.2.7. Effect of hypertonic PBS+BSA treatment on the fertilization and subsequent growth of mouse oocytes. No. ova used for each condition is shown on the figure.

treatment did not have any adverse effect on oocytes.

The overall results indicate that mouse oocytes at metaphase II can be readily and reliably recovered from hybrid $B_6D_2F_1$ female mice with an overall fertlization rate of 90% and subsequent blastocyst formation rate of 82%.

CHAPTER III

CRYOMICROSCOPY SYSTEM
&
ISOTHERMAL FREEZING STAGE

3.1. Introduction

The utility of cryomicroscopy in the study of cells exposed to low temperatures is well established (Diller & Cravalho 1970). As the scientific objectives in cryobiology evolve, so do the requirements placed on instrumentation systems, leading to a steady process of development and refinement. In this process, recent emphasis has been placed on the use of computers for software control of the temperature protocol (McGann, 1979) as well as for image analysis (Dietz et al., 1984; Steponkus et al., 1984a; Korber et al., 1986). Another area of interest has been the design of microscope stages which support unique thermal control requirements (Scheiwe & Korber, 1982c; Scheiwe & Korber, 1984) and offer improved manufacturability and reliability (Schwartz & Diller, 1982).

In our view, a cryomicroscopy system should perform the following functions:

Temperature Control: The thermal history of a microscope sample must be programmed, accurately executed, and recorded during an experiment. Initiation of sample freezing is considered part of the temperature control function.

Image Storage and Event Correlation: The microscope images must be recorded so that subsequent detailed observation and analysis can be performed. Events occurring during a temperature excursion must be annotated with the corresponding temperature and time from the beginning of the excursion.

Image Analysis: Features in the recorded images such as cell areas or ice-interface positions must be measured.

Data Reduction: Theoretical biophysical models are used to interpret the observed events and data, gathered from the image analysis. The end results of data reduction are parameters that can be used to assess freezing theories, ultimately allowing prediction of future cell behavior.

A system of hardware and software implementing the above functions is shown in the overview of Fig.3.1. Images are formed by either an upright Zeiss Universal Research Microscope or a Zeiss model ICM-405 inverted microscope. Phase contrast and bright field illuminations are used for permeability and nucleation experiments, respectively. The present system is used with Ikegami model ITC-62 and Panasonic WV-3890 B video cameras displayed in black and white, and color, respectively, on a Panasonic BT-S 1300 N monitor. Video recordings are made on a Panasonic AG-6300 VHS tape machine. Overall integration of temperature

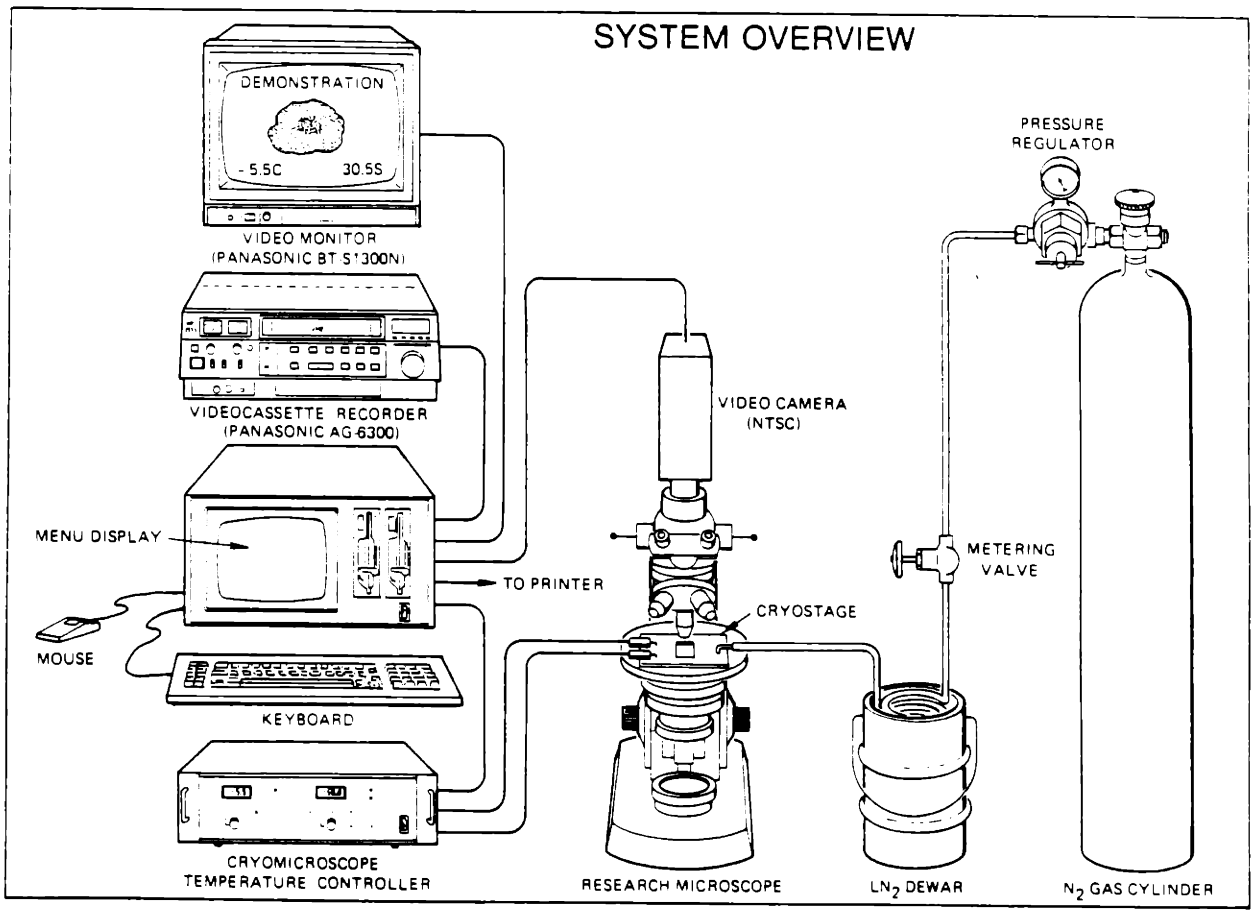

FIGURE.3.1. Pictorial overview of cryomicroscope research system (from Cosman et al. 1988).

control, image processing and data reduction functions is achieved by a microcomputer equipped with analog, digital, and video interfaces. Special software was developed to provide flexibility and ease of operation.

3.2. Cryomicroscopy System

Temperature Control

The system elements responsible for the temperature control function include the cryostage, freezing initiator, nitrogen gas supply, temperature controller, microcomputer and software control program. The basic arrangement of these elements follows reported practice (Diller & Cravalho, 1970; Cosman et al., 1982; Korber et al., 1986). Gaseous nitrogen, cooled by passage through a coil immersed in LN_2, is the refrigerant for the cryostage. Sample temperature is measured by a thermocouple at a point on the heated cryostage window. The temperature controller provides the window heater with the power needed to counterbalance the refrigerant and thus maintain the sample at the desired temperature or setpoint. A time-varying setpoint is created by the microcomputer when running the temperature control software.

The ultimate performance of a cryomicroscope system is bounded by the thermal and optical properties of the cryostage itself. These properties depend, in large part, upon the method of cooling the sample

window. Two basic cooling methods have been used to date; convective and conductive. In convective stages, a gas coolant stream, which is maintained below the coldest required temperature, flows past or impinges on the back surface of the sample window. By contrast, the sample window of a conduction stage is cooled at its edges by direct contact with the metal body of the stage. The stage body is in turn cooled by the gas stream. The primary advantage of the conduction approach is its small optical thickness since it lacks a coolant flow channel below the sample window. This feature is important since shorter optical distances usually result in higher quality microscope images. Conduction stages are characterized by high thermal gradients which extend radially from the center of the field of view (McGrath 1974). These gradients are equal to the difference in temperature between the control point (at the window's center) and the coolant stream. This difference is at least as large as the maximum temperature excursion required for the experiment, often exceeding 100°C. The automatic initiation of sample freezing, which frequently results from this large thermal gradient can be an advantage or disadvantage depending upon the experiment. Automatic freezing can, for instance, be a drawback for experiments requiring control of the degree of sample undercooling.

Convective stages, on the other hand, operate with significantly lower thermal gradients across the surface of the window. This property is especially beneficial in volumetric response experiments for two reasons: First, since a wider region of the field of view will

accurately track the desired thermal protocol, data from a greater number of cells may be obtained.Second, the osmotic concentration profile arising from the temperature gradient, and resultant non-equilibrium condition in the extracellular medium is reduced. The maintenance of this extracellular equilibrium is important for slowly-cooled cells in water permeability investigations. The penalties usually associated with low thermal gradients are greater optical thickness and the need for manual or mechanical initiation of sample freezing.

A new convective stage shown in the cross-section of Fig.3.2 has been constructed for use with our cryomicroscope research system. The design of the heating window follows reported practice (Diller & Cravalho, 1970). Briefly, the heating window contains the thermocouple (5 μm foil copper-constantan) installation as well as a tin oxide electrically conductive coating. This layer is epoxied onto another cover glass sheet to assure the insulation of the conductive layer. An enlarged cross section of the heater is shown in Fig.3.2. Cold gaseous nitrogen stream flows underneath the heating window. Compensatory heating is performed by dissipation of electrical energy in the transparent electricelly conductive coating. Our new freezing stage has improved optical performance and further reduces temperature gradients when compared to current convective designs. These advantages are conferred by two new design features. Optical performance is improved by reducing the thickness of the stage in the window area to approximately 0.1 inch (2.54 mm). The second design improvement in the

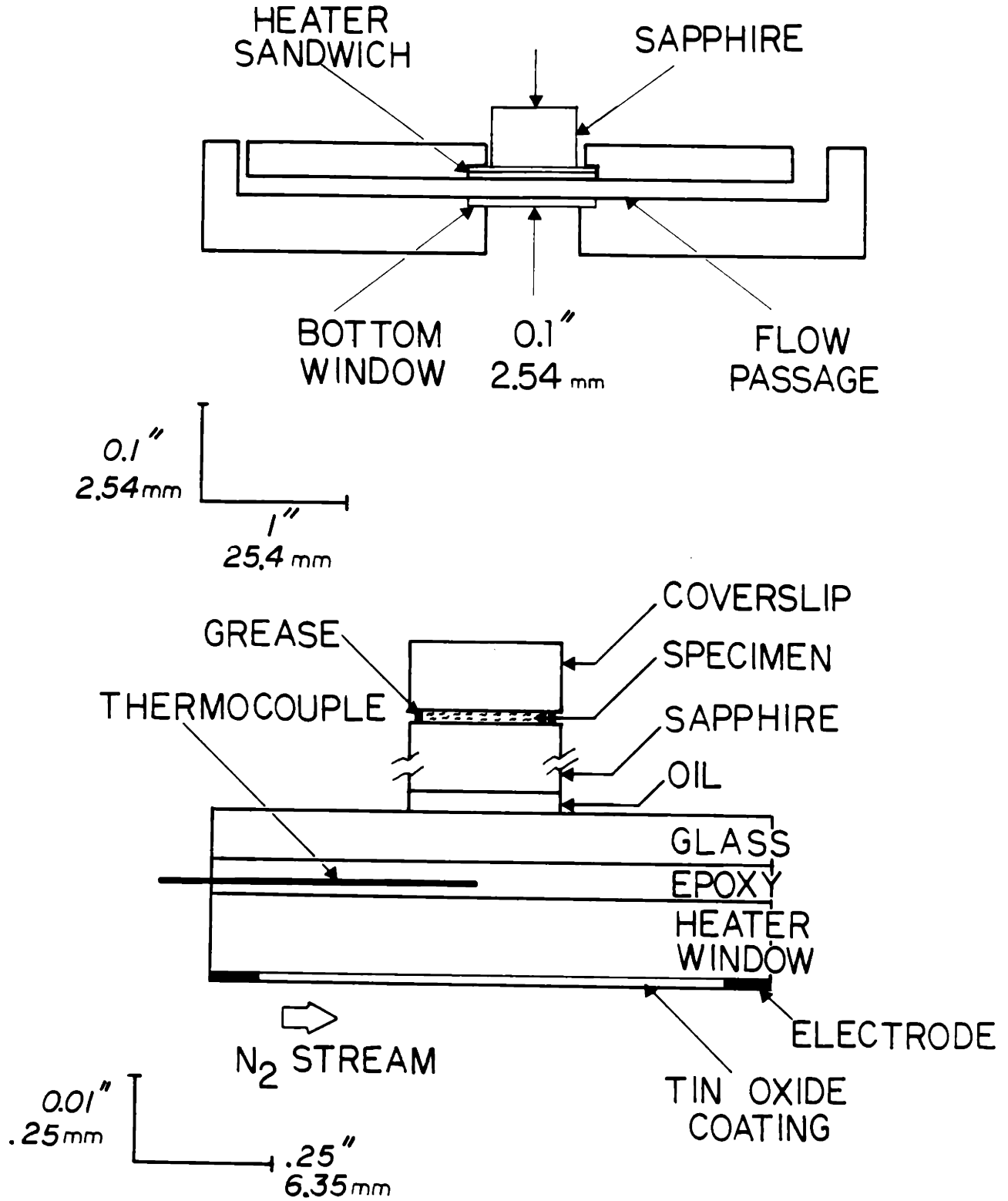

FIGURE.3.2. Expanded cross-section of the cryostage.

new cryostage is the use of an optically flat sapphire layer in the sample window assembly. Sapphire is employed here because of its high thermal conductivity when compared with other transparent materials. We have investigated the effect of sapphire thickness on the maximum thermal gradients across the window and have found 0.063 inch (1.6 mm) to be a good compromise between the competing requirements of reduced gradients and rapid thermal response. With the coolant stream temperature and flow rate adequately set, sample cooling rates of several hundred ^{o}C per minute have been achieved for temperatures as low as -60^{o}C. Measured gradients for these flow conditions were in the range of 0.1^{o}C per 20 millimeter at sample temperatures near 0^{o}C. The initiation of the sample freezing was achieved by manual triggering of ice growth by contacting the edge of the sample with a cold needle.

Cryomicroscope temperature controllers have undergone an evolution paralleling advances in electronics. The function of the controller is to compare continuously the actual sample temperature with the desired sample temperature throughout an experiment and to effect required changes in heater power necessary to reduce this difference or error. The algorithm used to calculate the amount of power needed for the heater, based on this error, is referred to as the feedback control algorithm. The modern era in cryomicroscope temperature controllers began with the Diller-Cravalho system which incorporated analog proportional feedback. Different control system algorithms have been implemented including proportional (Diller, 1981), pseudo derivative feedback (Steponkus et al., 1984a), and proportional plus

integral(Scheiwe & Korber, 1982c). In most cases these techniques have been realized using analog components, although the computer-in-the-loop approach, enabling software control of the feedback algorithm, has also been implemented (Shah et al., 1987). In that the primary limitations of temperature controller performance are the dynamics of the cryostage itself, we have employed a simple analog, proportional architecture in our current system.

Technology changes have had an even greater impact on the methods of programming and storing desired temperature protocols and of providing the corresponding time-varying reference signal to the control loop. Early digital techniques offered an improvement in protocol flexibility when compared to analog ramp generators (Cosman et al., 1979) but remained difficult to use. The advent of inexpensive microcomputers and digital-to-analog converters has enabled greater flexibility in the execution of temperature protocols as well as greater ease of use. Most modern temperature control systems make use of microcomputer technology. Microcomputers offer the additional advantages of the ability to linearize the thermocouple signal from the cryostage and to control the timing of events such as ice initiation. An IBM™ compatible computer is the platform used in this cryomicroscope system.

The software is menu driven and allows the desired temperature protocol to be specified in either of two ways: by entering a series of linear segments that are each defined by their cooling rates and durations, or by defining the segments in terms of their final

temperatures and durations. From this definition, the program executes the protocol by mathematically generating the appropriate time-varying setpoint. The setpoint is converted to an analog voltage and sent to the temperature controller. Systems have been reported (Shah et al., 1987) which store the entire temperature history in the computer's memory prior to execution. This scheme provides the faster execution time needed if the computer is incorporated into the control feedback loop. Protocol duration, however, is limited by available memory. Since our computer is not part of the feedback loop, high speed is not required and the setpoint is generated in real time. Thus, the protocol may be of arbitrary length.

Image Storage and Event Correlation

Cryomicroscopy involves the observation and analysis of the reactions of cells to thermal change. In order to accomplish this, microscope images must be recorded and correlated with temperature and time during an experiment. Several methods of recording images and correlating them with experimental conditions have been devised. Still or motion picture photography has been used to capture microscope images while temperature is noted using a constant speed chart recorder. Significant events were annotated as they occurred by written notations on the chart paper or by a footswitch-operated event-marking pen. Video cameras and recorders are the preferred method of storing images, possessing several advantages:

-Dynamic processes are captured by virtue of rapid image update (25-30 pictures/sec)

-The recording medium is inexpensive and reusable.

-No processing is required, allowing inspection of images as soon as they are captured.

-Computer control and analysis are facilitated by the electronic nature of the storage system.

Direct correlation with time and temperature have been accomplished by recording these data directly on the video image. Two methods in use are optical combination of numeric displays with the microscope image (Scheiwe & Korber, 1983), and electronic combination of the numeric and video information. Electronic combination of images has been performed by modified commercial video equipment (Steponkus et al., 1984a) and by custom electronic hardware (Cosman, 1983).

Image storage system employs electronic superposition since it provides greatest flexibility. This function is implemented by a special video interface which allows the computer, by software control, to superimpose text and graphics onto the microscope image. During the execution of the temperature control protocol, elapsed time, temperature, experiment title and event markers are displayed and recorded with the video image. Here, timing signals are derived from

the video chain (1/6 field rate or 0.1 sec intervals) which provides the software with an accurate clock for generating the temperature protocol, and avoids visual flicker by updating the display synchronously with the camera. Written notes can also be saved on the video recording by entering them through the keyboard before and after an experiment is run. Thus, images stored with this system are fully annotated, facilitating subsequent analysis and data reduction.

Image Analysis

Quantitative data must be extracted from the recorded images of a cryomicroscope experiment in a form utilizable by data reduction algorithms. Particularly important to the Cryobiologist are measurements of cell volume changes for determining permeabilities. A variety of methods have been used to extract these data. Mechanical planimetry of still photos, yielding cross sectional area from which cell volume can be approximated, is one technique. The drawbacks of this method are that it is tedious and requires difficult, rapid photography to capture dynamic events. Paper tracings of video images have also been analyzed by mechanical planimetry (Scheiwe & Korber, 1982c).

Recent developments in the field of video imaging have brought electronic methods of area analysis. One of these techniques is the computation of cell area enclosed by a computer-generated circle. The operator adjusts the position and diameter of the circle, using a joystick, to match that of the cell under study. The computer keeps track of circle diameters entered as a function of time (Steponkus et al., 1984a).

Fully automatic, computerized image analysis has also been reported. In this case an image is converted to digital form and then analysed by a computer which is programmed to recognize cell boundaries and calculate the enclosed areas. While demonstrating progress toward high speed data analysis, current automatic systems are subject to problems such as the confusion of ice boundaries with cells (Schwartz & Diller, 1983a-b).

The method used in our system can best be described as computer-aided or semi-automatic. It gives the investigator flexibility in performing image analysis due to a high level of integration between the computer and the video system. To perform analysis, the computer places the video recorder in the playback freeze-frame mode and superimposes a cursor on the image. Using a mouse or tracing pad, the cursor can be moved, by the investigator, to any location on the image while the

computer automatically reads and stores its coordinates. This capability gives the system the means of making virtually any planar measurement. For example, by plotting points around the periphery of an object such as a cell, bubble or other particle, the software can compute the enclosed area using a polygonal approximation. Moving the cursor to the edge of an ice dendrite and then to an adjacent dendrite allows the computer to calculate the distance between them. Putting the cursor at the edge of the ice front on a given video frame and then replotting this point as the computer steps the playback recorder through successive frames yields a list of position vs. time, allowing the velocity of an ice interface or other object to be calculated.

In addition to geometric analysis, the timing of observed events is important to cryobiological investigation. The elapsed time at which extracellular and intracellular nucleation occur can be measured accurately with this system. The software which performs this task steps through the playback of the videotape frame by frame. A button is pressed each time an event is observed. The computer then generates a list of events matched to the time at which they occurred.

We expect this degree of system integration to increase research productivity in performing current types of experiments and data analysis procedures. We also anticipate that the system's capabilities

will support future research needs.

3.3. Thermal Performance of the Isothermal Freezing Stage

In any study of cell freezing, precise temperature measurement and control are fundamentally important. The importance of accurate temperature measurement is amplified further when the ice nucleation inside the cells is analyzed. It is well documented that the kinetics of ice nucleation in non-biological systems is a complex exponential function of the temperature and undercooling. However, this has not been emphasized enough in cryobiology literature. Even state-of-the art freezing stage designs have large thermal gradients and in most of the cases, thermal gradients in the field of view of the cryomicroscope are not reported. Steponkus et al. (1983) reported a gradient of $0.25^{o}C/40\mu m$ near the thermocouple for a conductive stage. For mouse oocytes with a diameter of 79 μm this would imply a temperature gradient of $0.5^{o}C$ across the cell volume. It will be shown in Chapter VIII that this much of a temperature gradient may effect the results dramatically. It is the purpose of this section to experimentally investigate the effects of incorporating a sapphire window onto the heating window.

Square sapphire plates 12.7x12.7 mm square of various thicknesses were applied onto the heating window (22x22 mm sq.) with the aid of a Zeiss immersion oil. A 2 μl sample of distilled water was placed at the

center of the sapphire window of the stage and covered with a glass slip (12x12 mm sq.) forming a thin, liquid film. A method similar to Steponkus et al. (1983) was employed to measure the temperature gradients in the viewing area without perturbation of the temperature profile by the presence of a probe. The distilled water is first frozen by rapid cooling to -25°C. The temperature was raised rapidly (≃100°C/min) to -5°C and then was increased in 0.1 to 0.2°C increments from -5°C until all the ice melts. An estimate of the 0°C isotherm was made by the location of the ice-water interface.

Fig.3.3 shows the effect of the sapphire thickness on the temperature gradient. The thermal gradient on the viewing stage was two dimensional as observed from the shape of the ice-water interface. Fig.3.3 reports the gradient at the symmetry axis of the window along the thermocouple. As can be seen from this figure temperature gradients of approximately 8, 3, 1, 0.5, and 0.1 were observed over an area of 10x10 mm sq. for sapphire thicknesses of 0, 5, 13, 25 and 63 mls, respectively. The temperature gradient at the down stream side of our cryostage was much less than the up stream side. This is due to the construction of flow channels and was not further investigated. When a 0.063 inch (1.6 mm) thick sapphire glass was employed, there were no temperature gradients for all practical purposes over the 10x10 mm

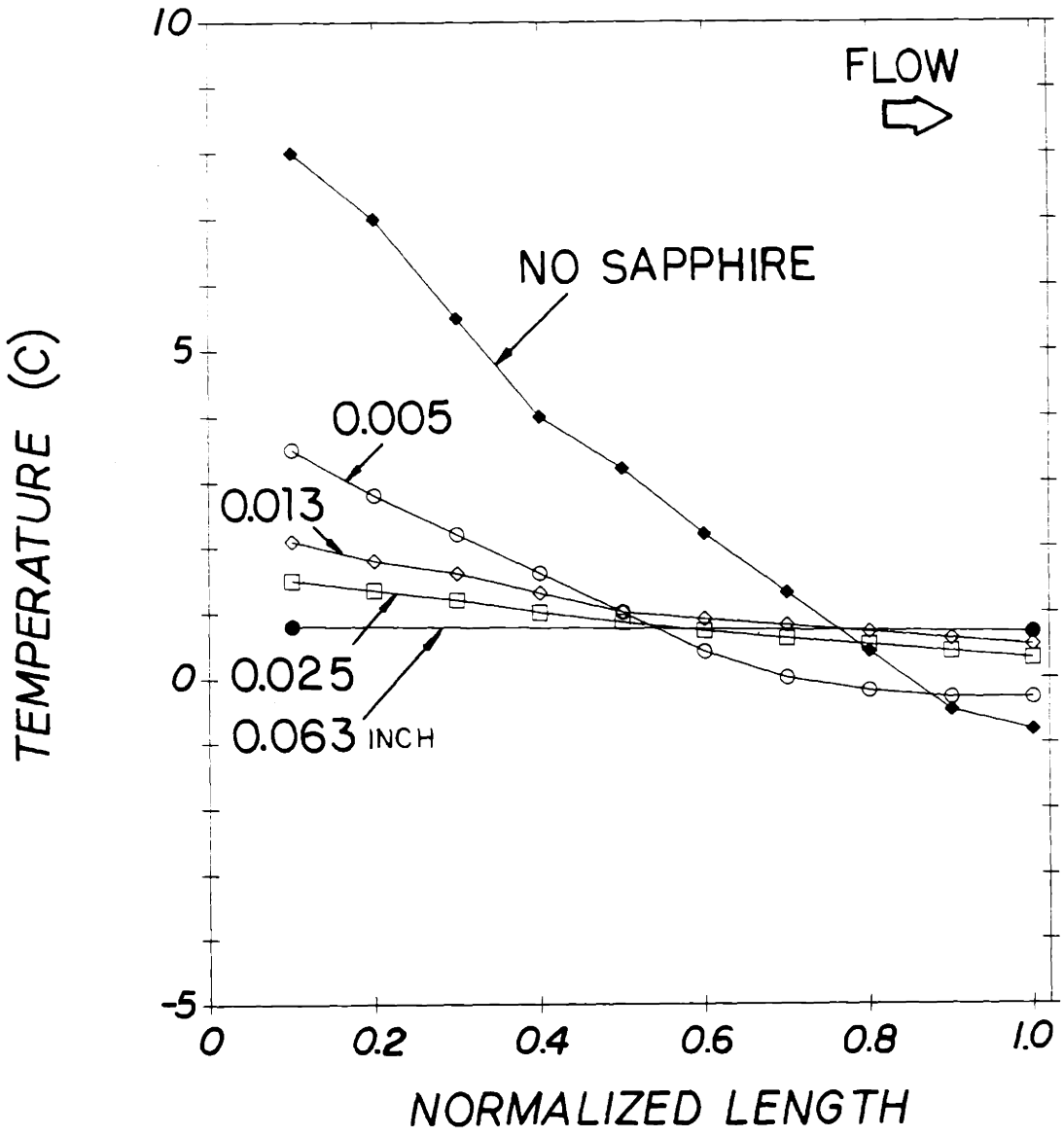

FIGURE.3.3. Temperature at the thermocouple as a function of the location of the ice-solution interface across the window (10 mm) for different thicknesses of sapphire plates incorporated onto the cryostage. Cold gas inlet is from the right and the outlet is from the left side of the figure. The temperature was estimated from the location of the ice-water interface.

square of the window. The melting of ice was spontaneous with an increment of 0.1°C in temperature as would be expected for isothermal melting. These results are summarized in Fig.3.4.

In addition to temperature gradients it is important to investigate the dynamic characteristics of the cryostage. The cooling rate performance of the freezing stage is extremely important for our purposes. The sapphire added to the window will increase the thermal mass of the window. Consequently, the dynamic response of the stage will be influenced. Measurements of the cooling rate were performed with sapphire glasses of different thicknesses. The microcomputer was programmed to follow a given cooling rate between 0 to -40°C and the actual temperature/time reading was obtained from the video monitor. Higher cooling rates were achieved with colder stream temperatures.

Fig.3.5 shows the maximum cooling rate obtained for a given thickness of the sapphire window as a function of stream temperature. As can be seen from this figure, the dynamics of the stage is slowed by adding the sapphire window onto the heating window. Cooling rates higher than 1,200°C/min were obtained without the sapphire for a stream temperature of -100°C. However, cooling rates of approximately 400 and 200°C/min was achieved when sapphire glasses of 0.013 inch (0.33 mm) and 0.063 inch (1.6 mm) were employed. This is a limitation for cells which

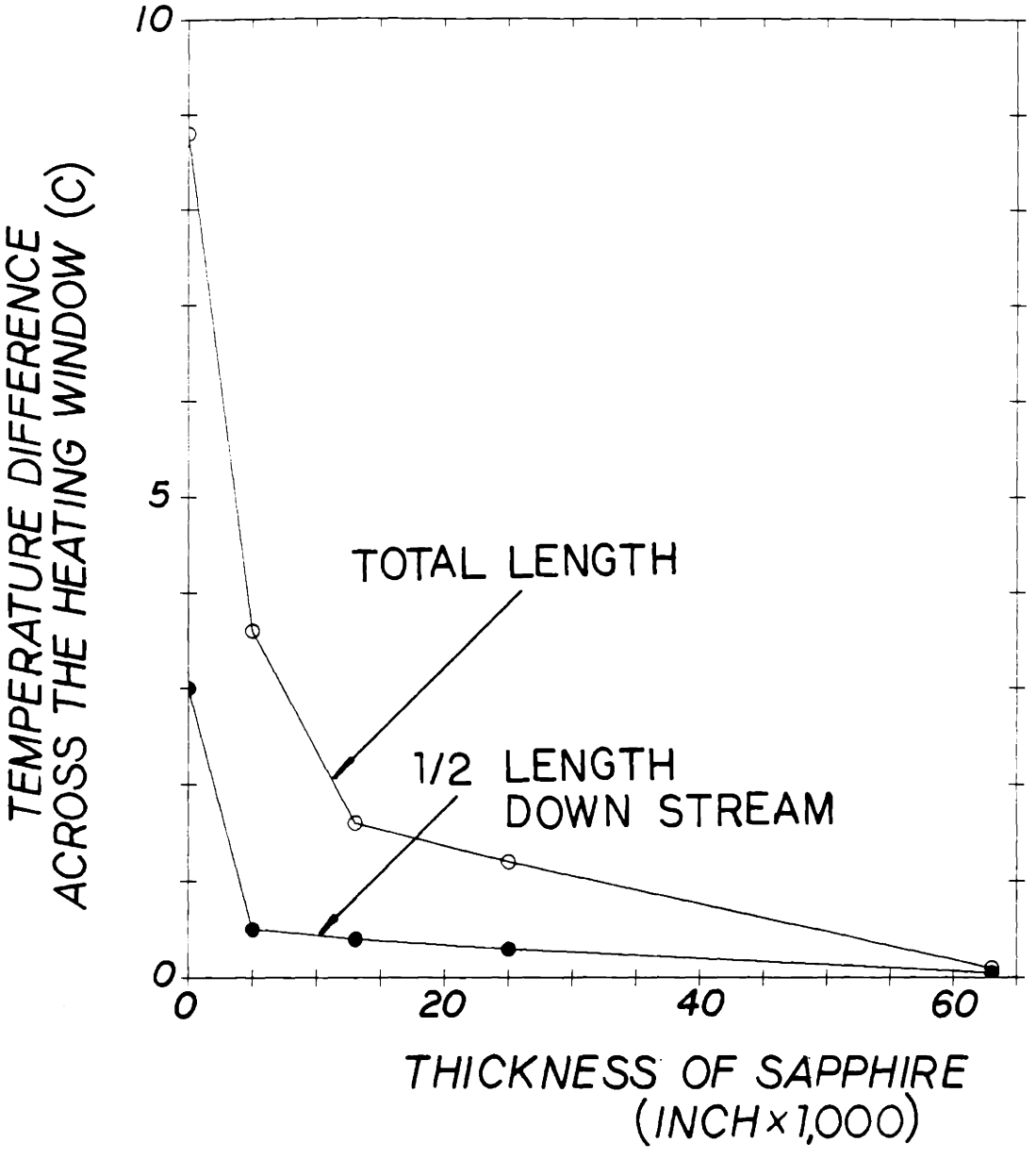

FIGURE.3.4. Temperature gradient across the cryostage window as a function of the thickness of the sapphire plate.

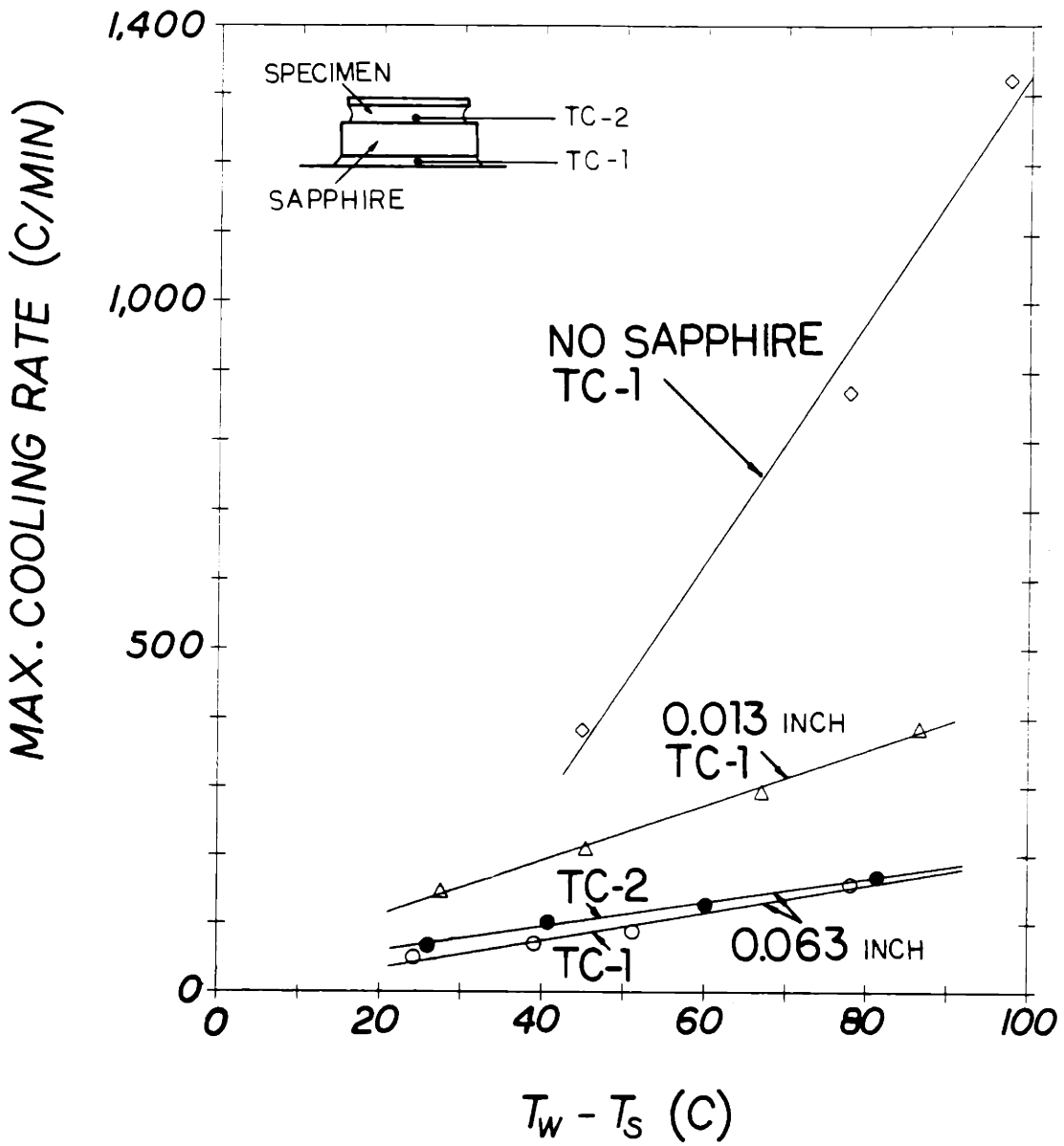

FIGURE.3.5. Maximum cooling capacity of the cryostage vs. the difference in window and stream temperatures as a function of the thickness of the sapphire plate placed onto the heating window. A second thermocouple (TC-2) was used to measure the maximum cooling rate at the top of the sapphire plate.

require fast cooling rates. In our studies with mouse oocytes there was no need to use cooling rates higher than 120°C/min, therefore, the sapphire glass with 0.063 inch (1.6 mm) was used for all subsequent freezing experiments in this study.

It is important to mention that all of the above measurements were done with a control thermocouple imbedded into the heating window as shown in Fig.3.2. This may lead to an error between the actual specimen temperature on the top of the sapphire window and the control thermocouple under the heating window. This is because there will be a time lag before the steady-state temperature can be established at the top of the sapphire window. To test this possibility, we incorporated another 5 μm copper-constantan foil thermocouple onto the sapphire window where the specimen was located. Dual measurements of temperature from both control and specimen thermocouples are shown in Fig.3.5 for a sapphire of 0.063 inch (1.6 mm) thick. As can be seen from this figure there is no appreciable error in the cooling rate measured with the control thermocouple compared to the actual specimen cooling rate.

In addition to the cooling rate we measured the vertical gradients with this dual thermocouple arrangement at steady-state situations. A temperature between 0 to -30°C was imposed on the control thermocouple with the aid of the microcomputer and the temperature measurements from

control and specimen thermocouples were compared at steady state conditions. There was no vertical temperature gradient that we could detect with our measurement technique. We assumed that the vertical gradient was always less than 0.1°C and had no effect in our measurements.

With the experimental analysis given above, it can be concluded that the temperature gradients for all the measurements performed in this study were less than 0.1°C over a field of 10x10 mm. In actual freezing experiments only a very small portion of the entire field is observed depending on the experiment therefore the actual temperature gradients are much less than 0.1°C.

CHAPTER IV

EXPERIMENTAL PROCEDURES AND OBSERVATIONS

4.1. Experimental Procedures

Permeability Experiments at Subzero Temperatures

Mouse oocytes at metaphase II were used for permeability experiments. Oocytes from 6 mice were collected (12 to 13 hours after HCG injection) and stored in a culture dish containing modified Earle's medium (EBSS) in a 5% CO_2 incubator as described in Chapter II. The oocytes were used within 3 hours following the collection. Direct observation of the oocytes during freezing was accomplished using the cryomicroscopy system described in Chapter III. Typically, 3 to 10 oocytes were placed onto the cryostage under a cover slip and sealed with silicone grease for each of the permeability experiment in isotonic Dulbecco's Phosphate Buffered Saline (PBS) solution with 4 mg/ml Bovine Serum Albumin (BSA). Each sample was supercooled to the extracellular ice seeding temperature (-2 to -3^{o}C) and the external medium was nucleated by touching the cryostage window with a spatula cooled in

liquid nitrogen. As soon as the ice front surrounded the oocyte(s), the cryomicroscope system was commanded to cool the specimen at 2°C/min (Orrico, 1988). These experiments were recorded on a video tape as described in Chapter III. One to 3 of these oocytes were visible at any given time in the view field of the cryomicroscope. A 16x objective and 2x photo-ocular were used. Phase contrast illumination was used for the permeability experiments. This allowed for an easier visual determination of the cell boundaries during freezing.

In order to obtain the permeability parameters from these experiments it was necessary to determine the inactive cell volume and the diameter distribution of oocytes. Static experiments were conducted to determine the osmotically inactive cell volume using five unfertilized mouse ova. This was accomplished by equilibrating oocytes for approximately 10 minutes in solutions of increasing osmolalities ranging from 285 to 2,215 mosm at ambient temperature. The hypertonic solutions were made by adding small amounts of NaCl to PBS and the osmolality of each solution was checked by an osmometer (Adv.Ins.Inc. Model 3L). Observations of the osmometric behavior of oocytes were made in 100 μl PBS+NaCl solutions covered with extracted silicone oil (Aldrich Chem.) to prevent evaporation. A Zeiss 405ICM inverted microscope was used for observations during the static experiments.

In addition to the osmometric behavior, the diameter distribution of oocytes was also determined using the same experimental procedure. The

diameter measurements were made by measuring their projected areas and converting them to diameter by assuming spherical shape. Eighty unfertilized ova were used for this purpose.

Intracellular Ice Nucleation Experiments

For nucleation experiments, oocytes from 9 mice were collected in a sequential manner. Typically, HCG was injected (44 to 48 hours after PMSG) into three sets of 2 to 4 mice in approximately one hour intervals the night before the experiments. The oocytes were then removed from the mice about 12 to 13 hours after the HCG injection in roughly one hour intervals. The experiments with each collection of 2 to 4 mice, were run during these intervals to minimize the time exposure of oocytes to *in vitro* conditions. Approximately 40 to 100 oocytes were collected from 2 to 4 mice. These oocytes were kept in petri dishes containing 100 μl PBS+BSA solution covered with silicone oil until they were used. For nucleation experiments, 10 to 30 oocytes at a time were placed onto the cryomicroscope stage. The oocytes were covered and sealed with in a similar manner as the permeability experiments. Two to 3 sets of nucleation experiments were run from one collection of 40 to 100 oocytes. Then a new set of 2 to 4 mice was sacrificed for the next set of experiments followed by the third collection and experiments. The oocytes were never put in culture media prior to nucleation experiments. They were always used within 60 minutes after the collection to minimize

the time exposure to the PBS+BSA solution. A control group of oocytes were fertilized for each experiment to assess the functionality of the oocytes collected. Since it was determined that the oocytes can be fertilized for at least 4 hours after the collection (16 hours after HCG injection), 10 oocytes were spared from each experiment and put in separate Petri dishes containing EBSS and placed in a 5% CO_2 incubator. All of the control oocytes were inseminated at the same time roughly, 3 hours after the beginning of the first experiment. Results of the experiments were used only if the fertilization rate of the control group was greater than 85% with 80% subsequent development to blastocyst stage. All the control experiments are summarized in Chapter II and the reader should refer to that chapter for detailed information. Table 4.1 summarizes the experimental protocol for nucleation experiments.

For nucleation experiments, 10 to 30 oocytes were placed on the cryomicroscope stage. The oocytes were covered and sealed in a similar manner as the permeability experiments. Ten to 20 of these oocytes were observed at a time with a 4x or 10x objective and 1.25x or 2x photo-ocular, depending on the distribution of the oocytes over the freezing stage. The photo-ocular was chosen such that the maximum number of oocytes could be observed during the cryomicroscopy. Bright-illumination was used for nucleation experiments thus allowing for an easier visual determination of the intracellular ice formation.

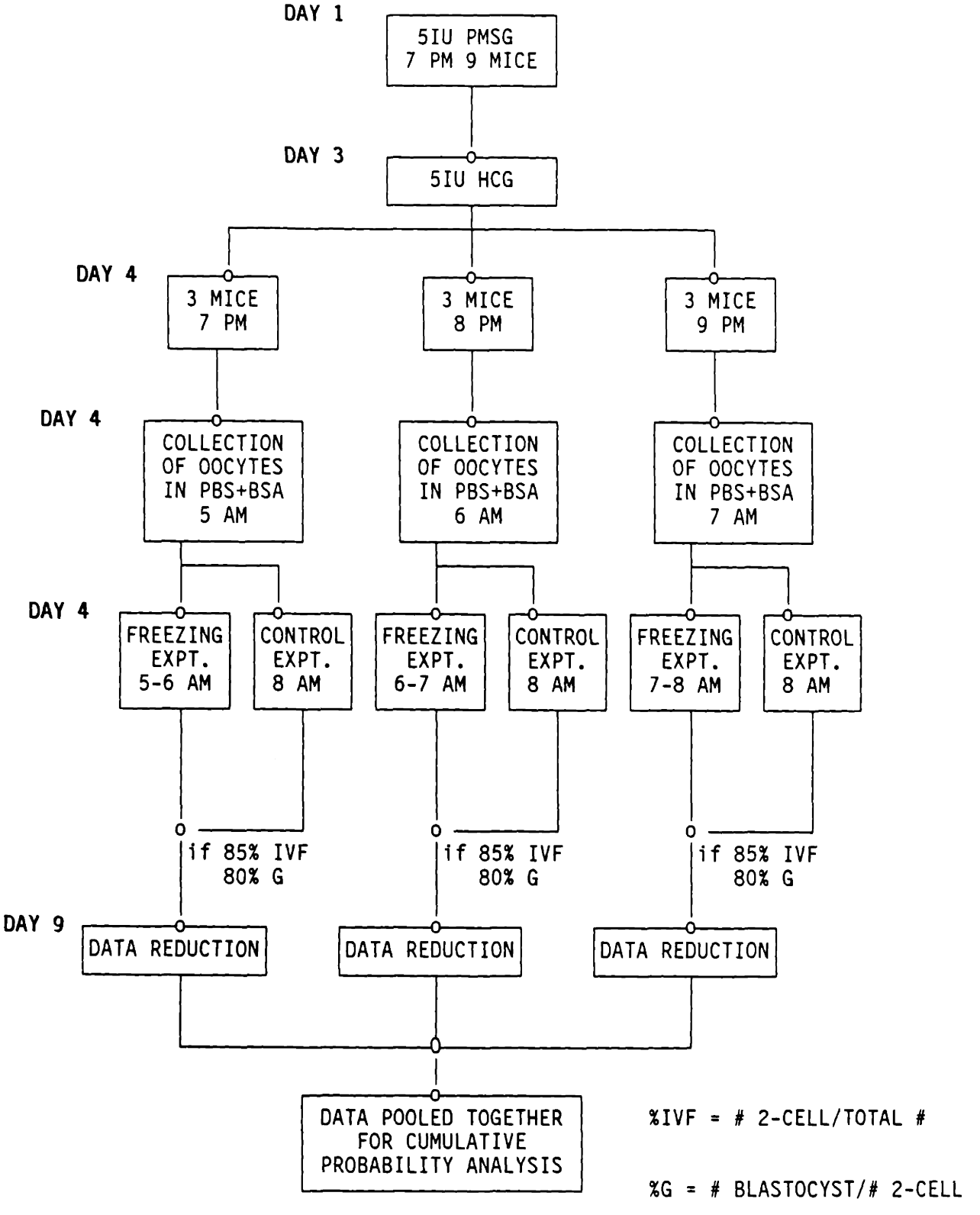

TABLE 4.1.
SCHEMATIC REPRESENTATION OF THE EXPERIMENTAL PROCEDURE
FOR NUCLEATION EXPERIMENTS WITH MOUSE OOCYTES

It is noteworthy to mention here that a sapphire plate of 0.063 inch in thickness was used for the experiments. The temperature gradient over the whole field was less than 0.1°C/20mm. After each run the melting temperature was determined from the cryomicroscopic recordings during slow warming and the temperature measurements were corrected to minimize experimental errors due to the possible variations in flow rate of gaseous nitrogen, liquid nitrogen level in the storage dewar, thickness of the oil layer underneath the sapphire plate, etc.

For some of the nucleation experiments, the tonicity of the suspending medium was altered to investigate the effect of dehydration on the nucleation kinetics. The osmolality of the solutions were adjusted by adding NaCl to obtain hypertonic solutions or by adding distilled deionized water to obtain hypotonic solutions. The final concentration was checked using an osmometer (Adv.Inst.Inc. Model 3L). The concentrations used were 210, 285, 510, 735, 820, and 1,035 mosm and all the solutions contained 4mg/ml BSA.

4.2. Subzero Temperature Permeability Experiments

Volumetric changes during cooling were determined for mouse oocytes at a cooling rate of 2°C/min. During cooling, the oocytes responded osmotically by decreasing in volume due to the decreased chemical potential of the external frozen solution. The area of each oocyte was

converted to volume by assuming spherical geometry. Since the assumption of spherical symmetry was made, only oocytes that shrunk in a reasonably spherical manner were used. Oocyte volumes were normalized with respect to the initial volume before cooling.

The volumetric response of all the oocytes observed is presented in Fig.4.1. The range of volumes observed among oocytes during freezing at any given temperature was considerably large. While the variation may be attributed to experimental variations, this is unlikely because the temperature was regulated within 0.05^{o}C and the temperature gradient over the field of view was always less than 0.1^{o}C. Errors in the calculation of volume from two dimensional measurements and cell to cell variations in permeability may be the cause of variation.

Metaphase II mouse oocytes equilibrated in solutions of PBS+NaCl with varying tonicities at 24^{o}C behaved as perfect osmometers over a range of osmolalities between 285 to 2,215 osm. Fig.4.2 shows the results of such experiments. The data points were fit by the method of least squares to determine the theoretical osmotically inactive volume by extrapolating the best fit line to an infinitely concentrated solution. This resulted in an inactive cell volume of 0.214 for unfertilized mouse ova with a correlation coefficient of 0.995, indicating that the ova closely follow the ideal Boyle-van't Hoff relation. The results of the diameter experiments with eighty oocytes yielded a mean value diameter value of 79.41 μm and a standard deviation

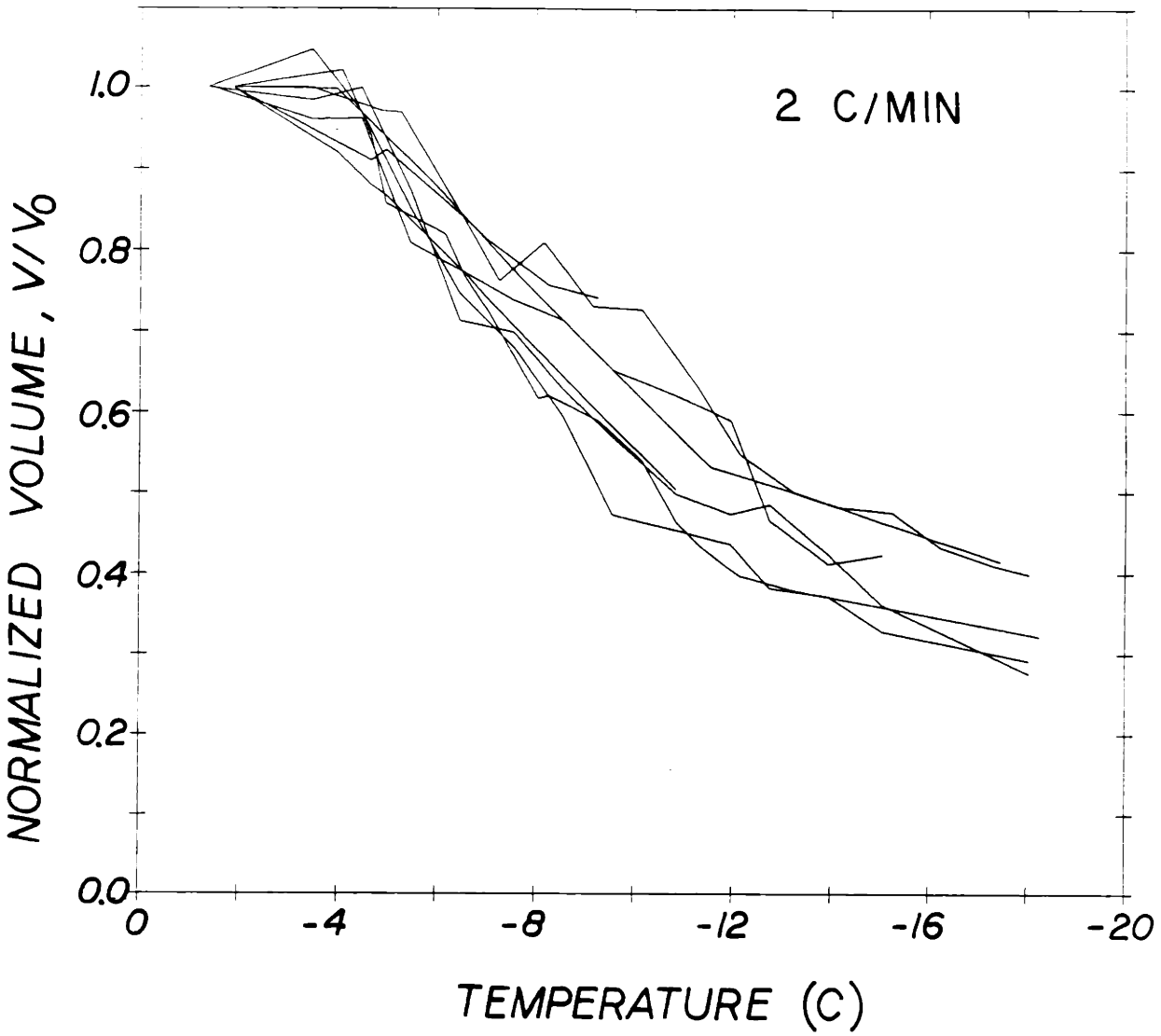

FIGURE.4.1. Experimental normalized total volume vs. temperature curves for mouse oocytes cooled at 2°C/min. A sapphire plate of 0.063 inch was used for the experiments. Eight oocytes are reported. Oocytes that deviated from spherical shape during dehydration were discarded to minimize the experimental errors.

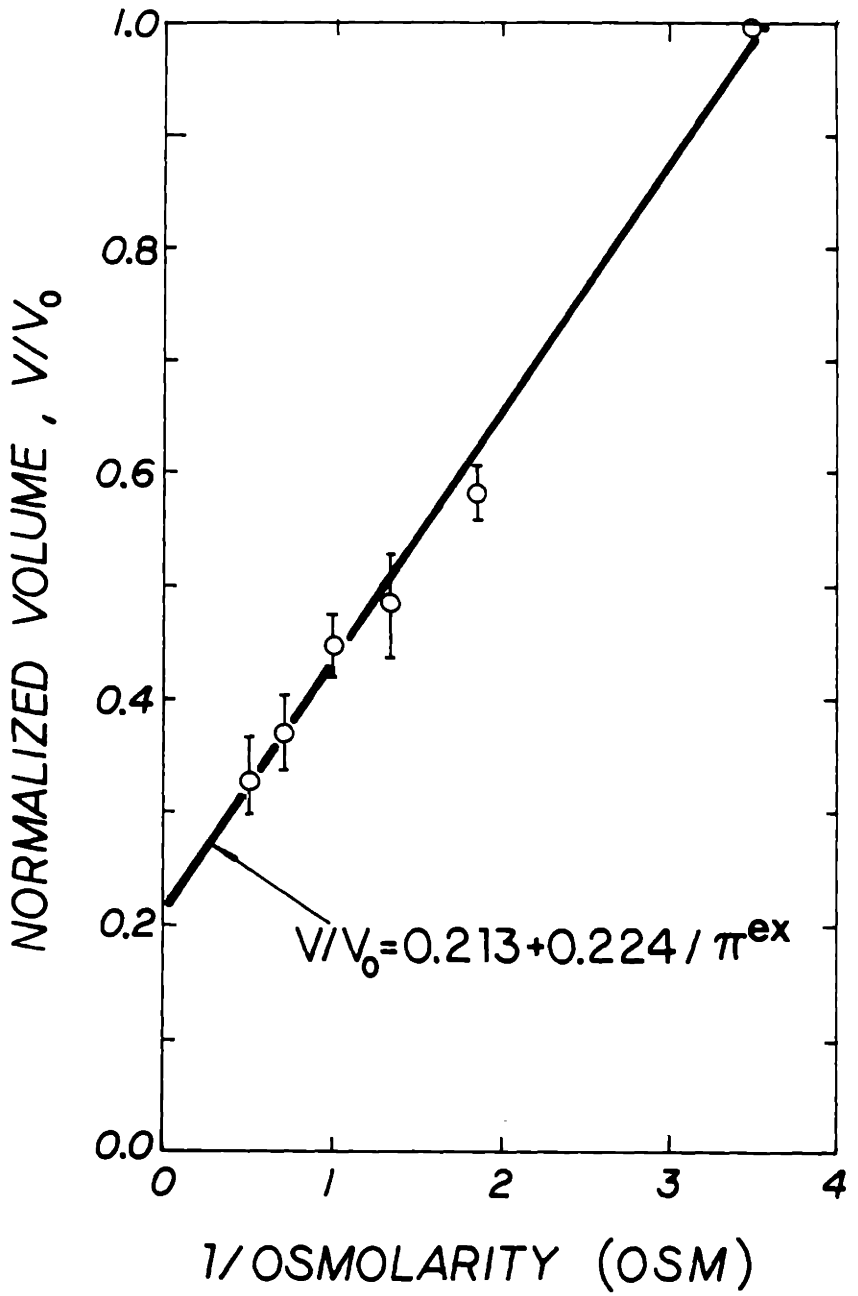

FIGURE.4.2. Static osmometric behavior of mouse oocytes in different hypertonic PBS+BSA solutions. Five oocytes were used for these experiments. Bars show the standard deviations.

of 4.62 μm. The distribution revealed close agreement with a theoretical normal distribution (Orrico, 1988). Fig.4.3 shows the experimental diameter distribution of the metaphase II mouse oocytes.

4.3. Intracellular Ice Nucleation Kinetics Experiments

This section includes the presentation of the experimental observations for intracellular ice formation in unfertilized mouse ova. When oocytes are frozen at rapid rates (120^{o}C/min) in isotonic solutions of PBS + BSA, the ice-nucleation of intracellular solution commenced at about -8^{o}C and the oocytes were frozen at about -18^{o}C (see Fig.4.4, curve with 285 mosm label). The formation of ice inside the oocytes were detected by the sudden darkening of the contents of the oocytes. This darkening is believed to be caused by small ice crystals and/or air bubbles (Steponkus & Dowgert, 1981; Korber, 1988). The fraction of oocytes frozen was a strong function of the final temperature to which they were cooled. The incidence of internal ice formation was increased greatly as the minimum temperature was decreased. The fraction of oocytes frozen increased from 0% to 100% over a temperature range of approximately 10^{o}C. Since the cooling rate of 120^{o}C/min was high enough to impede any water transport, this result gave us the kinetics of intracellular ice formation decoupled from water transport. The thermodynamic state of the intracellular milieu is also well defined at high cooling rates because the water transport is negligible. Thus, the

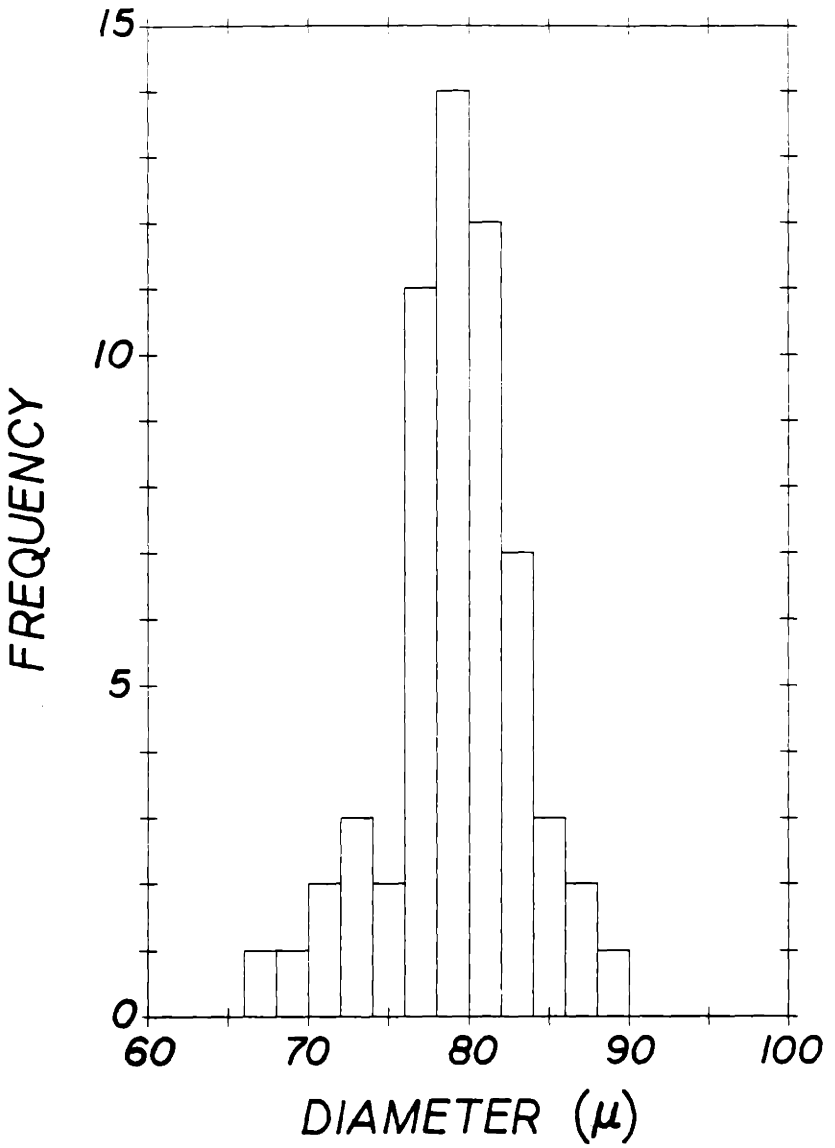

FIGURE.4.3. Diameter distribution of mouse oocytes in isotonic PBS+BSA solution. The mean diameter is 79.41 μm and the standard deviation 4.62μm.

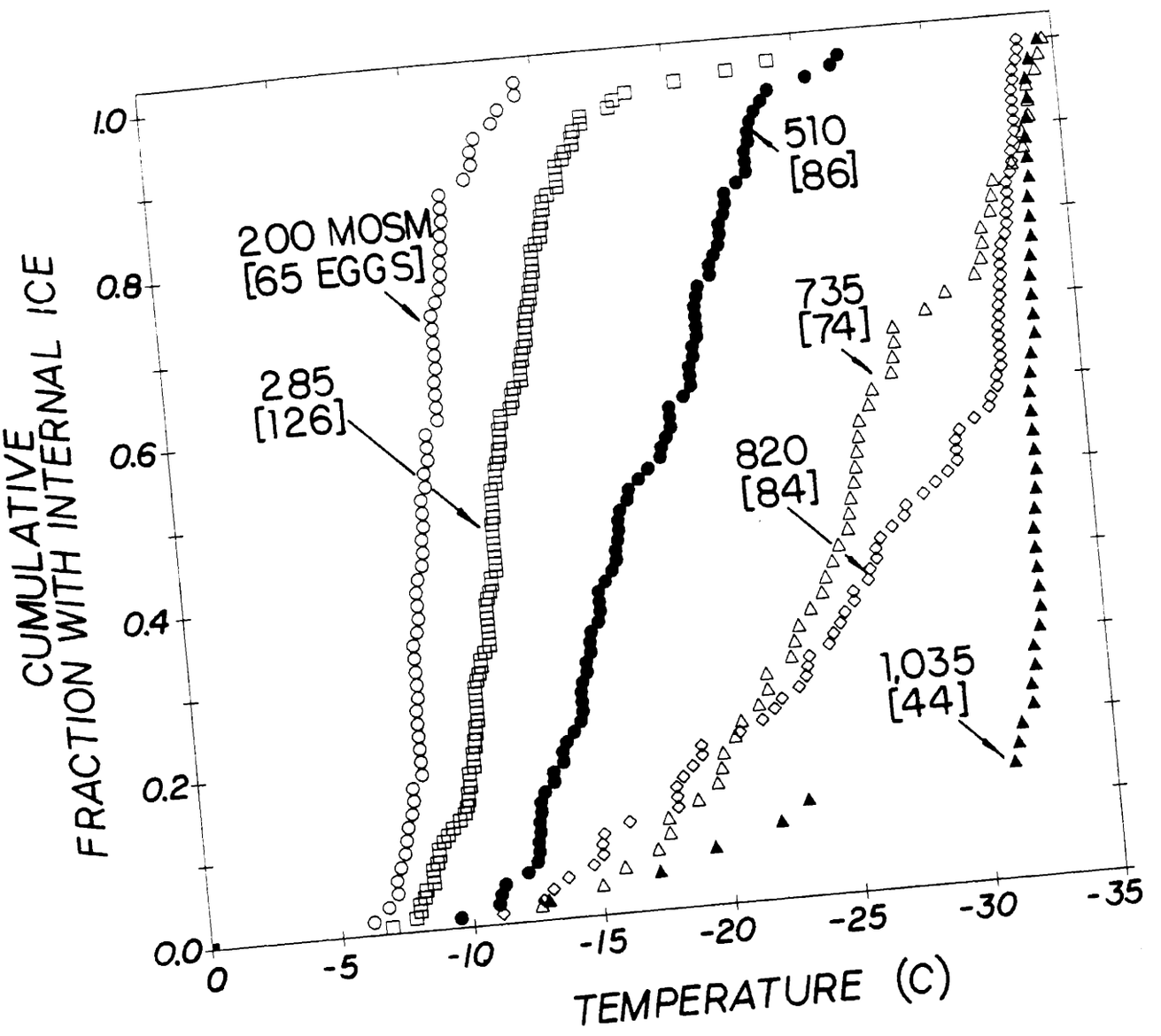

FIGURE.4.4. Cumulative fraction of mouse oocytes containing intracellular ice as a function of the temperature at which intracellular ice formation was observed to occur. Oocytes were cooled in various anisotonic solutions of PBS+NaCl+BSA between 200 to 1,035 mosm to -40°C at 120°C/min. No. oocytes used for each experiment is given in brackets. Data from 5 to 10 sets of experiments were pooled.

nucleation phenomena can be modelled using these rapid cooling experiments with high accuracy.

The effect of intracellular concentration on the nucleation frequency can be tested by freezing the oocytes at rapid rates in various concentrations of the suspending medium. This was done in six different concentrations of PBS+NaCl+BSA solutions ranging from 200 to 1,035 mosm. Oocytes were frozen in a given concentration of the suspending medium at 120°C/min to determine the incidence of intracellular ice formation. As can be seen from Fig.4.4, the dependence of intracellular ice formation on the initial concentration of the suspending medium was pronounced. Increasing the concentration of the solution caused the ice-nucleation kinetics to shift to lower temperatures. In 200 mosm, nucleation started about -6°C and reached 100% at about -12°C. However, in 285, 510, and 735 mosm the initial oocyte nucleated at about -8°, -10°, and -12°C, respectively. Subsequently, all the oocytes were frozen at -18° for 285, -26° for 510, and -32°C for 735 mosm, respectively. This drastic shift in the temperature range over which intracellular ice nucleation occurred could not be explained by simple depression of the freezing temperature. The freezing point is only depressed 1.4°C by increasing the concentration from 285 mosm to 1,035 mosm. Whereas, the mean nucleation temperature for intracellular ice formation decreased from -12.5 to -30.5°C for the same increase in concentration.

One very interesting observation in Fig.4.4 is the fact that for concentrations higher than 735 mosm the kinetics of ice-nucleation shows a break point at approximately -31°C. In 820 and 1,035 mosm, the fraction of oocytes with internal ice initially increased slowly. At approximately -31°C all of the remaining oocytes nucleated almost spontaneously over a temperature range of less than 3°C. This shift in the mechanism of nucleation can be better seen from Figs.4.5. These plots show cumulative probability of internal ice formation as a function of observed nucleation temperatures. The y-axis is rescaled such that a normal distribution will yield a straight line. For concentrations from 200 to 510 mosm, the data follows a straight line favoring a normal distribution. However, starting at 735 mosm (and especially in 810 and 1,035 mosm), a sudden change in the slope of normal distribution plots can be seen at about -31°C. There are two normal distributions defined with two different slopes. The change in the slopes of these curves is a consequence of the change in the nucleation kinetics. Oocytes that follow a very slow initial ice nucleation kinetics switch suddenly to a much faster nucleation kinetics at approximately -31°C. This dramatic shift in nucleation kinetics may be due to a change in the mechanism of intracellular ice formation. This will be analyzed in detail in the following chapters.

Crystallization temperatures for the formation of intracellular ice exhibit a dependency on the volume fraction of fictitious species (salt+proteins) of the intracellular solution (see App. A). The volume

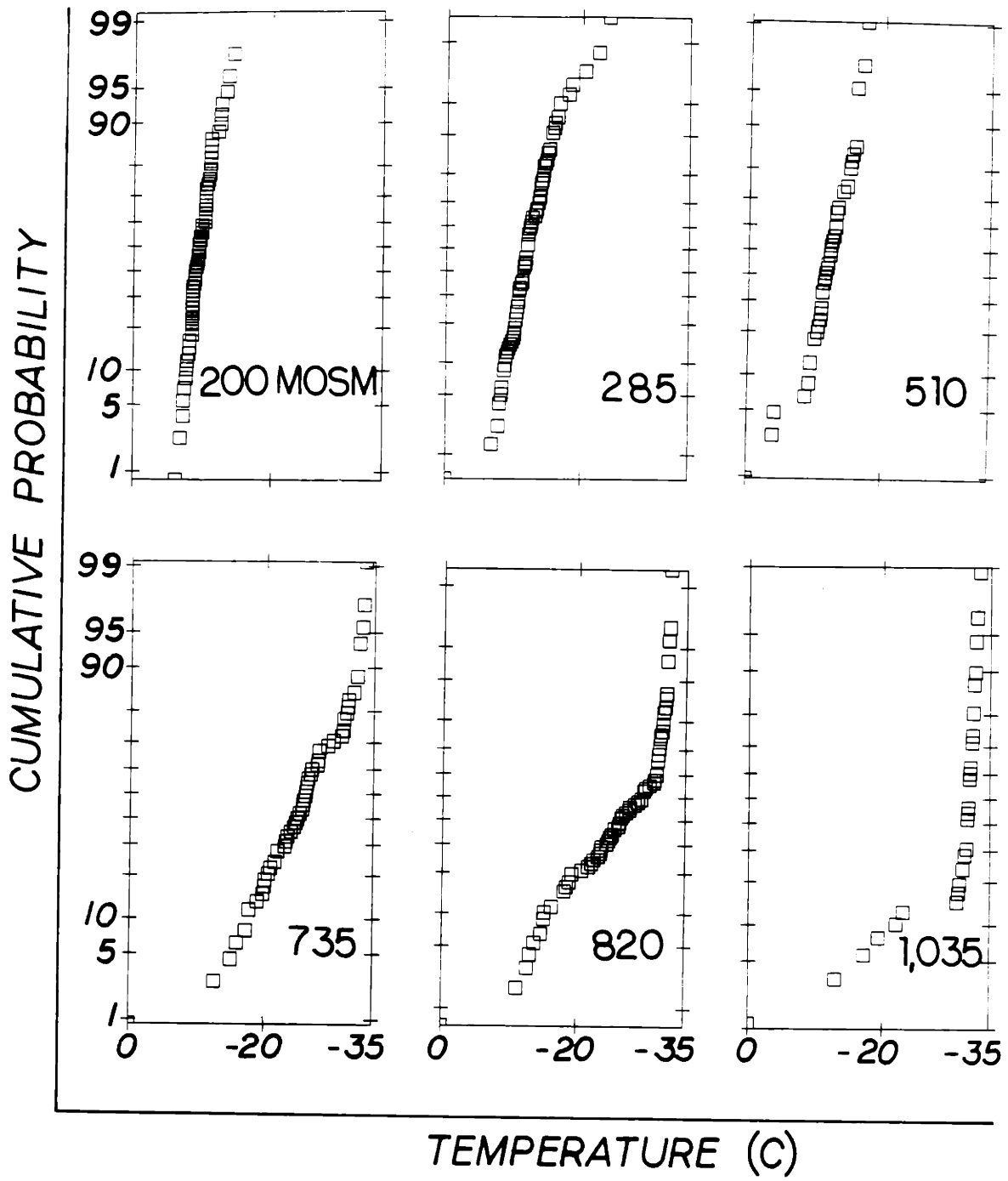

FIGURE.4.5. Cumulative probability of intracellular ice formation as a function of temperature for mouse oocytes suspended in anisotonic PBS+NaCl+BSA solutions between 200 to 1,035 mosm. The y-axis was scaled such that a linear line would yield normal distribution. Each data point corresponds to an oocyte.

fraction of fictitious species (= V_b/V_c) was calculated from Eq.(6.87). The results of such calculations for osmolalities ranging from 200 to 1,035 mosm in our experiments are depicted in Fig. 4.6. The detailed calculation of the volume fraction of fictitious species will be given in Chapter VI. The freezing temperature for 50% of the oocytes to nucleate is decreased from about -10°C down to -32°C by increasing the volume fraction of fictitious species from 0.15 to 0.5. The freezing temperatures for 10% and 90% of the oocytes to nucleate intracellularly varied from about -9° and -12°C down to -22° and -32°C when the solute volume fraction is increased from 0.15 to 0.5, respectively. Also shown on Fig.4.6 is the average homogeneous nucleation temperatures of electrolyte droplets at the size of an oocyte. The homogeneous nucleation temperatures are calculated using the equation derived by Rasmussen & MacKenzie (1972) and are good only for a first cut analysis for complex intracellular solutions. As the solute volume fraction increases, the difference between the freezing temperatures of the oocytes and the homogeneous nucleation temperature decreases. Appendix B describes the detailed calculation of the homogeneous nucleation temperature.

During the cryomicroscopy experiments, some of the oocytes showed a very rapid internal ice formation with almost no change in the grey level of the internal content. The crystallization of the internal solution was very difficult to see. It occurred suddenly with a flashlike motion within the cell borders. This type of internal ice

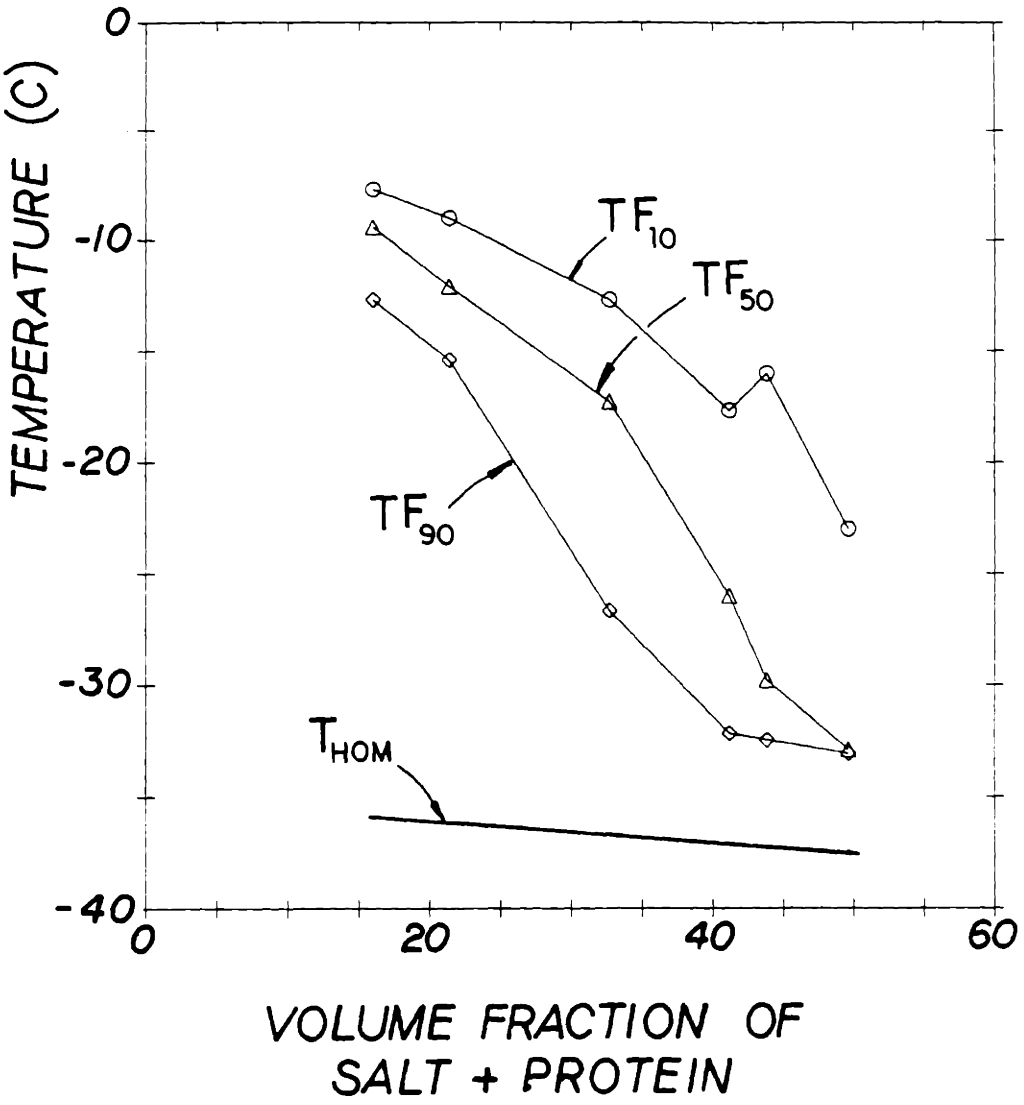

FIGURE.4.6. Temperature at which 10, 50, and 90% of the oocytes containing ice as a function of volume fraction of fictitious species when oocytes were cooled in various anisotonic solutions. Volume fraction was calculated as described in App.A. Homogeneous nucleation temperature is also shown in the figure (App.B).

formation was first observed by Scheiwe & Korber (1982a-b; 1987) and called **twitching** type as opposed to **darkening** type of ice formation observed in most of the instances. The darkening process usually covered the whole cell starting from one side towards the other side in a matter of 0.2 to 0.6 seconds. The twitching type of crystallization occurred spontaneously at a rate higher than the time resolution of the framing system used (0.1 second). The twitching type of ice formation could only be detected by dynamic investigation of the video tapes and was not observed at freezing in low concentrations of the suspending medium. The frequency of twitching type crystallization was increased as the concentration of the suspending medium was increased. In 1,035 mosm, almost all the oocytes showed twitching type of mode of ice growth. However, there was no clear cut transition between darkening to twitching types of intracellular ice formations. In addition, there was no correlation between the type of crystallization (darkening vs. twitching) and shift in nucleation mechanism at -31^{o}C. No darkening type growth was observed below -24^{o}C. Whereas, all the oocytes showed twiching type of ice growth below -24^{0}C. There was a transition zone between -17 to -24^{o}C were both types of crystallizations were observed simultaneously. Since the second nucleation mechanism occurred below -31^{o}C, the twitching type of crystallization was always observed for the second nucleation mechanism. However, first nucleation mechanism occurred over a broader temperature range and both darkening and twitching types of crystallization were observed depending on the concentration of the suspending solution (see Fig.4.4). It is probably

the size of the dendrites causing the change in the grey level of the intracellular ice depending on the undercooling of the cytoplasm yielding darkening or twitching types of growth. Further experimental investigation is necessary to derive definite conclusions for the mechanisms of these two types of ice growth observed during freezing of oocytes.

Examples of the morphological appearance of mouse oocytes undergoing rapid freezing in various solutions are given in Figs.4.7 to 4.10. The oocytes were photographed at different temperatures from the video-monitor. As can be seen from these figures, at low concentrations the darkening type of nucleation is very obvious and easy to detect. However, at higher concentrations it is almost impossible to detect the internal ice-nucleation from still pictures. Oocytes with intracellular ice formation are pointed out with arrows. One could only detect 'twitching' type nucleation after many careful revisions of the video tapes. Oocytes with intracellular ice formation showed damaged morpholgy after the freeze-thaw protocol.

We have also investigated the effect of the cooling rate on the nucleation kinetics. The distribution of the observed intracellular nucleation temperatures is shown in Fig.4.11. All of these experiments were done in an isotonic PBS+BSA solution. At rates lower than $40^{o}C$/min, there was appreciable volume change due to the dehydration of the oocytes altering the thermodynamic state of the internal milieu.

FIGURE.4.7. Sequence of micrograph illustrating the kinetics of intracellular ice formation for mouse oocytes cooled at 120°C/min in 200 mosm. Arrows indicate the occurence of intracellular ice formation. Oocytes were damaged after thawing back to suprazero temperatures. Scale shows 100 μm.

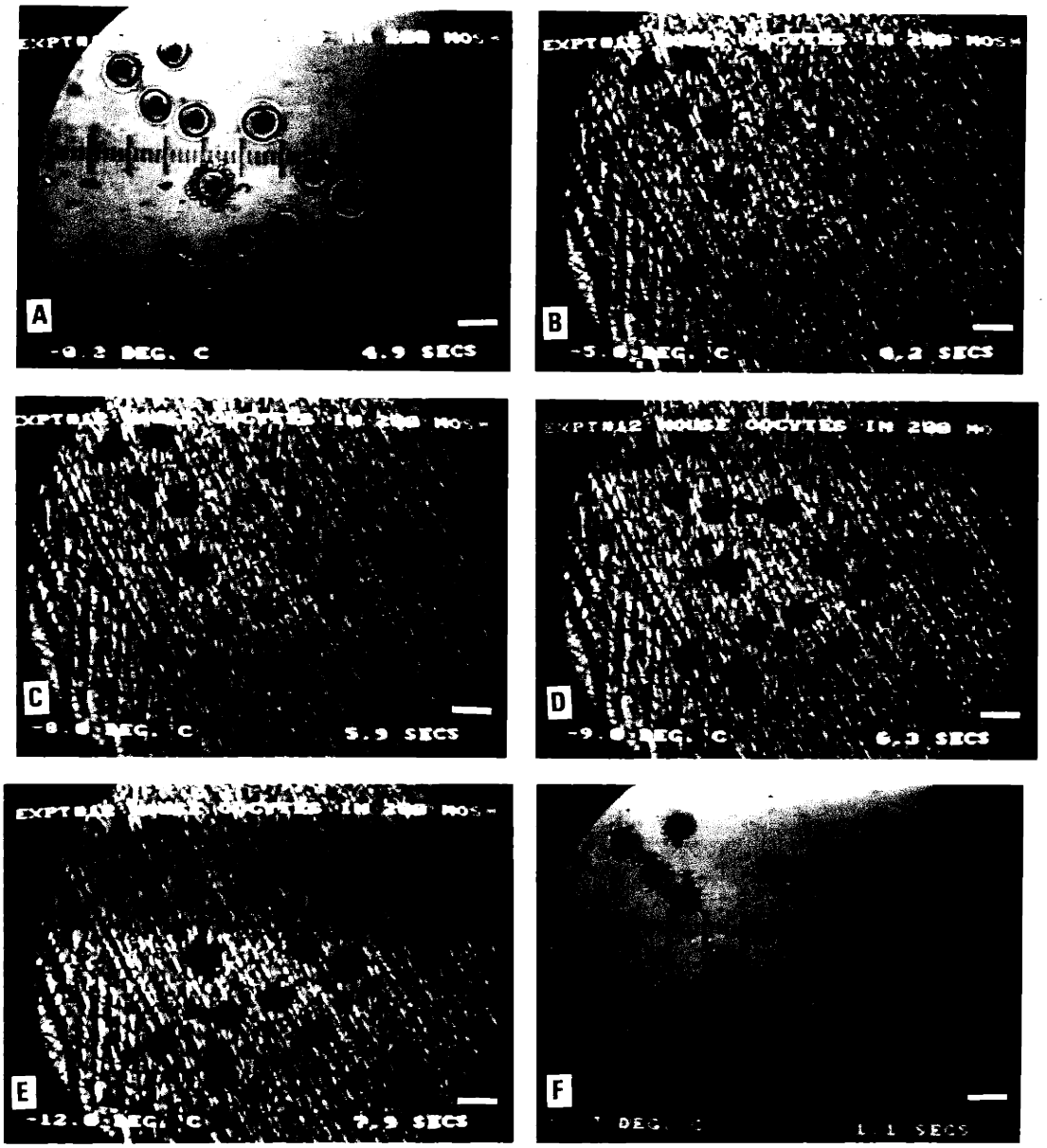
A
-0.2 DEG. C
4.9 SECS
B
-5.0 DEG. C
6.2 SECS
C
-8.0 DEG. C
5.9 SECS
D
-9.0 DEG. C
6.3 SECS
E
-12.0 DEG. C
7.9 SECS
F
1.1 SECS

PLATE-1

FIGURE.4.8. Sequence of micrograph illustrating the kinetics of intracellular ice formation for mouse oocytes cooled at 120°C/min in 285 mosm. Arrows indicate the occurence of intracellular ice formation. Oocytes were damaged after thawing back to suprazero temperatures. Scale shows 100 μm.

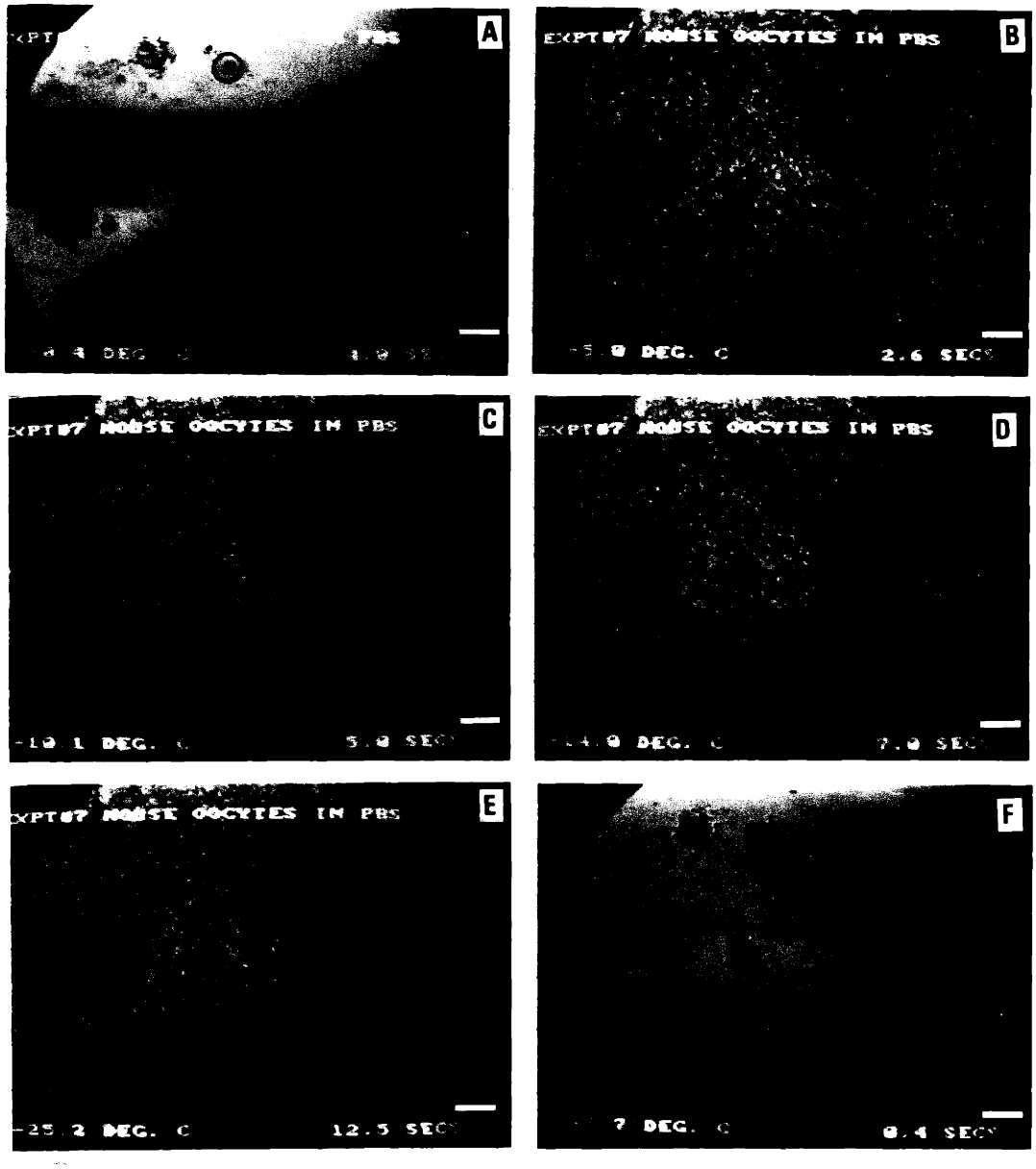
A
B
EXPT#7 MOUSE OOCYTES IM PBS
2.6 SEC
C
EXPT#7 MOUSE OOCYTES IM PBS
D
EXPT#7 MOUSE OOCYTES IM PBS
E
EXPT#7 MOUSE OOCYTES IM PBS
F

PLATE-2

FIGURE.4.9. Sequence of micrograph illustrating the kinetics of intracellular ice formation for mouse oocytes cooled at 120°C/min in 510 mosm. Arrows indicate the occurence of intracellular ice formation. Oocytes were damaged after thawing back to suprazero temperatures. Scale shows 100 μm.

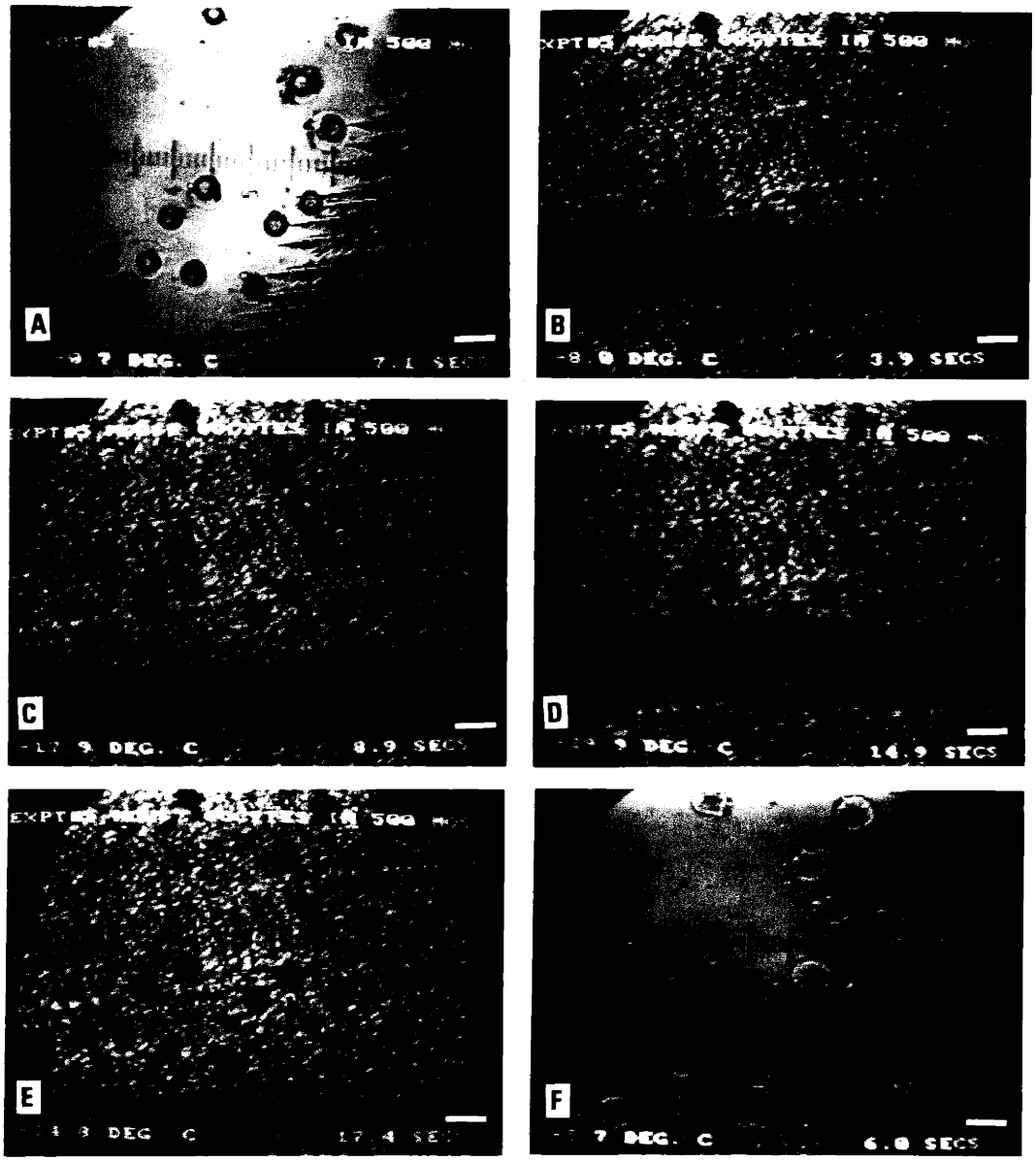

PLATE-3

FIGURE.4.10. Sequence of micrograph illustrating the kinetics of intracellular ice formation for mouse oocytes cooled at 120°C/min in 1,035 mosm. Arrows indicate the occurence of intracellular ice formation. Oocytes were damaged after thawing back to suprazero temperatures. Scale shows 100 μm.

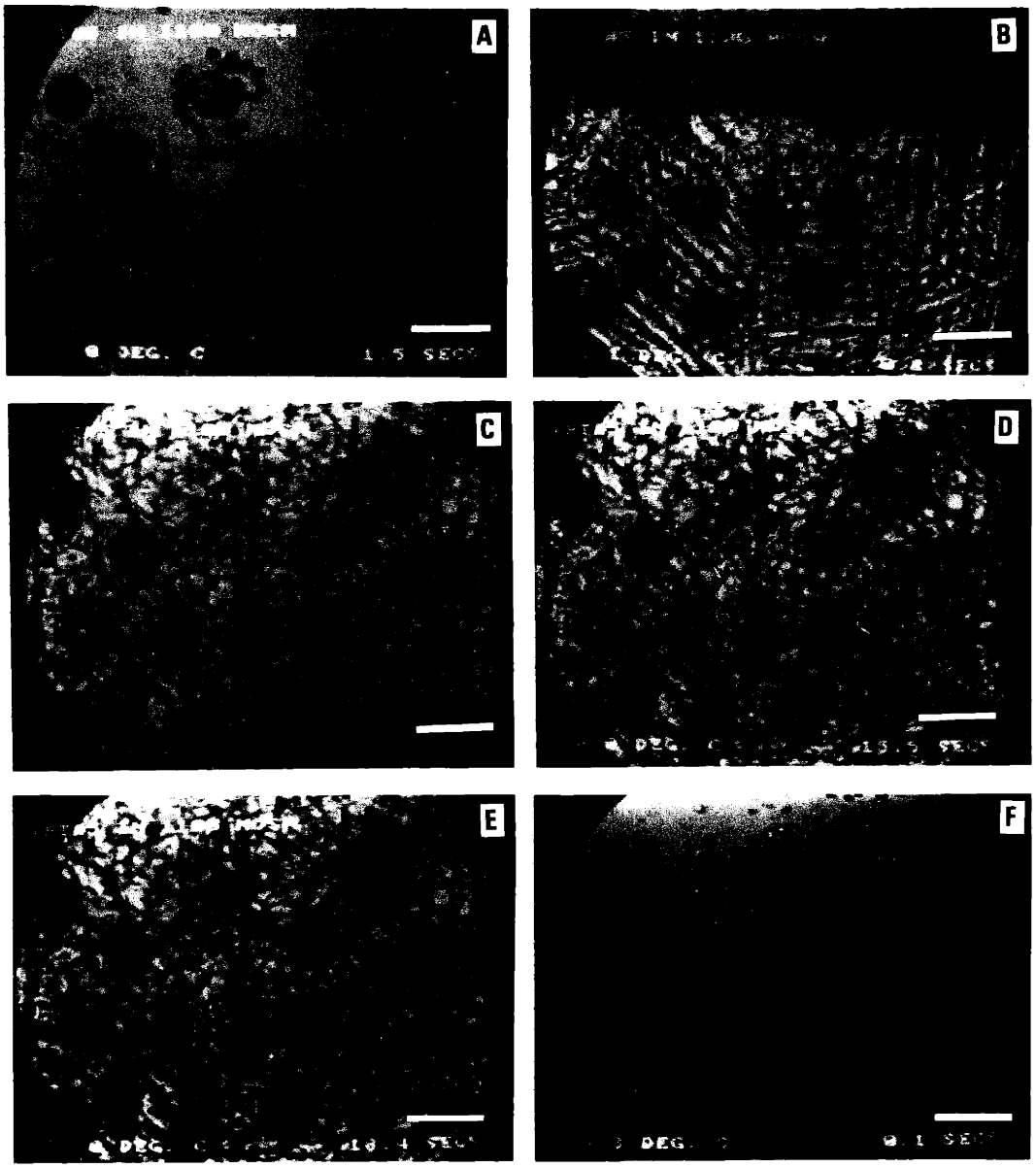

PLATE-4

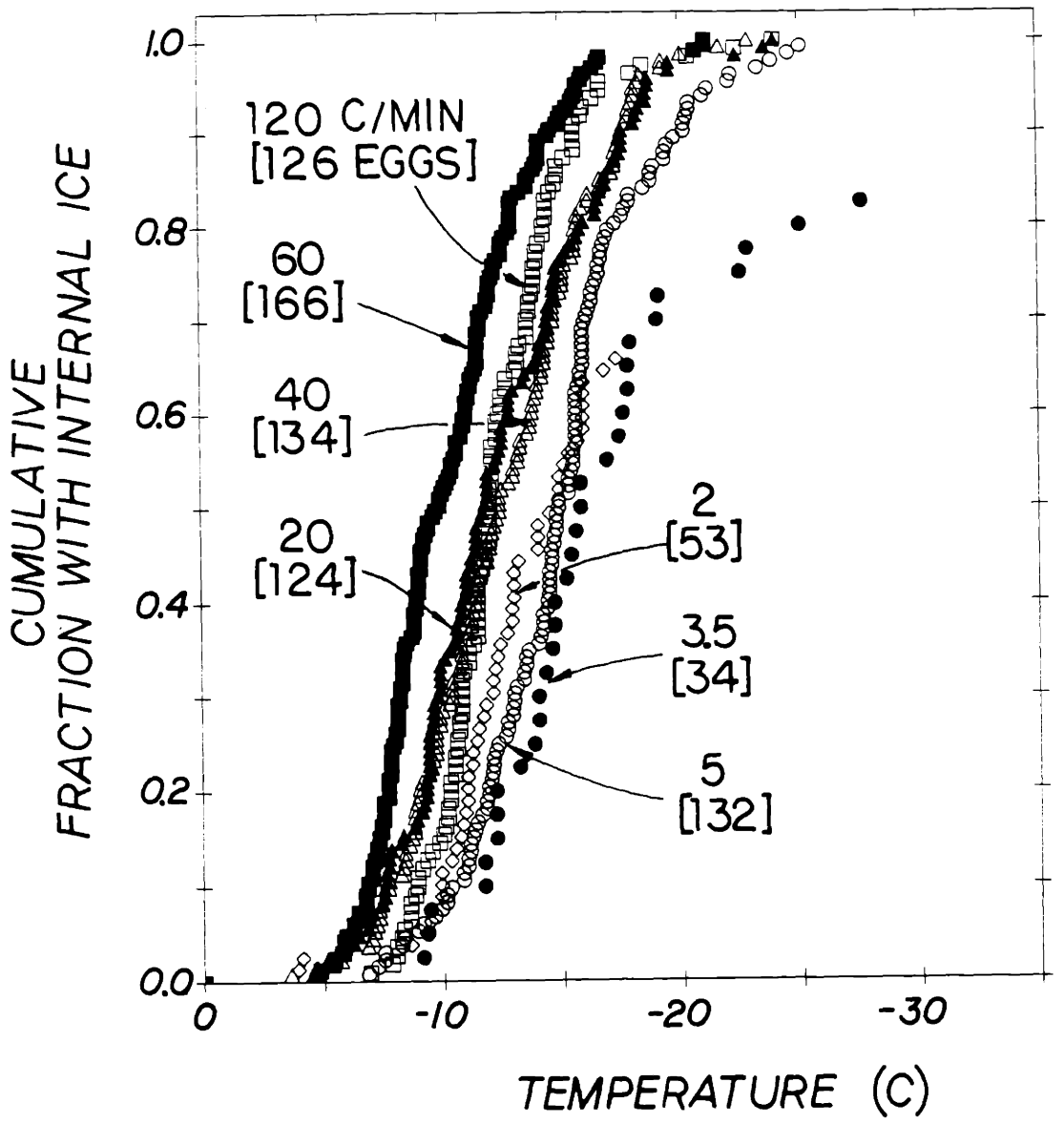

FIGURE.4.11. Cumulative fraction of mouse oocytes with intracellular ice formation vs. temperature for various cooling rates. Experiments were done in isotonic PBS+BSA solution. Extracellular ice was seeded at -0.615°C. Each data point represent an oocyte. No. oocytes are given in brackets. Data from 5 to 10 sets of experiments were pooled together. Oocytes were cooled to a final temperature of -40°C.

Fig.4.12 shows experimental results on a rescaled cumulative probability plot yielding a linear relation for a normal distribution. As can be seen from these plots, the distributions of internal ice formation incidence were normal for cooling rates ranging from 2° to 120°C/min. No shift in the nucleation mechanism was observed during these freezing experiments. This is due to all of the oocytes nucleating intracellularly before the temperature reaches -20°C or dehydrating enough so that they do not form ice intracellularly below -20°C. In addition, no twitching type of intracellular ice nucleation was observed during these experiments because the intracellular freezing temperature was always above -20°C during freezing in isotonic solutions. Fig.4.13 shows the mean nucleation temperatures of ice formation as calculated from Fig.4.11. Bars show standard deviations. The mean nucleation temperatures were almost constant throughout the all cooling rates.

The classical way of presenting the nucleation data is to plot the fraction of cells with intracellular ice as a function of the cooling rate. A transition spectrum of cooling rates from 1° to 5°C/min can be identified from such a representation as shown in Fig.4.14. At 1°C/min none of the oocytes contained ice, however, at 5°C/min all the oocytes contained ice. This typical sharp transition is observed for many other types of cells (Mazur, 1984). A micrograph sequence of the cooling rate effect on intracellular ice formation is shown in Fig.4.15 for oocytes cooled at 2°C/min to a final temperature of -40°C. Two oocytes that did

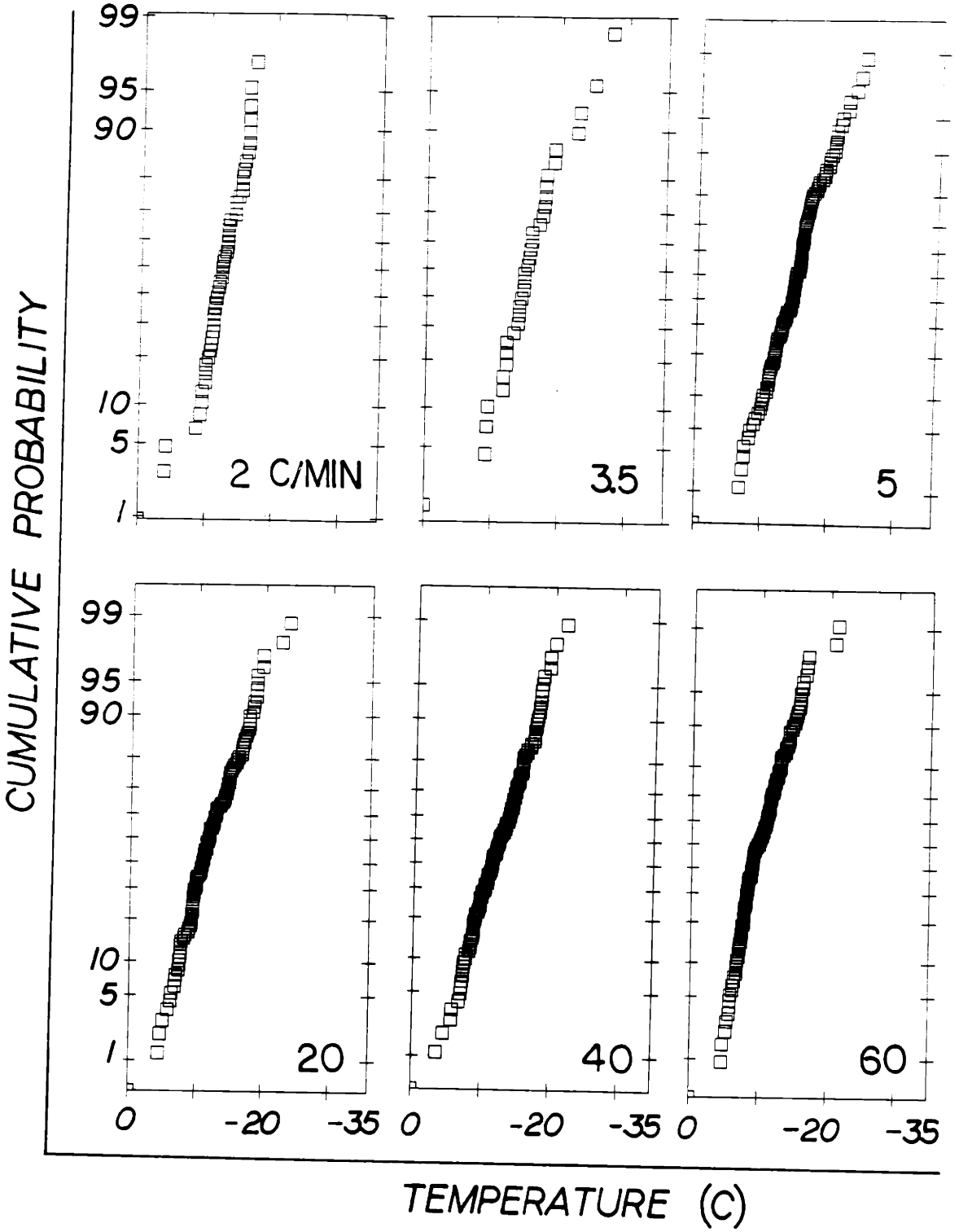

FIGURE.4.12. Cumulative probability of intracellular ice formation in mouse oocytes vs. temperature cooled at different rates. Oocytes were suspended in isotonic PBS+BSA solution. Extracellular ice was seeded at -0.615°C. Each data point represents an oocyte. Cumulative probability axis is scaled such that a linear line yields a normal distribution.

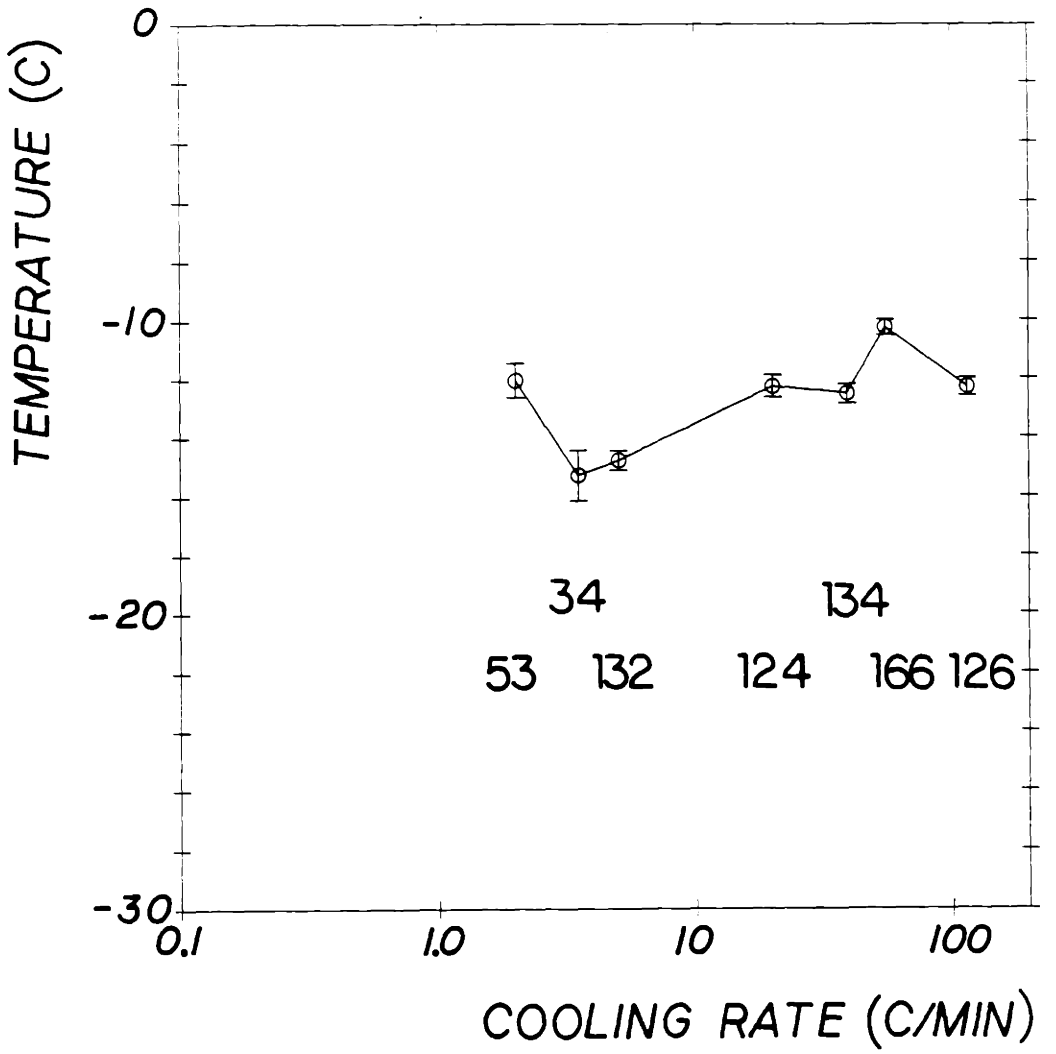

FIGURE.4.13. Temperature at which fifty percent of oocytes containing intracellular ice as a function of cooling rate when cooled in isotonic solutions. Bars show standard deviations. Numbers of oocytes are shown in brackets. Oocytes were cooled to a final temperature of -40°C. Samples were suspended in isotonic PBS+BSA and extracellular ice was seeded at -0.615°C.

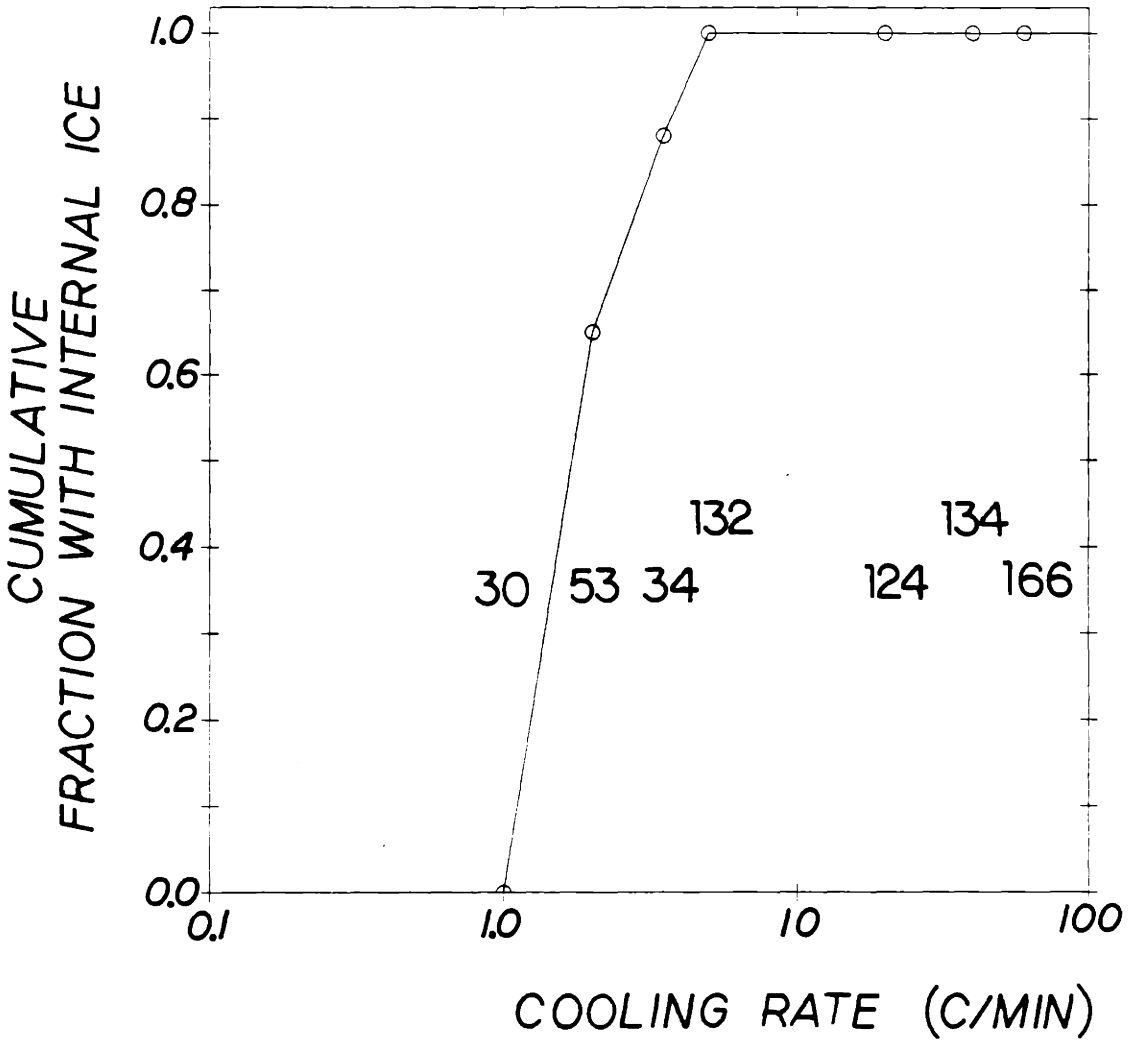

FIGURE.4.14. Cumulative fraction of mouse oocytes with intracellular ice formation as a function of the cooling rate. Numbers in brackets represent the number of oocytes. Oocytes were cooled to a final temperature of -40°C. Samples were suspended in isotonic PBS+BSA and extracellular ice was seeded at -0.615°C.

FIGURE.4.15. Sequence of micrograph illustrating mouse oocytes cooled at 2°C/min in isotonic solution to -40°C. Arrows indicate oocytes with intracellular ice formation. Two of the oocytes that did not form intracellular ice appeared normal after thawing as shown in (e). Five minutes later, these two oocytes were degenerated (f). Scale shows 100 μm.

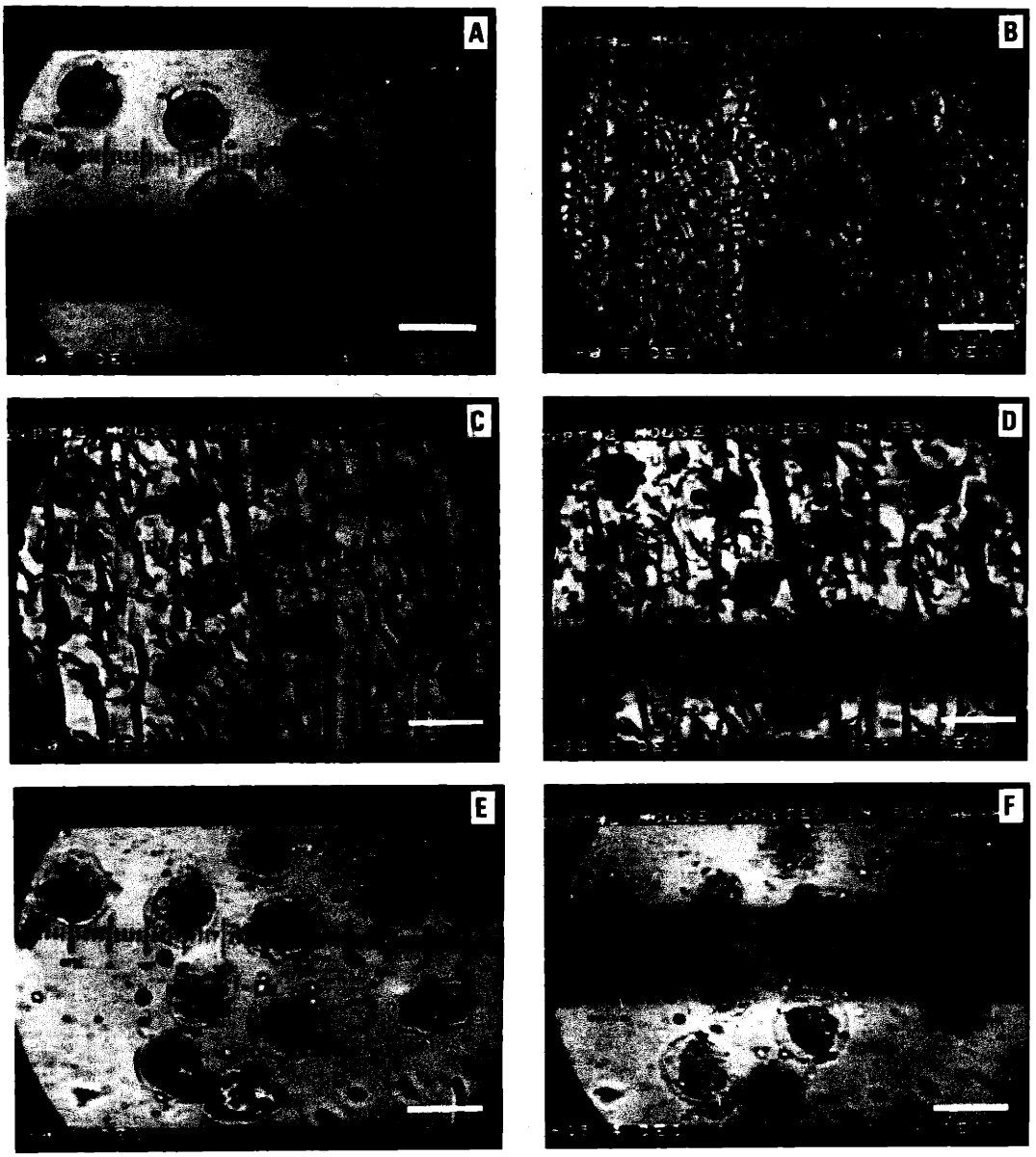

PLATE-5

not form internal ice looked morphologically normal immediately after thawing, however, they lost their normal structure in less than 30 seconds at 25°C.

In addition to rapid and slow cooling rate experiments, constant temperature experiments were conducted in isotonic PBS+BSA solutions. The results in Fig.4.16 for three different temperatures show that the lower the temperature, higher the proportion of oocytes with internal ice formation. The fraction of oocytes with internal ice were 50%, 60%, and 95% for -6.4°, -7.72°, and -8.85°C, respectively. Fig.4.17 shows a typical sequence of micrographs displaying the intracellular nucleation pattern of oocytes at various constant temperatures.

Some experiments were also run in the absence of external ice. The oocytes were carefully cooled such that both the oocytes and the extracellular solution (isotonic PBS+BSA) were undercooled. The intracellular ice did not form in 43 of the oocytes used for these experiments until immediately after the appearance extracellular ice at -20°C. This was significantly different than the first case where intracellular nucleation occurred from -8 to -14°C. A micrograph of an undercooling experiment is shown in Fig.4.18. As can be seen clearly from this figure, oocytes that were cooled in the absence of extracellular ice did not form intracellular ice until -20°C. At -20°C, both the suspending solution and the oocytes were nucleated spontaneously. The only conclusion that can be drawn from these

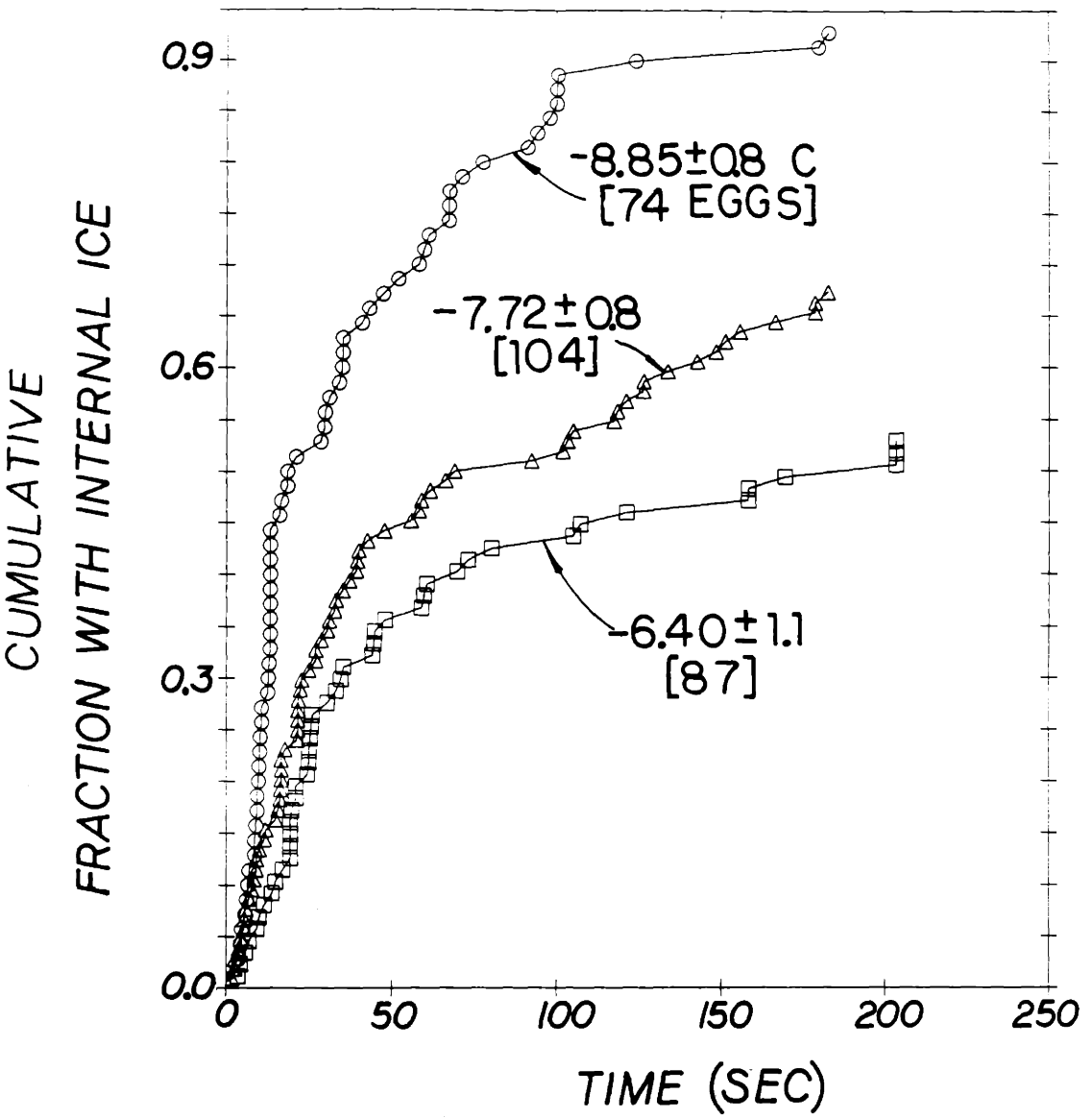

FIGURE.4.16. Cumulative fraction of mouse oocytes with intracellular ice formation as a function of time at different constant temperatures. Numbers in brackets shows the number of oocytes pooled from 3 to 5 sets of experiments. Samples were suspended in isotonic PBS+BSA and extracellular ice was seeded at -1°C prior to rapid cooling to the desired constant temperature.

FIGURE.4.17. Sequence of micrograph illustrating the kinetics of intracellular ice formation in mouse oocytes at constant temperature. Sample was suspended in isotonic PBS+BSA and extracellular ice was seeded at -1°C prior to rapid drop of temperature to -8°C. Arrows indicate the oocytes with intracellular ice. Scale shows 100 μm.

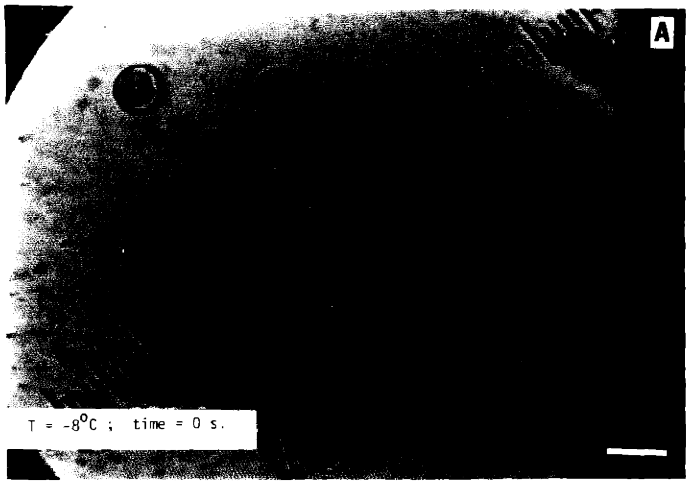

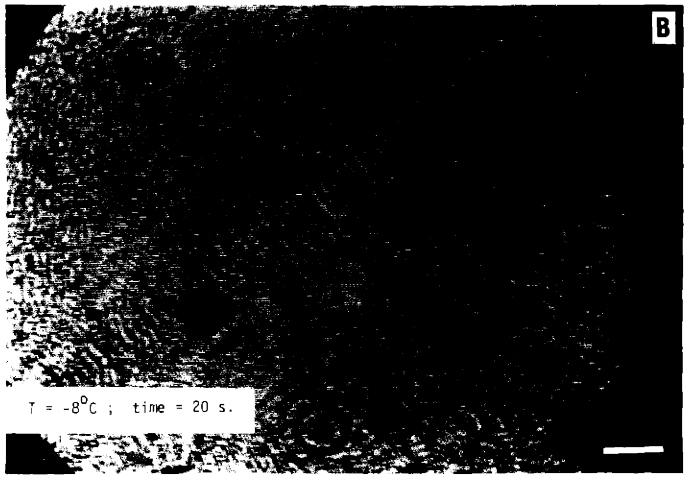

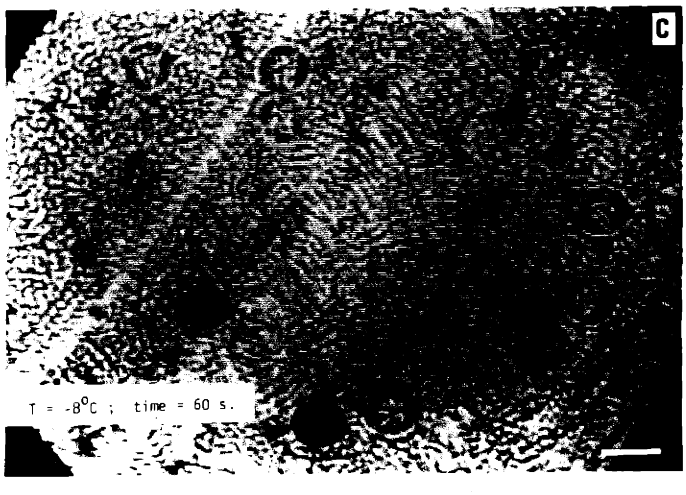

PLATE-6

FIGURE.4.18. Sequence of micrograph illustrating the mouse oocytes in isotonic PBS+BSA undercooled to -21°C at 120°C/min in the absence of extracellular ice. The suspending solution and the oocytes nucleated spontaneously at -21°C. Scale shows 100 μm.

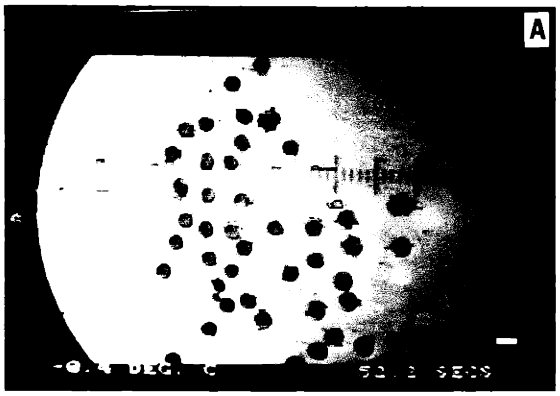

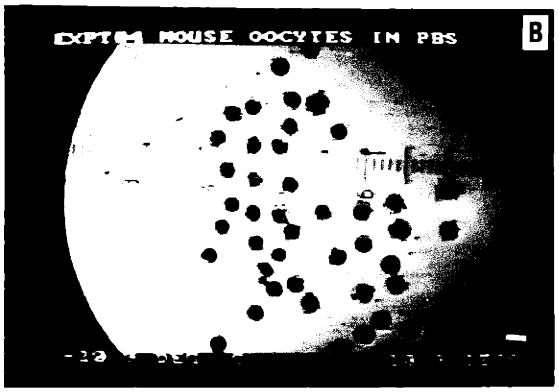

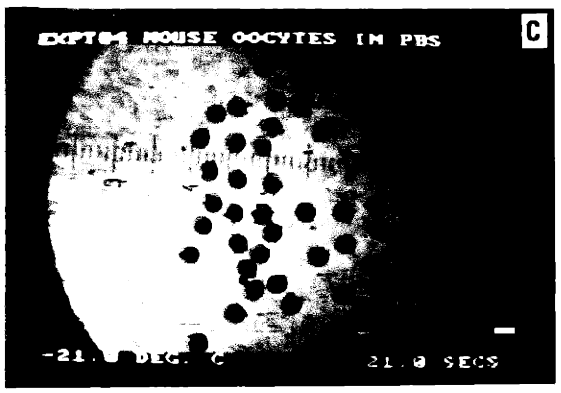

PLATE-7

experiments is that the intracellular nucleation is catalyzed by the presence of the extracellular ice. No current model explains the mechanism by which external ice causes the formation of the internal ice. The mechanism of the internal ice formation cannot be simply determined from these experiments by simple observation of the results. Therefore, rather than pursuing an extensive experimental investigation into the kinetics of ice formation in oocytes, it is more important to develop a theoretical model to analyze the kinetics and the thermodynamics of intracellular nucleation. The model may serve as a guideline for future experimental work to gain a better understanding of the physics for the mechanism of ice formation inside biological cells.

CHAPTER V

THERMODYNAMICS OF WATER AND ION TRANSPORT DURING FREEZING OF BIOLOGICAL CELLS

5.1. Thermodynamics of Water Transport During Freezing

Introduction

The mass transport of water across the plasma membrane and the amount of water remaining within the cell during freezing play a very significant role in cell damage. In recent years, several models have been developed to describe the physicochemical events occurring during the freezing and thawing of biological cells. The first of such models was Mazur's publication in 1963. Mazur developed a mathematical model to predict the water content of cells subjected to freezing, the essence of which became the basis of almost all subsequent treatments. For a cell suspended in a freezing medium and subjected to sub-freezing temperatures, ice preferentially forms outside the cell in the freezing medium. Due to the precipitation of the pure ice, the partially frozen extracellular solution has a lower chemical potential than the water in the intracellular solution. As a result, the thermodynamic equilibrium that exists across the cell membrane between the cell contents and the

freezing medium is upset, and the cell responds by expressing water across the cell membrane. Three biophysical parameters that are shown to be important in determining the thermodynamic states of intracellular solution during freezing are: (1) surface area-to-volume ratio (SA/V); (2) the hydraulic conductivity of the plasma membrane (L_{pg}); and (3) the activation energy of the hydraulic conductivity (E_{Lp}, i.e. its temperature dependence). Mazur's model predict that high SA/V and L_{pg}, and low E_{Lp} values would increase the water transport during a freezing protocol.

Most of the work since Mazur's historical publication in 1963 is concentrated on (i) improving some of the simplifying assumptions; (ii) develop new experimental techniques to measure the permeability parameters; and (iii) correlate theory with experiments using sophisticated curve fitting techniques. Theoretical improvements in the modelling include non-ideality of the protoplasm and intracellular temperature gradients (Mansoori, 1975), effect of extracellular undercooling and concentration dependence of water permeability (Silvares, 1974; Silvares et al., 1975), solution non-ideality (Levin et al., 1977a), concentration polarization across the plasma membrane (Levin et al., 1977b), multi-component non-ideal internal solution (Levin et al., 1978), cluster of packed cells (Levin et al., 1977c), thermal gradients across the cell volume (Hua et al., 1982), water permeability as a function of internal and/or external concentration (Scheiwe & Korber, 1983; Schwartz & Diller, 1983a-c), non-linear cooling rates (Cosman & Cravalho, 1978; Novikov et al., 1985), distributed

analysis of cell parameters (Cosman, 1983; Orrico et al., 1988). The improvements in the area of experimental techniques to determine response of cells during freezing starts with the design of the modern cryomicroscopy system by Diller & Cravalho in 1970. Improved image analysis techniques (see Chapter III), various freezing stage designs (see Chapter III), diffusion chamber designs (McGrath, 1985; Porsche et al., 1986), unidirectional freezing stages (Kourosh & Diller, 1984; Rubinski & Ikeda, 1985), are some of the important advancements in the field if not all. Combined with these improved experimental techniques is the use of non-linear regression analysis applied to differential equations to determine water permeability parameters by statistically fitting the theoretical models to sets of experimental data of cell as a function of temperature (Stusnick & Hurst, 1972; Levin et al., 1979; Toner, 1985).

In the rest of this section, we will underline the basic principles of water transport across the plasma membrane and determine the water permeability parameters for mouse oocytes. A distributed analysis will be used to show the deviation of the behavior of oocytes from the mean behavior during freezing due to the individual variations in their permeability parameters. Computer simulations will be included to investigate the water content and the undercooling of the cytoplasm during freezing.

Theory of Water Transport

The biological cell immersed in its suspending medium may be modelled as an isolated cell in a salt solution consisted of salt, n_s^{ex}, and water, n_w^{ex} in the absence of cryophylactic agents. The cell interior is assumed to be composed of only salt (completely dissociated) given by number of moles of salt, n_s^{in}, and water, n_w^{in}, and an osmotically inactive cell volume, V_b, composed of hydration water, proteins and macromolecules. The physical model is shown schematically in Fig.5.1. The control volume is divided into two compartments by ideally semi-permeable cell plasma membrane. The two compartments are in chemical equilibrium across the membrane until the ice is formed in the extracellular solution converting a given portion of n_w^{ex} to n_{ice}^{ex}. Since ice is pure water this increases the electrolyte concentration of the extracellular compartment and the chemical disequilibrium prevails favoring the flux of water from internal compartment to external compartment. The water flux for a thin membrane, J_w, is given by an expression of the form

$$J_w = \frac{L_p}{v_w^2} (\mu_w^{in} - \mu_w^{ex}) \qquad (5.1)$$

where μ_w^{in} and μ_w^{ex} are, respectively, the chemical potentials of the water within the intra- and extra-cellular solutions, L_p is the water permeability of the plasma membrane, and v_w is the apparent molar volume of water (Katchalsky & Curran 1981). The chemical potential of water in each compartment may be written, under the assumption that

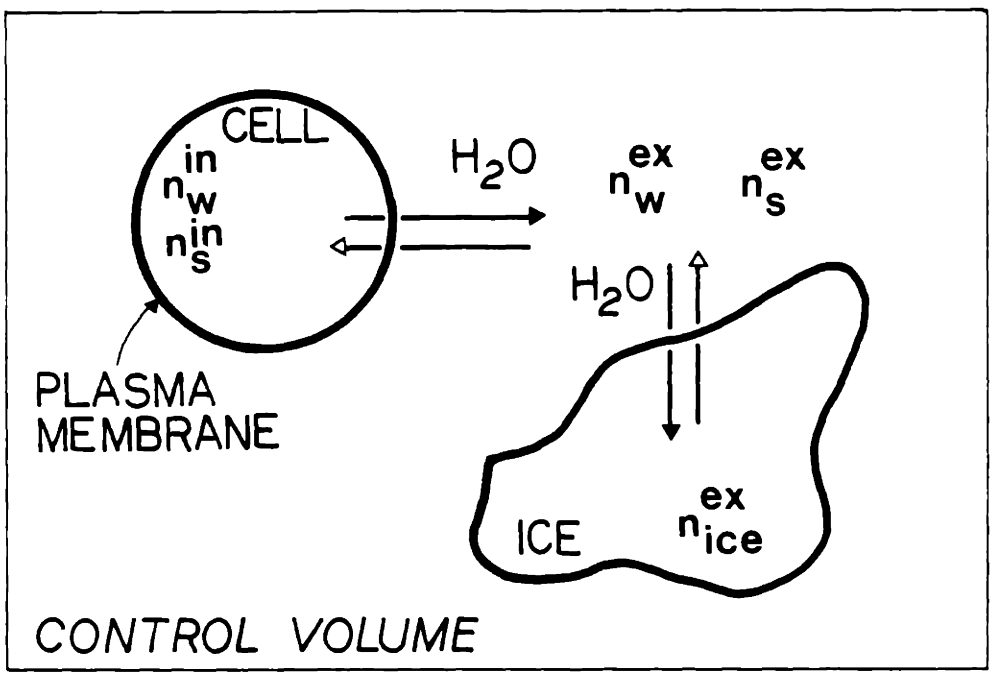

FIGURE.5.1. Model for water transport across the membrane of an unprotected oocyte.

the solution is an ideal one, as

$$\mu_w = \mu_w^*(T) + RT \ln(a_w) + v_w p \qquad (5.2)$$

where $\mu_w^*(T)$ is the reference chemical potential, a_w is the activity of water, p is the hydrostatic pressure, T is the temperature and R is the gas constant. Using Eqs.(5.1) and (5.2), we can write

$$J_w = \frac{L_p}{v_w^2} \{(\mu^{*in}(T) - \mu^{*ex}(T)) + v_w(p^{in} - p^{ex}) + RT \ln(a_w^{in}/a_w^{ex})\} \qquad (5.3)$$

Mansoori (1975) and Hua et al. (1975) analyzed the temperature gradients across the cell volume and showed that it is reasonable to assume that there are no significant temperature gradients within the small cells. Hua et al.'s result suggests that the temperature gradient across the membrane during freezing is less than 0.01 K and its effect on water transport is negligible. Hence, we can let $\mu_w^{*in}(T) = \mu_w^{*ex}(T)$ in Eq.(5.3). In addition, Schwartz & Diller (1983b) analyzed the effect of hydrostatic pressure in the freezing of yeast cells. Their result suggests that osmotic forces are significant in dictating transmembrane fluxes. Therefore, the turgor pressure term can also be ignored in Eq.(5.3) to obtain

$$J_w = \frac{L_p}{v_w^2} RT \ln (a_w^{in}/a_w^{ex}) \qquad (5.4)$$

The molar flux of water for constant apparent volume and a cell

permeable to the solvent but impermeable to solutes is defined by

$$J_w = -\frac{1}{A_c}\frac{dn_w^{in}}{dt} = -\frac{1}{A_c v_w}\frac{dV_w}{dt} = -\frac{1}{A_c v_w}\frac{dV_c}{dt} \qquad (5.5)$$

where V_w and V_c (= $V_w + V_b$) are the water and total cell volumes, and A_c is the cell surface area. Substituting Eq.(5.5) in Eq.(5.4), one can get

$$\frac{dV_c}{dt} = -\frac{L_p}{v_w} A_c RT \ln (a_w^{in}/a_w^{ex}) \qquad (5.6)$$

During freezing of cells, the temperature is changed at a constant rate $B = -dT/dt$. A coordinate transformation from time to temperature can be done as follows

$$\frac{dV_c}{dT} = \frac{L_p A_c RT}{v_w B} \ln (a_w^{in}/a_w^{ex}) \qquad (5.7)$$

In order to evaluate Eq.(5.7) values are needed for a_w^{in}, a_w^{ex}, and L_p.

* Water Activity in the Intracellular Solution (a_w^{in}): the intracellular solution can be modelled as an ideal solution for which the water activity is equal to its mole fraction

$$a_w^{in} = x_w^{in} \qquad (5.8)$$

The intracellular mole fraction of water, x_w^{in}, is a function of the

cell solute content and it can be written as

$$x_w^{in} = \frac{V_w}{V_w + 2n_s^{in}\upsilon_w} = \frac{(V_c - V_b)}{(V_c - V_b) + 2n_s^{in}\upsilon_w} \quad (5.9)$$

assuming fully dissociated salt with a dissociation constant of two.

* Water Activity in the Extracellular Solution (a_w^{ex}): if the extracellular medium is modelled as an ideal solution in continuous equilibrium with a pure crystalline phase (ice), The Gibbs phase rule states that two intensive properties, such as temperature and pressure, are sufficient to describe the system. Therefore, a Gibbs-Helmholtz relation can be used to relate extracellular water activity to the temperature at constant pressure

$$\frac{d}{dT}(\ln a_w^{ex})|_p = \frac{\Delta H_f}{RT^2} \quad (5.10)$$

where ΔH_f is the latent heat of fusion of water. Assuming that ΔH_f is constant over the temperature range of interest Eq.(5.10) can be integrated to give

$$\ln a_w^{ex} = \frac{\Delta H_f}{R} \left(\frac{1}{T_R} - \frac{1}{T} \right) \quad (5.11)$$

where T_R is the melting temperature of pure water (273.15 K). Other studies have assumed that ΔH_f varies with temperature (Mazur, 1963;

Schwartz & Diller 1983a-c; Toner 1985) but it is determined that the effect of this variation is not significant.

* Water Permeability of the Plasma Membrane: Mazur (1963) showed that a major source of error can be introduced by an incorrect estimation of water permeability at subzero temperatures. Shabana and McGrath's (1988) recent analysis quantified further the sensitivity of water transport equation to L_p. Water permeability may be both temperature and composition dependent. Although the temperature dependence of water permeability can be explained on the basis of theoretical transport models (Levin et al., 1976b), there are no a priori reasons to believe that L_p is composition dependent.

Rich et al. (1968) measured the osmotic water permeability for human and dog red cells as a function of external medium osmolality and found that it depends on the extracellular solution concentration. They reported that the water permeability falls by a factor of 2.45 when the external osmolality is increased from 199 to 516 mosm/kg. A similar decrease was also observed for dog red cells. Another study on the effect of concentration on water permeability has been published by Blum & Forster (1970). Their result agreed with Rich et al. (1968). Terwilliger & Solomon (1981) hypothesized that large osmotic gradients tend to introduce errors that exaggerate the dependence of L_p on osmolality. Their experimental results showed no concentration dependence for small osmotic perturbations of osmolality around the

isotonic concentration (184 to 365 mosm). Recently, Diller & Bradley (1984) measured the water permeability of human granulocytes in both hypotonic and hypertonic solutions in the range of 145 to 833 mosm/kg. They obtained a linear dependence of permeability on extracellular osmolality which does not correspond to the exponential correlations used by prior investigators. Some other researchers have also reported a decrease in the water permeability with an increase in the external concentration when cryoprotectants, such as Me_2SO or glycerol, are used (Papanek, 1978; Rule et al., 1980). There are other reports on osmolality dependence of the water permeability at subzero temperatures (Scheiwe & Korber, 1983; Schwartz & Diller, 1983c). Most of these studies assumed various empirical relationships for composition dependence of permeability and none of them are conclusive. Given the lack of knowledge on composition dependence of water permeability, we will assume that L_p can be expressed simply as a function of temperature

$$L_p = L_{pg} \exp\left[- \frac{E_{Lp}}{R} \left(\frac{1}{T} - \frac{1}{T_R} \right) \right] \qquad (5.12)$$

where L_{pg} is the reference hydraulic conductivity at 0°C, E_{Lp} is the activation energy for permeation of water, and T_R is the reference temperature (273.15 K). In this study T_R is chosen to be 273.15 K instead of 293.15 K as in most of the permeability studies. The reason for this choice is that we are concerned with freezing behavior of cells. It seems more reasonable to use a reference temperature in the subzero range rather than extrapolate suprazero results to subzero temperatures.

Finally combining Eqs.(5.9), (5.11), (5.12) in Eq.(5.7), the expression for change in water volume in response to freezing of extracellular solution can be obtained

$$\frac{dV_c}{dT} = \frac{L_{pg}\, A_c\, RT}{v_w\, B} \exp\left[- \frac{E_{Lp}}{R} \left(\frac{1}{T} - \frac{1}{T_R} \right) \right] \times \left\{ \ln \left[\frac{(V_c - V_b)}{(V_c - V_b) + 2n_s^{in}\, v_w} \right] - \frac{\Delta H_f}{R} \left(\frac{1}{T_R} - \frac{1}{T} \right) \right] \tag{5.13}$$

In this equation the cell area, A_c, may be related to cell volume by assuming a spherical geometry such that

$$\frac{A_c}{A_o} = \left[\frac{V_c}{V_o} \right]^{2/3} \tag{5.14}$$

where A_o and V_o refer to initial surface area and cell volume, respectively. The initial condition for Eq.(5.13) is

$$V_c = V_o \qquad \text{at} \qquad T = T_{init} \tag{5.15}$$

The non-linear differential equation can be solved by means of a 4th order Runge-Kutta scheme. It is worth mentioning here that Runge-Kutta solution does not require very small step size used in iterative procedures (Mazur, 1963). In iterative schemes, a step size of 0.005°C is necessary to obtain accurate results (Mazur 1963). However, step sizes as large as 1°C can be used with Runge-Kutta scheme. In this study, a step size of 0.1°C was used to solve the water transport equation. The results of Eq.(5.13) can be represented as volume change

vs. temperature curves which can be directly correlated with experimental results. The numerical fitting technique of Marquart (1963) and Bevington (1959) are used to obtain "best-fit" values for permeability parameters from experimental volume vs. temperature curves. The fitting technique is also used for nucleation parameters in this study and is briefly outlined in Chapter VI (section 6.6).

The effects of various assumptions on water transport are summarized in Table 5.1.

Experimental Results

The permeability at 0 C, L_{pg}, and the activation energy, E_{Lp}, of unfertilized ova were determined simultaneously by fitting experimentally measured volumes of ova (Fig.4.1) to theoretically predicted volume/temperature curves using non-linear regression analysis. The mean value and standard deviation of L_{pg} were found to be 0.044 and 0.008 μm/min-atm and the mean value and standard deviation of E_{Lp} were found to be 13.3 and 2.5 kcal/mol for unfertilized ova. Leibo (1980) conducted permeability experiments at constant suprazero temperatures with unfertilized mouse ova. He reports a value of 0.44 μm/min-atm for permeability at 20 C and a value of 14.5 kcal/mol for activation energy. If Leibo's value of L_p is extrapolated to 0 C using Eq.(5.12) and Leibo's value of E_{Lp}, one finds L_{pg} to be 0.074 μm/min-atm. This extrapolated value agrees closely with the L_{pg} for fertilized

TABLE 5.1

ASSUMPTIONS IN WATER TRANSPORT MODEL

AND ESTIMATED MAGNITUDE OF ERROR

ASSUMPTION	ERROR	AUTHOR
1. Intra- & extra-cellular solution ideality	Small	Mazur 1963 Mansoori 1975 Levin et al. 1977a
2. Extracellular phase equilibrium between ice and solution	Negligible	Mazur 1963
3. Constant latent heat of fusion	Neglible	Mazur 1963 Schwartz & Diller 1983c Toner 1985
4. Constant no. moles of intra-cellular solution	Negligible	Mazur 1963 Silvares 1974
5. Concentration dependence of the water permeability	Moderate	Silvares 1974 Schwartz & Diller 1983c Scheiwe & Korber 1983
6. Thermal equilibrium between the cell and the environment	Negligible	Mazur 1963 Hua et al. 1982 Mansoori 1975
7. Transmembrane pressure equilibrium between the cell and the environment	Negligible	Schwarzt & Diller 1983b
8. Intracellular chemical potential equilibrium	Small to Moderate	Pushkar et al. 1976 Levin et al. 1978

ova found in this study.

Table 5.2 summarizes the mean values and the standard deviations for L_{pg}, E_{Lp}, and SA/V. Results of this study and others indicate that there is a great deal of individual variation in these parameters in the same cell type (Cosman, 1983). In order to predict the osmotic behavior during freezing of mouse ova or any cell which has biophysical parameters widely distributed, it is not sufficient to assume that a given cell will behave as the "mean" cell would. The probability of a cell having a certain set of biophysical parameters must be coupled with that cell's osmotic behavior. In the next section a probabilistic, distributed parameter approach is presented to model the behavior of ova during freezing.

Distributed Parameter Modelling.

Two major assumptions are made in the distributed parameter model: 1) the distribution of the biophysical parameters is due to actual variation in the parameters from ovum to ovum and not uncertainty in the experimental measurements and 2) the three distributed parameters used in this study, L_{pg}, E_{Lp} and SA/V, are assumed to be completely independent of each other. The numerical integration of Eq.(5.13) can be written symbolically:

$$V_c = \text{function}(L_{pg}, E_{Lp}, SA/V, T) \qquad (5.16)$$

The results of this study presented indicate that L_{pg}, E_{Lp} and SA/V are

TABLE 5.2

METAPHASE II MOUSE OOCYTE PROPERTIES

PROPERTY	MEAN	STANDARD DEVIATION	UNITS
L_{pg}	0.044	0.008	μm/min-atm
E_{Lp}	13.3	2.5	kcal/mole
SA/V	79.41	4.92	1/μm

distributed parameters. The notation Λ_L, Λ_E and Λ_S denote the distribution or probability density function of permeability, activation energy and surface area-to-volume ratio, respectively. Using this notation, one finds at a specified cooling rate:

$$\Lambda_V = \text{function}(\Lambda_L, \Lambda_E, \Lambda_S, T) \qquad (5.17)$$

Eq.(5.17) states that at each temperature a probability density function of volume Λ_V can be found by combining the probability density functions of the distributed parameters into the integration of Eq.(5.13). Practically, the volume probability density function can be determined by a computer model. In this model, the probability density functions of L_{pg}, E_{Lp} are approximated by a finite number of representative values of these parameters. Associated with each value of the parameters is a probability. This probability can be most easily described as the likelihood that this value will occur relative to the other representative values. In the model, Eq.(5.13) is integrated with a particular combination of representative values, and a volume/temperature curve is generated. The values of this curve are then rounded so that they can be sorted into a specified number of discrete volume levels. This integration of Eq.(5.13) is repeated with another combination of parameters, and another volume/temperature curve is generated. These integrations continue until every combination of the parameters has been used. A weight is associated with each combination of parameters. This weight is simply the probability that that particular combination will occur, and it is equal to the product of the probabilities associated with each of the parameters in that combination.

In this study the probability density functions of each parameter were approximated by five points spaced one standard deviation apart starting two standard deviations less than the mean and continuing to two standard deviations more than the mean. This range corresponds to 98.7% of the cumulative distribution. Thus, there were 5^3 or 125 possible combinations of the three parameters. Fig.5.2 shows the volume probability density functions for various temperatures of the probability matrix for unfertilized mouse ova. As one can see, the probability density function is constrained to start at 100% probability when normalized volume is one at the extracellular nucleation temperature. As the cooling continues at -2°C/min, the function becomes more spread out, until at about -16 C the function becomes skewed since the volume is constrained at the equilibrium volume. The spreading occurs because of the distributed values of the biophysical values. Results agree well with the observed experimental volume curves depicted in Fig.4.1.

A very important conclusion of this analysis is that any study of ice-nucleation at low cooling rates will have a large experimental discrepancy because of this distributed behavior of oocytes during freezing. However, at higher cooling rates, there will be no time for water transport and oocytes will remain constant at their initial volume during freezing until they form intracellular ice. Since the initial diameter distribution is narrow (Fig.4.3), the undesired effect of distributed response of oocytes during freezing can be overcome by using

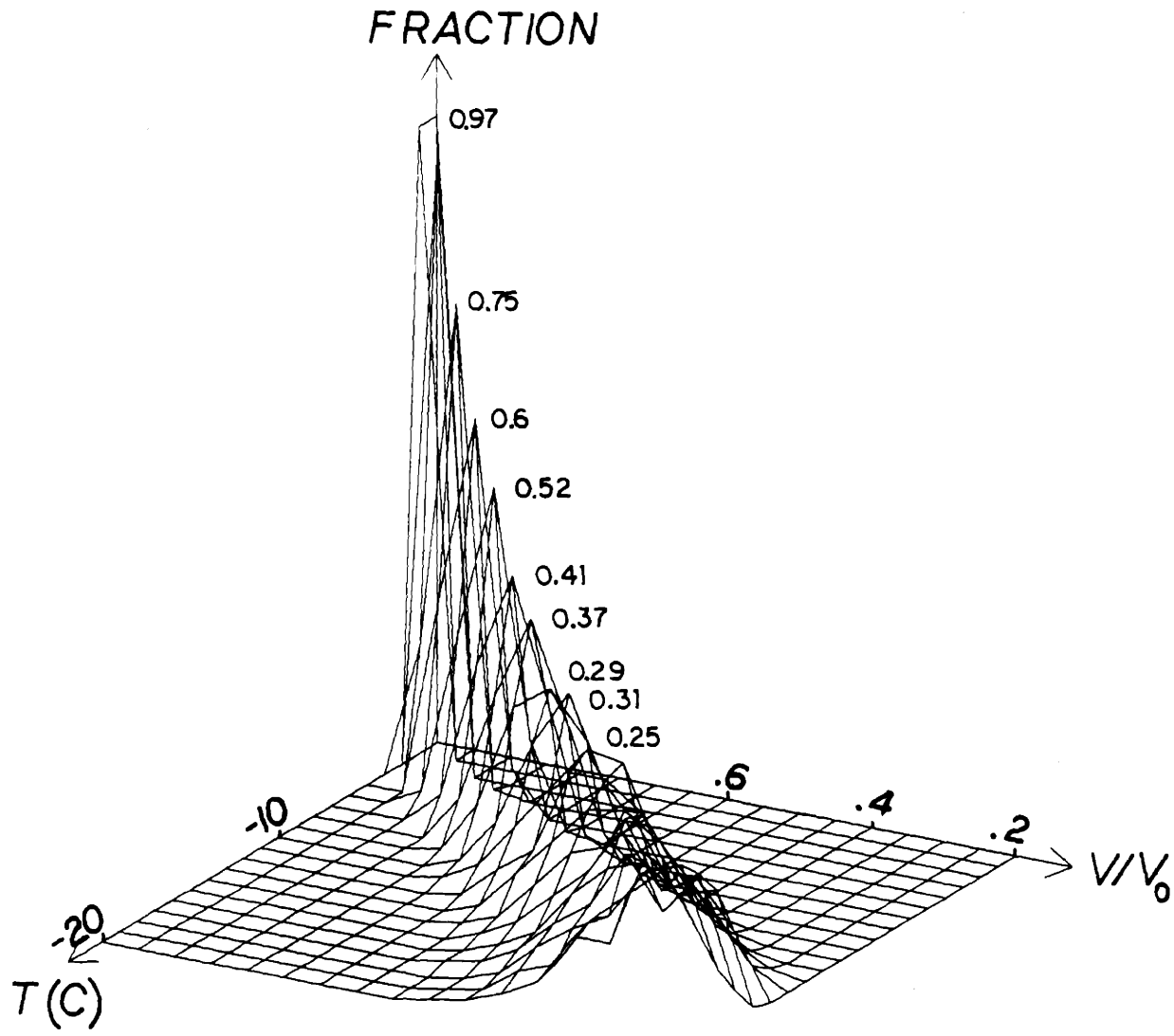

FIGURE.5.2. Volume probability density functions at various temperatures during freezing at -2°C/min.

high enough cooling rates to impede any water transport. In the next section we will analyze some of the experimental parameters that affect the behavior of oocytes using the simple mean behavior of the oocytes.

Computer Simulations

Computer simulations of water transport from mouse oocytes during freezing were performed using the mean behavior of oocytes. Fig.5.3 shows the effect of the cooling rate, B, on the predicted displacement from equilibrium states for oocytes when the freezing starts at the equilibrium freezing point. The curve displays the normalized cell water volume as a function of temperature. The equilibrium curve represents the normalized water volume in a single oocyte cooled infinitely slowly to various subzero temperatures. This curve is generated from Eq.(5.13) assuming $dV_c/dT = 0$ at equilibrium. The figure illustrates a highly significant effect of the cooling rate on the water content of an oocyte at any subzero temperature. At approximately -10°C the water content of the oocyte cooled at 2°C/min is about 50% of its initial water content. At the same intermediate temperature the predicted water content of an oocyte cooled at a faster rate is higher. At rates above 40°C/min, the water transport is negligible. There is only 8% and 3% water loss from an oocyte cooled to -20°C at rates of 40 and 120°C/min, respectively.

The amount of the undercooling of the cytoplasm can be calculated using Fig.5.3. Given the cell volume at an intermediate temperature the

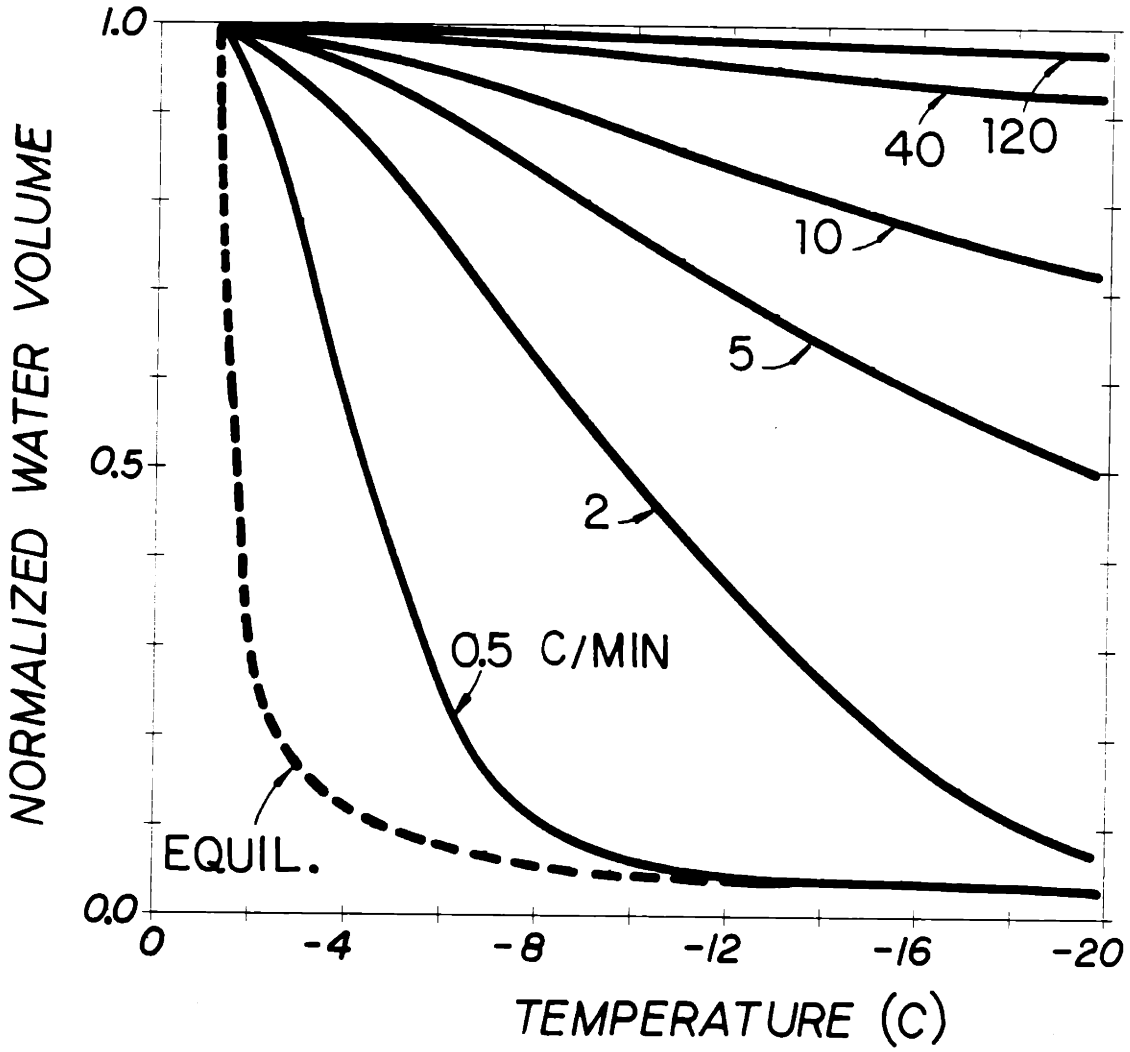

FIGURE.5.3. Theoretical normalized water volume vs. temperature of mouse oocytes as a function of cooling rate. Extracellular seeding temperature is -0.615°C.

concentration of the intracellular solution can be estimated from the static behavior of oocytes depicted in Fig.4.2. Then the osmolality of the intracellular solution can be converted to the equilibrium freezing temperature of the cytoplasm using the well known $T_f = -1.858 \times osm$ relation. The cytoplasmic undercooling is the difference between the actual temperature and the equilibrium freezing temperature of the cytoplasm. The amount of intracellular undercooling as a function of temperature obtained from Fig.5.3 is shown in Fig.5.4 as a function of different cooling rates. As can be seen from this figure, the amount of the intracellular undercooling becomes appreciable when the cooling rate exceeds $0.5^{o}C/min$.

Another factor that effects the freezing behavior of oocytes is the amount of initial external undercooling prior to the start of the cooling. If the freezing of the oocytes starts at a temperature lower than the equilibrium freezing temperature of the suspending medium than there will be less time for oocytes to dehydrate during cooling. Consequently there will be more water retained in the oocytes at any given temperature. This behavior is illustrated in Fig.5.5. The normalized water content of an oocyte cooled at a rate $2^{o}C/min$ down to $-15^{o}C$ is 22, 31, 52, and 83% for extracellular undercoolings of 1, 5, 9, and $13^{o}C$ prior to the formation of the external ice, respectively.

The behavior of mouse oocytes when they are exposed to external ice at constant temperature is shown in Fig.5.6. As can be seen from this figure, the time constant to reach the equilibrium volume after exposure

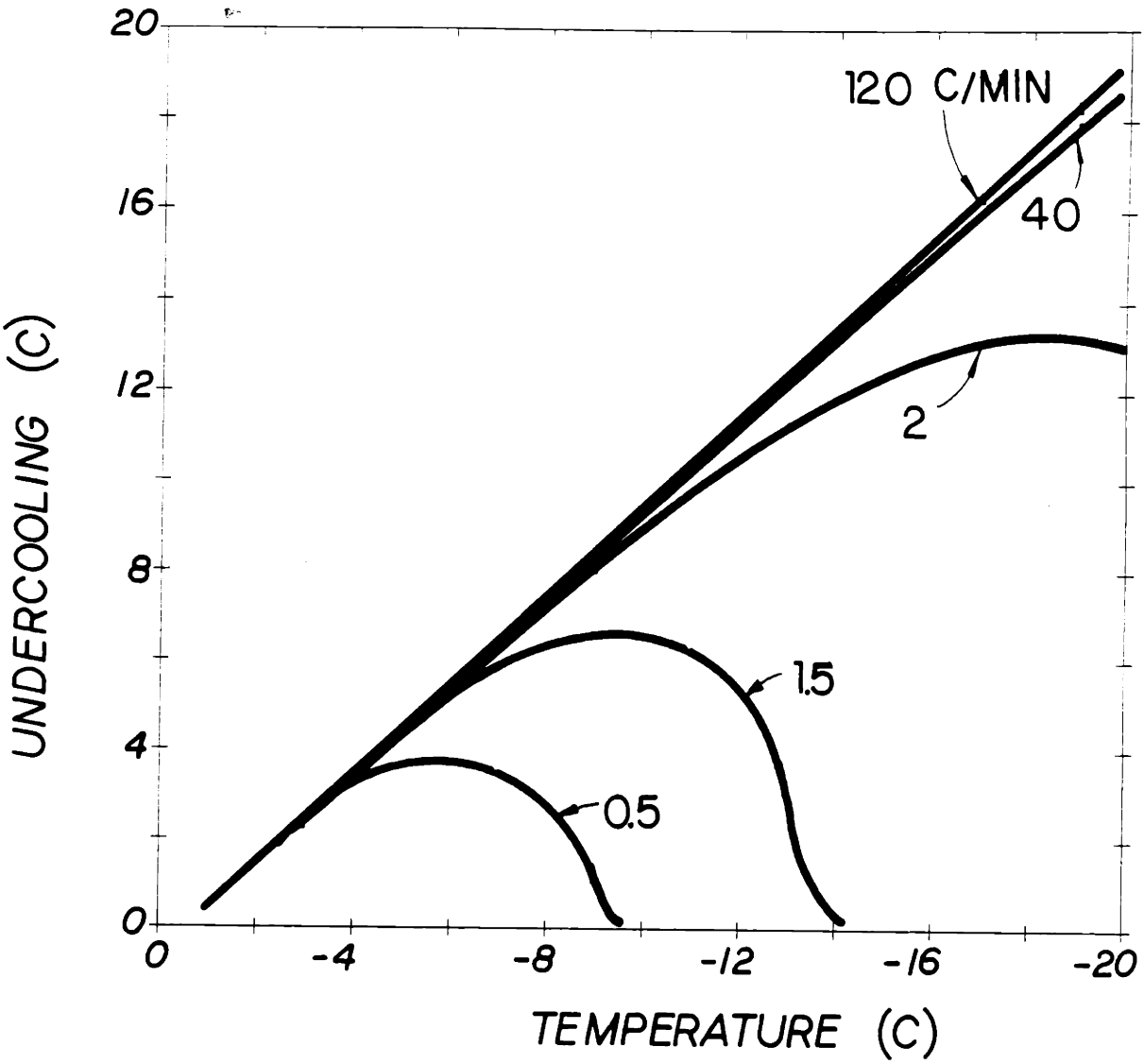

FIGURE.5.4. Theoretical undercooling of the cytoplasm of an oocyte as a function of temperature for oocytes suspended in isotonic PBS. Extracellular seeding temperature is -0.615°C. Cooling rates are indicated for each curve.

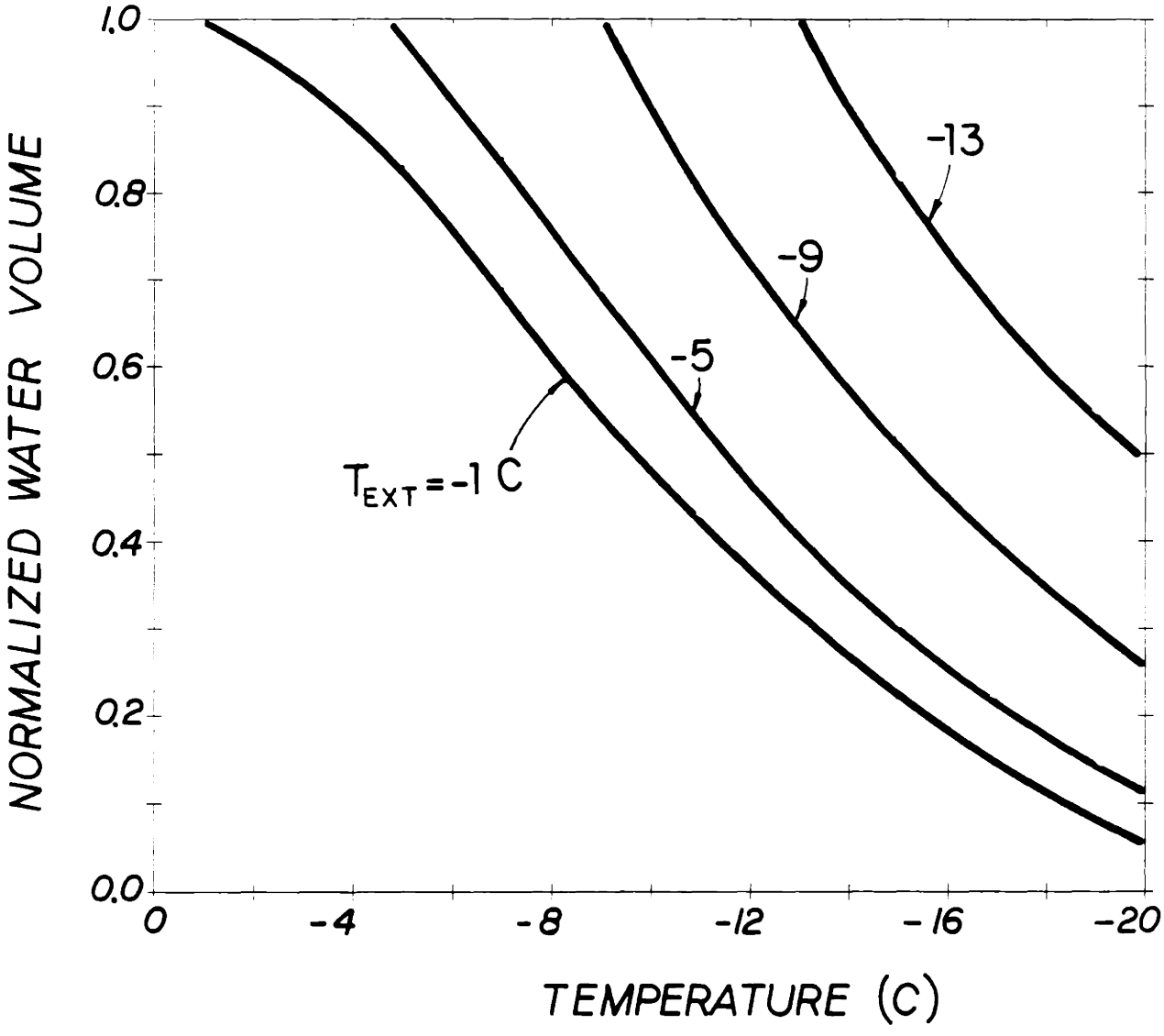

FIGURE.5.5. Theoretical normalized volume vs. temperature curves for various extracellular seeding temperatures. Oocytes are suspended in isotonic PBS solution. Cooling rate is 2°C/min.

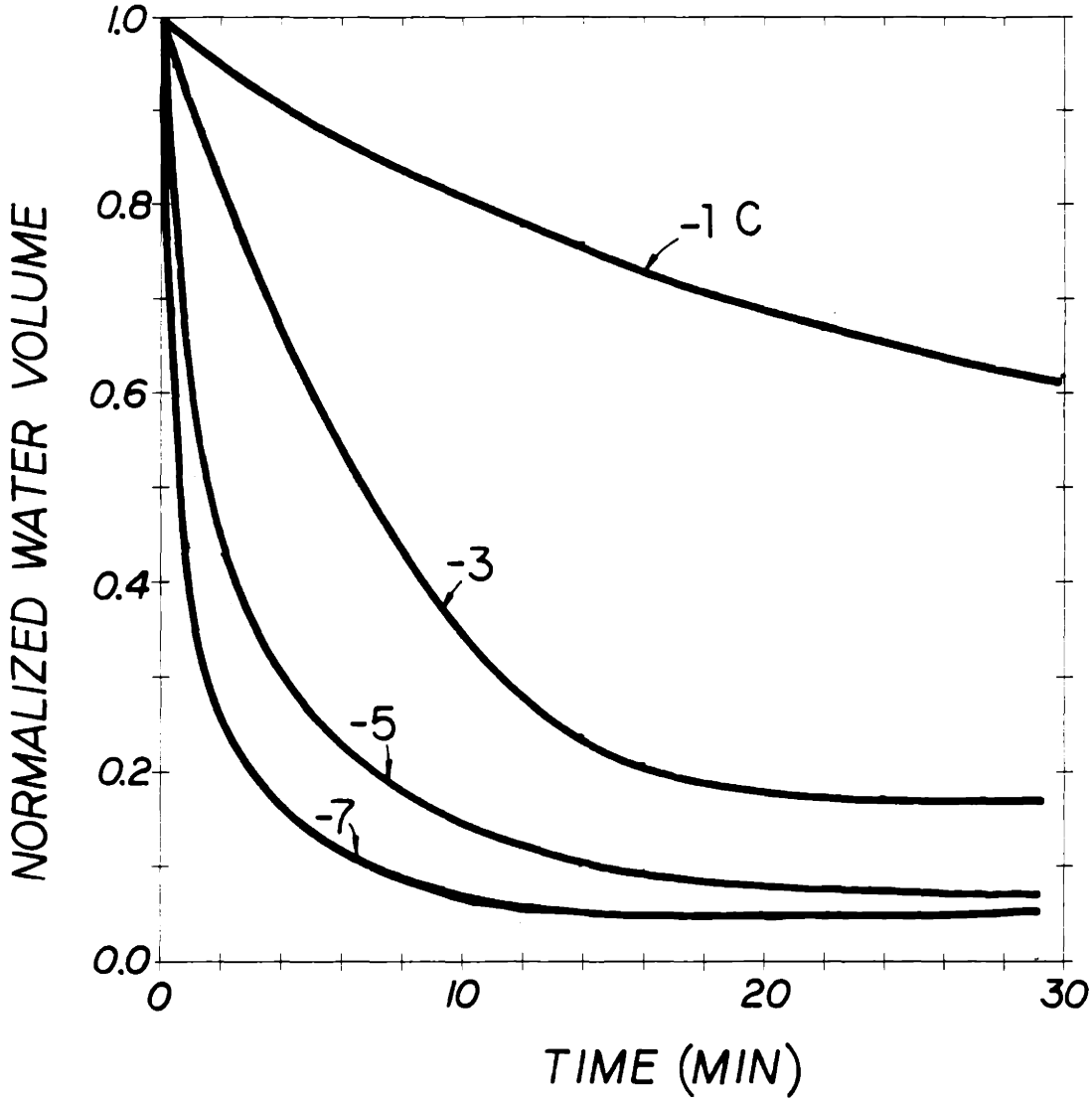

FIGURE.5.6. Theoretical normalized water volume vs. temperature curves at constant temperatures. Oocytes suspended in isotonic PBS solution.

to external ice becomes shorter for higher temperatures. This is due to high driving force exerted on the oocytes by the formation of external ice at lower temperatures. This constant temperature behavior is important for the analysis of the ice nucleation kinetics inside the oocytes.

In summary, we have used the mean permeability parameters of oocytes to predict their behavior during freezing. It is shown that the water content and the undercooling of the intracellular milieu can be altered significantly during freezing. This behavior is fundamentally important in ice nucleation inside the oocytes and will be discussed in the next chapter.

5.2. Ion Transport and Trans-Membrane Potential During Freezing of Biological Cells

Introduction

The sole effect of external ice formation during freezing of biological cells is not the water efflux. One also needs to investigate the diffusion of ionic species during freezing. It is well known from electro-diffusion theories that any alteration on the ionic composition of the suspending medium will result in a non-steady state movement of ions across the plasma membrane to reach a new intra- and extra-cellular equilibrium condition. Such a change will change the thermodynamic

state of the plasma membrane which we strongly believe to play a major role in intracellular ice formation (this will be discussed in Chapter VII). This chapter will present a review of the basic electrodiffusion theory as applied to mouse oocytes during freezing.

The bulk of the cytoplasm and the external solution is electrically neutral with an equal number of positive and negative charges. However, cells have an electrical charge layer on their plasma membrane resulting from a charge separation over a very narrow region on either side of the membrane. In a cell at rest, the outside of the cell is at the more positive potential, but of course this does not necessarily imply that the outside surface carries a net positive charge. The membrane is able to maintain a separation of charge because it constitutes a permeability barrier to the diffusion of ions. This separation of charge is responsible for the resting membrane potential, E_R. The more general term membrane potential (E_m) refers to the potential across the membrane at any moment, including resting and activation states of the membrane.

The accurate measurements of the resting membrane potential as well as ion flux measurements (Keynes & Lewis, 1951) across membranes showed the insufficiency of earlier theories of electrodiffusion based on the semi-permeable nature of most biological cell membranes with respect to ions. In 1949, Hodgkin & Katz described the observed membrane potential by ion diffusion potential theory and a difference in ionic mobilities (see also Goldman, 1943).

Although the Goldman-Hodgkin-Katz (GDH) theory has been used widely to investigate the membrane potential of many biological cells, there have been cases where the model was not adequately describing the electrochemical phenomena (see Ohki, 1986)). This led investigators to improve the ion diffusion model by introducing the existence of net electrical charge on membrane surfaces. This net electrical charge will give rise to a surface potential. Diffusible cations will be attracted to the surface and anions will be repelled due to the fact that membranes are negatively charged. This would create an electrical double layer described by a potential decreasing as one proceeds out into the solution. The fixed electrical charges on the membrane surface may have a significant influence on the magnitude of the potential difference acting across the membrane (Pethig, 1986). The electrical double layer effects were first formulated by Gouy (1917) and Chapman (1913) (GC) and later extended by Grahame (1947). The model has been extensively reviewed by Brown (1974) and recently extended by Ohki (1986), and Ohki & Ohshima (1986). Application of the constant field (GHK) and the surface potential theories to squid axon gave relatively good results which are the same degree of deviation to the experimental data (Ohki, 1986). However, the overall experimental results were found to be explained better by the surface diffusion potential equation.

The use of surface potential theory requires the knowledge of membrane surfaces charge densities. The conventional method to estimate surface charge density from cell electrophoretic mobility by assuming zero thickness of the surface charge layer may result in largely

underestimated values of those for the membrane having the non-zero thickness of the surface charge layer (Ohki & Ohshima, 1986). Given the uncertainties involved in experimental techniques and the theoretical difficulties associated with a very complex situation such as freezing of cells, we have decided to use diffusion potential theory in our analysis. This will give us an order of magnitude estimate about the changes occurring in the plasma membrane during freezing. The only time that the theory of electrodiffusion was applied to freezing of cells was Silvares's (1974) work on red blood cells. Silvares showed that the use of GHK theory as applied to freezing can adequately describe the changes in membrane potential. In the rest of this chapter we will develop the theoretical model for diffusion potential theory as applied to mouse oocytes.

Theory of Ion Transport Across Biological Membranes During Freezing

The migration of charged particles through biological membranes will take place due to the total driving force consisting of the concentration gradients for various charged particles and the electrical field effects. The frictional forces opposes the movement of the charged particle. A steady condition is reached when the driving force, F_d, and the resistance force, f_R, acting on the moving particle are equal. Hence, the particle moves with a constant velocity, v, such that

$$v = \frac{F_d}{f_R} \qquad (5.18)$$

The frictional resistance for a spherical particle can be expressed by Stoke's formula

$$f_R = 6\pi\eta r_p \tag{5.19}$$

where η is the viscosity of the suspension, r_p is the radius of the particle. Using Eq.(5.18) and (5.19), the velocity can be written as

$$v = \frac{F_d}{6\pi\eta r_p} \tag{5.20}$$

The force acting on one particle is equal to the force acting on one mole of particles divided by Avagadro's number, N_{AV}

$$F_d = \frac{\text{(total driving force)}}{N_{AV}} \tag{5.21}$$

The flux, Φ, can be written as the velocity of particles multiplied by the molar concentration of the substance such as

$$\Phi = vc \tag{5.22}$$

Substituting Eqs.(5.19), (5.20) into Eq.(5.22) yields

$$\Phi = \frac{1}{N_{AV}\, 6\pi\eta r_p}\, c\ \text{(total driving force)} \tag{5.23}$$

In this equation the factor $1/N_{AV}6\pi\eta r_p$ is defined as the mobility of the

ion and is represented by the symbol U. In the presence of a gradient of electrical potential and a gradient of chemical potential, the resulting process of electrodiffusion may be described as the sum of diffusion and migration fluxes. Hence, Eq.(5.23) yields

$$\Phi = - cU \, \text{grad}(\mu + z_v F_r \Psi) \qquad (5.24)$$

where z_v is the ionic valence, F_r is the Faraday constant and Ψ electrical potential. For the one dimensional case this equation reduces to

$$\Phi = - cU \left(\frac{\partial \mu}{\partial y} + z_v F_r \frac{\partial \Psi}{\partial y} \right) \qquad (5.25)$$

In the case of dilute solution $\mu = \mu_o + RT \ln c$ approximation for the chemical potential is valid and Eq.(5.25) can be expressed as

$$\Phi = - cU \left(RT \frac{\partial \ln c}{\partial y} + zF \frac{\partial \Psi}{\partial y} \right) \qquad (5.26)$$

$$\Phi = - RT \, U \frac{\partial c}{\partial y} - zF \, c \frac{\partial \Psi}{\partial y} \qquad (5.27)$$

since $d(\ln c) = dc/c$.

Goldman (1943) assumed that the potential profile between the two planes of the plasma membrane is linear, in other words the electrical field between them is constant. Under this assumption, Eq.(5.27) can be integrated to yield the well known "constant-field equation" for ion j

$$\Phi_j = z_v F_r U_j \frac{E_m}{\delta} \frac{c_j^{in} - c_j^{ex} e^{-zF E_m/RT}}{e^{-zF E_m/RT} - 1} \qquad (5.28)$$

where c^{in} and c^{ex} are the molar concentrations at the internal and external walls of the plasma membrane, E_m ($= \Psi^{in} - \Psi^{ex}$) is the membrane potential, δ is the thickness of the plasma membrane. Hodgkin and Katz (1949) made use of partition coefficients, k_p, in order to be able to use bulk concentration of ions in solution, $[c]^{in}$ and $[c]^{ex}$, rather than c^{in} and c^{ex}

$$\begin{aligned} c^{in} &= k_p [c]^{in} \\ c^{ex} &= k_p [c]^{ex} \end{aligned} \qquad (5.29)$$

By introducing the permeability constant for ion j as given by

$$P_j = \frac{RT U_j k_j}{\delta} \qquad (5.30)$$

and rearranging Eq.(5.28) for major constituents of the cell cytoplasm, namely Na^+, K^+ and Cl^- one can obtain (where $\xi = F_r/RT$):

$$\Phi_{Na^+} = P_{Na^+} \frac{\xi E_m}{e^{-\xi E_m} - 1} \left\{ [Na^+]^{in} - [Na^+]^{ex} e^{-\xi E_m} \right\} \qquad (5.31)$$

$$\Phi_{K^+} = P_{K^+} \frac{\xi E_m}{e^{-\xi E_m} - 1} \left\{ [K^+]^{in} - [K^+]^{ex} e^{-\xi E_m} \right\} \qquad (5.32)$$

$$\Phi_{Cl^-} = P_{Cl^-} \frac{\xi E_m}{e^{-\xi E_m} - 1} \left\{ [Cl^-]^{in} e^{-\xi E_m} - [Cl^-]^{ex} \right\} \qquad (5.33)$$

(z_V = -1 for chloride anions in Eq.(5.33). The electric neutrality can be satisfied only if the sum of fluxes of all cations are equal to the sum of fluxes of all anions such that

$$\Phi_{Na^+} + \Phi_{K^+} = \Phi_{Cl^-} \tag{5.34}$$

By substituting Eqs.(5.31)-(5.33) in Eq.(5.34), the expression for the membrane potential can be obtained as

$$E_m = \frac{RT}{F} \ln \left(\frac{P_{K^+} [K^+]^{ex} + P_{Na^+} [Na^+]^{ex} + P_{Cl^-} [Cl^-]^{in}}{P_{K^+} [K^+]^{in} + P_{Na^+} [Na^+]^{in} + P_{Cl^-} [Cl^-]^{ex}} \right) \tag{5.35}$$

Goldman's equation in the above form neglects the possible complications caused by the effects of electrogenic pumps on the membrane potential. The use of GHK equation in the presence of an electrogenic pump in the frog muscle was analyzed by Gedulding (1968). His result suggests that if pumps are only "slightly" electrogenic (i.e. less than 10^{-11} mol/cm^2/sec) the net diffusion current will not substantially affect the constant field equation. Since the active fluxes of Na^+ and K^+ were found to be 24×10^{-12} and 9×10^{-12} mol/cm^2/sec for mouse oocytes (Powers and Tupper, 1975), the constant field equation will be assumed to retain its validity. In addition, Frumento (1965) included the effect of active transport in the constant field equation. However, the active transport can be neglected at subzero temperatures (Frumento, 1965; Biggers et al., 1977).

Computer Simulations

The physical system used is displayed in Fig.5.7 where a single oocyte is immersed in an isotonic solution. The values of internal exchangable ionic concentrations and permeabilities given on Fig.5.7 are obtained from Powers & Tupper (1974, 1975). The concentration of the extracellular solution is isotonic PBS solution. Initially the system is in electrochemical and osmotic equilibrium.

Now assume that at time t = 0, the ionic concentration of the extracellular medium is increased to a certain uniform value throughout the external compartment due to the precipitation of pure ice at the beginning of the freezing. This will upset both the ionic and osmotic equilibrium across the plasma membrane. Ionic species and water will start moving across the plasma membrane to reach the new equilibrium state with the external milieu. The rate at which they can reach this new equilibrium state is a function of their transport characteristics across the plasma membrane and the rate of cooling in the case of freezing. This transient response cannot be modelled with Eq.(5.35). Equations modelling the coupled transport of ions and water should be solved simultaneously (Silvares, 1974). However, there are certain differences in ionic and osmotic responses which may allow to use Eq.(5.35) in a complex transient situation.

The water permeability of the plasma membrane is several orders-of-magnitude higher than the ionic permeabilities given in Fig.5.7. The

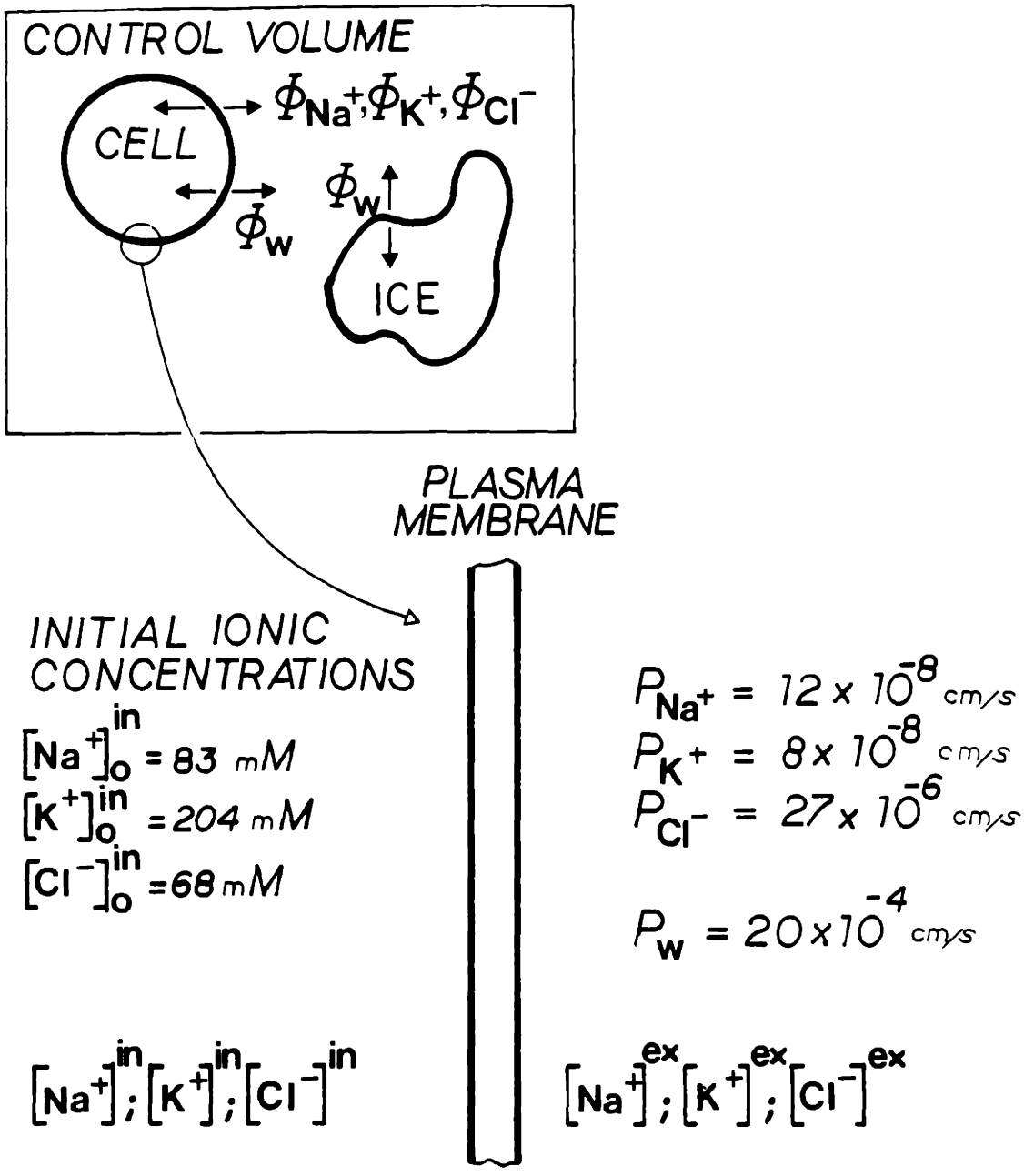

FIGURE.5.7. Schematic illustration of the ionic components in the mouse oocytes. Membrane ionic permeabilities (P_j) are also given.

water permeability value determined in the previous section can be converted to the same units as ionic permeabilities as follows

$$L_p(37^oC) \simeq 0.8 \frac{\mu m}{min\text{-}atm} \simeq 14 \frac{cm^3}{dyn\text{-}sec} \quad (5.36)$$

$$P_w = \frac{L_p RT}{v_w} \simeq 20x10^{-4} \text{ cm/s} \quad (5.37)$$

This value is two orders-of-magnitude higher than the Cl^- permeability and four orders-of-magnitude higher than Na^+ and K^+ permeabilities. Therefore one can assume that the osmotic equilibrium is reached before the ionic equilibrium. This means that even after the osmotic equilibrium is reached there will be some ion transport. The importance this ion transport can be best understood by analyzing the absolute ion and water content of the cytoplasm. Roughly the number of moles of ions inside the cell can be estimated form the values given in Fig.5.7 to be approximately $8x10^{-11}$ moles. This is much less than the total number of moles of water inside the cell which can be estimated to be $1x10^{-8}$ (see also Appendix A). Since both the water content and the water permeability are several orders-of-magnitude higher than the ionic content and permeabilities, one can assume that the ionic equilibrium is established predominantly by the osmotic response of the cell. Thus internal ionic concentrations can be estimated from the initial concentrations and the change in cell volume by neglecting the actual diffusion across the plasma membrane.

During freezing at very fast rates, there will be no water and ion

transport, therefore, the internal ionic concentrations remain constant. The transmembrane potential can then be calculated from Eq.(5.35). At low cooling rates there will be a substantial water transport, and the internal ionic concentrations can be readily calculated from the cell volume as mentioned above. Once the internal ionic concentrations are estimated then the transmembrane potential can be evaluated from Eq.(5.35). In addition, it is shown that Cl^- is passively distributed across the plasma membrane in mouse oocytes and Cl^- permeability is much higher than Na^+ and K^+ permeabilities (Powers and Tupper 1975, 1977). Thus in calculation the Na^+ and K^+ dependent terms can be eliminated from Eq.(5.35). This is important because Eq.(5.35) becomes independent of ionic permeabilities and it only depends on the intra- and extracellular Cl^- concentrations. This means that the error introduced in our calculations by assuming constant ionic permeabilities is probably minimized.

Given the assumptions and approximations stated above, the transmembrane potential can be estimated during freezing of oocytes if the external ionic concentrations are known. The external solution in the present analysis is a simple phosphate buffered saline solution as NaCl being the major component. An analytical expression relating the molarity to the temperature during freezing can be derived using osmotic coefficients. However, it is simpler to predict the external concentration from the equilibrium phase diagram of NaCl. The following equation is derived for NaCl from the Handbook of Physics & Chemistry (Weast 1973)

$$[NaCl] = 0.0101xT^3 - 4.31xT^2 + 307.9xT - 10.86 \quad (5.38)$$

where T is in celsius and [NaCl] is in mM (see Appendix C).

Fig.5.8 represents the variation of the membrane potential in oocytes cooled at different rates. At the beginning of the freezing process (-1°C), the fast growth of ice in the extracellular solution causes a sharp increase of the membrane potential. As the temperature continues to drop, the oocyte dehydrates (see Fig.5.3). The rate of increase of the internal Cl^- concentration will depend upon the dehydration (i.e. cooling rate) whereas the external Cl^- concentration is dictated by the equilibrium phase behavior given by Eq.(5.38). There is a competition between the increase in intra- and extra-cellular Cl^- concentrations. Once the cell starts dehydrating as a function of the cooling rate, the rate of increase in internal Cl^- concentration may reach values higher than the rate of increase of the external Cl^- concentration, and the transmembrane potential may start decreasing in a certain range of temperature as shown in Fig.5.8. At sufficiently low cooling rates, the minimum equilibrium cell volume may be reached, thereafter internal Cl^- will remain constant and E_m increases due to the increase in external Cl^- concentration. This is clearly seen for cooling rate of 0.5°C/min in Fig.5.8. As shown in Fig.5.3 the oocyte reaches the minimum cell volume at approximately -8°C which corresponds to the increase in membrane potential displayed in Fig.5.8. The change in membrane potential is substantial for almost all cooling regimes. Our estimations show that values as high as -90 mV can be reached during

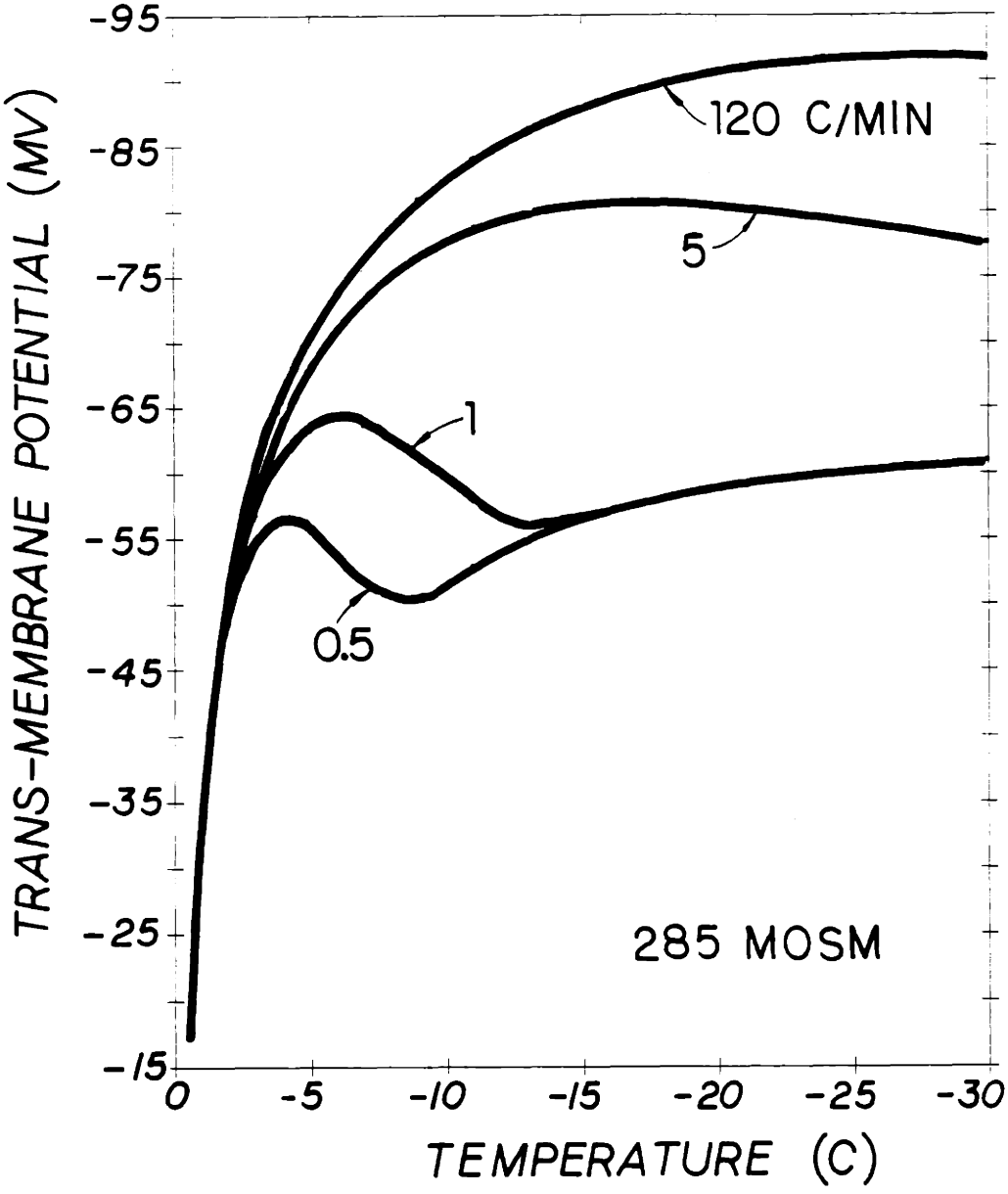

FIGURE.5.8. Variation of the trans-membrane potential in mouse oocytes as a function of temperature. Cooling rates are indicated for each curve. Oocytes are suspended in isotonic PBS solution and extracellular ice is seeded at -0.615^{o}C.

freezing.

In addition to the membrane potential change in isotonic solutions, we have investigated the effects of freezing on the oocytes in hypertonic solutions. Fig.5.9 displays the membrane potential as a function of temperature for a cooling rate of 120^{o}C/min in different concentrations of PBS+NaCl+BSA. When an oocyte starts the freezing protocol in a dehydrated state, the initial internal Cl^- of that oocyte is higher than an oocyte in isotonic solution while the external concentration is specified by the two-phase equilibrium curve and it is the same for both oocytes. Therefore, the trans-membrane potential is always smaller for an oocyte dehydrated prior to the freezing.

In summary, under the assumptions of constant ionic permeabilities and negligible active transport, the transmembrane potential is equal to the equilibrium electric potential difference. The equilibrium ion distribution during freezing is established by osmotic dehydration of the oocyte rather than by the diffusion of ionic species across the plasma membrane.

Orientational Polarizability of Plasma Membrane During Freezing

Like any material, membranes will become polarized in the presence of an electrical field applied across them. Polarization usually occurs due to formation of dipoles or orientation of dipoles within the

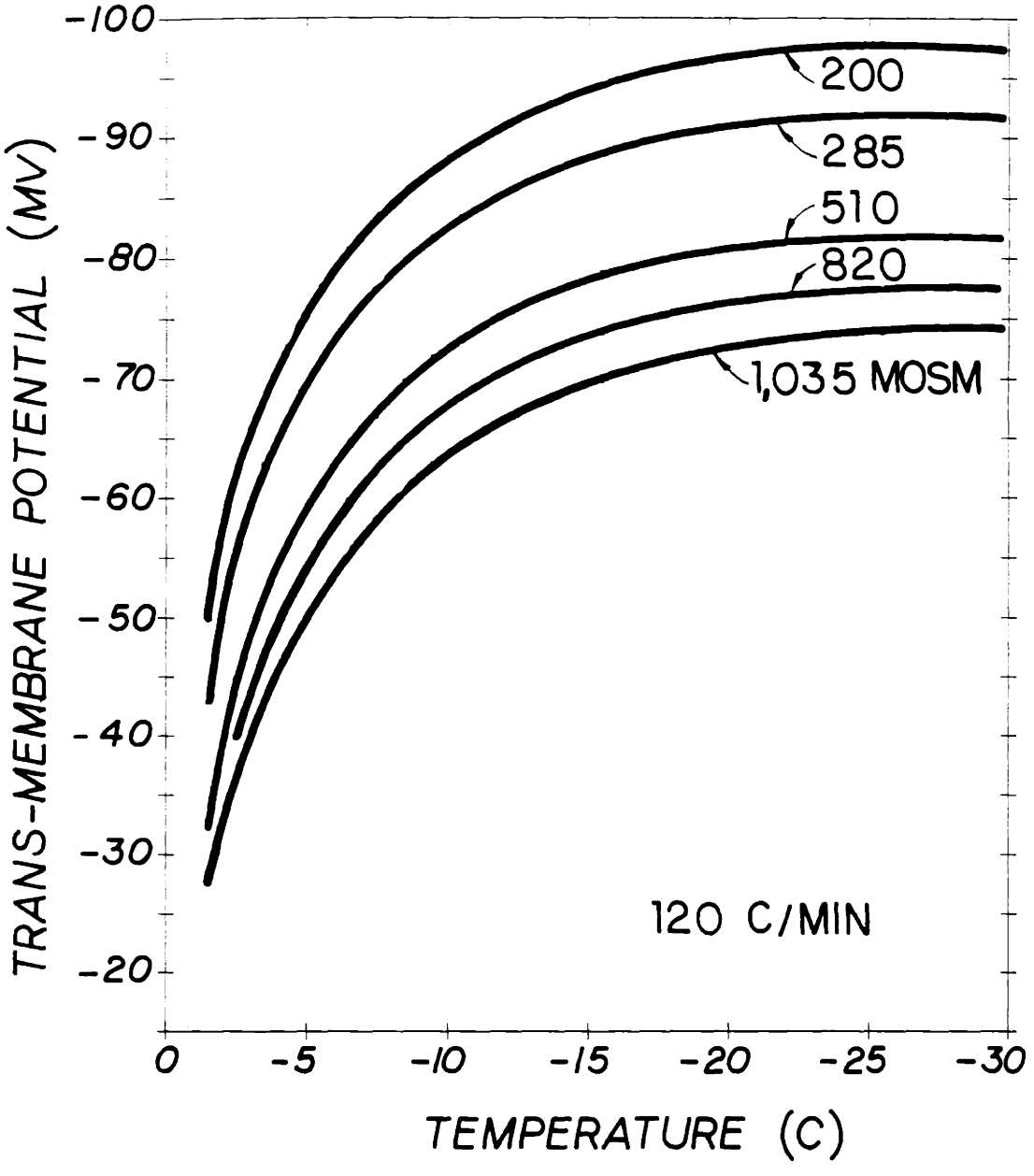

FIGURE.5.9. Variation of the trans-membrane potential in mouse oocytes as a function of temperature. Cooling rate is 120°C/min. Concentrations of the suspending PBS+NaCl solutions are indicated for each curve.

membrane or at the interface between the membrane and the electrolyte solution (Zimmermann 1982). Existing dipole molecules in biological membranes are water, lipids, and proteins. These dipoles normally may be randomly oriented. However, they align themselves in the direction of the field lines in the presence of an external field to an extent depending on field strength and temperature.

During freezing of cells as discussed in the previous section, the trans-membrane potential is hyperpolarized due to the formation of external ice and increased ionic strength in the external milieu. One of the possible effects of hyperpolarization is aligning of the dipoles in the membrane with the electrical field. In this section, a simple theory will be developed to estimate the percentage of dipoles that align themselves during freezing. The reader should refer to Pethig (1979) and Zimmermann (1982) for more detailed discussion of the dielectric properties of biological membranes.

When an electrical field is applied across a membrane composed of proteins, lipids, and water each having a permanent dipole moment, the dipoles will be subjected to a torque. This torque will try to align the dipoles with the electrical field in the presence of thermal agitations opposing the orientation. The potential energy U_d of a dipole moment $\bar{\mu}_d$ in a field $\bar{E}_m$ is given by (Pethig 1979)

$$U_d = - \bar{\mu}_d \bar{E}_m = - \mu_d E_m \cos \varsigma \qquad (5.39)$$

where ς is the angle between the dipole moment and the field direction.

Boltzmann distribution law can be used to relate the thermal average of cos ς, $\langle\cos\varsigma\rangle$, and the relative probability of finding a dipole oriented in an element of solid angle $d\varsigma$ as follows

$$\langle\cos\varsigma\rangle = \frac{\int \exp(-U_d/kT)\cos\varsigma\, d\varsigma}{\int \exp(-U_d/kT)\, d\varsigma} \qquad (5.40)$$

The integration of Eq.(5.40) over all solid angles can be carried out to determine a relationship between the thermal average of cos ς and the function $\mu_d E_m/kT$ (= Λ). The integration yields

$$L(\Lambda) = \langle\cos\varsigma\rangle = \coth\Lambda - \frac{1}{\Lambda} \qquad (5.41)$$

where $L(\Lambda)$ is called the Langevin factor (Pethig 1979). The Langevin factor gives the percentage of dipoles at a given dipole moment that are aligned due to the applied electrical field.

Eq.(5.41) can be coupled with Eq.(5.35) to predict the dipole orientation during freezing. Fig.5.10 shows the solution of Eq.(5.41) for a freezing protocol in isotonic saline at 120^{o}C/min. The Langevin function $L(\Lambda)$ is plotted as a function of temperature during freezing for different dipole moments. As can be seen from this figure, molecules with larger dipole moments will align at higher proportions with the electrical field. According to this first-cut analysis, there is a dramatic change in the orientation of the proteins due to the hyperpolarization of the membrane. For proteins with 300 debye dipole moment, the percentage of dipoles aligned with the membrane potential

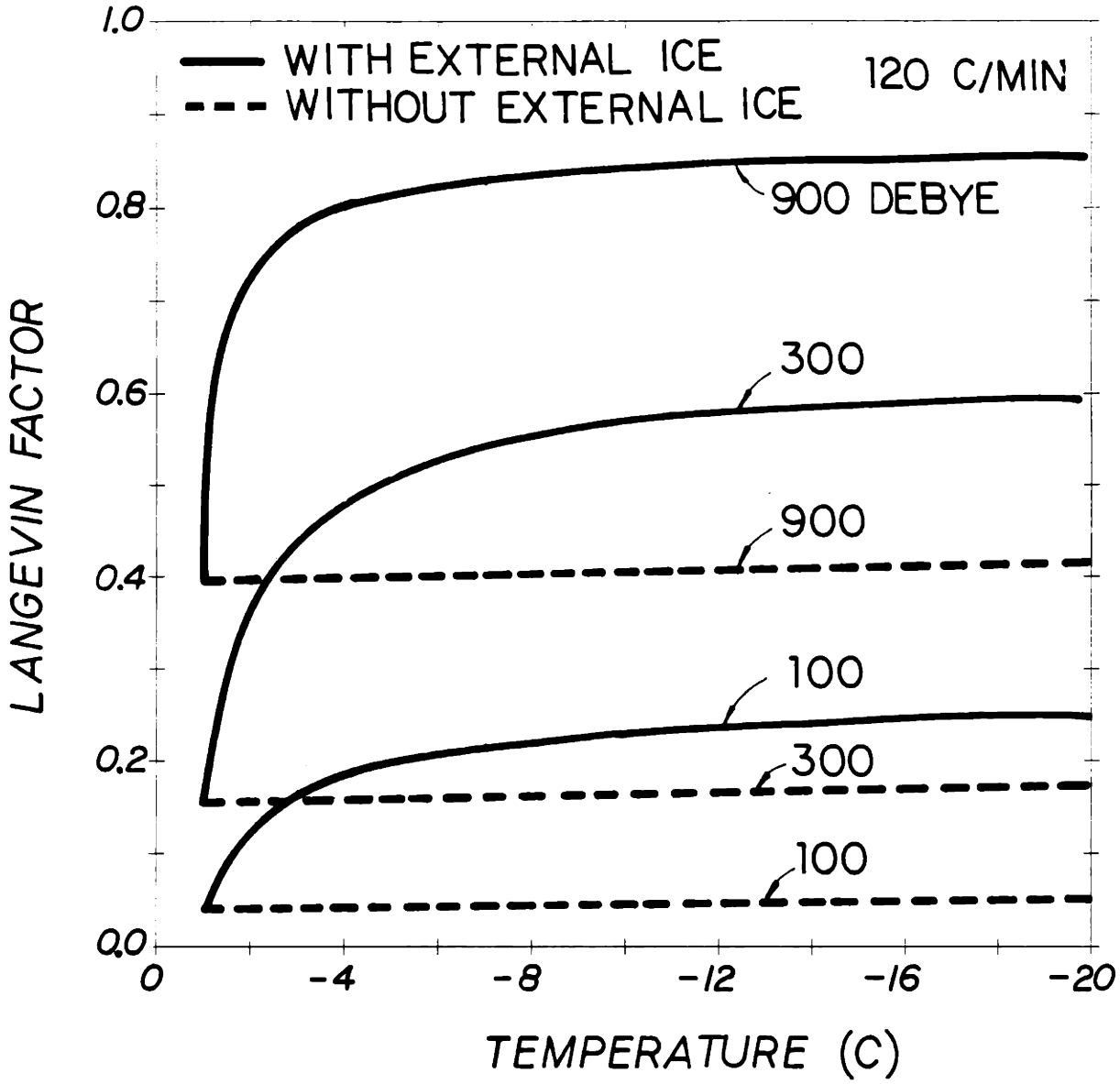

FIGURE.5.10. Dipole orientation (Langevin factor) as a function of temperature during freezing at 120°C/min. Dipole moments are indicated for each curve. Dashed lines represent the Langevin factor during cooling in the absence of extracellular ice.

increases from approximately 16% at 0°C prior to freezing to 58% at -8°C after the seeding of the external ice.

The dipole moment for most of the proteins is on the order of 300 debye and greater, whereas water molecules have a dipole of 1.8 debye. Therefore, the orientation of water molecules will be very small and can be easily ignored. However, a major contribution to orientational polarization should be expected for membrane proteins as well as for membrane lipids (Pethig 1979). The orientational polarization of membrane components may have enhancing effect on ice nucleation and these issues will be further discussed in the following chapters.

CHAPTER VI

THERMODYNAMICS AND KINETICS OF INTRACELLULAR ICE-NUCLEATION DURING FREEZING OF BIOLOGICAL CELLS

6.1. Introduction

The growth of a new phase within a mother phase must be preceded by the process referred to as "nucleation" such as the crystallization of ice from the undercooled (or supercooled) water (Chalmers, 1959; Turnbull, 1965b). There are two general mechanisms of ice nucleation. First, **homogeneous** nucleation (or spontaneous nucleation) in which case the ice phase, β, must be initiated by water molecules, α, combining together to form a cluster of molecules in the solid phase which can grow spontaneously. In the second case, nucleation of the ice phase occurs on foreign particles (heterophase impurities), the ice is said to form by **heterogeneous** nucleation (or catalyzed nucleation). The largest cluster which may exist before crystallization proceeds is usually referred as the critical cluster. Catalyst surfaces help organizing water molecules required for a critical cluster to initiate the nucleation. Irrespective of the mechanism of ice formation, the cluster consists only of water molecules (see Fig.6.1). Thus the theory of

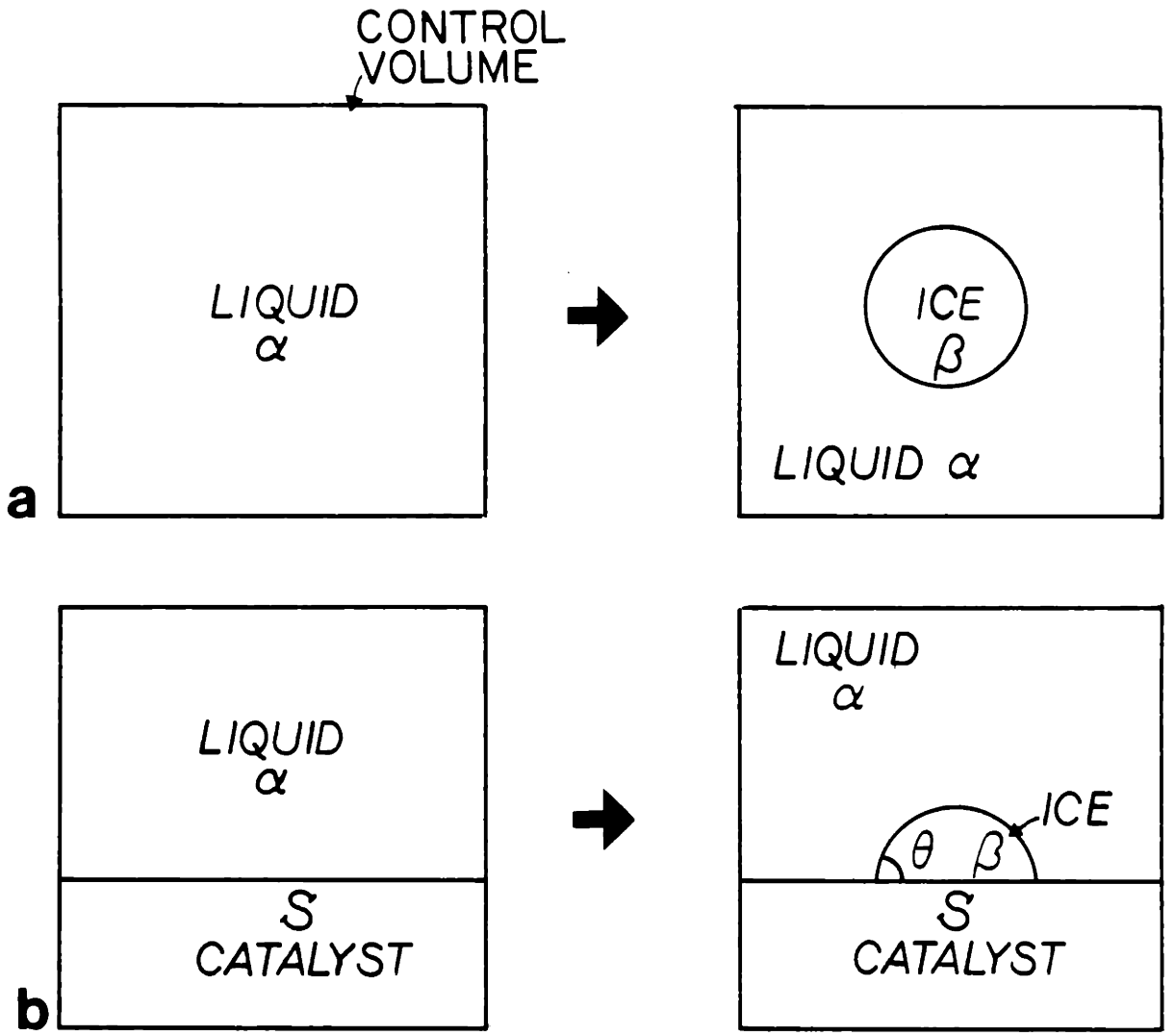

FIGURE.6.1. Schematic comparison of (a) homogeneous and (b) heterogeneous nucleation of ice in an undercooled water, with a flat catalytic surface.

nucleation applies equally to homogeneous and heterogeneous processes. For more detailed and comprehensive accounts of nucleation theory the reader is referred to the excellent review articles of Hollomon & Turnbull 1953; Walton 1969; and Christian 1975, and books of Fletcher 1969, 1970; Hobbs 1974; Pruppacher 1978.

In the classical nucleation theory, the formation of clusters are represented as sequences of bimolecular processes. Such clusters are assumed to arise by a series of reactions, i.e. one molecule adding to another to form a dimer, then another molecule adding to the dimer, etc, plus the reverse reactions,

$$\begin{aligned} \alpha + \alpha_m &\rightleftharpoons \beta_m \\ \alpha + \beta_m &\rightleftharpoons \beta_{m+1} \\ \alpha + \beta_{m+1} &\rightleftharpoons \beta_{m+2} \\ &\vdots \\ \alpha + \beta_{i-1} &\rightleftharpoons \beta_i \end{aligned} \qquad (6.1)$$

where α represents an atom of phase α (water), β_i a cluster of phase β (ice) containing i atoms and m is the number of atoms in the smallest cluster of β. Sundquist & Oriani(1962) assumed that two molecules could interact as a new phase. However, the hexagonal ring being the smallest structure in an ice lattice, Rasmussen & MacKenzie (1973) assumed that the smallest sized cluster capable of demonstrating icelike properties is a six-membered ring. Basically, as the temperature of the liquid phase is reduced below its equilibrium freezing point, small particles of solid phase called clusters are constantly being formed by statistical thermal fluctuations. These fluctuations are called

heterophase fluctuations resulting in the momentary formation of small groups of molecules in the atomic arrangement associated with the solid crystalline phase (Frenkel 1955; Fletcher 1970). As the degree of undercooling is increased, the number of these unstable clusters increase. According to nucleation theory, the fluctuations will only grow if they exceed a certain critical size for a given degree of undercooling. Thus at a particular temperature, one of the clusters reaches a critical size and becomes metastable. Nucleation as the formation of a new phase can then be defined as the formation of a post critical cluster of size i^*+1,

$$\alpha + \beta_{i^*} \underset{k^-_{i+1}}{\overset{k_i^+}{\rightleftharpoons}} \beta_{i^*+1} \qquad (6.2)$$

The rate of this equation will depend on the rate at which monomers react additively with the cluster, the number of surface monomers, and the distribution of critical clusters.

Heterogeneous nucleation may take place when a solid surface or heterophase impurity particle is present in the liquid (Turnbull 1950a; Fletcher 1958, 1960); then the cluster may be formed on this surface. Therefore, some of the catalyst-medium interfacial energy is removed, and the cluster so formed will have a lower free energy than an independent cluster facilitating its growth. Consequently, it is possible to form clusters in heterogeneous nucleation at temperatures higher than the case of homogeneous nucleation. In this chapter, a detailed derivation of the equations governing the thermodynamics and the kinetics of ice-nucleation in condensed systems will be given.

Then, these equations will be applied to biological cells to predict the likelihood of intracellular ice formation during freezing.

6.2. Surface Thermodynamics

The method most widely employed for treating interfaces was largely developed by Gibbs (1875; see collected papers; Gibbs 1961) who discussed the thermodynamics of interfaces in terms of a conceptual "dividing surface" between phases (Fig.6.2). The thermodynamic treatment of interfaces by Gibbs does not concern itself with details of the interfacial region such that any extensive property, X, of a system consisting of two phases α and β separated by an interface, s, can be written as the sum of three contributions:

$$X = X^{\alpha} + X^{\beta} + X^{s} \qquad (6.3)$$

where X^{α} is the value of the property for the α phase, X^{β} is the corresponding value for the β phase, and X^{s} is defined as a surface excess that is the amount by which the real value of X differs from that in the hypothetical discontinuous system. In this notation, the interface volume is assumed to be zero. Therefore, it is necessary to determine as to what contribution the interface makes to the work done in any process in order to use first and second laws of thermodynamics. This leads to the definition of interface tension, σ, as the reversible

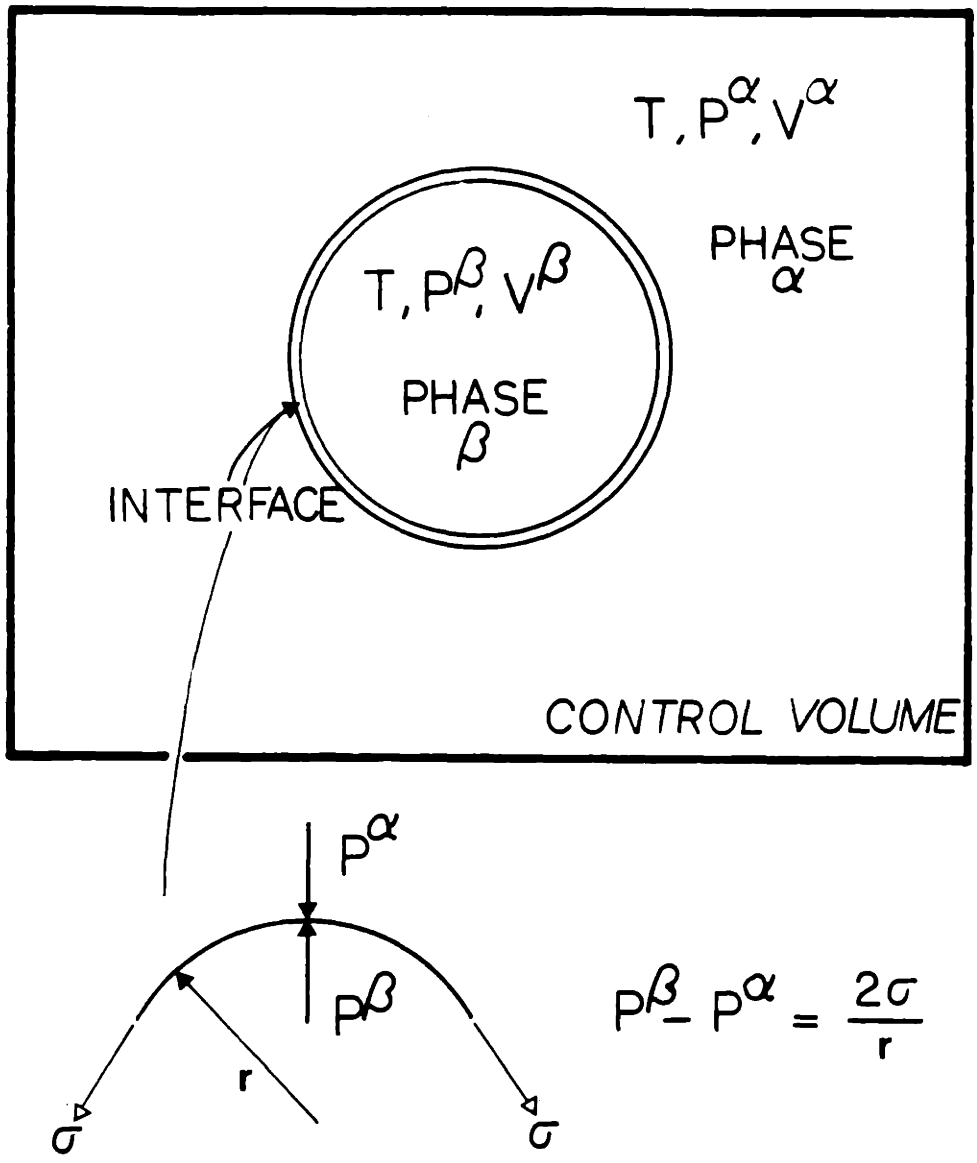

FIGURE.6.2. Schematic drawing of a circular surface phase, s, between two phases α and β according to Gibbs treatment of surfaces.

work needed to form an interfacial area of dA^S at constant system temperature, pressure and chemical potentials of the components, so that

$$\sigma = \lim_{dA^S \to 0} (dW/dA^S) \qquad (6.4)$$

where dW is the work involved in the reversible formation of the element of area dA^S (Blakely, 1986). The terms surface tension and surface energy are used interchangeably for liquids that do not support residual stress. Because interfaces give rise to physical forces in systems, a work term including σ should be included in the combined first and second laws of thermodynamics. For a planar interface

$$dE = TdS - PdV + \sum_{\gamma} \mu_\gamma dn_\gamma + \sigma dA^S \qquad (6.5)$$

where E is the internal energy of the system, S is the entropy, σdA^S is equal to the work done against the surface tension force to create the new interface, μ_γ is the chemical potential of the γ'th component, n_γ is the number of moles of γ'th component, T is the temperature, P is the pressure, and V is the volume of the system. Using the definition of surface excess quantities for a planar inerface

$$dE^S = TdS^S + \sum_{\gamma} \mu_\gamma{}^S dn_\gamma{}^S + \sigma dA^S \qquad (6.6)$$

The PdV work term does not appear in Eq.(6.6) because the surface plan has very small volume compared to the other phases. This may be integrated through the use of Euler's theorem to obtain

$$E^S = TS^S + \sum_{\gamma} n_\gamma{}^S \mu_\gamma{}^S + \sigma A^S \qquad (6.7)$$

The internal energy E may not be the most appropriate thermodynamic potential in considering nucleation processes, and σ can be defined by using the surface Helmholtz free energy, F^S, such as

$$F^S = \sum_{\gamma} n_\gamma{}^S \mu_\gamma{}^S + \sigma A^S \qquad (6.8)$$

Now, at constant temperature and volume, the Helmholtz free energy of the combined liquid and solid phases, and the interface can be written using Eq.(6.1)

$$F = F^\alpha + F^\beta + F^S \qquad (6.9)$$

where F^α, F^β represent Helmholtz free energies of phases α (liquid) and β (solid), respectively. The individual free energies can be written for a system at constant temperature and volume

$$\begin{aligned} F^\alpha &= \sum_{\gamma} n_\gamma{}^\alpha \mu_\gamma{}^\alpha - p^\alpha V^\alpha \\ F^\beta &= \sum_{\gamma} n_\gamma{}^\beta \mu_\gamma{}^\beta - p^\beta V^\beta \end{aligned} \qquad (6.10)$$

Combining Eq.(6.9) with Eqs.(6.10), (6.8) one obtains the Helmholtz free energy of the system as follows

$$F = \sum_{\gamma} n_\gamma{}^\alpha \mu_\gamma{}^\alpha - p^\alpha V^\alpha + \sum_{\gamma} n_\gamma{}^\beta \mu_\gamma{}^\beta - p^\beta V^\beta + \sum_{\gamma} n_\gamma{}^S \mu_\gamma{}^S + \sigma A^S \qquad (6.11)$$

The Helmholtz free energy of formation of the system, $(\Delta F)_{T,V}$, at temperature, T, and volume, V, can be defined as the difference between the above free energy, F, and the free energy, F_o, of the system in the initial state

$$(\Delta F)_{T,V} = F - F_o \tag{6.12}$$

with,

$$F_o = \sum_{\gamma} n_\gamma \mu_{\gamma o}^{\alpha} - P_o^{\alpha} V \tag{6.13}$$

where,

$$\begin{aligned} V &= V^{\alpha} + V^{\beta} \\ n_\gamma &= n_\gamma^{\alpha} + n_\gamma^{\beta} + n_\gamma^{s} \end{aligned} \tag{6.14}$$

Since the temperature and the pressure of the system can be assumed to be uniform for a planar interface, it can be written that $\mu_\gamma^{\alpha} = \mu_{\gamma o}^{\alpha}$ and $P^{\alpha} = P_o^{\alpha}$. By substituting Eqs.(6.11), (6.13), (6.14) in Eq.(6.12), an expression for the Helmholtz free energy of formation of the system can be found as

$$(\Delta F)_{T,V} = \sum_{\gamma} n_\gamma^{\beta}(\mu_\gamma^{\beta} - \mu_\gamma^{\alpha}) - V^{\beta}(P^{\beta} - P^{\alpha}) + \sum_{\gamma} n_\gamma^{s}(\mu_\gamma^{s} - \mu_\gamma^{\alpha}) + \sigma A^{s} \tag{6.15}$$

In the case of a spherical interface, the pressure P^{β} within the condensed phase can be related to the pressure P^{α} within the liquid phase by Laplace's law (Dufour & Defay 1963)

$$P^{\beta} - P^{\alpha} = 2\sigma/r \tag{6.16}$$

Using Eq.(6.16), and assuming a spherical particle

$$V\beta(P\beta - P\alpha) = 4\pi r^3/3\ (2\sigma/r) = 2\sigma A^S/3 \qquad (6.17)$$

Thus Eq.(6.15) becomes

$$(\Delta F)_{T,V} = \sum_{\gamma} n_\gamma{}^\beta(\mu_\gamma{}^\beta - \mu_\gamma{}^\alpha) + \sum_{\gamma} n_\gamma{}^S(\mu_\gamma{}^S - \mu_\gamma{}^\alpha) + \sigma A^S/3 \qquad (6.18)$$

It is necessary to underline here that for a spherical interface the chemical potential of the new phase is defined at $P\beta$, while the chemical potential of the condensed phase is defined at $P\alpha$. Using the classical formula (Prigogine & Defay 1954), one can obtain

$$\frac{\partial \mu_\gamma{}^\beta}{\partial P\beta}\Big|_{T,n_\gamma{}^\beta} = v_\gamma{}^\beta \qquad (6.19)$$

where $v_\gamma{}^\beta$ is the specific molar volume of the component γ in phase β. By integrating Eq.(6.19) and neglecting the compressibility of the phase β,

$$\mu_\gamma{}^\beta(T,P\beta,n_\gamma{}^\beta) = \mu_\gamma{}^\beta(T,P\alpha,n_\gamma{}^\beta) + v_\gamma{}^\beta\ (P\beta - P\alpha) \qquad (6.20)$$

Since

$$\sum_{\gamma} n_\gamma{}^\beta\ v_\gamma{}^\beta = V\beta \qquad (6.21)$$

and assuming that the surface adsorptions are negligible, one can obtain from Eqs.(6.16)-(6.18), (6.20), (6.21)

$$(\Delta F)_{T,V} = \sum_{\gamma} n_{\gamma}^{\beta}(\mu_{\gamma}^{\beta}(T,P^{\alpha},n_{\gamma}^{\beta}) - \mu_{\gamma}^{\alpha}(T,P^{\alpha},n_{\gamma}^{\alpha})) + \sigma A^{S} \quad (6.22)$$

Or, as a short hand notation

$$(\Delta F)_{T,V} = \sum_{\gamma} n_{\gamma}^{\beta}\,\Delta\mu_{\gamma} + \sigma A^{S} \quad (6.23)$$

or

$$= \sum_{\gamma} (4\pi r^3/3\upsilon_{\gamma}^{\beta})\,\Delta\mu_{\gamma} + (4\pi r^2)\,\sigma \quad (6.24)$$

or

$$= \sum_{\gamma} i\,\Delta\mu_{\gamma} / N_{AV} + (36\pi)^{1/3}\, i^{2/3}\, \upsilon^{\beta 2/3}\, \sigma / N_{AV}^{2/3} \quad (6.25)$$

where $\Delta\mu_{\gamma}$ ($= \mu_{\gamma}^{\beta} - \mu_{\gamma}^{\alpha}$) and i is the number of molecules in the cluster of radius r. This equation can be interpreted as the free energy of formation of clusters is equal to the sum of the difference between the average per unit volume chemical potentials within the cluster compared with that in the bulk and the energy expended in creating the interface so that

$$\Delta F = \Delta F_{BULK} + \Delta F_{INTERFACE} \quad (6.26)$$

It is to be noted that Eq.(6.23) refers only to a stationary cluster since changes in translational, rotational and vibrational components have been ignored. This approximation is probably reasonable since all are relatively small contributions in a condensed phase. Lothe & Pound (1962) analyzed the effect of neglecting these quantum statistical contributions to the cluster's free energy of formation.[1] Their result

****

1./These effects are originally discussed by Frenkel (1955), although the credit is usually given to Lothe & Pound (1962) in the literature.

show that the only appreciable contribution is the rotational component. The rotation of the clusters in the liquid will certainly be hindered. Their upper limit calculations showed that the contribution for free rotation is thought to be important. The model amounted to an increase of 10^{20} in expected nucleation rate. It could explain the anomalous pre-exponential observed by Turnbull (1952) in the solidification of supercooled mercury droplets which is a 10^{7} discrepancy between the experimental and theoretical pre-exponential factors. However, Lothe & Pound's (1962) explanation was challenged by Sundquist & Oriani (1962); and Dunning (1969) who showed that inclusion of quantum statistical contributions change the theoretically predicted critical undercooling by a negligible amount and the original treatment is correct. A later analysis by Deryaguin (1972) confirms this conclusion.

The Helmholtz free energy of formation in the case when there is only a single component in the drop or crystal such as formation of a crystal of pure ice in pure water or in a salt solution can be derived from Eqs.(6.23)-(6.25) as follows

$$(\Delta F)_{T,V} = n\beta \ \Delta\mu_b + \sigma A^s \qquad (6.27)$$

or

$$= (4\pi r^3/3\upsilon\beta) \ \Delta\mu_b + (4\pi r^2) \ \sigma \qquad (6.28)$$

or

$$= i \ \Delta\mu_b \ / \ N_{AV} + (36\pi)^{1/3} \ i^{2/3} \ \upsilon\beta^{2/3} \ \sigma \ / \ N_{AV}^{2/3} \qquad (6.29)$$

where $\Delta\mu_b$ ($=\mu^\beta - \mu^\alpha$) is the thermodynamic driving force for the bulk pure water-ice system. At temperatures below the thermodynamic melting point $\Delta\mu_b$ is negative while σ is positive. Therefore, the free energy of formation of a cluster is initially positive and goes through a

maximum as the cluster size is increased. At the maximum a cluster of the final phase, β, is in unstable equilibrium with the surrounding initial phase (see Fig.6.3). The maximum in the value of ΔF_i, called ΔF_i^*, gives the thermodynamic barrier to nucleation at the particular temperature considered. The kinetics of the process overcoming this energy barrier is treated by the nucleation theory. The cluster size corresponding to the maximum Helmholtz free energy of formation is designated as the critical cluster. Maximizing ΔF_i with respect to r (or i) in Eqs.(6.27)-(6.29) we obtain the following relationships for r^* (or i^*)

$$r^* = - \frac{2\sigma}{(\Delta\mu_b/v\beta)} \tag{6.30}$$

and

$$i^* = - \frac{32\pi}{3} \frac{\sigma^3 v\beta^2 N_{AV}}{\Delta\mu_b{}^3} \tag{6.31}$$

and the following relationship for ΔF_i^*

$$\Delta F^* = \frac{16\pi}{3} \frac{\sigma^3}{(\Delta\mu_b/v\beta)^2} \tag{6.32}$$

Among the assumptions in the derivation of the above interface thermodynamics relations that the independence of the interfacial free energy, σ, on the cluster size has been examined critically by many investigators (Buff & Kirkwood 1950; Hollomon & Turnbull 1953; Cahn & Hilliard 1958, 1959). Instead of assuming a sharp interface with zero volume as in Gibbs treatment, they have assumed a diffuse interface (see Fig.6.4). The diffuse interface model in the Cahn-Hilliard theory of

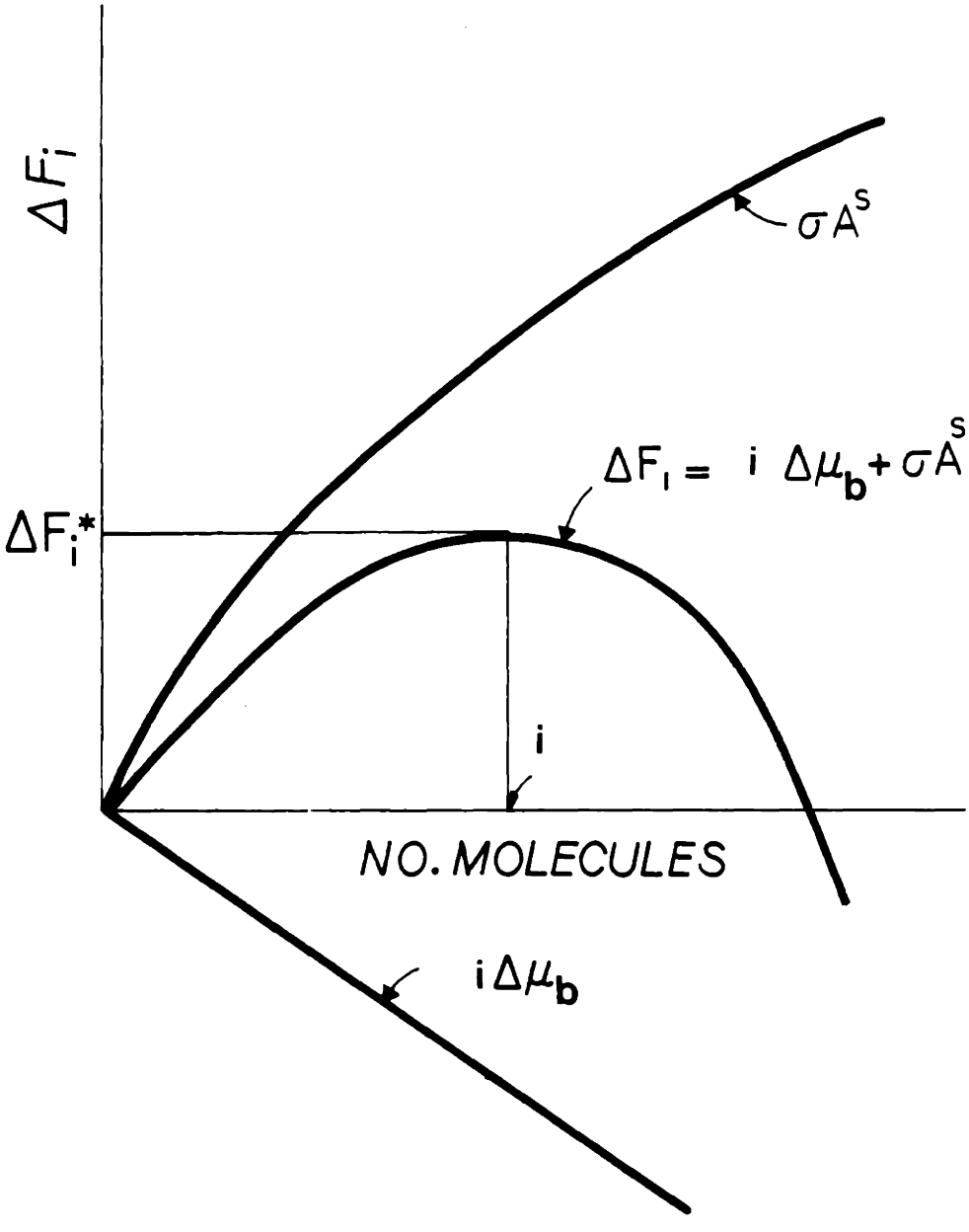

FIGURE.6.3. Helmholtz free energy of formation, ΔF_i, of a cluster.

nucleation assumes that the free energy of the cluster can be expressed as the sum of two terms, the first representing a uniform compact cluster and the second surface gradients. The total Helmholtz free energy for a diffuse cluster can be then expressed as

$$F = N_V \int_V [f_o(x) + K_d (\nabla x)^2] \, dV \qquad (6.33)$$

where N_V is the number of molecules per unit volume, x is any intensive property of the system other than temperature and pressure, f_o is the free energy of a homogeneous system, K_d is a parameter (Cahn & Hilliard 1958; Uhlmann & Chalmers 1965). The parameter K_d can be calculated from theoretical considerations and is constant for regular solutions. The interfacial free energy may then be defined in terms of the interfacial density gradient

$$\sigma = \int_{\rho 1}^{\rho 2} [K_d \, \Delta f(\rho)]^{1/2} \, d\rho \qquad (6.34)$$

where Δf is the difference in actual free energy of the system and the free energy which would be present if the properties of the bulk phases were continuous right up to the interface, and ρ is the density. Tolman (1949) determined that for a diffuse interface

$$\sigma(r) = \sigma_\infty \; / \; (1 + 2\delta/r) \qquad (6.35)$$

where δ is a proportionality constant, σ_∞ is the surface free energy of a planar interface, and $\sigma(r)$ is the surface free energy per unit area of

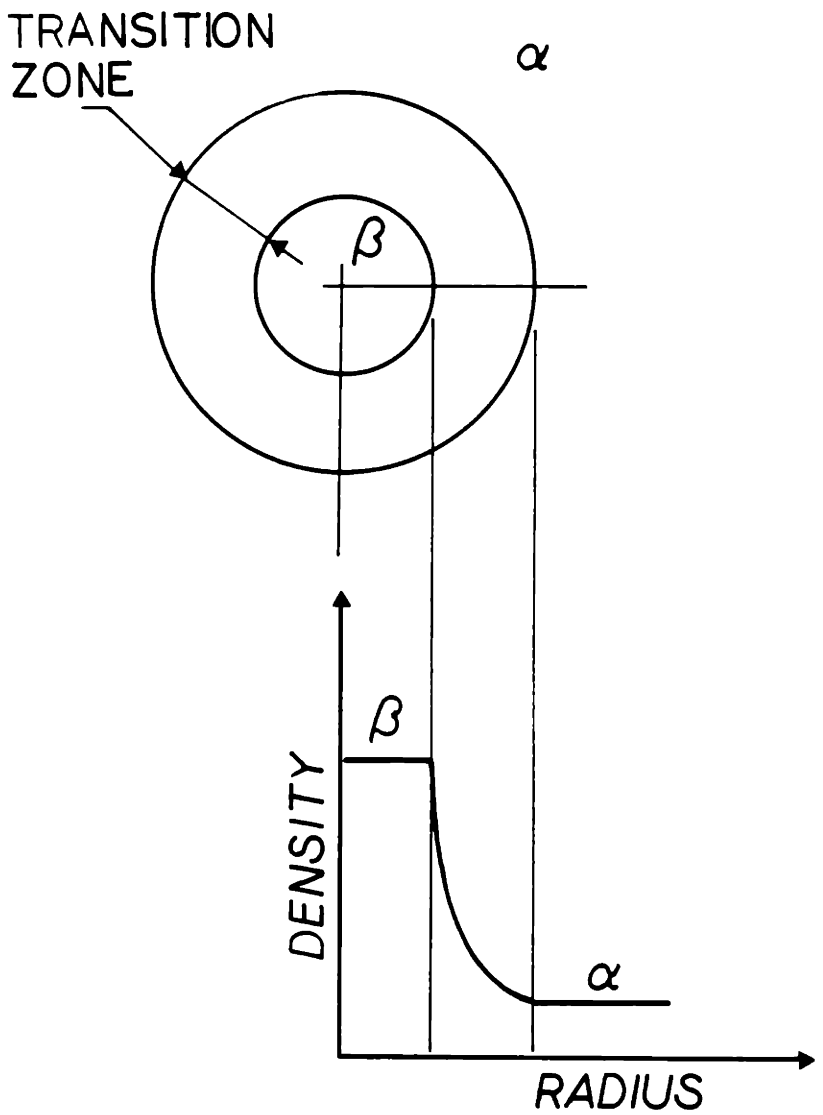

FIGURE.6.4. Variation of density (or any other property) across the transition zone between solid and liquid phases for a spherical cluster according to Cahn & Hilliard (1958, 1959) diffuse interface model.

a curved surface of a sphere. Similar versions of Tolman's formula are recently derived by other investigators (Rasmussen 1982; Rasmussen et al. 1983; Jayaraman et al. 1986). As can be seen from Eq.(6.35) the surface free energy diminishes with the radius. According to Tolman (1949) and Buff & Kirkwood (1950), δ is on the order of 10^{-8} cm. Hence, this effect is still negligible for droplets of 10^{-4} cm in radius (see Fig.6.5) and becomes significant only for radii below 10^{-5} cm (Defay 1930; Tolman 1949; Buff & Kirkwood 1950; Koieng 1950; Dufour & Defay 1963). However, in a later paper, Buff (1955) showed that the direction of change in $\sigma(r)$ is uncertain for a very small r. In view of this and the lack of knowledge of cluster-liquid interfacial energies, it is, probably more appropriate to use a size independent relation for σ to analyze the kinetics of ice-nucleation.

Also shown on Fig.6.5 is the estimated number of ice molecules contained in the droplets of various radii as calculated from

$$i = \frac{4\pi r^3}{3v\beta} N_{AV} \qquad (6.36)$$

assuming spherical geometry. As can be seen from this figure for values of approximately $r/\delta > 10$ which corresponds to approximately 120 water molecules in the cluster, the change in σ with r is negligible and all the different approximations yield similar results.

The radius of the critical cluster and the number of water molecules forming the critical cluster can be estimated using Eqs.(5.13), (6.30), (6.36).

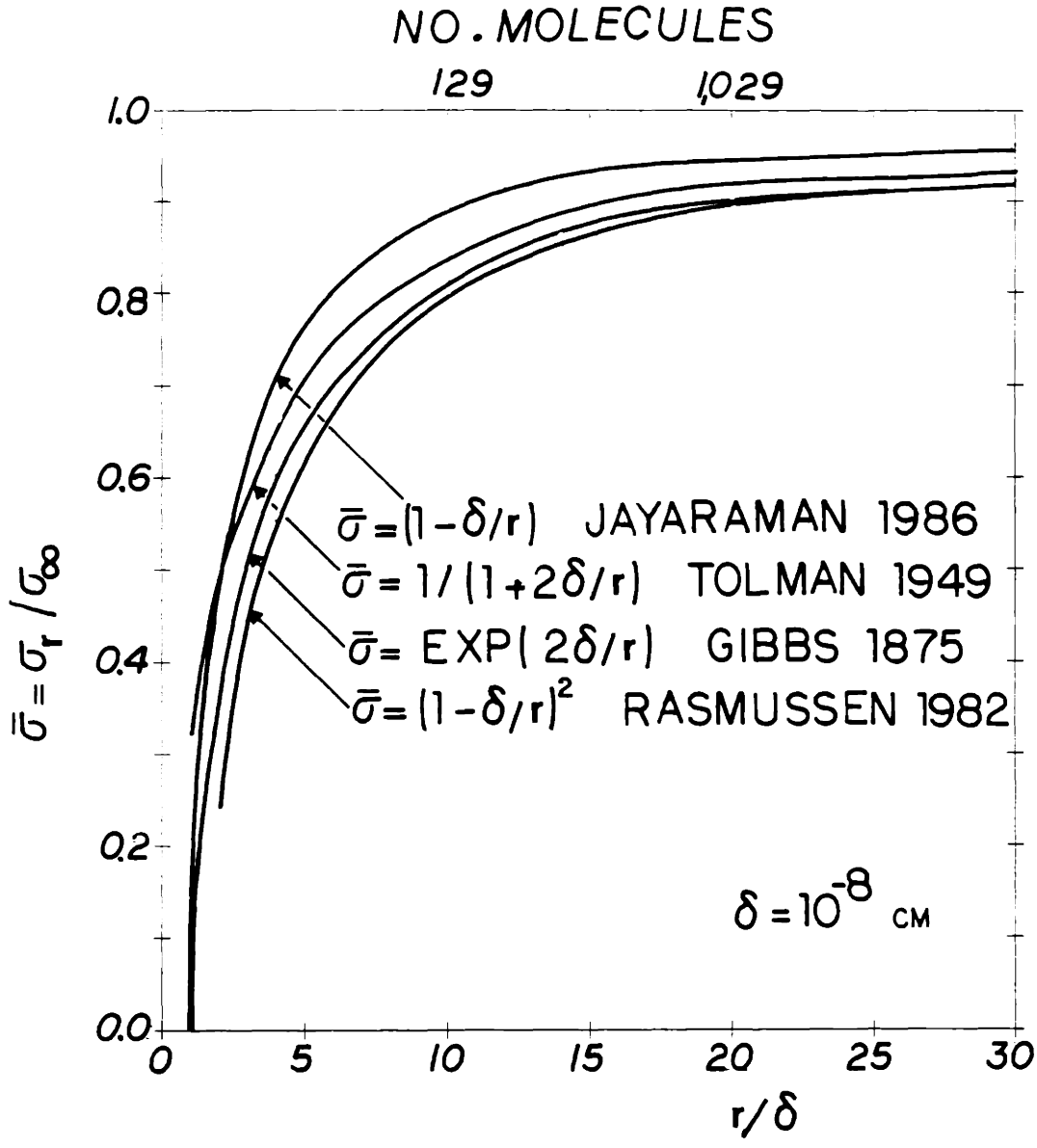

FIGURE.6.5. Variation of surface free energy with the size of the cluster.

Fig.6.6 shows results of such calculations for 285 and 1,035 mosm solutions for mouse oocytes cooled at 120°C/min. As can be seen from this figure, the number of water molecules in the critical cluster is larger than 1,000 molecules at -20°C in 285 mosm and it is larger than 350 molecules at -30°C in 1,035 mosm. Therefore, the ice-solution interfacial energy can be assumed to be independent of the cluster size. In conclusion, the nucleation model applied to mouse oocytes can be treated in the framework of thermodynamics.

6.3. Theory of Homogeneous Nucleation in Condensed Systems

Formation of clusters in an homogeneous phase is called "homogeneous nucleation." Volmer & Weber (1926) were able to calculate the rate of liquid nucleation from vapors by assuming that the concentration of the critical clusters was the characteristic of equilibrium, and that the back flux of supercritical clusters could be neglected in Eq.(6.2) for $i \geq i^*$. Post-critical clusters would grow rapidly, in effect being removed from the system. For $i > i^*$ they therefore set the cluster population $N_{i,t}$ to zero (see Fig.6.7). For $i \leq i^*$ they assumed that the cluster population is the equilibrium population. Mathematically, this can be summarized as follows

$$\begin{cases} i < i^* & N_i = N^v \exp(-\Delta F_i/kT) \\ i \geq i^* & N_i = 0 \end{cases} \qquad (6.37)$$

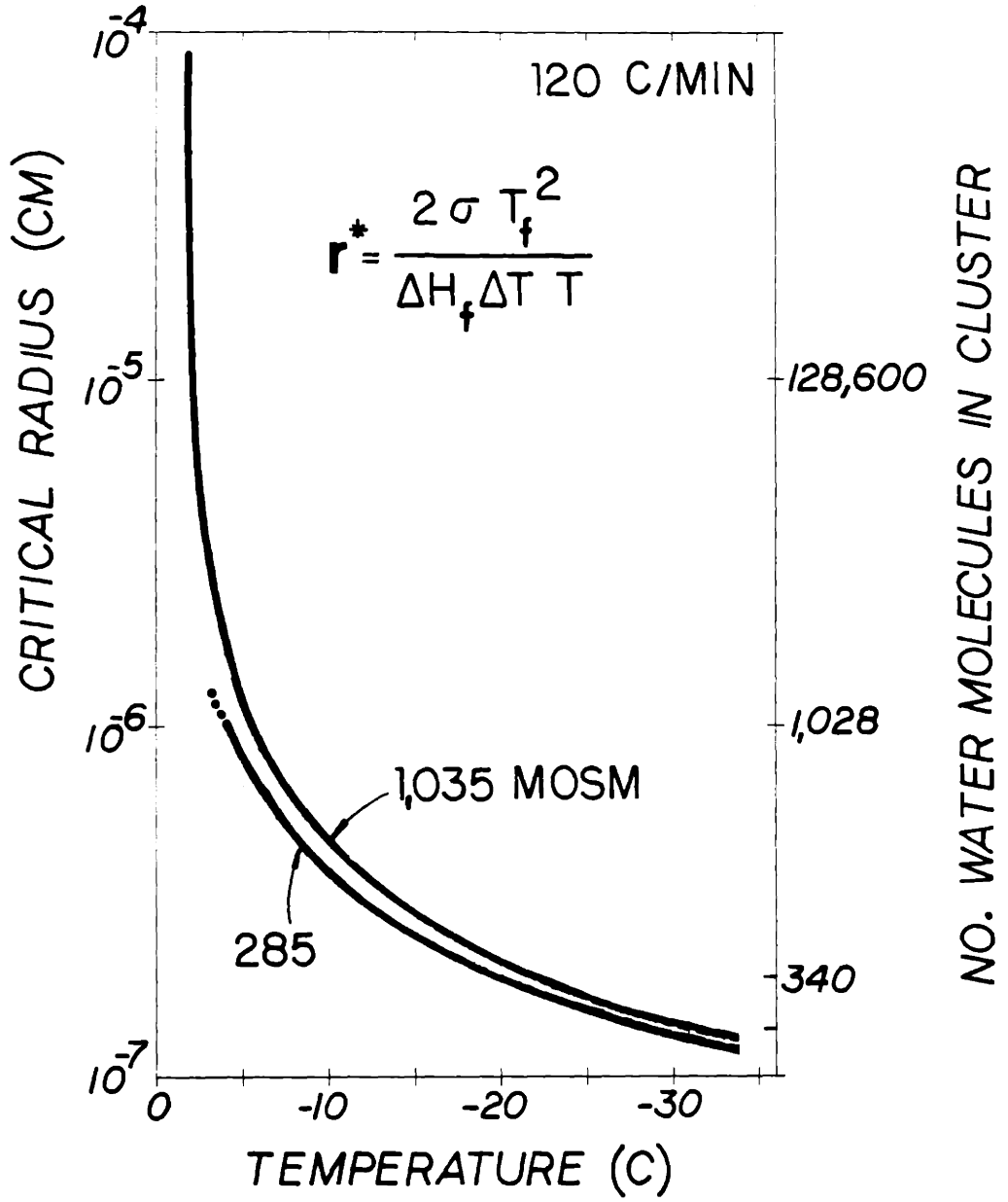

FIGURE.6.6. Critical radius for intracellular solution of mouse oocytes cooled at 120°C/min in various hypertonic PBS+NaCl+BSA solutions.

where N_i is the statistical distribution function for clusters containing i atoms, N^{ν} is the number of atoms in the mother phase α, and ΔF_i is the standard free energy change resulting from the conversion of α into clusters. The main defect of the theory lies in the assumption that the equilibrium thermodynamics is applied to a kinetic situation. This difficulty has been circumvented by the steady-state treatments of Becker and Doring (1935), Farkas (1927), and later by Zeldovich (1927), and Buckle (1961). The resulting initial theory served as a basis for the development of a nucleation rate expression in condensed systems by Becker in 1938. The synthesis of this theory with absolute reaction rate lead Turnbull and Fisher in 1949 to a nucleation rate expression, the essence of which became the basis of almost all subsequent treatments.

Considering again the interchange of clusters β_i, β_{i+1} represented in Eq.(6.2), the net transfer can be given generally as a function of time and of i by

$$I_{i,t} = N_{i,t}\, k_i^{+} - N_{i+1,t}\, k^{-}_{i+1} \qquad (6.38)$$

where $N_{i,t}$ is the number of clusters of size i present in the system at time t, k_i^{+} and k^{-}_{i+1} are the forward and backward rate constants, respectively. At equilibrium $N_{i,t} = N_i^{e}$ and the net rate is zero so that

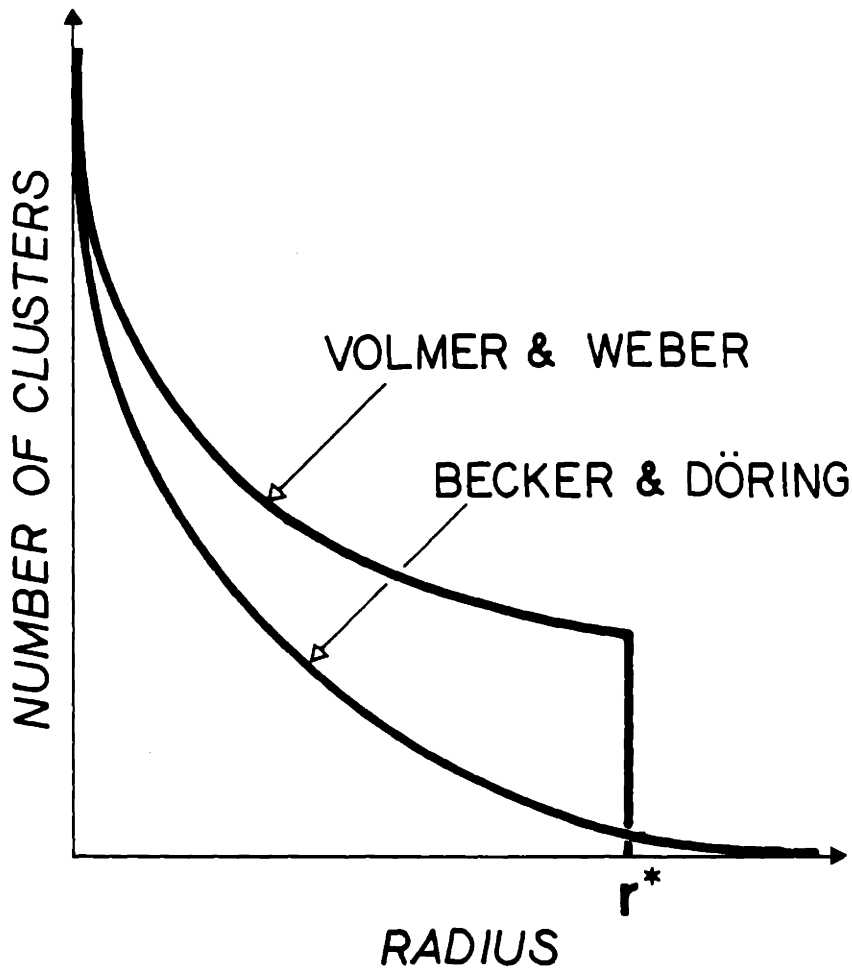

FIGURE.6.7. Distribution of ice-like clusters in water at a temperature below 0°C according to Volmer & Weber (an equilibrium distribution is assumed) and Becker & Doring (steady-state problem).

$$I_{i,t} \equiv 0 \equiv N_i^e k_i - N^e_{i+1} k^-_{i+1} \qquad (6.39)$$

The net forward rate in the transient regime can be derived from Eqs.(6.38), (6.39) as

$$I_{i,t} = N_i^e k_i^+ \left[\frac{N_{i,t}}{N_i^e} - \frac{N_{i+1,t}}{N^e_{i+1}} \right] \qquad (6.40)$$

The next problem in formulating the nucleation kinetics is to derive expressions for the rate constant k_i^+. Turning to the reaction in Eq.(6.1) as the basis of the kinetics, we see that the reaction involves the addition of single molecules to clusters. In the case of condensed phase reactions, there are many molecules essentially in contact with the cluster and it is a matter of bonding and reorientation that is involved. When a molecule, α, in contact with a cluster β_i is about to join it, the molecule must first pass through an activated state before it joins β_i to form β_{i+1} similarly to the theory of reaction rates (Eyring, 1935). Suppose that the free energy of a cluster β_{i+1} exceeds that of β_i by Δf_i. Then, using the reaction rate theory in the manner of Turnbull & Fisher (1949), one obtains (see Fig.6.8)

$$\nu_i^+ = \nu_o \exp(-\Delta f_i/kT) \qquad (6.41)$$

where ν_i^+ is the average jump rate of molecules in the forward reaction, Δf_i is the free energy of activation for a monomer to cross the interface between the liquid and the cluster, and ν_o is the frequency

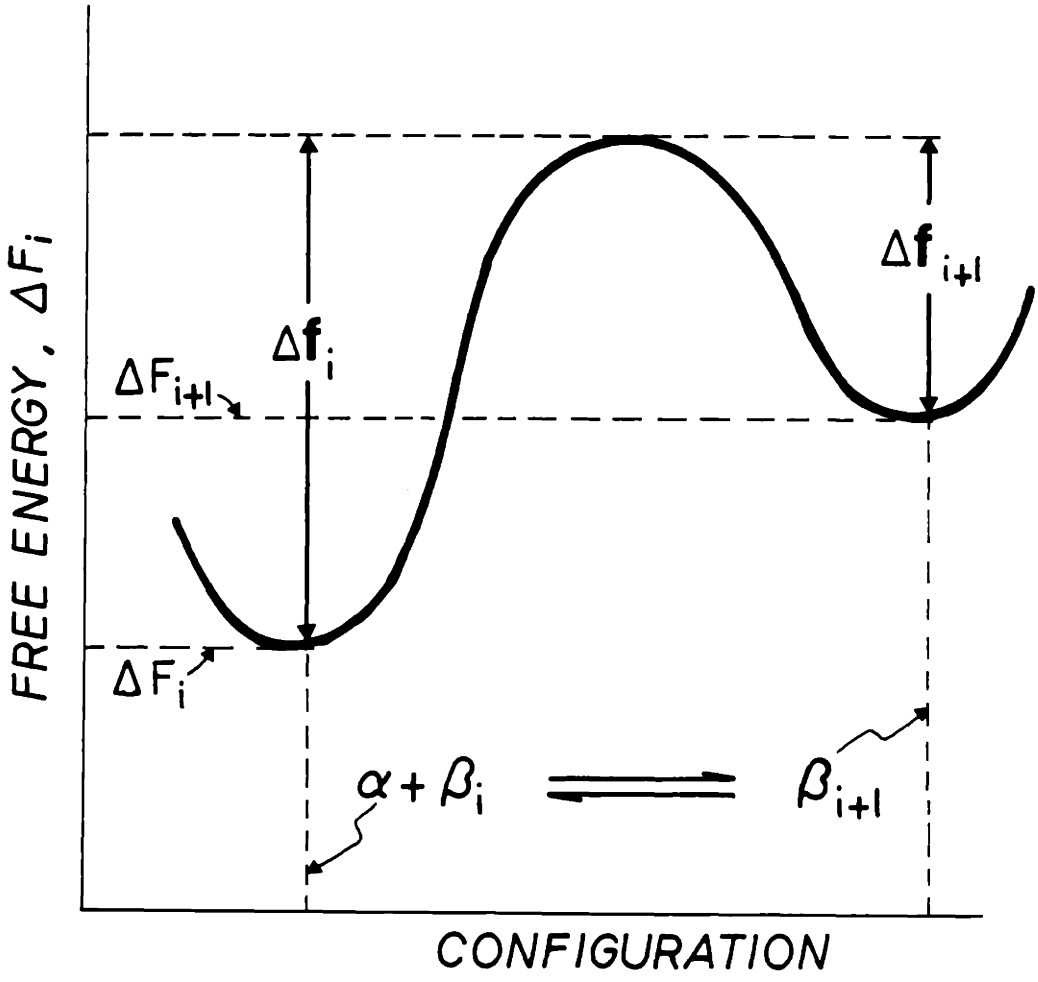

FIGURE.6.8. Illustration of the free energy relation in the Turnbull-Fisher treatment of nucleation theory (from Turnbull & Fisher 1949).

factor. The frequency factor can be defined using rate theory (Eyring, 1935)

$$\upsilon_o = kT/h \tag{6.42}$$

where k is the Boltzman's constant, and h is the Plank's constant. The forward rate constant is the product of the number of molecules that could be placed with their centers on a sphere that just encloses all the molecules in the cluster, O_i, with the forward jump rate, so that

$$k_i^+ = O_i \, \upsilon_i^+ \tag{6.43}$$

From Eqs.(6.40)-(6.43), one can obtain

$$I_{i,t} = N_i^e \, O_i \, \upsilon_o \exp(-\Delta f_i/kT) \left[\frac{N_{i,t}}{N_i^e} - \frac{N_{i+1+t}}{N^e_{i+1}} \right] \tag{6.44}$$

If a quasi steady-state is assumed such that a steady-state distribution of clusters is always established, the net forward rate of the reaction in Eq.(6.44) is constant, independent of time and of i. The net steady-state forward rate, I^s, is then given by

$$I^s = N_i^e \, O_i \, \upsilon_o \exp(-\Delta f_i/kT) \left[\frac{N_i^s}{N_i^e} - \frac{N^s_{i+1}}{N^e_{i+1}} \right] \tag{6.45}$$

It is to be noted that Δf_i is a function of i only. To make progress it is now necessary to suppose that (see Fig.6.8)

$$\Delta f_i = \Delta f + \frac{1}{2} \left[\frac{\partial \Delta F_i}{\partial i} \right] \tag{6.46}$$

where Δf is the free energy of activation for the transfer of molecules across the interface, and is independent of i. In addition to Δf to evaluate I^s, we need to know the steady-state distribution of clusters. Even though we do not know the distribution function for N_i^s, we know that for very small clusters it must be identical with the equilibrium distribution population function ($i \to 0$, $N_i^s \to N_i^e$) and as the cluster size gets larger, the distribution function must approach zero ($i \to \infty$, $N_i^s \to 0$). These boundary conditions can be expressed mathematically as follows

$$\begin{cases} n \leq p & N_i^s = N_i^e \\ n \geq s & N_i^s = 0 \end{cases} \qquad (6.47)$$

where $p < i^* < s$. We will see that it is not necessary to specify the values of either p or s provided that they are outside the critical region. From Eqs.(6.45)-(6.47), we may write a series of equations for all values of i from p to s and adding these equations we can obtain

$$\frac{I^s h}{kT} \exp(\Delta f/kT) \sum_{p}^{s} \frac{1}{N_i^e \, O_i \exp\{(1/2kT)\ (\partial \Delta F_i/\partial i)\}} = \left[\frac{N_p^s}{N_p^e} - \frac{N^s{}_{s+1}}{N^e{}_{s+1}}\right] = 1 \qquad (6.48)$$

Evaluating I^s from Eq.(6.48) analytically requires some further assumptions. The only important terms in the sum are those having i values near $i = i^*$ since there is a sharp maximum of $1/N_i^e$ at i^*. In

all the important terms, O_i will thus differ slightly from O_i^* and can be taken outside the sum by assuming that it is constant. In addition $\partial \Delta F_i / \partial i$ will be very small (it is zero at $i = i^*$) and we may therefore equate the exponential term in Eq.(6.48) to unity in the sum. The summation is then reduced to

$$\frac{I^S h}{O_i^* kT} \exp(\Delta f / kT) \sum_p^s (1/N_i^e) = 1 \qquad (6.49)$$

In evaluating N_i^e from Eq.(6.37), N^ν is taken to be equal to N as the total number of molecules in the system, and ΔF_i is replaced by the first two nonzero terms in a Taylor expansion about i^* as follows

$$\Delta F_i \simeq \Delta F_i^* + \frac{i^2}{2} \left[\frac{\partial^2 \Delta F_i}{\partial i^2} \right]_{i=i^*} \qquad (6.50)$$

The linear term, $\partial \Delta F_i^* / \partial i$ at $i = i^*$, is zero since ΔF_i^* has its maximum at $i = i^*$. When a cluster of critical size is formed, chemical equilibrium prevails in the system consisting of α and β phases, therefore, the free energy of a spherical critical cluster is given from Eq.(6.18)

$$\Delta F_i^* = \sigma A^{S^*} / 3 \qquad (6.51)$$

Using Eqs.(6.18),(6.36),(6.51) we have

$$- \left[\frac{\partial^2 \Delta F_i}{\partial i^2} \right]_{i=i^*} = \frac{2 \Delta F_i^*}{3 i^{*2}} \qquad (6.52)$$

By substituting Eq.(6.52) in Eq.(6.50), and replacing the sum term by an integral from p to s taking N_i^e as a continuous function of i, one can obtain

$$\sum_{p}^{s} (1/N_i^e) = \frac{1}{N} \exp(\Delta F_i^*/kT) \int_p^s \exp\left[-\frac{\Delta F_i^*}{3\, i^{*2}\, kT} i\right] di \quad (6.53)$$

Since only values of $1/N_i^e$ near i^* have influence on the integral, the limits can be changed $p = -\infty$ to $s = +\infty$ without affecting the results. The integral is then takes the form of the error integral and can be evaluated as follows

$$\sum_{p}^{s} (1/N_i^e) = \frac{1}{N} \exp(\Delta F_i^*/kT) \left[\frac{3\pi kT}{\Delta F_i^*}\right]^{1/2} i^* \quad (6.54)$$

Substutiting back to Eq.(6.49)

$$I^S = \frac{O_i^*\, kT}{h\, i^*} \left[\frac{\Delta F_i^*}{3\pi kT}\right]^{1/2} N \exp(-\Delta f/kT) \exp(-\Delta F_i^*/kT) \quad (6.55)$$

For a sphere, the number of monomers at the surface of a critical cluster in Eq.(6.55) is given by

$$O_i^* = (36\pi)^{1/3}\, \upsilon\beta^{2/3}\, i^{*2/3} \quad (6.56)$$

It is possible to envisage cluster shapes other than spherical. In view of the small size of the critical cluster and the other unknown factors involved, such complexity in equations is not really justified.

Eq.(6.55) differs from the Volmer & Weber (1926) solution by the factor

$$Z = \frac{1}{i^*} \left(\frac{\Delta F_i^*}{3\pi kT} \right)^{1/2} \qquad (6.57)$$

called Zeldovich factor (1927), although it was first derived by Farkas (1927). Its value is usually smaller than 1/20 and can be neglected for most practical processes (Turnbull & Fisher 1949).

By substutiting Eqs.(6.51), (6.56) in Eq.(6.55), one can obtain the following equation to model the homogeneous nucleation rate in condensed systems

$$I^S = K \exp\left(- \frac{\Delta f + \Delta F_i^*}{kT} \right) \qquad (6.58)$$

where

$$K = 2 \upsilon \beta 1/3 \frac{(\sigma kT)^{1/2}}{h} N$$

This equation is similar to that of Turnbull and Fisher (1949), however it is derived in a different manner (Christian 1975).

Another critical assumption that requires some explanation here is the steady-state nucleation (Turnbull 1948; Kantrowitz 1951; Kelton et al. 1983). The steady-state rate of nucleation requires some time to be established, especially in condensed phases during which transport is very slow. An order of magnitude analysis can be given by (Kantrowitz

1951) the relation

$$I(t) = I^S \exp(-\tau/t) \qquad (6.59)$$

where I(t) is the rate at time t, and τ is the time lag given by (Turnbull 1956)

$$\tau = \frac{i^{*2}}{0_i^* \, \upsilon_i^+} \qquad (6.60)$$

The time lag for nucleation of undercooled water calculated from Eq(6.60) is on the order of 10^{-9} seconds which is a negligible contribution (Wood & Walton 1970).

Experimental studies on homogeneous nucleation from the bulk systems of undercooled liquid are generally unsuitable to test the accuracy of Eq.(6.58) because bulk systems contain catalytic surfaces initiating heterogeneous nucleation. Turnbull (Turnbull 1950a-b; Turnbull 1965b) showed that the most promising method of testing the homogeneous nucleation theory in undercooled liquid is the measurement of I^S in a dispersion of fine droplets. Impurities are seggregated into proportionally few of the droplets and the homogeneous nucleation is achieved. The classic experiment on homogeneous nucleation (Turnbull 1956) used a foaming agent to divide a mass of liquid mercury into a large number of droplets. The droplets are sufficiently small in size and large in number to ensure that impurities were segregated into relatively few droplets so that homogeneous nucleation can be acheived

for the major portion of the droplets. Studies performed on some organic (DeNordwall & Staveley 1954; Langham & Mason 1958; Turnbull & Cormia 1961) and inorganic compounds (Buckle 1961), polymers (Cormia et al. 1962; Burns and Turnbull 1967; Koutsky et al. 1967), metals (Turnbull 1950c-d, 1952) and water (Wood & Walton 1970). One can estimate σ from these undercooling nucleation experiments using Eq.(6.58).

If the nucleation of small droplets of water were homogeneous, the σ values determined from nucleation experiments should be comparable to independently measured values. The σ values for ice-water from different experimental methods are shown in Table 6.1. Values for σ are all clearly of the same order of magnitude irrespective of the method of determination. Realizing that the values reported obtained by various experimental methods are calculated using different methods of averaging σ, and considering the uncertainities in the techniques used, the agreement between the values of the nucleation experiments and other techniques are quite satisfactory. This establishes the validity of homogeneous nucleation.

6.4. Theory of Heterogeneous Nucleation in Condensed Systems

Although theories of homogeneous nucleation have had some success in explaining certain features of the kinetics of nucleation in condensed systems, most observable nucleation phenomena are of the heterogeneous

TABLE 6.1.

SURFACE ENERGY OF ICE-WATER INTERFACE FOR PURE WATER

METHOD	$\sigma x10^{+3}$ (J/m^2)	PLANE	TEMP. (^oC)	REFERENCES
Nucleation	27.53	hexagonal prism	-36.5	Wood & Walton (1970)
Nucleation	24.22	spherical cluster	-36.55	Wood & Walton (1970)
Nucleation	19.70	over all faces	-40	Dufour & Defay (1963)
Nucleation	22.00	over all faces	-40	Fletcher (1970)
Nucleation	32.10	over all faces	-40	Schaefer (1952)
Nucleation	32.10	spherical cluster	-40	Turnbull (1950c)
Nucleation	18.00	over all faces	-40	Franks et al. (1984)
Crystal Growth	31.80	// to c-axis	~0	Fernandez & Barduhn (1967)
	20.00	// to c-axis		Kotler & Tarshis (1968)
Morpholog. Stability	22.00	// to c-axis	0	Hardy & Coriell (1969)
Contact Angle	33.00	over all faces	-40	Ketcham & Hobbs (1969)
Grain-Boundary Grooves	44.00	// to c-axis		Jones (1973)
	29.10	// to c-axis	-0.4	Hardy (1977)

type. The energetics of heterogeneous nucleation has been described by Gibbs (1961) and Volmer (1929) and the kinetics in condensed systems has been analyzed by Turnbull (1950a); Turnbull & Vonnegut (1952). Application of this theory to ice formation from water has been extensively carried out by Fletcher (Fletcher 1960, 1963, 1969, 1970).

The heterogeneous nucleation occurs by formation of clusters on impurities or surfaces in contact with the liquid phase. The temperature at which the clusters become stable and grow is a function of the size and the degree of promotion of ice structure of the substrate sites. Substrates typically increase cluster stability, thereby facilitating the nucleation at higher temperatures than would be possible for homogeneous nucleation. The major difference between homogeneous and heterogeneous nucleations is the term, ΔF_i^*, the free energy of formation of a critical sized cluster. The simplest case is to consider an ice cluster of the form of a spherical cap on a plane solid surface characterized by the contact angle θ (see Fig.6.9a). The contact angle, θ, is related to the solution-cluster, $\sigma^{\alpha\beta}$, solution-substrate, $\sigma^{\alpha S}$, and cluster-substrate, $\sigma^{\beta S}$, interfacial energies as follows

$$\sigma^{\alpha S} = \sigma^{\beta S} + \sigma^{\alpha\beta} \cos\theta \qquad (0 \leq \theta \leq \pi) \qquad (6.61)$$

As shown in Fig.6.9a, the lattice parameters of the solid substrate do not match those of the ice cluster, the ice lattice will either deform elastically at the ice-substrate interface so as to match the solid

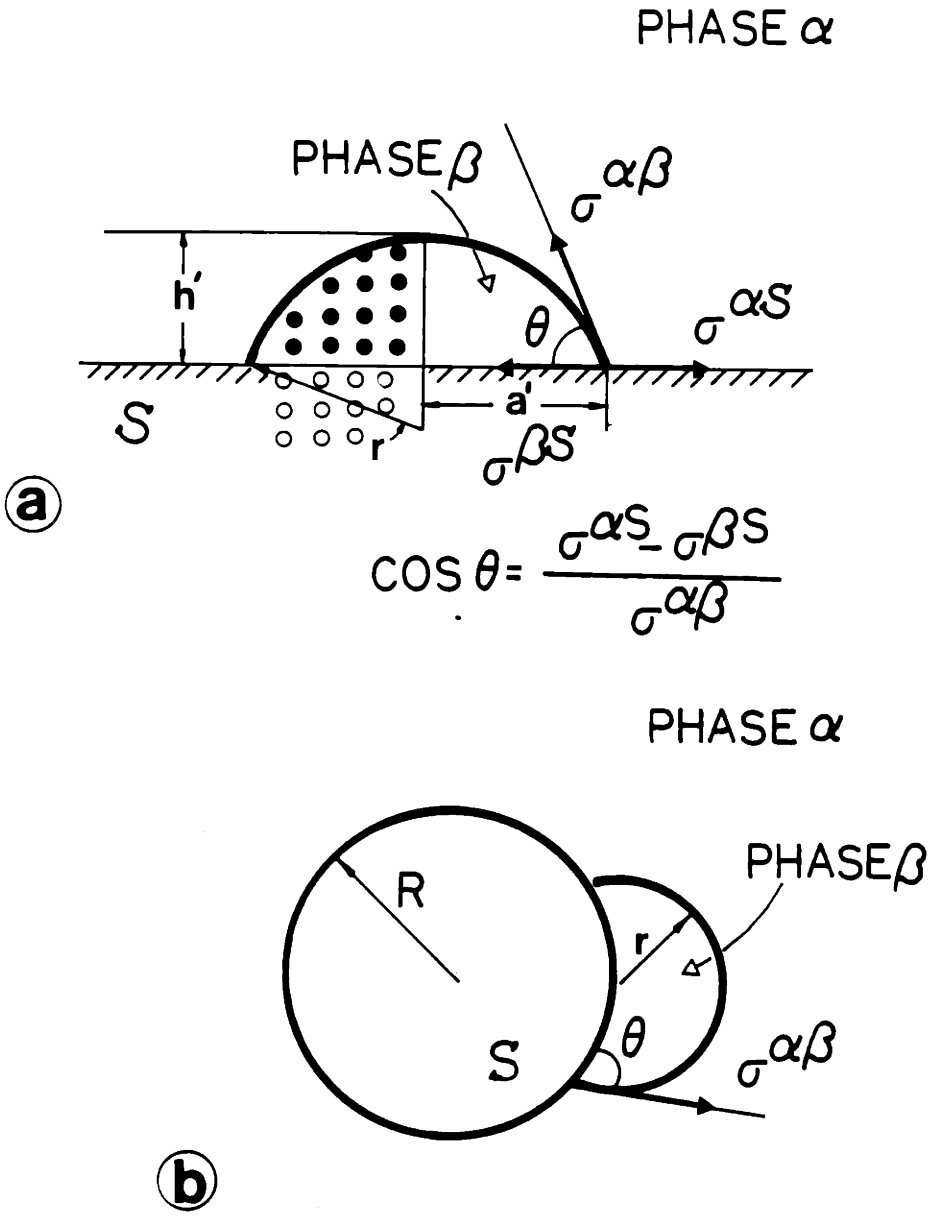

FIGURE.6.9. Heterogeneous nucleation from the α phase: (a) heterogeneous nucleation on a flat plate; (b) heterogeneous nucleation on a spherical particle. Also shown in (a) is the latice misfit between a cap shaped ice cluster and an insoluble substrate.

lattice thereby giving coherent growth, or that the ice will have dislocations. The degree of misfit between the ice and substrate lattices, δ, can be expressed following the procedure of Turnbull & Vonnegut (1952)

$$\delta = \left| \frac{a - a_o}{a_o} \right| \qquad (6.62)$$

where a and a_o are the lattice parameters for the substrate and ice, respectively. The elastic strain, ϵ, developed in the cluster is given by

$$\epsilon = \left| \frac{z - a_o}{a_o} \right| \qquad (6.63)$$

where z is the lattice parameter of strained cluster. The amount of misfit will then be given by $\delta - \epsilon$.

The free energy required to form the cap, ΔF_{het}, will then be given by including the elastic strain term in Eq.(6.27) (Turnbull & Vonnegut 1952)

$$\Delta F_{het} = n^{\beta} (\Delta\mu_b + v^{\beta} C\epsilon^2) + \sigma^{\beta S} A^{\beta S} + \sigma^{\alpha\beta} A^{\alpha\beta} - \sigma^{\alpha S} A^{\alpha S} \qquad (6.64)$$

where the last three terms take all the σA^S terms into consideration, and $C\epsilon^2$ (C constant) is due to elastic strain. The formal theory of nucleation catalysis is based on the assumption that the strain in cluster is zero ($\epsilon = 0$). The kinetics of heterogeneous nucleation of

mercury, tin crystals, ice formation, and oriented growth are satisfactorily described on the basis of the formal theory and ϵ can be neglected.

By taking into consideration the following geometrical relations for the volume and area of a spherical segment shown if Fig.6.9b

$$\begin{aligned} h' &= r\,(1 - \cos\theta) \\ V &= \pi h'^2\,(3r - h')\,/\,3 \\ a' &= r\sin\theta \\ A^S &= 2\pi r h \end{aligned} \qquad (6.65)$$

and substutiting Eqs.(6.61), (6.65) in Eq.(6.64)

$$\Delta F_{het} = \left(\frac{1}{3}\pi r\,(1 - \cos\theta)^2\, r\,(2 + \cos\theta)\,\Delta\mu_b + \pi r^2 \sin^2\theta\,\sigma^{\beta S} + 2\pi r^2\,(1 - \cos\theta)\,\sigma^{\alpha\beta} - \pi r^2 \sin^2\theta\,\sigma^{\alpha S}\right) \qquad (6.66)$$

When a cluster of critical size is formed, chemical equilibrium requires from Eq.(6.66) since $\Delta\mu_b = 0$

$$\Delta F^*_{het} = \frac{\sigma^{\alpha\beta} A^{S*}}{3}\,\frac{(1 - \cos\theta)^2\,(2 + \cos\theta)}{4} \qquad (6.67)$$

Using Eqs.(6.51), (6.67)

where $$\Delta F^*_{het} = \Delta F^*_{hom}\, f(\theta) \qquad (6.68)$$

$$f(\theta) = \frac{(1 - \cos\theta)^2 (2 + \cos\theta)}{4} \qquad 0 \leq f(\theta) \leq 1$$

We can see from Eq.(6.68) that the effect of the substrate is to reduce the formation energy of the corresponding critical spherical cluster by a factor $f(\theta)$. Variation of $f(\theta)$ with θ is presented in Fig.6.10. When $\theta = \pi/2$, the free energy to form a critical cluster in the interior of phase α is twice that to form one on the substrate. As $\theta \to \pi$, the free energy of the heterogeneous nucleation increases to that required for the homogeneous nucleation. On the contrary as $\theta \to 0$, the free energy decreases to zero. When $\theta = 30^o$ the activation energy is less than 1% of that required for homogeneous nucleation.

The nucleation rate for clusters formed on the substrate can be found by a procedure analogous to that used for homogeneous nucleation. If the number of atoms which are in contact with the substrate is N^s, then the equilibrium distribution of clusters of size i can be written as

$$N_i = N^s \exp(- \Delta F_i^{het} / kT) \qquad (6.69)$$

Thus, the corresponding steady-state nucleation rate can be derived as (see Turnbull, 1956) in a similar manner to Eq.(6.58)

$$I^s_{het} = K_{het} \exp(- \frac{\Delta f + \Delta F^*_{het}}{kT}) \qquad (6.70)$$

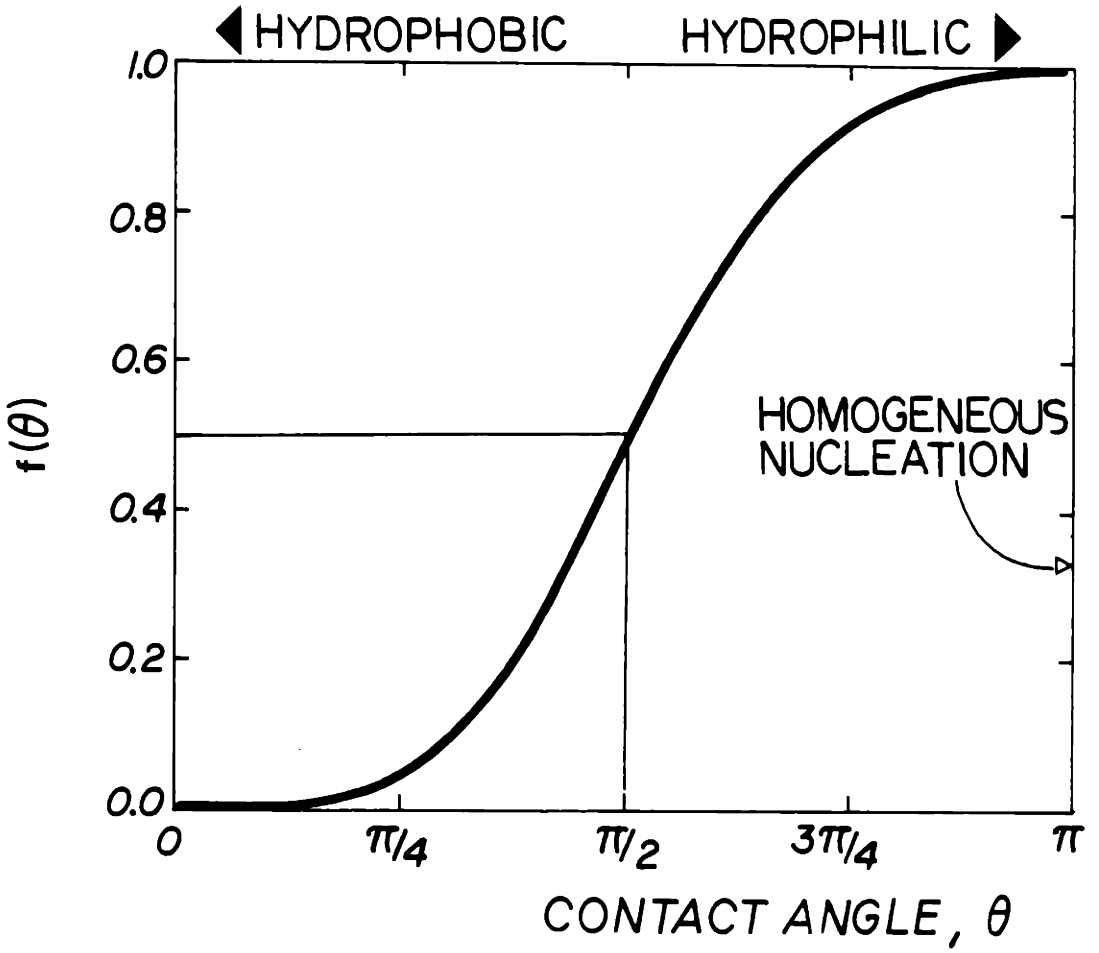

FIGURE.6.10. Variation of $f(\theta)$ with the contact angle in heterogeneous nucleation.

where

$$K_{het} = 2\upsilon\beta^{1/3} \frac{(\sigma\alpha\beta kT)^{1/2}}{h} N^S f(\theta)^{1/6}$$

Usually, the pre-exponential term K_{het} is smaller than that in Eq.(6.58) by a factor 10^7, the ratio of the number of water molecules per surface area to the number per volume.

If the nucleating particle is a sphere of radius R_c as shown in Fig.6.9b and the ice cluster grows on it as a spherical cap, then (Fletcher 1958)

$$f(m,x) = \frac{1}{2}\{1 + [\frac{1 - mx}{h}]^3 + x^3 [2 - 3 (\frac{x - m}{h}) + (\frac{x - m}{h})^3] + 3 m x^2 [(\frac{x - m}{h}) - 1]\} \qquad (6.71)$$

where

$$h = (1 + x^2 - 2 mx)$$

$$m = \cos\theta$$

$$x = R_c/r^*$$

The function f(m,x) has also been evaluated for other geometries and the general behavior is similar to that for the spherical case (Fletcher, 1963). The assumption of spherical geometry is reasonable, and even when this is not true the influence of cluster shape will not be significant unless extreme geometries are encountered. Fig.6.11 shows the variation of the geometrical factor f(m,x) in terms of the ratio x. As can be seen from this curve as the radius of the impurity increases

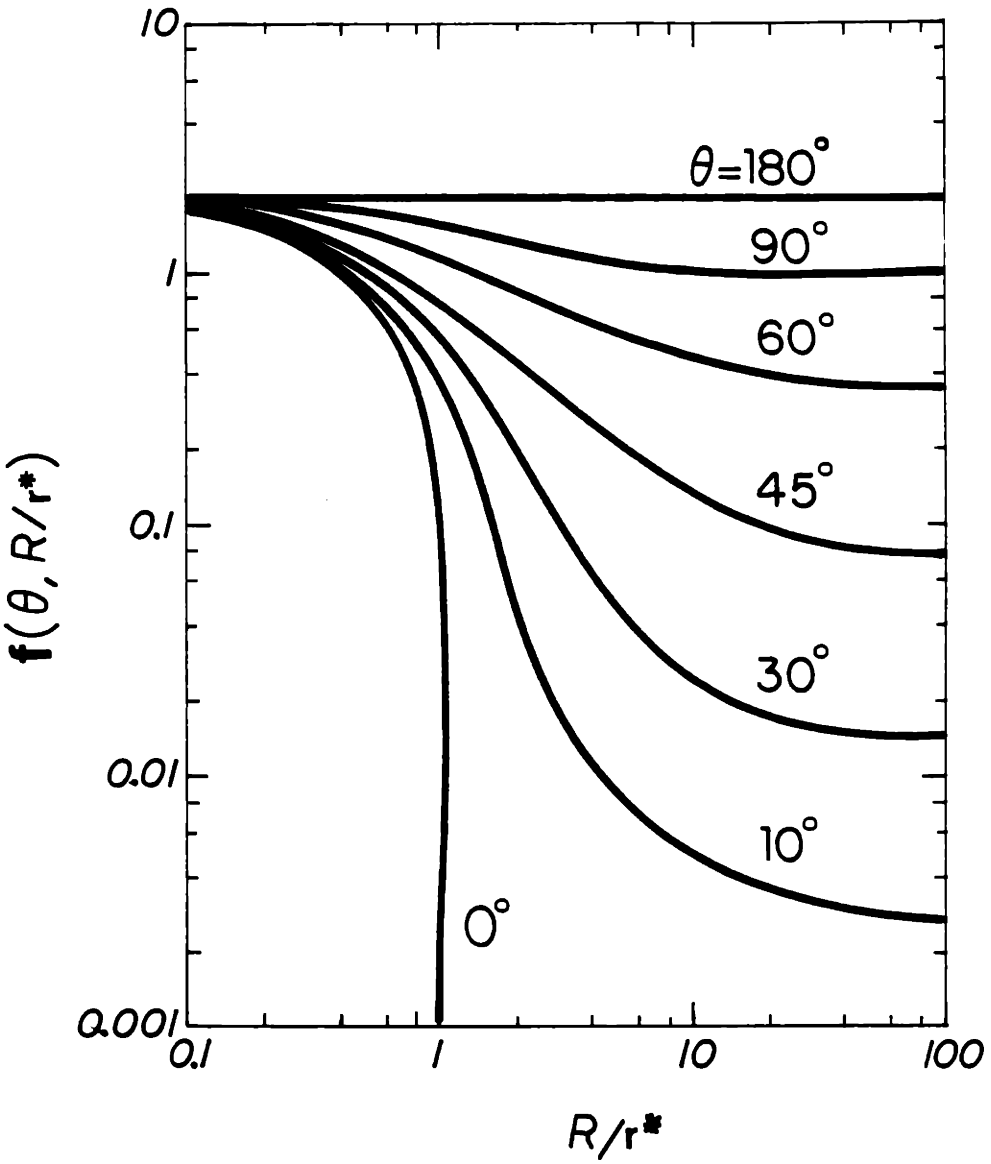

FIGURE.6.11. The geometrical factor f(cos θ,R/r*) in terms of the ratio R/r* as a function of θ.

the variation in factor f(m,x) becomes smaller reaching the value for flat plane when $R \to \infty$.

Mode of Action of Ice Nuclei

A major research effort has been devoted to establish the specific characteristic features of the substrate and its mode of action. Small lattice misfit between the crystallographic structures of silver iodide (AgI) and ice and exceptionally effective nucleating ability of AgI appear to confirm that lattice misfit does play a role in heterogeneous nucleation (Vonnegut 1947). More recently, however, it has become evident that the match of the crystal structure of the substrate with that of ice is not the only factor involved in promoting ice nucleation.

Another factor that increases the nucleation efficiency of a substrate is that it should possess a degree of hydrophobicity. Karasz et al. (1956) pointed out that AgI is essentially hydrophobic in nature and that the surface of AgI and ice are probably energetically incompatible. Zettlemoyer et al. (1961; 1963) confirmed these results. Several types of silicas were found to be more effective in initiating ice nucleation when they were hydrophobed. Some of these hydrophobed silica surfaces were as effective as AgI.

In addition to hydrophobicity requirement, Fletcher (1959) has predicted that the ideal nucleating surface should have zero net charge.

Edwards and Evans (1962) have found that the ice nucleating efficiency of AgI is a maximum at the isoelectric point and have confirmed Fletcher's hypothesis. Earlier work by Weyl (1949) showed that a surface containing polarizable atoms is likely to be slightly hydrophobic and this could explain the controversial observations of Hosler (1951) that most good ice nuclei contain highly polarizable atoms. Later, Gokhale & Goold (1968) found that if AgI particles were introduced into water drops when the temperature was above 0°C, the drops had to be cooled to -13 to -15°C before they could start the freezing. Whereas, AgI particles were the most effective in surface nucleation. AgI particles sprinkled on undercooled millimetre size water droplets were effective as ice nuclei at -5°C. Examples of various foreign particles to nucleate the freezing of the undercooled water droplets include the studies by Gokhale & Spengler (1972), Sax & Goldsmith (1972), Gokhale & Lewinter (1971), and Pitter & Pruppacher (1973). The phenomenon has been termed **contact nucleation.** The mechanism by which surface contact promotes ice nucleation is still contreversial (Cooper 1974; Fukuta 1975a,b), however, the experimental evidence is clear that the surface nucleation of droplets is more effective than suspended particles in the droplets. Contact nucleation (or surface nucleation) may especially be important in ice nucleation inside the cells when cells are surrounded by external ice. One may envisage situations where the external ice may alter the surface of the plasma membrane so that the ice can form on the plasma membrane heterogeneously. This will be discussed further in the next chapter.

Several organic compounds that are encountered in biological cells are also shown to possess ice nucleating ability. Examples of such organic compounds include α-phenazine (Head 1962), metaldehyde (Fukuta 1963), steroids (Head 1961; Fukuta & Mason 1963), and amino acids, peptides and proteins (Power & Power 1962; Barthakur & Maybank 1963; Fukuta and Mason 1963). However, these compounds are active ice nucleators only when they are in crystalline form, and they are rendered ineffective in solution (Power & Power 1962). In addition, another interesting area of natural ice nucleation is the bacterial ice nucleation. A detailed review of bacterial ice nucleation is discussed in Lindow (1983).

In summary, the general requirements for a good ice nuclei can be outlined from the brief review given above: (1) small lattice mismatch with ice, (2) a slight degree of hydrophobicity and (3) a low net surface charge. Although these criteria appear to be valid, the mechanism of heterogeneous nucleation is not completely understood at this time.

6.5. Theory of Ice Nucleation in Biological Cells

There are major differences between simple water drops and biological cells so that the nucleation theory should be altered accordingly. The intracellular solutions of biological cells are multicomponent aqueous electrolyte solutions of usually completely

dissociated inorganic and protein salts (Clegg 1984; Powers & Tupper 1975; Biggers et al. 1977). Hydration effects are also important in biological solutions containing electrolytes and charged proteins. When a charged ion or a plane (proteins) is brought into contact with water, the intense electric field surrounding the electrolyte and the proteins attracts a layer of water molecules around it due to dipole characteristics of water. The ion-dipole and dipole-dipole interactions do not stop at the first layer of water and is strong enough to influence further layers (Ling 1972). Therefore, some of the water in biological cells is attached to electrolytes and macromolecules and not available as free water (Levin 1976a). In the present analysis, it will be assumed that the intracellular solution is a hydrated pseudo-binary mixture of water-protein-salt solution. Although such a model may be too simplistic to represent the real intracellular solution, it is very useful in understanding the physics of the nucleation process without being overwhelmed by complicated models. Fig.6.12. describes the simplified model of the complex intracellular solution that will be the basis of the following sections. As shown in this figure, when the freezing starts the cell (plasma membrane) is exposed to extracellular ice-water equilibrium solution of NaCl. The plasma membrane, however, prevents the penetration of the external ice into the cell. As described in detail in Chapter V, the cell starts dehydrating in response to the external driving force. The system is changing its temperature, volume and composition during the freezing complicating further the analysis of ice-nucleation in biological cells. In summary, we are dealing with a complex system of water-protein-salt solution

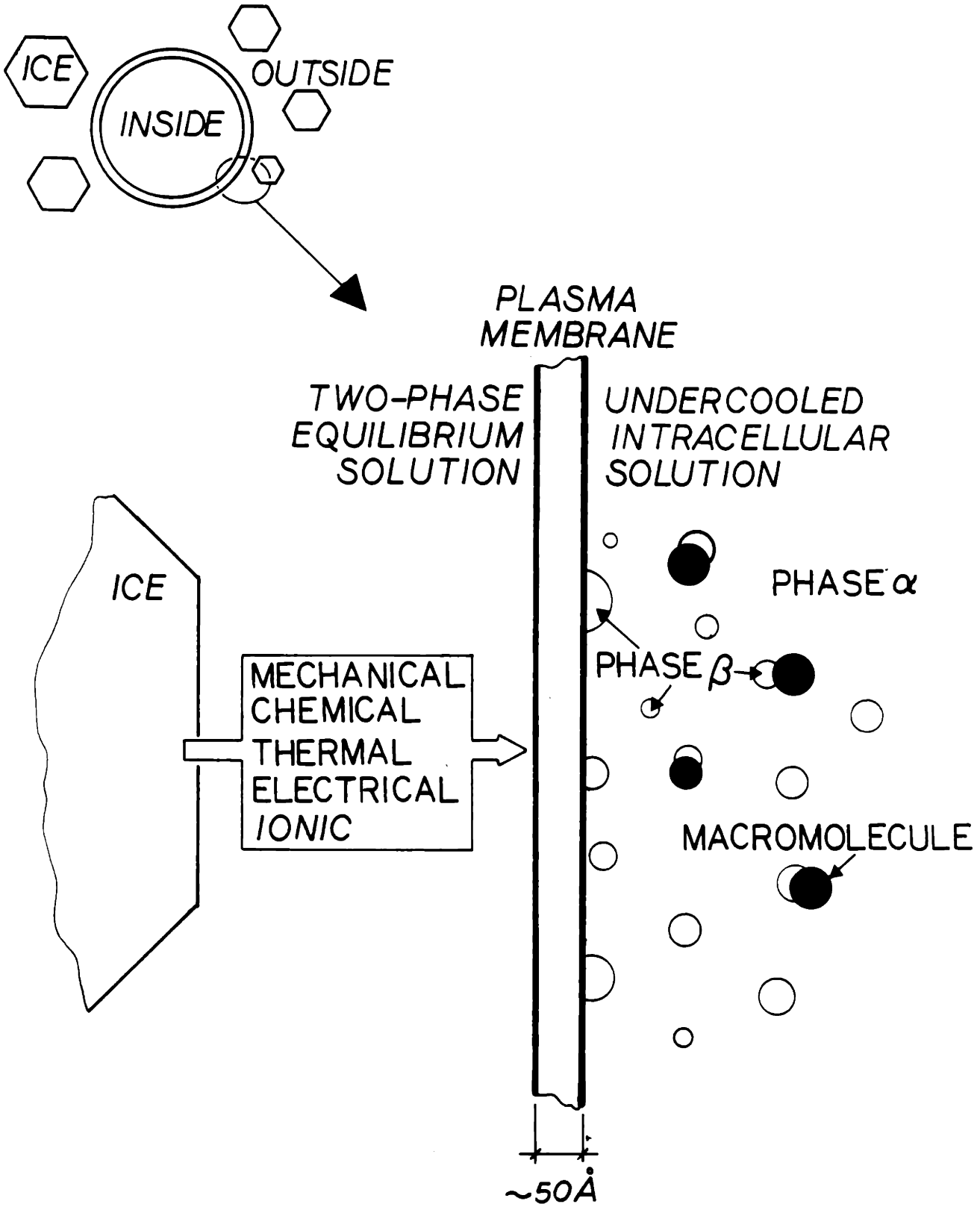

FIGURE.6.12. Schematic model for heterogeneous nucleation mechanisms in biological cells. Heterogeneous nucleation of phase β (ice) may be catalyzed by the plasma membrane or the supramolecular particles.

which is bound with a plasma membrane exposed to partially frozen electrolyte solution and which varies its composition and volume during freezing.

Effect of Electrolytes on Ice-Nucleation

Undercoolings of droplets containing various electrolytes have been investigated (DePena et al. 1962; Reischel & Vali 1975) to understand the effect of dissolved substances on the mechanism of phase change. It is well known that solutes in water cause a depression of the equilibrium freezing point by lowering the water vapor pressure. Although the equilibrium behavior has been investigated extensively, little is known on the effect of solutes on the non-equilibrium freezing point (i.e. temperature at which ice nucleation is initiated in the undercooled solution). There exists discrepancy among reports (Hoffer 1961; DePena et al. 1962; Pruppacher 1963; Pruppacher & Neiburger 1963; Uzu & Sano 1965) with respect to the influence of a dissolved substance on the freezing temperature of a droplet.

Pruppacher (1963) has suggested on the basis of his droplet experiments that the effect of water-soluble substances is to lower the freezing temperature and the rise found in old literature is mainly due to the insoluble particles introduced in droplets by the addition of solutes. His conclusion was challanged by Uzu & Sano (1965). They suggest that ions of electrolytes are effective ice nucleants increasing

the non-equilibrium freezing point. In order to test the possibility of introducing insoluble particles into the droplet preparations, they also observed the freezing of non-electrolytes prepared by the same way as electrolytes. Their results with non-electrolytes showed no dependence of non-equilibrium freezing temperature on a wide range of concentrations. Hence, they concluded that the insoluble particles, if introduced into water by chance, might have little effect on heterogeneous nucleation as proposed by Pruppacher (1963).

These studies were, however, concerned with rather large droplets which showed undercoolings typical of heterogeneous nucleation. Homogeneous nucleation of various aqueous solutions has been investigated by Wood & Walton (1969), and Rasmussen & MacKenzie (1972). Their result suggested that the dissolved electrolytes in water depress the homogeneous nucleation temperature more than the equilibrium freezing temperature. More research is undoubtely necessary in order to incorporate all the possible effects of dissolved solutes into nucleation equations. In the rest of this section we will try to incorporate some of these effects into our nucleation frequency equations in order to predict the behavior of biological cells during freezing.

In freezing of aqueous solutions of electrolytes the diffusion of solute does not need to be considered in the solid phase because the distribution coefficient, k, representing the ratio of solute concentration between solute and liquid is extremely small ($k = 10^{-6}$

...10^{-8}, Korber 1988). This means that the solid phase remains very pure and its free energy change with composition is negligible. The standard free energy change of forming an ice cluster in an electrolyte solution can then be written simply

$$\Delta F_i = n^{\beta} \Delta\mu_s + \sigma^{\alpha\beta} A^s \qquad (6.72)$$

where $\sigma^{\alpha\beta}$ is the ice-solution interfacial energy, and $\Delta\mu_s$ is the driving force to transfer a water molecule from the electrolyte solution to a bulk ice crystal. The effects of solutes on the nucleation can be primarily explained through their influence on the values of $\Delta\mu_s$ and $\sigma^{\alpha\beta}$. At a given temperature, the thermodynamic driving force between a cluster and an electrolyte solution is greater than the driving force between a cluster and a pure water slowing down the nucleation process. This effect, however, is greatly diminished when $\Delta\mu_b$ and $\Delta\mu_s$ are compared at a given supercooling in a dilute solution. For most of the practical purposes, the intracellular solution can be assumed to be dilute on a molar basis and the differences between $\Delta\mu_b$ and $\Delta\mu_s$ can be neglected. The detailed calculation of the thermodynamic driving force for dilute aqueous solutions will be given later in this section.

The effect of electrolytes on the solid-liquid interfacial energy is analyzed by Wood & Walton (1969). However, their experiments are not very conclusive and reliable relationships for the variation of $\sigma^{\alpha\beta}$ with the concentration cannot be derived. Their result indicates that the ice-solution interfacial energy increases sligthly by increasing the

concentration which is in disagreement with Volmer's (1939) and Antonow's (1907) rules. Both of these rules suggest that

$$\sigma_{\text{solid-liquid}} = \sigma_{\text{solid-vapor}} - \sigma_{\text{liquid-vapor}} \qquad (6.73)$$

where liquid-vapor interfacial energy increases linearly with salt concentration (Adamson, 1960). Hence from Eq.(6.73), one should expect a decrease in solid-solution interfacial energy. Recently, Oxtoby (1986) calculated the solid-liquid surface free energy using density functional theory. The result calculated for $\sigma^{\alpha\beta}$ was

$$\sigma^{\alpha\beta} \propto \rho_o^{2/3}\, T\Delta S_f = \rho_o^{2/3}\, \Delta H_f \qquad (6.74)$$

where ρ_o is the average density of the liquid, a relationship proposed first on empirical grounds by Turnbull (Turnbull 1965a; Woodruff 1973). The value of ΔH_f decreases slightly when electrolytes are added to water, and ρ_o increases with the addition of electrolytes, the net effect depending on the concentration and temperature as well as the type of the solute. In any case the variation of $\sigma^{\alpha\beta}$ with electrolyte concentration is small and will be neglected in this study.

Another effect of electrolytes on the nucleation kinetics will be through their effect on the equilibrium population of clusters (Eq.(6.37)). Dufour and Defay (1963) showed that Eq.(6.37) can easily be modified for the formation of clusters in salt water. Their result suggest that

$$N_i = (N' + N_S) \exp(-\Delta F_i / kT) \qquad (6.75)$$

where N_S is the number of molecules of solute and N' is the number of molecules of solvent. Since cells can be considered dilute on a molar basis, the effect of N_S is negligible. Same relationship can be written for heterogeneous nucleation by replacing volume terms with substrate surface area terms. However, the most important effect of electrolytes on the nucleation frequency is probably through their effect on the activation energy for molecular transport and this will be analyzed separately in the next section.

Activation Energy for Molecular Transport in Aqueous Cytoplasm

The activation energy, Δf, in Eq.(6.41) for molecular transport of a molecule in α phase to the surface of the cluster is the same as viscous flow as proposed by Turnbull & Fisher (1949). Using the Eyring approach to rate processes (Eyring 1935; Glasstone et al. 1941), the activation energy for molecular transport can be expressed as a function of solutions viscosity by

$$\Delta f = kT \ln \frac{\eta v^{\alpha}}{hN_{AV}} \qquad (6.76)$$

where v^{α} is the molar volume of phase α, N_{AV} is the Avagadro number, η is the viscosity. Substituting Eq.(6.76) in Eqs.(6.41), (6.42) yields

$$\upsilon = \frac{kTN_{AV}}{\eta v^{a}} \qquad (6.77)$$

In order to evaluate Eq.(6.77) during freezing of biological cells, the concentration and temperature dependence of viscosity are needed. Since transport processes are considered to be "volume transfer" processes rather than "mass transfer" processes, they should be treated accordingly on a volume basis and not molar basis. A suspension of rigid particles (i.e. electrolytes and macromolecules) in a continuous medium will have a higher viscosity than the medium alone, because of the interference by the particles with the stream-lines of the flow pattern. An effect of this kind will be expected during freezing of hydrated water-protein-salt solutions of biological cells. When biological cells are suspended in isotonic solutions, the mole fraction of water is always greater than 0.993 and can be considered dilute on a mole basis. However, the volume fraction of free water is usually less than 80% and cannot be considered dilute on a volume basis even at isotonic conditions (Loewenstein & Cohen 1964; Abramczuk & Sawicki 1974). Therefore, the change in volume during freezing will have an important effect on the viscosity and obviously on the kinetics of ice nucleation.

The first attempt to treat mathematically the viscosity of suspensions of rigid spherical obstructions in a continuum is due to Einstein (1906, 1911) who derived

$$\eta/\eta_W = 1 + 2.5\phi_S \qquad (6.78)$$

where η_W is the viscosity of the pure liquid, and ϕ_S is the volume fraction of the solute. The derivation introduces certain simplifications which are valid only for infinitely dilute suspensions of spherical particles. A way of approach to the problem of higher concentrations which introduces the mutual interaction of the particles and their collisions is derived by Vand (1947)

$$\ln (\eta/\eta_W) = \frac{2.5\phi_S}{1 - Q\phi_S} \qquad (6.79)$$

where Q = 0.609375 is the interaction parameter. Eqs.(6.78), (6.79) are plotted as a function of the solute volume fraction in Fig.6.13. Eq.(6.79) is shown to be accurate up to the viscosities five to ten times that of water (Robinson & Stokes 1959) for strongly hydrated electrolyte solutions as well as solutions of large non-electrolyte molecules. The above theory assumes that the aqueous cytoplasm of biological cells is well mixed solution containing various ions and macromolecules. All these are dissolved in water. This kind of description of the cytoplasm is referred as the "solution description". The other extreme for cytoplasmic structure is referred as to an "organized description" in which all the solutes, macromolecules are associated with cellular ultrastructures. Therefore, aqueous compartments in between cellular ultrastructure is assumed to be pure water even when cells dehydrate. The viscosity of such a solution model

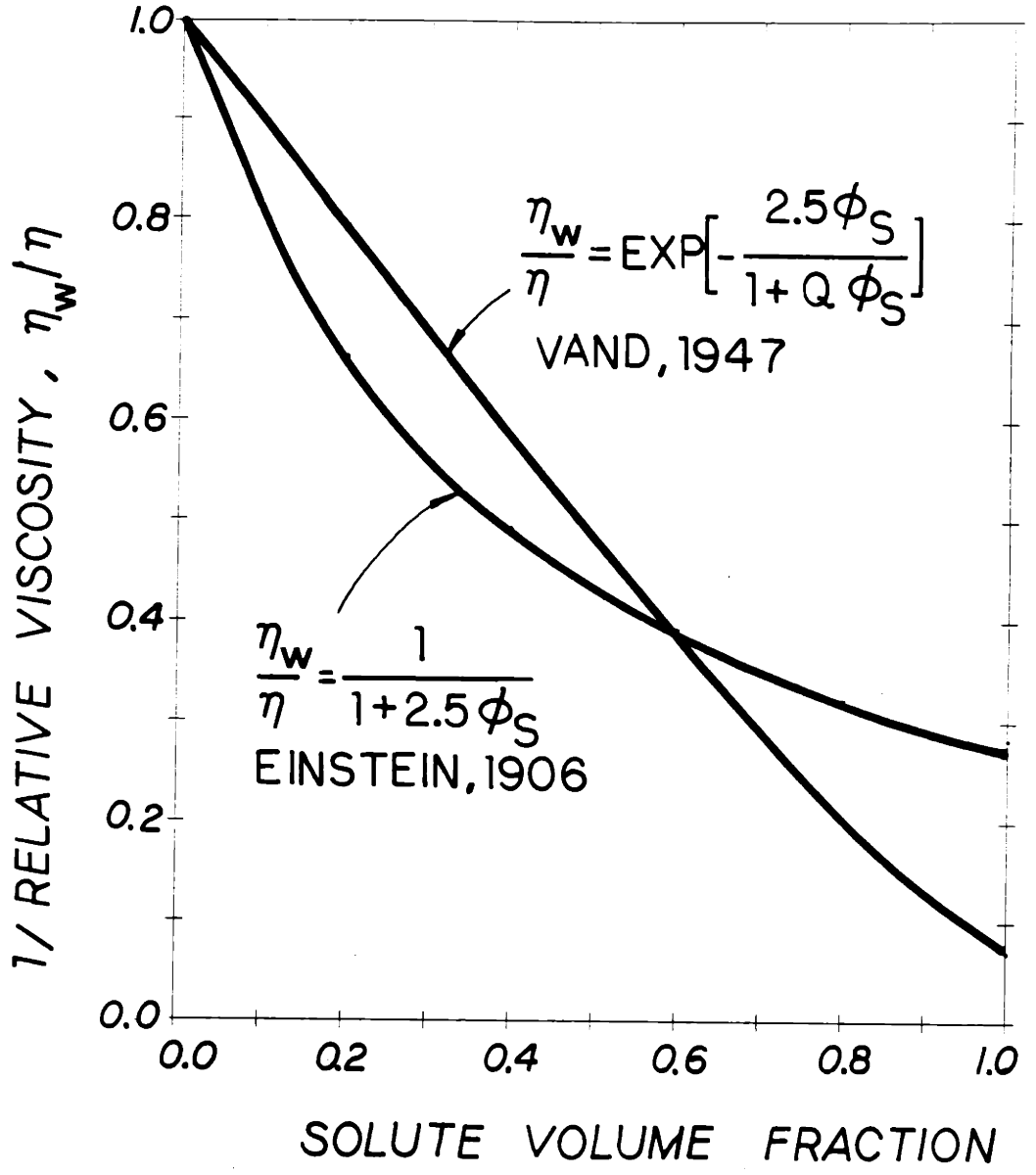

FIGURE.6.13. Concentration dependence of solution viscosity as a function of solute volume fraction according to Einstein (1906, 1911) and Vand (1947).

would be essentially the same as pure water and independent of the dehydration of the cell in marked contrast to "solution description" of the aqueous cytoplasm used in our analysis. Interested reader should refer to an excellent review article by Clegg (1984) and to a recent book by Keith (1979).

The prediction of the volume fraction of the solute, ϕ_s, in biological cells is a complex problem because of the presence of hydrated multi-electrolytes and macromolecules and worked out in detail for red blood cells by Levin (1976), and Levin et al. (1978). A similar derivation will be followed here for unfertilized mouse eggs. The volume fraction of the solutes and the proteins, ϕ_m, can be defined as follows on a hydrated basis for a pseudo-binary mixture

$$\phi_m = \frac{n_m v_m^h}{n_w^F v_w + n_m v_m^h} \tag{6.80}$$

where n_m is the number of moles of the fictitious solution species (i.e. proteins plus salt present within the cell), v_m^h is the apparent hydrated molar volume of the protein and the salt, n_w^F is the number of free water moles available for water transport, and v_w is the molar volume of water. The number of moles of solution species can be calculated from

$$n_m = n_p + v_s n_s^{in} \tag{6.81}$$

where n_p is the number of moles of proteins, n_s^{in} is the number of moles

of the salt in the cell, and v_s (=2) is the dissociation constant. The apparent hydrated molar volume of fictitious solute is a weighted average and can be written as follows

$$v_m^h = \frac{n_s^{in} v_s^h + n_p v^h}{n_m} \qquad (6.82)$$

where v_s^h and v_p^h are the hydrated molar volume of salt and proteins, respectively. The number of moles of free water in Eq.(6.81) can be expressed

$$n_w^F = n_w^{in} - n_w^B \qquad (6.83)$$

where n_w^B is the number of moles of bound water in the cell and is given by

$$n_w^B = h_m n_m \qquad (6.84)$$

where h_m is the apparent hydration number of solution species (i.e. apparent moles of bound water associated with the apparent moles of fictitious solution species). The apparent hydration number is defined as

$$h_m = \frac{n_s^{in} h_s + n_p h_p}{n_m} \qquad (6.85)$$

where h_s and h_p are the hydration number of the salt and the proteins,

respectively. Substituting Eqs.(6.81)-(6.85) in Eq.(6.80), one can determine the volume fraction of salt and protein in the cell (see App.A). The solution of Eqs.(6.80)-(6.85) for unfertilized mouse eggs yield a solute volume fraction of 22% in isotonic conditions. This means that only 78% of the total cell volume is free water for transport and the intracellular milieu cannot be assumed to behave as a dilute solution on a 'volume' basis. The viscosity of the intracellular water-protein-salt solution can, therefore, be calculated with reasonable accuracy using Eq.(6.80) provided that the true volume fraction can be estimated. The assumed values to calculate ϕ_m are subject to considerable uncertainity and reasonable only for a first-cut analysis. An easier method of predicting ϕ_m is desirable. Since the volume fraction occupied with hydrated macromolecules is much higher than the volume fraction occupied with hydrated electrolytes (see App. A),

$$n_s{}^{in}\upsilon_s{}^h \;/\; n_p\upsilon_p{}^h \;(\simeq 0.03) \;\ll\; 1 \qquad (6.86)$$

then Eq.(6.80) can be approximated by the following relation

$$\phi_m \;=\; \frac{n_p\upsilon_p{}^h}{n_w{}^F\upsilon_w + n_p\upsilon_p{}^h} \;\simeq\; \frac{V_p{}^h}{V_w{}^F + V_p{}^h} \;\simeq\; \frac{V_b}{V_c} \qquad (6.87)$$

where V_c, and V_b are the cell volume, and inactive cell volume, respectively. The solutions of Eqs.(6.80), (6.87) are shown in Fig.6.14 as a function of the osmolality of the suspending medium. As can be seen from this figure, Eq.(6.87) is a good approximation to Eq.(6.80) given the uncertainities involved in the various assumptions.

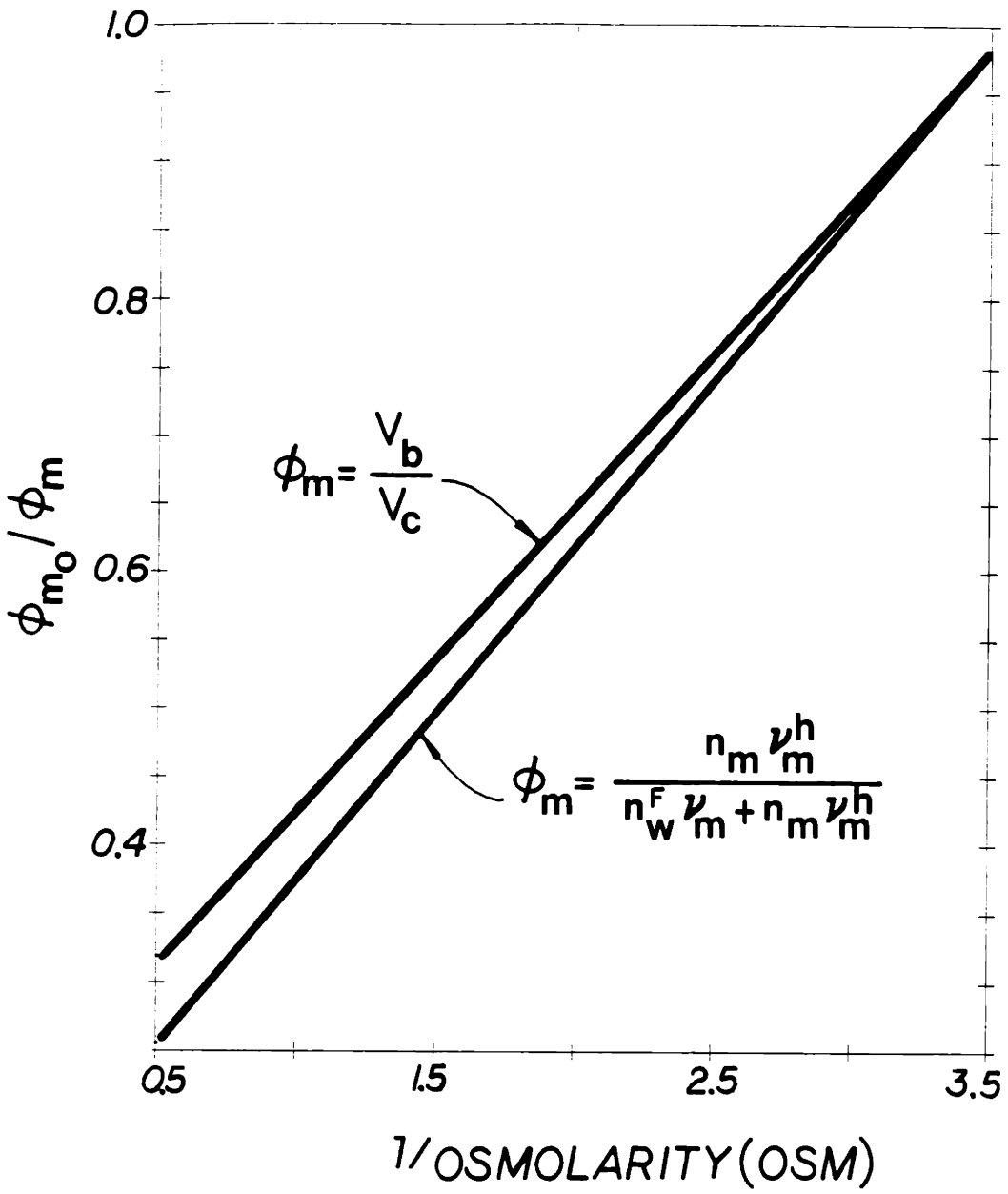

FIGURE.6.14. Variation of the ratio of the initial volume fraction of salt and protein to volume fraction of salt and protein in anisotonic solutions.

In summary, the dependence of viscosity on concentration can be simply estimated from Eq.(6.87).

In addition to the concentration effects on the viscosity during freezing of biological cells, the change in temperature will alter the viscosity as well. If the viscosity of the intracellular solution is assumed to have the same temperature dependence as pure water, then the Eq.(6.79) can be rewritten as

$$\eta/\eta_w(T) = \exp\left(\frac{2.5\phi_m}{1 - Q\phi_m}\right) \qquad (6.88)$$

The temperature dependence of the viscosity of fluids is often described using the Vogel-Fulcher form $\eta \propto \exp(E/(T - T_o))$ (Vogel 1921; Fulcher 1925). However, the recent mode-coupling theories (Bengtzelius et al. 1984; Angell 1988) showed that a better fit can be obtained by a power law temperature dependence of the form

$$\eta_w(T) = A\,(T/T_c - 1)^{\lambda} \qquad (6.89)$$

where A = 0.139 cP, T_c = 225 K, and λ = -1.64 for water (Taborek et al. 1986). Eq.(6.89) is plotted as a function of temperature in Fig.6.15. The viscosity increases drastically by decreasing temperature at the temperature range of 0 to -20 C and the agreement between experimental data and theoretical formula is very good.

Once the temperature and concentration of the viscosity are

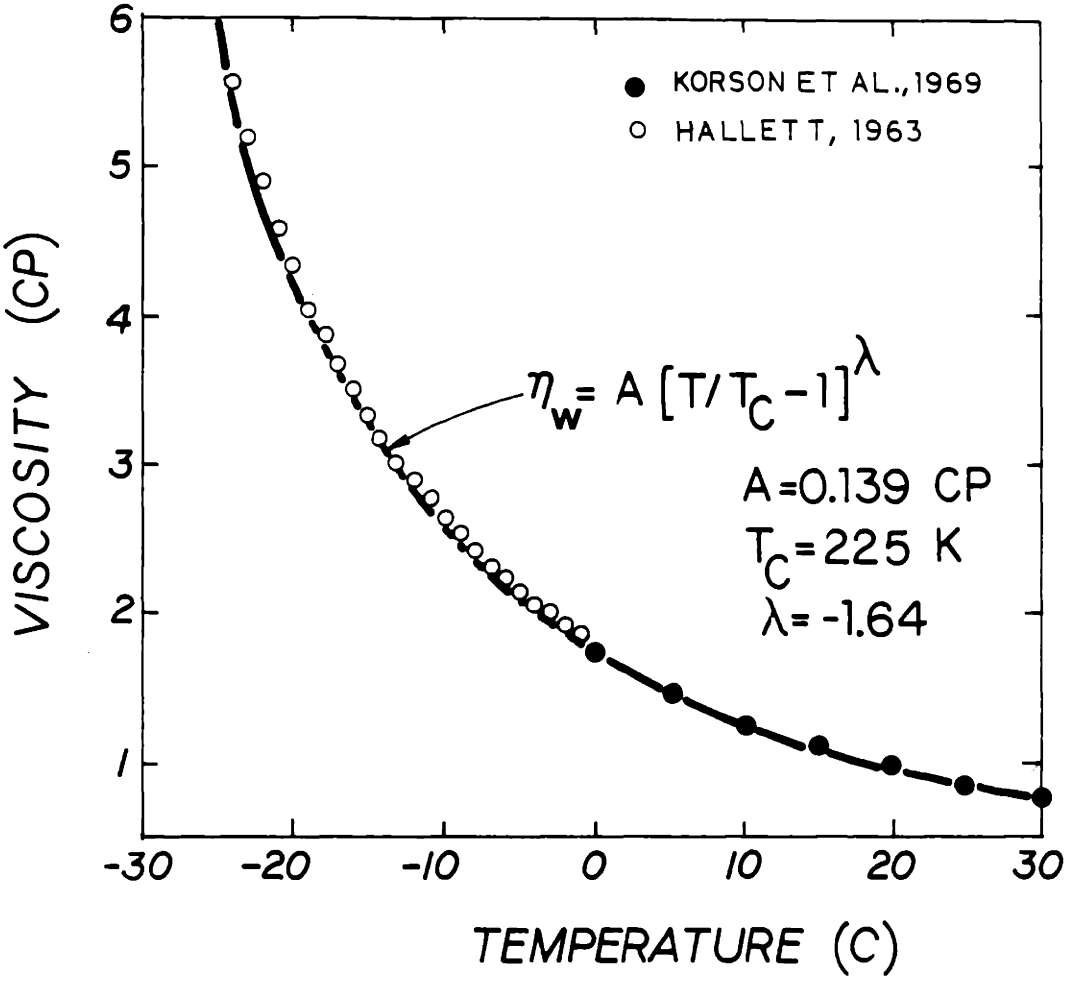

FIGURE.6.15. Temperature dependence of viscosity (Data points from Hallett 1963; Korson et al. 1969).

determined, its effect on the nucleation rate can be shown. The viscosity affects the nucleation rate through its influence on the rate of molecule addition as calculated in Eq.(6.77). Fig.6.16. shows the normalized rate of molecule addition, $\upsilon(T,\phi_m)$ / $\upsilon(0,0)$, as a function of temperature for various volume fractions. As can be seen from this figure that the rate of molecule addition (i.e. the nucleation rate) becomes less sensitive to temperature and concentration changes at higher volume fractions and lower temperatures. In Fig.6.17 the change in the viscosity of the cell cytoplasm is shown as calculated from the solution of the water transport equation derived in Chapter V. At slow cooling rates, the oocyte experiences enough dehydration so that the viscosity increases drastically at the beginning of the freezing. However, the change in oocyte's volume can be ignored at higher rates and the viscosity of the cytoplasm follows a path similar to Eq.(6.88).

Thermodynamic Driving Force for Crystallization in Aqueous Cytoplasm

The thermodynamic driving force for crystallization of an undercooled liquid, $\Delta\mu_s$, is an important parameter appearing in the formulation of the rate of nucleation. Since the rate of nucleation has an exponential dependence on $\Delta\mu_s$, the accuracy of an estimate of $\Delta\mu_s$ is important. The chemical potential difference between ice and solution is related to the Gibbs free energy of the system.

The exact temperature dependence of the Gibbs free energy can be

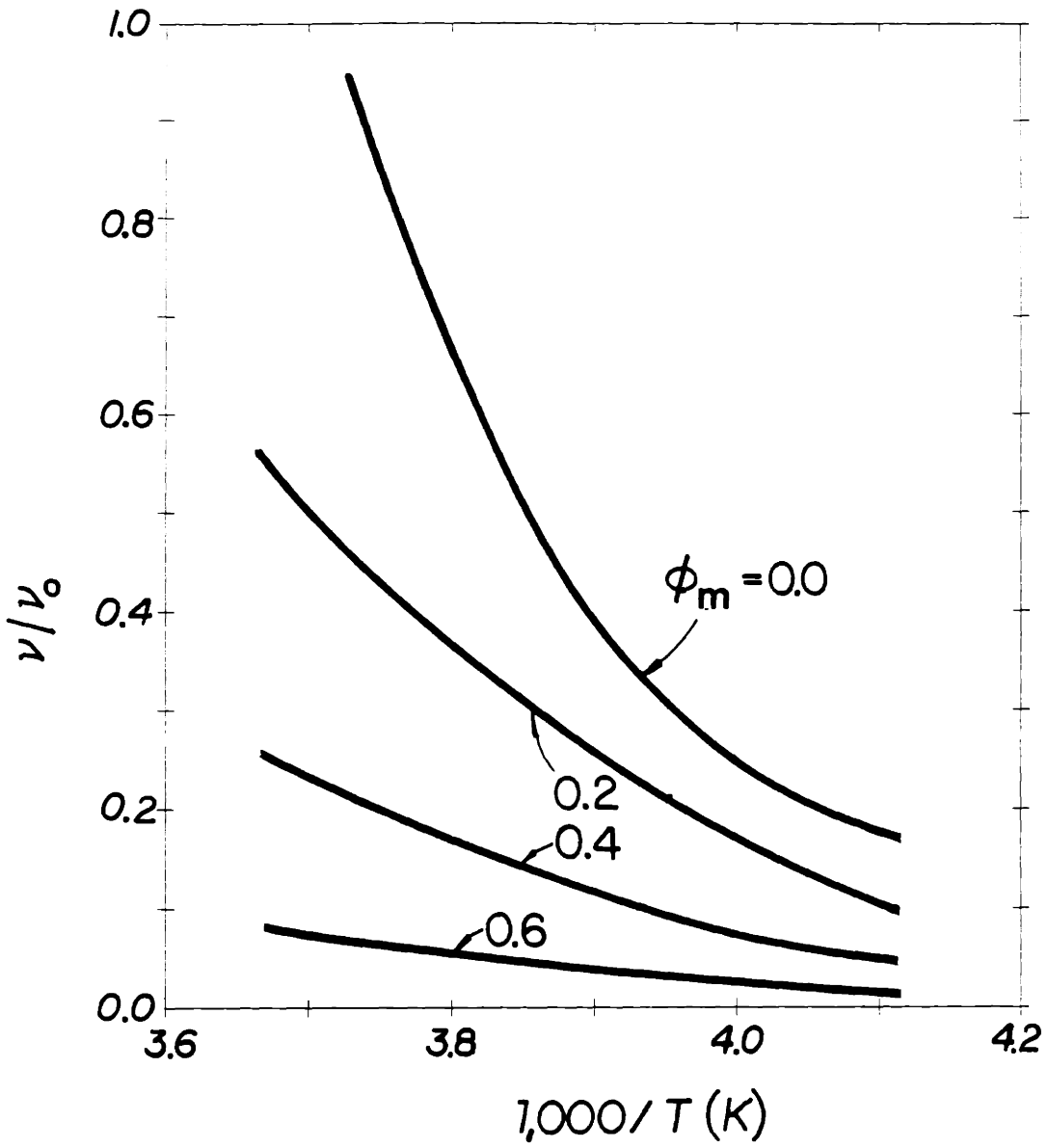

FIGURE.6.16. Rate of molecule addition to the cluster as a function of temperature for various volume fraction of fictitious species.

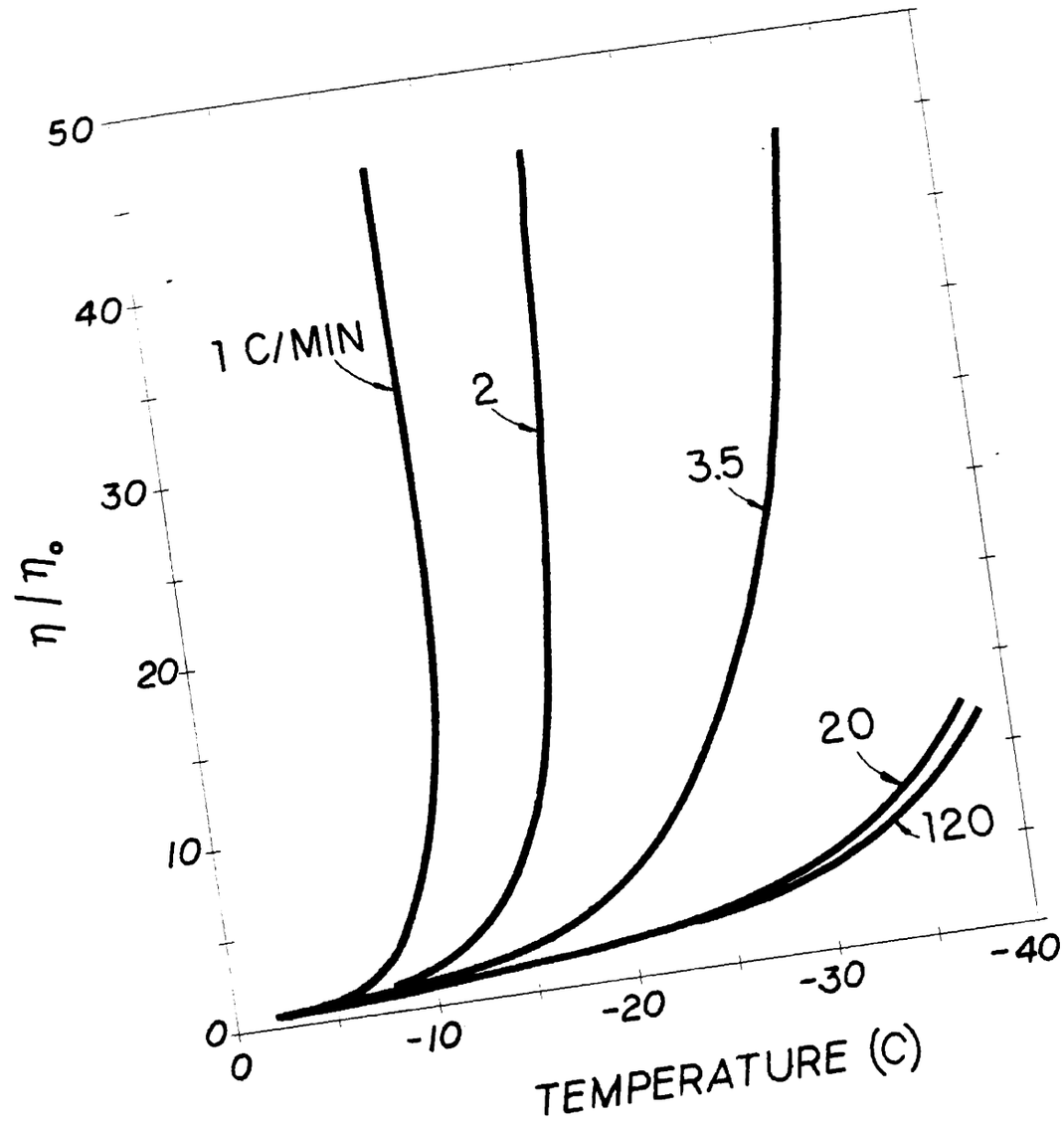

FIGURE.6.17. Variation of cytoplasmic viscosity as a function of temperature during freezing of mouse oocytes. Cooling rates are indicated for each curve. Oocytes are suspended in isotonic PBS and extracellular ice is seeded at -0.615°C.

calculated if the heat capacities of both liquid and solid phases are known as a function of temperature. Since the intracellular milieu of cells can be assumed to be dilute on a molar basis, the Gibbs free energy for pure water can be used to a good approximation at low dehydration limits during freezing. The Gibbs free energy between the liquid and the crystalline phases is given by

$$\Delta G = \Delta H - T\Delta S \tag{6.90}$$

where

$$\Delta H = \Delta H_f - \int_T^{T_f} \Delta C_p \, d \tag{6.91}$$

and

$$\Delta S = \Delta S_f - \int_T^{T_f} \Delta C_p \, \frac{dT}{T} \tag{6.92}$$

where ΔH_f is the enthalpy of fusion, ΔS_f is the entropy of fusion, T_f is the melting temperature, and ΔC_p ($= C_p^{\alpha} - C_p^{\beta}$) is the difference in specific heats of α and β phases. Rasmussen & MacKenzie (1973), and Angell et al. (1973) determined the specific heats of undercooled water from its respective melting point to its respective homogeneous nucleation temperature. The temperature dependence of the difference in specific heats between water and ice is shown in Fig.6.18. The difference in specific heats of α and β can be given approximately by the following formula

$$\Delta C_p = L_1 + L_2 \, \Delta T^4 \tag{6.93}$$

where ΔT ($= T_f - T$), L_1 ($= 36.92$ J/mol-^oC), and L_2 ($= 2.826 \times 10^{-5}$ J/mol/$^oC^5$). Substituting Eq.(6.93) in Eqs.(6.90)-(6.92), and by

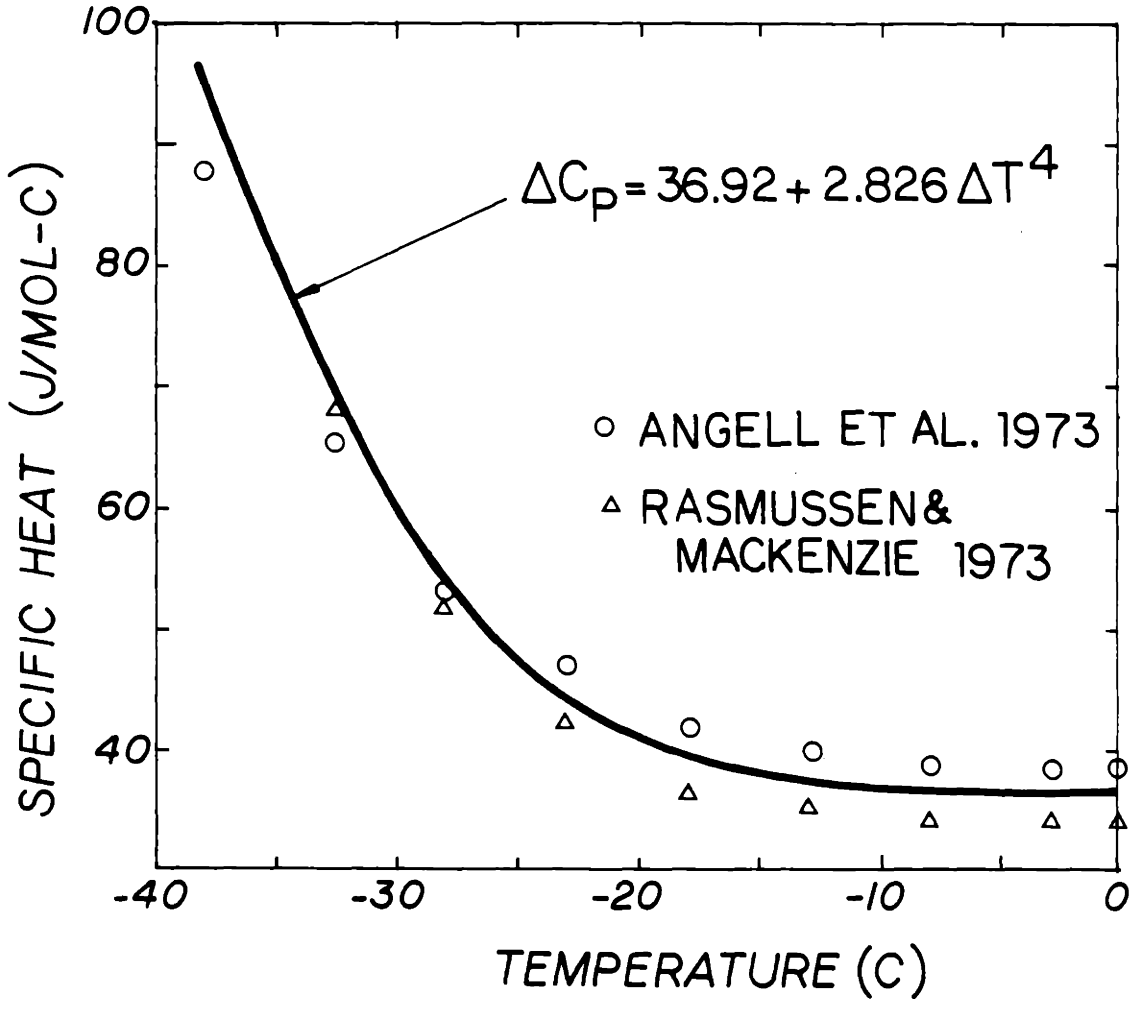

FIGURE.6.18. Temperature dependence of the specific heat for water-ice (Data points from Angell et al. 1973; Rasmussen & MacKenzie 1973).

integrating

$$\Delta G = \frac{\Delta H_f}{T_f}\Delta T - \Delta T\left(a + b\frac{\Delta T^4}{5}\right) + T \ln (T_o/T)\,(a + bT_o^4) \quad (6.94)$$

$$+ bT\left\{4\,T_o^3(T_o - T) - 3\,T_o^2(T_o^2 - T^2) + \frac{4}{3}T_o(T_o^3 - T^3) + \frac{1}{4}(T_o^4 - T^4)\right\}$$

This equation can be used to calculate the thermodynamic driving force of crystallization in undercooled dilute solutions. However, it is complicated and it should be compared with other well-known simpler relations. A review by Thompson & Spaepen (1979) summarizes various approximations used in the literature. The simplest and probably the most widely used approximation is Turnbull's assumption of $\Delta C_p = 0$ which leads to

$$\Delta G = \frac{\Delta H_f\,\Delta T}{T_f} \quad (6.95)$$

Turnbull's equation is usually used for pure metals (Turnbull, 1950c). Hoffman (1958) tried to ameliorate Eq.(6.95) by assuming that the enthalpy difference between the undercooled liquid and crystalline phases may be represented by a linear function. Hoffman's final result is as follows

$$\Delta G = \frac{\Delta H_f\,\Delta T}{T_f}\,\frac{T}{T_f} \quad (6.96)$$

This approximation is proved to be accurate for materials which have a

large ΔC_p at T_f. An appropriate adaptation of Hoffman's approach is made by Thompson & Spaepen (1979). In this approximation, ΔC_p is assumed to be a constant equal to $\Delta H_f/T_m$ so that the final result is given by

$$\Delta G = \frac{\Delta H_f \, \Delta T}{T_f} \quad \frac{2T}{T_f + T} \qquad (6.97)$$

Thompson and Spaepen's approximation is suggested for easy glass forming alloys. Fig.6.19. shows a comparison of all these three approximations with Eq.(6.94). It is interesting to see that Hoffman's equation is very close to the actual curve obtained by Eq.(6.94) and Hoffman's equation will be used in the rest of this study.

Since the cells dehydrate during freezing, the concentration of the intracellular solution increases while the temperature is lowered which supresses the equilibrium freezing temperature. Hence, the amount of undercooling of the cell cytoplasm changes during freezing (see Fig.5.4). Appropriate values of ΔT should be substituted in Eq.(6.96) to estimate the thermodynamic driving force for crystallization during freezing. The results of such calculations are shown in Fig.6.20.

Another factor that effects Eq.(6.96) is the composition dependence of ΔH_f. The variation of the latent heat of fusion for sodium chloride aqueous solutions is determined by Defay and Sanfield (1959). Their result suggest that ΔH_f decreases sligthly with increasing concentration of NaCl. At a concentration of 10x isotonic the change in ΔH_f is less

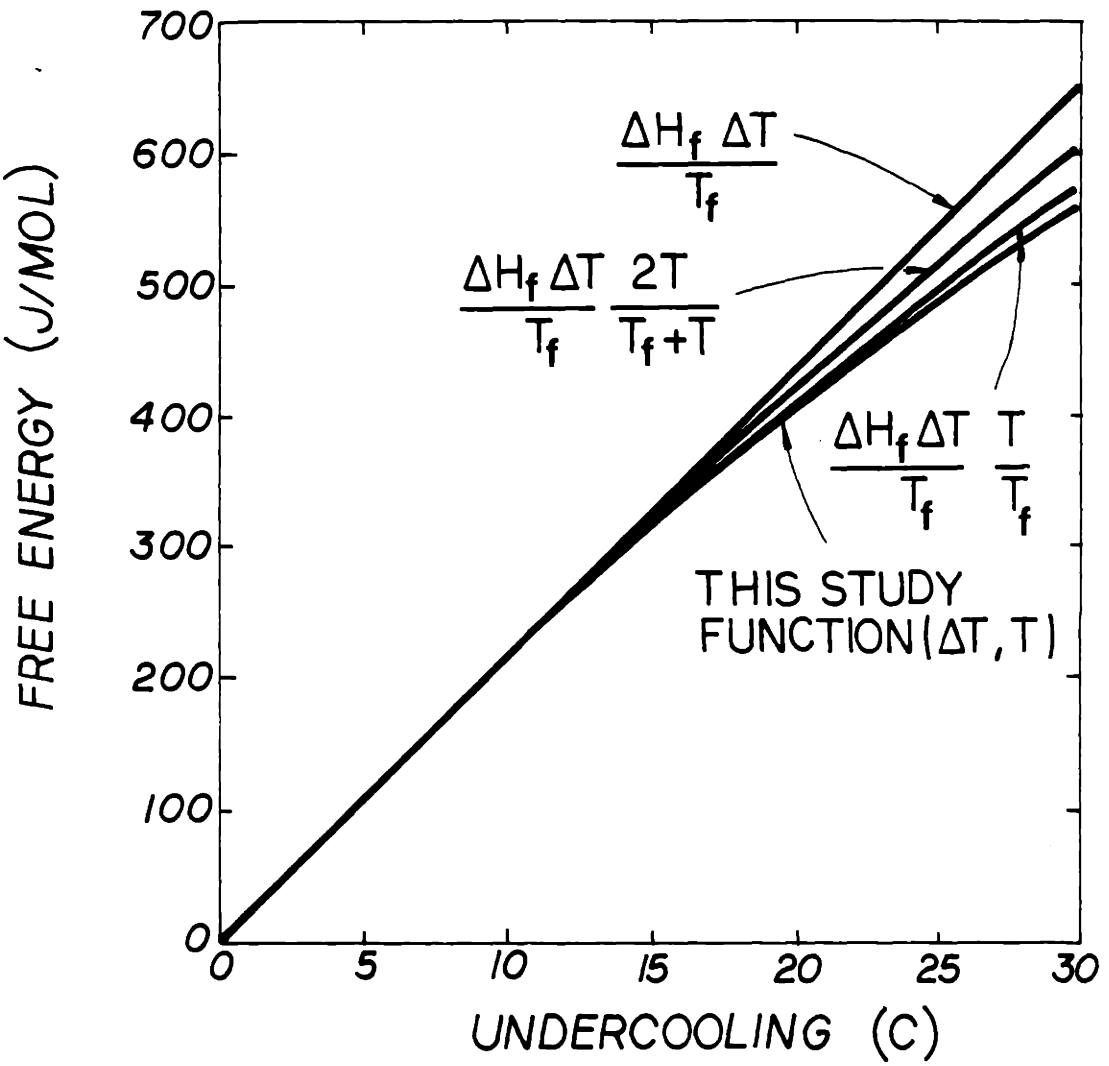

FIGURE.6.19. Thermodynamic driving force vs. undercooling for water.

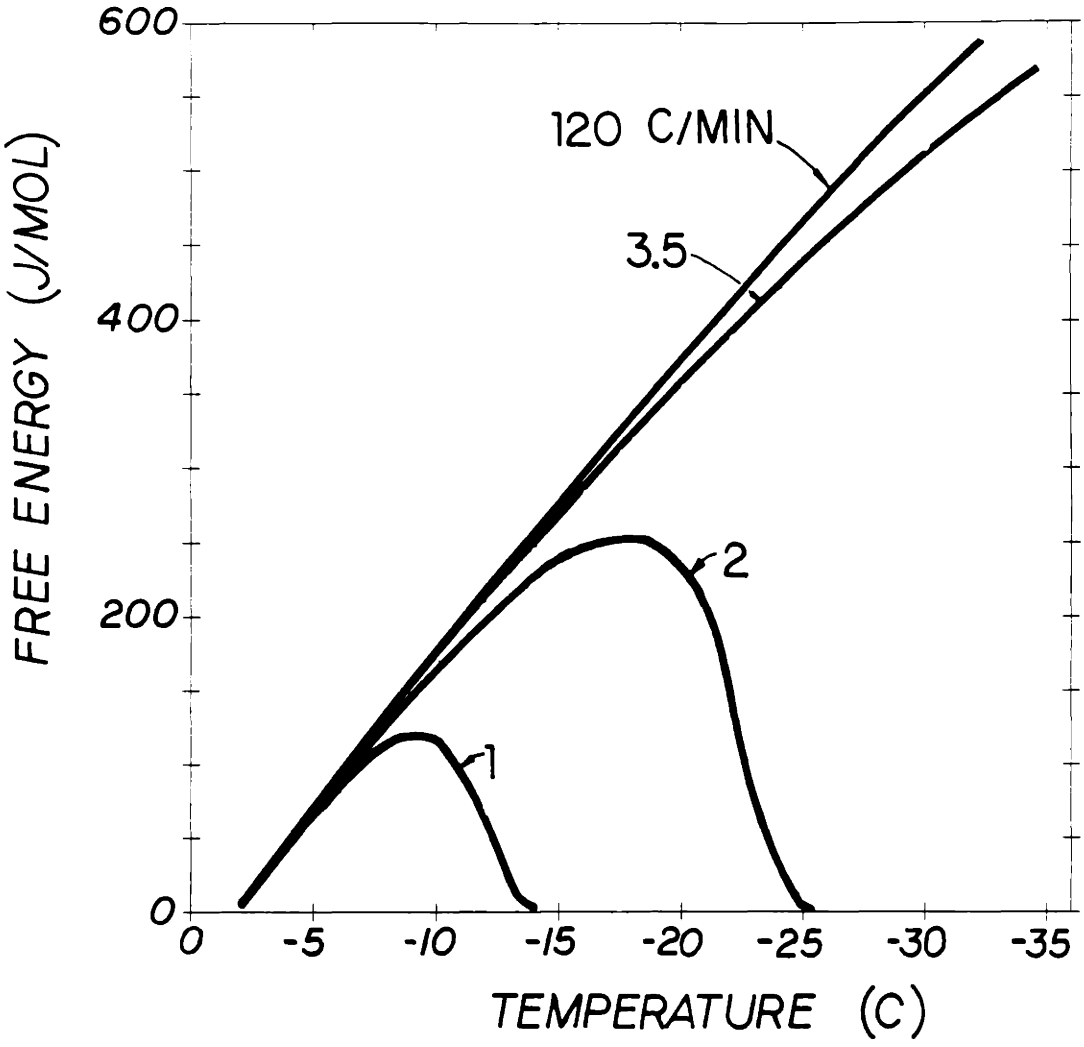

FIGURE.6.20. Thermodynamic driving force as a function of temperature during freezing of mouse oocytes. Cooling rates are indicated for each curve. Oocytes are suspended in isotonic PBS and the extracellular ice is seeded at -0.615^{o}C.

than 2% and can be neglected for any practical purposes.

Summary of the Kinetic Equations Describing the Intracellular Ice-Nucleation

During freezing of biological cells, cells dehydrate in response to the chemical driving force caused by the extracellular ice. Hence, the concentration, the temperature and the undercooling of the intracellular solution change simultaneously while the freezing progresses. Therefore, the nucleation frequency which is a function of the cell volume, the temperature, and the internal concentration can only be estimated if the kinetics of dehydration from the cells is known during freezing. This can be achieved by coupling ice nucleation kinetics equations with water transport equation. The summary of all the equations is as follows:

$$\frac{\partial V_w}{\partial T} = \frac{L_p A_c RT}{\upsilon_w B}\left\{ \ln \frac{V_w}{V_w + 2n_s i n \upsilon_w} - \frac{\Delta H_f}{R}\left[\frac{1}{T_R} - \frac{1}{T}\right]\right\} \quad (6.98)$$

$$I^s_{het} = \Omega_{het} \exp\left(\frac{\kappa_{het}}{\Delta T^2 T^3}\right) \quad (6.99)$$

$$\Omega^{het} = \Omega_o (\sigma T/\sigma_o T_o)^{1/2} [f(\theta)/f(\theta_o)]^{1/6} \frac{(T/T_c - 1)^{\lambda}}{(T_o/T_c - 1)^{\lambda}} (\eta_o/\eta) A_c/A_0 \quad (6.100)$$

and

$$\Omega_o = 2 \upsilon^{\beta} \frac{(\sigma_o kT_o)^{1/2}}{h} \frac{h N_{AV}}{\eta_o \upsilon^{\alpha}} [f(\theta_o)]^{1/6} N_o'$$

$$\kappa^{het} = \kappa_o \, (T_f/T_o)^4 \, [f(\theta)/f(\theta_o)] \, (\sigma/\sigma_o)^3$$

and (6.101)

$$\kappa_o = \frac{16 \, v^{\beta^2} \, \sigma_o^3}{3k \, \Delta H_f^2} \, T_o^4 \, f(\theta_o)$$

where,

$$\eta/\eta_w(T) = \exp\left(\frac{2.5\phi_m}{1 - Q\phi_m}\right) \qquad Q = 0.609375$$

$$\eta_w(T) = A \, (T/T_c - 1)^{\lambda} \qquad A = 0.139 \text{ cP}; \; T_o = 225 \text{ K}; \; \lambda = -1.64$$

$$\phi_m = V_b / V_c$$

$$f(\theta) = (2 + \cos\theta) \, (1 - \cos\theta)^2 / 4$$

$$T_f = - \pi^{in}/0.538 = - 0.224/(V_c/V_o - 0.213)/0.538 \quad \text{(see Fig.4.2)}$$

$$\Delta T = T_f - T$$

$$L_p = L_{pg} \exp\left[- \frac{E_{Lp}}{R} \left(\frac{1}{T} - \frac{1}{T_f} \right) \right]$$

where Ω_{het} is a kinetic constant that basically depends on molecular and transport properties of the system, and κ_{het} describes the free energy of formation of the critical size cluster and is of thermodynamic origin. In Eqs(6.100), (6.101), terms are grouped such that Ω_o and κ_o includes all the constant terms at isotonic conditions. The remaining terms are all the temperature and concentration dependent terms relative to the isotonic conditions. Using this notation, one can analyze the relative effect of anisotonic solutions to the nucleation kinetics.

In Eq.(6.100) it is assumed that the change in the no. moles of water in contact with the substrate is proportional to the change in the surface area of the substrate and it is not affected by the concentration change in the cell. This assumption is only valid for $N_S \ll N'$.

Solution of coupled Eqs.(6.98)-(6.101) requires numerical schemes. The water transport equation (Eq.(6.98) is solved using 4th order Runge-Kutta scheme with a temperature step size of 0.1^oC. The resulting water volumes are used to determine freezing temperature, undercooling and viscosity of the internal solution as described above. Then, these values are introduced in nucleation kinetics equation (Eqs.(6.99)-(6.101)). Nucleation kinetics equations are integrated using 3/8 Simpson rule with a temperature step size of 0.1^oC.

We assume heterogeneous nucleation and thus I^S_{het} represents the steady-state number of clusters formed per unit time per unit surface area. Similar equations can be written for homogeneous nucleation using Eq.(6.58) instead of Eq.(6.70).

In summary, we have developed a model to describe the kinetics of internal ice formation in biological cells when they are exposed to extracellular ice. Equations describing both the water transport and ice formation are coupled to predict the likelihood of intracellular ice formation. In the next two chapters, the consequences of this theoretical model are presented including quantitative comparisons of

theory and experiments as further verification of the validity of the model.

6.6. A Method of Estimating Nucleation Parameters from Experimental Data.

This section is concerned with the calculation of the nucleation parameters (i.e., Ω_o and κ_o) from experimental freezing data. In order to achieve this goal, one needs to determine the nucleation frequency, I^S_{het}, from the freezing experiments. Nucleation frequency is not amenable to experimental observations, however, crystallization may be measured experimentally. If the crystallization time is negligible in comparison with the nucleation time then one can assume that the nucleation frequency is identical to crystallization rate. In the case of biological cells, the crystallization of the cytoplasm occurs spontaneously, hence, the nucleation frequency can be computed from the direct measurement of the crystallization rate. In other words, once the critical cluster forms, the cell interior solidifies spontaneously as discussed in Chapter IV. Thus, the nucleation rate for a system composed of identical cells can be written as

$$I^S = \frac{1}{N_t^u V_w} \frac{\partial i^*}{\partial t} \tag{6.102}$$

where $\partial i^*/\partial t$ is the frequency of critical cluster formation, N_t^u is the

total number of unfrozen cells, and V_w is the water content of one cell. Obviously, frozen cells cannot be considered as part of the system, therefore, the term $N_t^u V_w$ varies as nucleation proceeds. Eq.(6.102) assumes that the transient in the nucleation rate is over and a steady-state is achieved. Since the critical cluster formation leads to spontaneously observable nucleation, one can write the variation in the number of unfrozen cells as

$$\frac{\partial N_t^u}{\partial t} = - \frac{\partial i^*}{\partial t} \qquad (6.103)$$

Combining Eqs.(6.102), (6.103) yields the rate of nucleation in terms of the number of unfrozen cells such as

$$I^s = - \frac{1}{V_w N_t^u} \frac{\partial N_t^u}{\partial t} \qquad (6.104)$$

This equation can be integrated to give

$$\ln (N_t^u / N_o) = - \int_0^t V_w I^s \, dt \qquad (6.105)$$

where N_o is the initial number of cells for the system composed of identical cells. It is more appropriate to write this equation as a function of the probability of nucleation, P_t, in which case

$$P_t = (N_o - N_t^u) / N_o = N_t / N_o \qquad (6.106)$$

where N_t is the number of cells frozen at time t. This equation assumes sporadic nucleation of identical cells. Substituting Eq.(6.106) in (6.104) yields

$$\ln (1 - P_t(V_w,t)) = - \int_0^t V_w(t)\ I^s(V_w,t)\ dt \quad (6.107)$$

This equation is similar to the equation derived by Carte (1956, 1959) based on the probability theory applied to large number of small droplets of equivalent sizes. A similar expression has also been applied by Turnbull (1950a), and Wood & Walton (1970). Eq.(6.107) is valid for homogeneous nucleation since we assumed that the production of critical clusters depends on the total volume of liquid present in the system. However, this is not true for heterogeneous nucleation in which case critical clusters form on a substrate as discussed in Section 6.4. For heterogeneous nucleation, the rate of nucleation will be proportional to the extent of the substrate that catalyses the ice nucleation and can be calculated in a similar way to homogeneous nucleation as described above.

In the freezing of biological cells, there may be two possible sites to catalyse the ice nucleation in the undercooled cytoplasm of cells surrounded by external ice: (1) the plasma membrane, or (2) the nucleators (macromolecules, organelles, proteins) present within the cytoplasm. If the plasma membrane is assumed to be the active catalytic surface, Eq.(6.107) can be rewritten as

$$\ln (1 - P_t(A_c,t)) = - \int_0^t A_c(V_w,t)\ I^s_{het}(A_c,t)\ dt \quad (6.108)$$

where A_c is the surface area of the cell which changes during freezing according to dehydration rate (Eq.6.98). On the other hand, if a

macromolecule inside the cell is assumed to be the active catalytic surface, Eq.(6.107) would yield

$$\ln (1 - P_t(A_m,t)) = - A_m \int_0^t I^s_{het}(A_m,t)\, dt \qquad (6.109)$$

where A_m is the surface area of the macromolecule or organelle and is constant. When the cells are cooled at a constant rate of cooling, B (= $-\partial T/\partial t$), Eqs.(6.108), (6.109) can be transformed to

$$\ln (1 - P_T(A_c,T)) = \frac{1}{B} \int_{T_o}^{T} A_c(V_w,T)\, I^s_{het}(A_c,T)\, dT \qquad (6.110)$$

and

$$\ln (1 - P_T(A_m,T)) = \frac{A_m}{B} \int_{T_o}^{T} I^s_{het}(A_m,T)\, dT \qquad (6.111)$$

Thus, the probability of freezing can be expressed as a function of the nucleation frequency and surface area of the nucleating site. When this equation is applied to heterogeneous nucleation such as in this study, the catalytic particles are assumed to enhance the efficiency of the random nucleation process without disturbing its stochastic nature. Explicitly, it is assumed that all the droplets (or cells in this study) have an equal probability of reaching the size of a critical cluster as a result of random fluctuations on the surface of foreign particles. Thus, the heterogeneous nucleation theory becomes equivalent to that given for homogeneous nucleation by Carte (1956; 1959). This statistical approach to the kinetics of ice nucleation is called the **stochastic hypothesis** of nucleation theory. The stochastic nature of freezing process can be attributed to the random fluctuation of water

molecules to form an ice-like cluster, and it has been successfully used for heterogeneous nucleation (Turnbull 1950a; Turnbull 1952; Cormia et al. 1962; Wood & Walton 1969).

Other models are also reported to relate the probability of ice formation to the frequency of nucleation. Levine (1950), Turnbull (1953), and Langham & Mason (1958) proposed the **singular hypothesis** of the nucleation theory. This hypothesis assumes that every particle contained inside a drop has one characteristic temperature at which freezing will be initiated in the drop. The probability distribution of ice nucleation is assumed to follow an empirical exponential relationship. The singular characteristic of drop freezing can be attributed to the nature, and chemical and crystallographic properties of the active sites contained in the drop. There is no reason to believe that an empirical exponential equation of singular hypothesis holds for all temperatures.

The relative importance of the kinetic effects (stochastic) and particle content (singular) on the heterogeneous nucleation of a drop was investigated experimentally by Vali & Stansbury (1966). From experiments on the the time-dependence of freezing, they deduced that the probability of freezing for a drop at a given temperature can be better represented by some combination of both stochastic and singular hypotheses. All of the experiments mentioned above were at the slow cooling rates. Thijssen et al. (1968) analyzed higher cooling rates and determined that a third probability function describing the probability per unit time that equilibrium is established should be included into

the equations. However, none of these studies are conclusive yet and further study of various parameters is necessary to resolve some of these important issues. In the present study, we will assume that the stochastic theory is valid in freezing of biological cells and ignore the effects of active sites on the randomness of the nucleation phenomena. This is again identical to assuming that each cell has the same heteronucleating particles with identical properties to alter the nucleation kinetics in an identical way among all the cells.

In the case of small droplets of liquids, the calculation of the nucleation parameters is relatively straightforward compared to biological cells. This is because nucleation parameters (Ω_{het},π_{het}) in Eqs.(6.100), (6.101) can be assumed to remain constant over a narrow range of temperatures that nucleation occurs. However, when cells are exposed to extracellular ice, the kinetics of intracellular nucleation occurs over a very broad range of temperatures between -5 to -35°C (Fig.4.4). In addition, the water content of cells and the internal concentration vary with time (or temperature) due to the dehydration of the cell in response to reduced external chemical potential by the formation of ice. Since Ω_{het} and π_{het} vary with changing cell volume (and concentration), it is almost impossible to analyze the kinetics of ice-nucleation inside the cells. In addition, there are significant cell-to-cell variations involved in the prediction of the water transport behavior of cells during freezing. This point is extensively discussed in Chapter V. The ice nucleation parameters are functions of cell water content and concentration, they are very sensitive to the kinetics of the water transport during freezing. One way to minimize

the uncertainties associated with the coupling of the water transport and the ice nucleation kinetics is to expose the cells to very rapid cooling rates. At high enough cooling rates, the water transport will be impeded (Fig.5.3) and cells can be treated as simple droplets of water-salt-protein mixtures of constant volume. In other words, one can simply decouple the water transport equation (Eq.(6.98)) from ice-nucleation equation (Eq.(6.99)) and analyze the ice-nucleation equation separately. Mathematically, this is equivalent to

$$\frac{\partial V_w}{\partial T} \rightarrow 0 \rightarrow A_c = \text{constant} \quad \text{if} \quad B \gg 1$$

$$\ln (1 - P_T(T)) = \frac{A_c}{B} \int_{T_o}^{T} I^s_{het}(T)\, dT \qquad (6.112)$$

and

$$\ln (1 - P_T(T)) = \frac{A_m}{B} \int_{T_o}^{T} I^s_{het}(T)\, dT \qquad (6.113)$$

Now, one can generate the freezing probability of cells to form internal ice (i.e. left side of Eqs.(6.112), (6.113)) from rapid cooling experiments as shown in Fig.4.4. Then the integral involving the nucleation parameters (i.e. right side of Eqs.(6.112), (6.113)) can be numerically fit to the experimental data to obtain Ω_o, κ_o. Eqs.(6.112), (6.113) together with Eqs.(6.99)-(6.101) can be solved using Simpson's 3/8 rule with a step size of 0.1^oC.

Numerical non-linear fitting technique of Marquardt (1963) and Bevington (1969) is used to obtain "best-fit" values for the nucleation parameters. The technique is explained in detail in the literature. Briefly, the goodness-of-the fit is measured by the sum of the square of the difference between the measured values and the corresponding values

predicted by the model such as

$$\chi^2(\Omega_o, \kappa_o) = \sum_i (P_i - P(T_i))^2 \qquad (6.114)$$

The problem is to minimize the functional χ^2 with respect to the parameters. The variance will then be an extremum if

$$\frac{\partial \chi^2}{\partial \Omega_o} \to 0 \; ; \quad \frac{\partial \chi^2}{\partial \kappa_o} \to 0 \qquad (6.115)$$

Since the function P(T) is non-linear in parameters, an iterative scheme should be used to satisfy Eq.(6.115). One typically continues iteration on the parameter values until the change in parameter values becomes smaller than a desired treshold value. Marquardt (1963) outlined the numerical scheme. In summary, one can determine the nucleation parameters from experimental data using the non-linear regression analysis coupled with the theoretical model describing the nucleation kinetics (Eqs.(6.112), (6.113)).

6.7. Conclusion

Theoretical and analytical techniques developed in Chapter VI to calculate the probability of cells with intracellular ice formation are based on the modified classical heterogeneous nucleation theory. The equations derived for nucleation rate in biological cells (Eqs.(6.99)-(6.111)) are coupled with water transport equation (Eq.(6.98)) to

predict the thermodynamic state of the undercooled cytoplasm. A method to estimate the nucleation frequency from observed probability of nucleation is suggested. This method is based on the assumption that each cell has the same heteronucleating particles with identical properties to alter the nucleation kinetics in an identical way among all of the cells. This allowed the correlation of the experimentally observed fraction of cells with internal ice and the nucleation rate. It is suggested that the uncertainties in the experimental conditions can be minimized if cells are cooled at rates fast enough to impede water transport during freezing. Hence, the "best-fit" values for nucleation parameters can be obtained by numerical solution of Eqs.(6.99)-(6.101) and (6.112) (or (6.113)) using non-linear regression analysis and experiments at high cooling rates.

As the above analysis revealed, the experimental and theoretical prediction of the nucleation kinetics in biological cells is a very complicated problem due to the complexity of the nucleation theory as well as the complexity of the behavior of biological cells. Studies such as this on the nucleation kinetics of cells are fundamental to the progress of the field. However, the results are very difficult to interpret. These considerations should cause the investigator to proceed in constant awareness of the complexity of the real physical problem, of the imperfections and dangers of all procedures. In the next chapters, the kinetics of ice nucleation in mouse oocytes based on the theory described in this chapter will be correlated with experimental observations. This will serve the purpose of evaluating the proposed theory.

CHAPTER VII

MECHANISMS OF INTRACELLULAR ICE FORMATION & DETERMINATION OF ICE NUCLEATION PARAMETERS

7.1. Introduction

In this chapter, the heterogeneous nucleation theory presented in the previous chapter will be applied to mouse oocytes as a model biological system. Possible nucleating sites to catalyze the heterogeneous nucleation will be discussed. Equations modelling the ice formation inside the biological cells will be solved for the freezing of oocytes at rapid rates in anisotonic solutions of sodium chloride to determine their ice-nucleation parameters. A sensitivity analysis of the proposed theory will then be carried out to better understand the important factors affecting the proposed nucleation theory for biological cells. Analytical results will be correlated with experimental results to verify the validity of the proposed mechanism of ice nucleation inside cells.

7.2. Mechanisms of Intracellular Ice Formation

In Chapter IV it was shown that the nucleation kinetics was changed when oocytes were dehydrated in hypertonic NaCl+PBS+BSA solutions prior to freezing (see Figs.4.4 and 4.5). Briefly, the kinetics of intracellular ice formation was slowed down drastically by increasing the concentration of the suspending medium from 200 to 1,035 mosm. Due to slow kinetics in hypertonic solutions, lower temperatures could be reached with major portion of the oocytes remaining unfrozen in hypertonic solutions. At concentrations above 735 mosm, an interesting phenomenon occurred. All of the oocytes remaining unfrozen at -31°C were frozen spontaneously in a temperature range of -31 to -34°C (overall average of -32.9°C), well above the estimated homogeneous nucleation temperature, approximately -37°C, of the cytoplasm (Rall et al. 1984). The dramatic increase in the rate of nucleation may be due to two different nucleation mechanisms that are active at different conditions. The cooling rate was the same for all experiments and the volume of the oocytes was given by the equilibrium osmometric behavior as shown in Fig.4.2. The rest of this chapter will focus on the specifics of these two different nucleation mechanisms.

It is helpful first to underline our hypothesis of the mechanism of intracellular ice formation and then justify its validity. Briefly, we propose that the ice nucleation kinetics inside mouse oocytes above -31°C is catalyzed heterogeneously by the plasma membrane via the effects

of the external ice surrounding the cell so we refer to it as **plasma membrane catalyzed nucleation** (or mechanism I). The rapid ice nucleation within oocytes between approximately -31 to -34°C is catalyzed by intracellular supramolecular structures (organelles, macromolecules) and we refer to it as **particle catalyzed nucleation** (or mechanism II). A discussion of these two distinct mechanisms of the ice nucleation inside cells follows.

Plasma Membrane Catalyzed Ice Nucleation

The internal freezing occurs at significantly higher temperatures in the presence of external ice than in its absence. The fraction of oocytes with internal ice increases from 0 at -6°C to 1 at -14°C when cooled at 120°C/min in isotonic PBS+BSA solution (Fig.4.4). The fraction of oocytes containing ice is zero at the same range of temperatures in the absence of external ice (Fig.4.18). It is, therefore, reasonable to conclude that external ice plays an important role in the initiation of the intracellular ice. Table 7.1 shows the differences between mean freezing temperature of various cells with and without the presence of the external ice. None of these data permit an unequivocal conclusion with respect to the seeding mechanism of the external ice leading to the formation of ice inside the cells.

TABLE 7.1

INTRACELLULAR FREEZING TEMPERATURES
WITH AND WITHOUT EXTRACELLULAR ICE PRESENT

Cell Type	Internal Freezing Temperaure: External Ice Present (°C)	External Ice Absent (°C)	Method of Eliminating Ext. Ice	References
Sea Urchin Eggs	-4 to -8	< -8	Suspension in Silicone Oil	Asahina 1961, 1962; Hubel et al. 1987
Spirogyra	-7.7	< -12.4	Undercooling	Morris & McGrath 1981
Yeast	-10 to -15	< -40	Safflower Oil	Mazur 1965; Rasmussen et al. 1975
Erythocytes	-10 to -15	< -35	Emulsion	Franks et al. 1984

According to our point of view, the internal ice is catalyzed heterogeneously by the plasma membrane via the effects of the external ice. The presence of external ice alters the plasma membrane by some unknown mechanism which makes the plasma membrane energetically favorable for ice nucleation on it. In the previous chapter, it is shown that the heterogeneous nucleation can be described by one parameter when the size of the nucleating particle (R) goes to infinity. This parameter is the contact angle between the ice-substrate and the substrate is the plasma membrane in our hypothesis of internal ice formation. The temperature at which nucleation occurs is a function of the contact angle such that lower values of the contact angle will decrease the value of $f(\cos \theta)$ (see Fig.6.10) shifting the ice nucleation to higher temperatures. Hence, the ice nucleation can be heterogeneously catalyzed on the plasma membrane between -6 to $-14^{o}C$ if the contact angle has the appropriate value. Our hypothesis is that the presence of the external ice alters θ through its effects on the plasma membrane to promote internal ice formation. The mechanism by which external ice may alter the plasma membrane is open to speculations. The plasma membrane being a very dynamic structure composed of charged lipids and proteins may respond to mechanical, chemical, electrical and ionic effects of the external ice by many ways which will be further discussed later in this section.

Correlation of experimental results with Eqs.(6.99)-(6.101) using non-linear regression analysis as described in the previous chapter

would yield the values for ice nucleation parameters, namely, Ω^I_o and κ^I_o. The calculations for oocytes frozen at 120°C/min in 285 mosm solution show that the nucleation parameters in the case of plasma membrane catalyzed nucleation are (Fig.7.1)

$$\begin{aligned} \Omega^I_o &= 3.56\text{x}10^{+9} \quad (1/m^2\text{-s}) \\ \kappa^I_o &= 4.60\text{x}10^{+8} \quad (K^5) \end{aligned} \tag{7.1}$$

The superscript 'I' refers to the nucleation mechanism I as described above and is called **plasma membrane catalyzed nucleation.** The variance of the theory and experiment is less than $4.25\text{x}10^{-4}$ favoring a 'good' correlation. The value for preexponential parameter being much smaller than homogeneous nucleation of saline droplets (10^{+56} $1/m^3$-s; Franks et al. 1983) suggests heterogeneous nucleation of ice. However, no definite argument can be made that the active nucleating site is the plasma membrane. Some order-of-magnitude estimations may be helpful as a first-cut analysis. The contact angle can be estimated assuming that the catalytic site has a very large radius (i.e. plasma membrane) compared to the critical cluster. From Eq.(6.101) and the value $4.6\text{x}10^{+8}$ K^5 for κ^I_o, one can calculate that the contact angle between ice-plasma membrane should be approximately 35°. Although this value is somewhat larger than 15.7° determined for cell-size liposomes (Tondorf et al. 1987), it is certainly close enough as to further increase the confidence in the soundness of the approach. There are no reported values of ice-plasma membrane contact angle for mouse oocytes. Hendlet et al. (1987) used the same experimental technique as Tondorf et al.

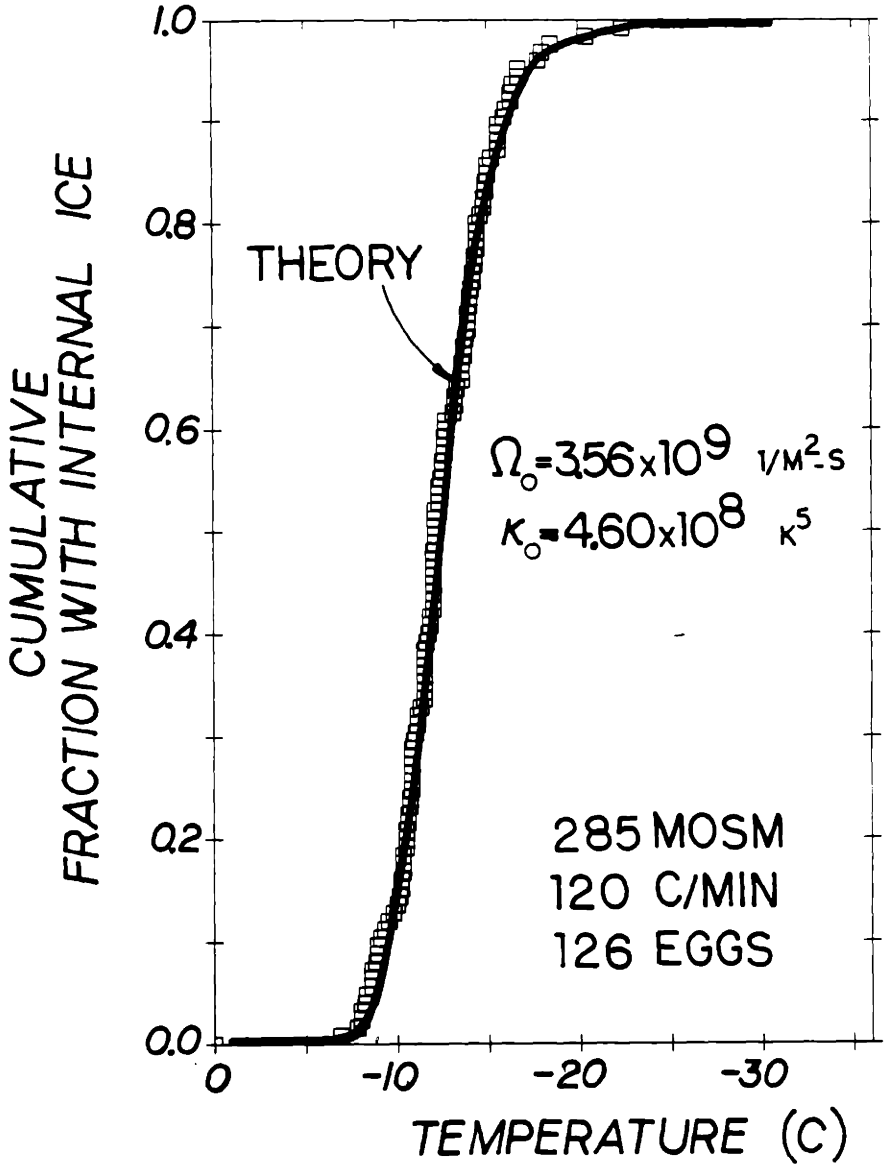

FIGURE.7.1. Determination of the nucleation kinetics parameters for mouse oocytes cooled at 120°C/min in isotonic PBS+BSA solutions. Each data point corresponds to an oocyte. Extracellular ice was seeded at -0.615°C.

(1987), however, their experimental set-up was not sensitive enough to obtain θ for mouse oocytes. It is important to mention here that it is the contact angle for the outer surface of the plasma membrane that is measured in these studies. However, our hypothesis proposes that the ice nucleation occurs on the inner surface of the cell membrane. It is well-established that cell membranes are asymmetrical and the contact angle for inner surface may be different than the outer surface (Kotyk et al. 1988).

It is clear that unequivocal confirmation of the active site responsible for heterogeneous nucleation cannot be obtained on the basis of the analysis given above. The important issue here is that our theory relies on the heterogeneous nucleation kinetics of ice as described in Chapter VI. If this is true than the experimentally observed kinetics of intracellular ice formation in cells should be adequately predicted using the theory developed. Correlation of experiments with the theory is going to be the real evaluation of the proposed hypothesis of the internal ice formation by heterogeneous nucleation on the plasma membrane. In the rest of this study, the merits of this hypothesis will be critically examined to evaluate its validity. However, before proceeding further, it is critical to comment on the possible effects of the external ice as how to alter the surface characteristics of the plasma membrane to make it a good ice nucleator.

Comments on Contact Angle for Heterogeneous Nucleation

On present evidence, we assume that the ice nucleation within cells during freezing occurs heterogeneously. The ice nucleator is assumed to be the plasma membrane and the estimated contact angle between ice-plasma membrane is 35°. Since ice does not nucleate within cells in the absence of external ice, the contact angle should be larger than 35°. Therefore, the presence of external ice somehow decreases the value of θ such that the cell membrane becomes more hydrophobic (i.e. water would not spread on it).

It is well-known that membranes are very dynamic structures. They respond to perturbations in their environment by many ways to accomodate for the new conditions. Possible changes in the external milieu with the formation of external ice can be summarized as follows:

1. Chemical effects: precipitation of pure ice increases the external electrolyte concentrations to several orders-of-magnitude higher than physiologic conditions. Desorption of the membrane components may occur (McGrath 1977).

2. Thermal effects: decreasing temperature changes the viscoelastic properties of the cell membrane (Thom 1988), decreases its fluidity (Kotyk et al. 1988), and cause lipid phase transitions (Quinn 1985).

3. Electrical effects: preferential incorporation of one ionic species into the ice lattice causes electrical transients in front of the ice-solution interface.

Externally applied electrical fields may destabilize the cell membrane and cause its breakdown at a critical potential (Zimmermann 1982).

4. Mechanical effects: ice-membrane adhesion may cause damage to the cell membrane (Tondorf et al. 1988; Hendlet et al. 1988). In addition, mechanical squeezing effects of the external ice may have important effects on the plasma membrane (Mazur et al. 1981).

5. Ionic effects: increased external ionic concentrations may lead to the hyperpolarization of the trans-membrane potential (see Chapter V). The trans-membrane potential can influence the membrane in a similar manner to the external electrical field effects (Zimmerman 1982).

All of the above effects beside the ionic effects will be discussed in Chapter IX in the context of membrane failure theory of intracellular ice formation. As will be shown in Chapter IX, none of the first 4 effects seem to be strong enough to cause membrane failure during freezing. Of course, this does not mean that they cannot alter the plasma membrane prior to the membrane failure. A discussion of possible effects of ionic changes follows.

It was shown in Chapter V that the cell membrane is hyperpolarized in response to an increasing external ionic strength. Trans-membrane potentials as high as -90mV (resting potential is about -15 mV) can easily be obtained with sudden exposure to external ice. Possible consequences of hyperpolarization of the trans-membrane potential are:

(1) increased fluidity of the plasma membrane (Corda et al. 1982); (2) change in membrane surface potential and hydrophobicity of the plasma membrane (Amory & Rouxet 1988; Kotyk et al. 1988); (3) alignment of dipole moment vector of integral membrane proteins with the membrane field (see Chapter V; Pethig 1979). The first one of these changes is probably not very important in initiating intracellular ice formation on the plasma membrane because the membrane fluidity is decreased during cooling in the absence of external ice without nucleation of the internal solution. The second one, surface potential, may be very critical, unfortunately, electrochemical models of cell membranes are still controversial and actual surface potentials are not very well-documented (Ohki 1986). The third effect can be very important. As shown in Chapter V, the orientation of lipid molecules and proteins can occur. For proteins with a dipole moment of 300 debye 16% of the proteins are aligned when the membrane potential is approximately -15mV prior to the seeding of the external ice. Once the freezing proceeds, the percentage of proteins oriented increases to 60% at -8^{o}C when the membrane potential reaches a value of roughly -80 mV (Fig.5.10). This dramatic change in orientation of the membrane proteins (as well as membrane lipids) may change the hydrophobicity of the membrane due to the possible electrostatic effects on water molecules adjacent to the plasma membrane (Matvinskii et al. 1983). In addition, the surface nucleation is exteremly effective as discussed in Section 6.4 supporting the possible involvement of the plasma membrane as the nucleation site.

In summary, we suggest that ionic changes in the suspending medium during freezing may be very important in causing intracellular nucleation. The exact mechanism by which membrane hyperpolarization and orientation of membrane proteins may influence the contact angle and/or the heterogeneous nucleation requires a better understanding of the physicochemical events occurring. Many further speculations as how the plasma membrane becomes a good nucleator in the presence of external ice may be stated, however, this is not very instructive due to the lack of basic knowledge concerning the biophysics of the plasma membrane and the heterogeneous nucleation mechanism.

Particle Catalyzed Intracellular Ice Nucleation

When oocytes were frozen in concentrations of PBS+NaCl+BSA exceeding 735 mosm, a shift in the nucleation kinetics is observed at approximately -31°C. All of the oocytes that were not frozen prior to -31°C formed intracellular ice between -31 to -34°C. The only firm conclusion that can be drawn regarding the nucleation mechanism from Figs.4.4 and 4.5 is that it must be by a heterogeneous mechanism. This is because intracellular ice always forms at temperatures above the homogeneous nucleation temperature of the suspending medium which is estimated to be approximately -37°C (Rasmussen & MacKenzie 1972; Rall et al. 1984; Scheiwe & Korber 1987). The temperature at which cell cytoplasm would nucleate homogeneously is calculated by assuming that each cell has the same nucleation behavior as an emulsion of equivalent-

sized drop of saline. The method of calculation for T_{hom} is given in Appendix B. The results of such calculations are summarized in Table 7.2 together with actual freezing results from mouse oocyte experiments. The differences between the actual and estimated homogeneous nucleation temperatures of the intracellular solution are 3.64, 3.82 and 4.18°C for initial solution concentrations of 735, 820 and 1,035 mosm, respectively. This value of the difference between actual and homogeneous nucleation temperatures is close to the value reported by Schiewe and Korber (1987) for granulocytes, namely 6.3 to 7.4°C, suggesting heterogeneous nucleation of the internal solution in the presence of external ice.

Although it can be assumed that the nucleation is heterogeneous, the catalytic site cannot be predicted from these experiments. However, there is a striking similarity between the sharp nucleation kinetics observed in the temperature range of -31 to -34°C and the heterogeneous nucleation of cells when they were cooled to subzero temperatures in the absence of external ice. Franks and co-workers (Franks & Bray 1980; Franks et al. 1983; Mathias et al. 1984; Franks 1985) have used an emulsion technique for suppressing extracellular ice formation to analyze the formation of intracellular ice in the absence of extracellular ice. Their undercooling studies have demonstrated that certain cells, namely, erythrocytes, yeast, and G. max, are able to undercool to substantial extents in the absence of external ice. However, they always freeze above the homogeneous nucleation

TABLE 7.2

Mean values of temperatures at which mouse oocytes formed intracellular ice in comparison to estimated homogeneous nucleation temperatures. Mean nucleation temperatures are calculated from Fig.4.4 by assuming that the mechanism I (plasma membrane catalyzed) was active above -31°C and mechanism II (particle catalyzed) was active below -31°C. The values for homogeneous nucleation temperatures were calculated as in Appendix B. Numbers in parantheses indicate differences by which the mean internal ice formation temperatures exceed the value of T_{hom}.

Osmolality (mosm)	T_{hom} (°C)	Mechanism I (°C)	Mechanism II (°C)
200	-35.57	-9.56±2.11 (26.01)	--
285	-35.72	-12.49±3.01 (23.23)	--
510	-36.14	-17.63±4.40 (18.51)	--
735	-36.56	-22.20±5.45 (14.36)	-32.92±1.15 (3.64)
820	-36.72	-21.74±6.28 (14.98)	-32.90±0.73 (3.82)
1,035	-37.12	-22.23±4.44 (14.89)	-32.94±0.83 (4.18)

temperature, 0.5 to 9°C, of the extracellular medium. The homogeneous nucleation temperature of the external solution is determined using the same emulsion technique in the absence of cells. This suggests that the ice nucleation inside the cells in the absence of external ice is most likely by a heterogeneous mechanism catalyzed by nucleators present within the cytoplasm. The similarity between the internal ice formation in the absence of external ice observed by Franks & co-workers and the ice nucleation inside the mouse oocytes observed in our experiments (between -31 to -34°C) in the presence of extracellular ice in hypertonic solutions cannot constitute a definite argument that the internal ice is catalyzed by an internal nucleator. It is noteworthy here that there are differences in the cooling rate, the concentration of intracellular milieu, and the volume of the cells considered by Dr. Franks and the present study. Another supporting evidence is given by intracellular ice formation experiments with drosophila embryos. Myers et al. (1987) analyzed the incidence of intracellular ice formation in embryos of Drosophila as influenced by dechorionation. Intracellular ice formation occurred over a very narrow temperature range (between -26 to -30°C) with a median temperature of -28°C for intact embryos. Following dechorionation, the embryos are exposed to the external ice and the intracellular ice formation occurred over a broder range (-13 to -30°C) with a median temperature of -24°C when cooled at 4°C/min.

Further evidence can be gained by analyzing the kinetics of heterogeneous ice nucleation for mouse oocytes, and then comparing the

results with Franks et al.'s (1983) analysis. One can predict the nucleation parameters, namely Ω^{II}_o and κ^{II}_o, for nucleation mechanism II using Eq.(6.99)-(6.101) and experiments in 1,035 mosm (Fig.4.4) as described in Chapter VI. Briefly, experimental data in Fig.4.4 will be correlated with Eqs.(6.99)-(6.101) using non-linear regression analysis to find the 'best-fit' values for nucleation parameters. Details of the solution techniques are given in Chapter VI. The result of this prediction is shown in Fig.7.2. The nucleation parameters are found to be

$$\begin{aligned} \Omega^{II}_o &= 1.84\text{x}10^{+50} \quad (1/m^2 - s) \\ \kappa^{II}_o &= 1.08\text{x}10^{+12} \quad (K^5) \end{aligned} \qquad (7.2)$$

The superscripts 'II' refer to what we call mechanism II (or particle catalyzed nucleation) as defined above. Data points between -10 and -30°C are not used in the estimation of nucleation parameters for particle catalyzed nucleation. The variance of the theory and experiment is less than 0.025 favoring a 'good' fit. The criterion for differentiating heterogeneous and homogeneous nucleation is the value of the preexponential factor. The value of the preexponential parameter being much less than estimated homogeneous nucleation (approximately 10^{+56} $1/m^3$-s for saline drops; Franks et al. 1983) favors heterogeneous nucleation of ice inside the cells under the given freezing conditions.

The parameters determined above can, now, be used to compare our results with the undercooling experiments of Franks & co-workers (Franks

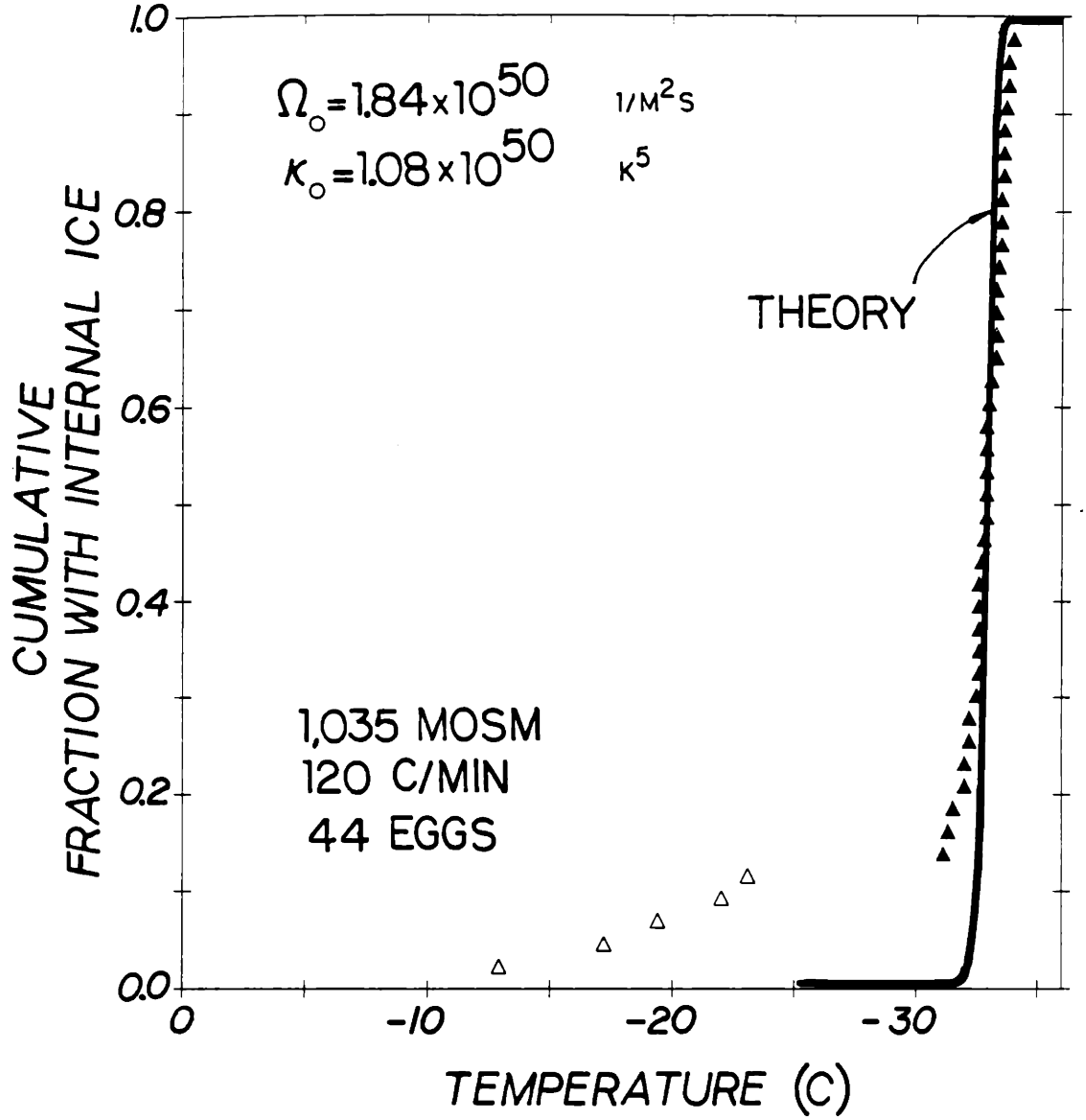

FIGURE.7.2. Determination of the nucleation kinetics parameters for mouse oocytes cooled at 120°C/min in 1,035 mosm PBS+NaCl+BSA solutions. Each data point corresponds to an oocyte. Extracellular ice was seeded approximately at -3°C.

& Bray 1980; Franks et al. 1983; Mathias et al. 1984). Fig.7.3 represents nucleation rates for saline solution, erythrocytes, G. max cells from Franks et al. (1983) as well as mouse oocytes from this study. The ice nucleation in mouse oocytes observed between -31 to -34°C in 1,035 mosm and the ice nucleation in erythrocytes and G. max cells in the absence of external ice are at the same order of magnitude. The values for mouse oocytes are between the values for pure saline and erythrocytes, and G. max cells (see Table 7.3). Franks et al. 1984 did not specify the actual nucleation parameters for yeast cells. However, they reported that it is somewhere between erythrocytes and G. max.

Further evidence for our hypothesis can be obtained by estimating the size of the supramolecular particles that are assumed to initiate the ice nucleation. The free energy of formation of a 'critical' cluster in the case of heterogeneous nucleation is lowered by the presence of nucleating particle as discussed in Chapter VI. The value by which a nucleating particle will lower the free energy of formation depends on the radius of the particle and its wettability by ice such that

$$\Delta G^{*}_{het} = \Delta G^{*}_{hom} f(R/r^{*}, \cos\theta) \qquad (7.3)$$

as discussed in detail in the previous chapter. The function $f(R/r^{*}, \cos\theta)$ is given Eq.(6.71). The value of $f(R/r^{*}, \cos\theta)$ can be estimated from the value of the exponential term, namely κ_0, and Eq.(6.101). Using a value of 22×10^{-3} J/m^2 for ice-solution interfacial energy, the function

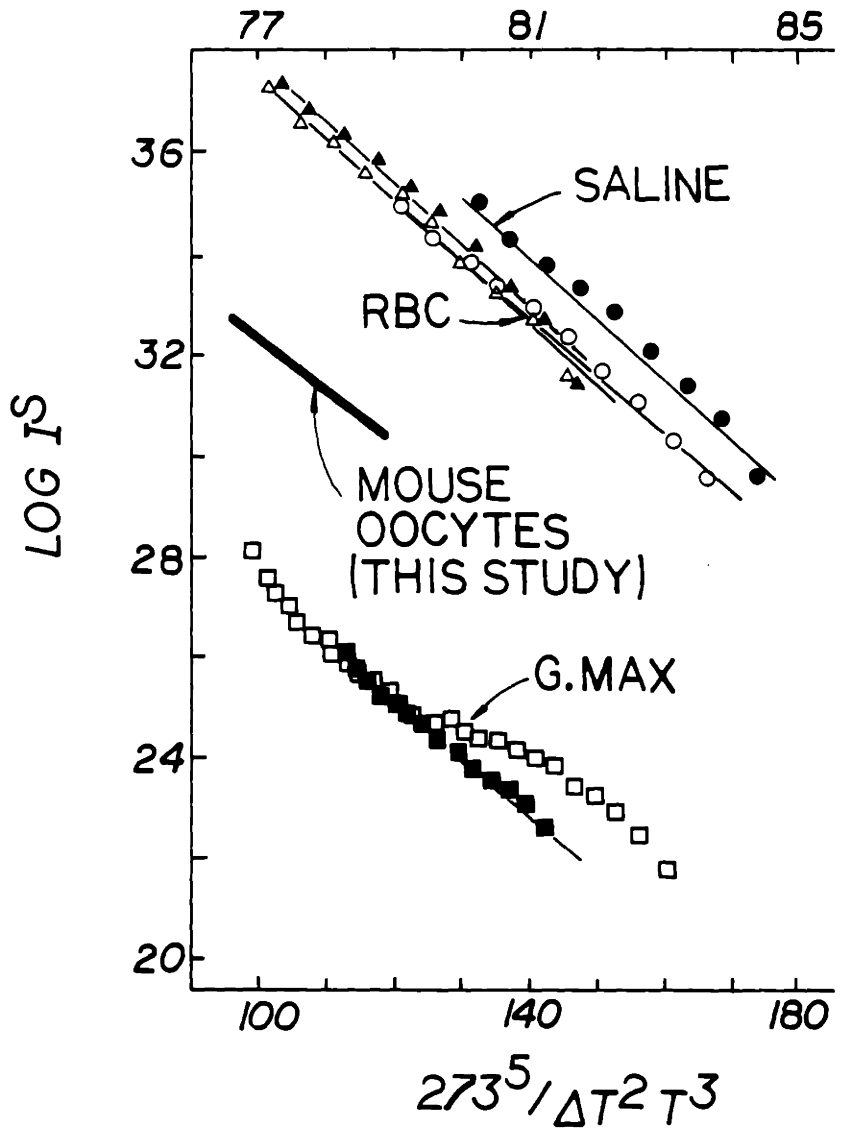

FIGURE.7.3. Plot of ln I^s vs $10^5/\Delta T^2 T^3$ (redrawn from Franks et al. 1983).

TABLE 7.3

Parameters Describing the Kinetics of Ice Nucleation in Saline Solution, Erythrocytes, G. max Cells (Franks et al. 1983) and Mouse Oocytes (this study)

Description	Ω_o ($1/m^2$-s)	κ_o (K^5)
Saline Solution	6×10^{57}	1.89×10^{12}
	4×10^{58}	1.92×10^{12}
Erythrocytes	1×10^{54}	1.72×10^{12}
	1×10^{54}	1.70×10^{12}
G. max Cells	4×10^{16}	1.67×10^{11}
	6×10^{14}	1.06×10^{11}
Mouse Oocytes:		
Particle Catalyzed	1.84×10^{50}	1.08×10^{12}
Plasma Membrane Catalyzed	3.56×10^{9}	4.6×10^{8}

$f(R/r^*,\cos\theta)$ of heterogeneous nucleation at -33°C is calculated to be 4.86. In addition, the radius of the critical cluster can be determined from Eq.(6.30) to be 1.25×10^{-7} cm. The calculation of one of the parameters describing the heterogeneous nucleation (i.e. R or $\cos\theta$) from $f(R,\cos\theta)$ requires the knowledge of the other. Many permutations of R and $\cos\theta$ may yield the same value for $f(R,\cos\theta)$. Fig.6.11 represents the function $f(R/r^*,\cos\theta)$ ($r^* = 1.25\times10^{-7}$ cm) for various values of $\cos\theta$ (or θ). As can be seen from this figure, $f(R,\cos\theta)$ is larger than 4.86 for approximately $\theta > 80^o$ ($\cos\theta = 0.17$). The radius, R, of the particle must be less than 4×10^{-7} cm in order to obtain $f(R/1.25\times10^{-7}\text{ cm},0.17) = 4.86$. In addition, Fletcher (1970) demonstrated that efficient ice nucleation only occurs for $R > 1$ nm. For R = 1 nm and $f(R,\cos\theta) = 4.86$, one can determine that the contact angle, θ, is roughly 15°. In summary, based on the first principles of heterogeneous nucleation theory, the upper and lower limits of θ and R are

$$\begin{aligned} 15^o &< \theta < 80^o \\ 10^{-7} &< R < 4\times10^{-7}\text{ cm} \end{aligned} \qquad (7.4)$$

These ranges for the contact angle and radius of the nucleating particle are very reasonable for intracellular organelles and macromolecules favoring the heterogeneous nucleation mechanism catalyzed by particles (Mazur 1965). In addition, particles smaller than the critical cluster may also serve as heterophase impurities to initiate the ice nucleation. These particles may serve as 'cores' for nucleation and increase the

nucleation temperature several degrees of centigrade (Turnbull 1986). However, exact numbers cannot be estimated because the type of the nucleating particle is not known.

In summary, it is concluded that the ice nucleation occurring in mouse oocytes between -31 to -34^{o}C in the presence of external ice is catalyzed by internal supramolecular structures. However, this should not be confused with the internal ice formation observed at higher temperatures as shown in Fig.4.4. We propose that only the fast kinetics seen below -31^{o}C is due to internal particles catalyzing the ice nucleation. It should also be emphasized that some plant cells do not contain supramolecular particles able to catalyze the ice nucleation (Burke et al. 1975, 1976). In such cases, the second mechanism of nucleation will be catalyzed homogeneously.

Combined Nucleation Mechanism

Once the parameters describing both of the nucleation mechanisms, Ω_o^I, Ω_o^{II}, κ_o^I and κ_o^{II}, are determined, the goal is to combine these two mechanisms to obtain the cumulative response of the oocytes during freezing (Table 7.3). A complex integral probability function can be defined to combine two coupled probability functions for plasma membrane and particle catalyzed nucleation mechanisms. Instead we will use a simpler approach to determine the cumulative response of oocytes during

freezing. The total number of oocytes nucleated at a time t is the superposition of the total number of oocytes nucleated according to both mechanisms. However, since the plasma membrane catalyzed nucleation operates at much higher temperatures and its rate is much slower than the particle catalyzed nucleation, one can assume that the plasma membrane catalyzed nucleation is active alone until the particle catalyzed nucleation becomes effective. At that time, the number of unfrozen oocytes is reduced by $(1 - P^I)$. So, there are only $N_o(1-P^I)$ oocytes available for the particle catalyzed nucleation. Therefore, one can simply write that

$$P = P^I + (1 - P^I)\, P^{II} \qquad (7.5)$$

The values for each nucleation mechanisms can be calculated during freezing from Eqs.(6.112), (6.113) and the combined nucleation probability can be estimated using the above equation.

When oocytes cooled rapidly (120°C/min) in various hypertonic solutions, the total probability of intracellular ice formation can be determined from Eq.(7.5) as shown in Fig.7.4 (solid curves labeled with $f(\theta)/f(\theta_o) = 1$). As can be seen form this figure the theory does not correlate well with the experimental results in hypertonic solutions. The higher is the initial concentration of the suspension medium the larger is the discrepancy between the theory and experiments. This discrepancy may be due to several simplifying assumptions in the derivation of nucleation equations (Eqs.(6.99)-(6.101)). Although, the

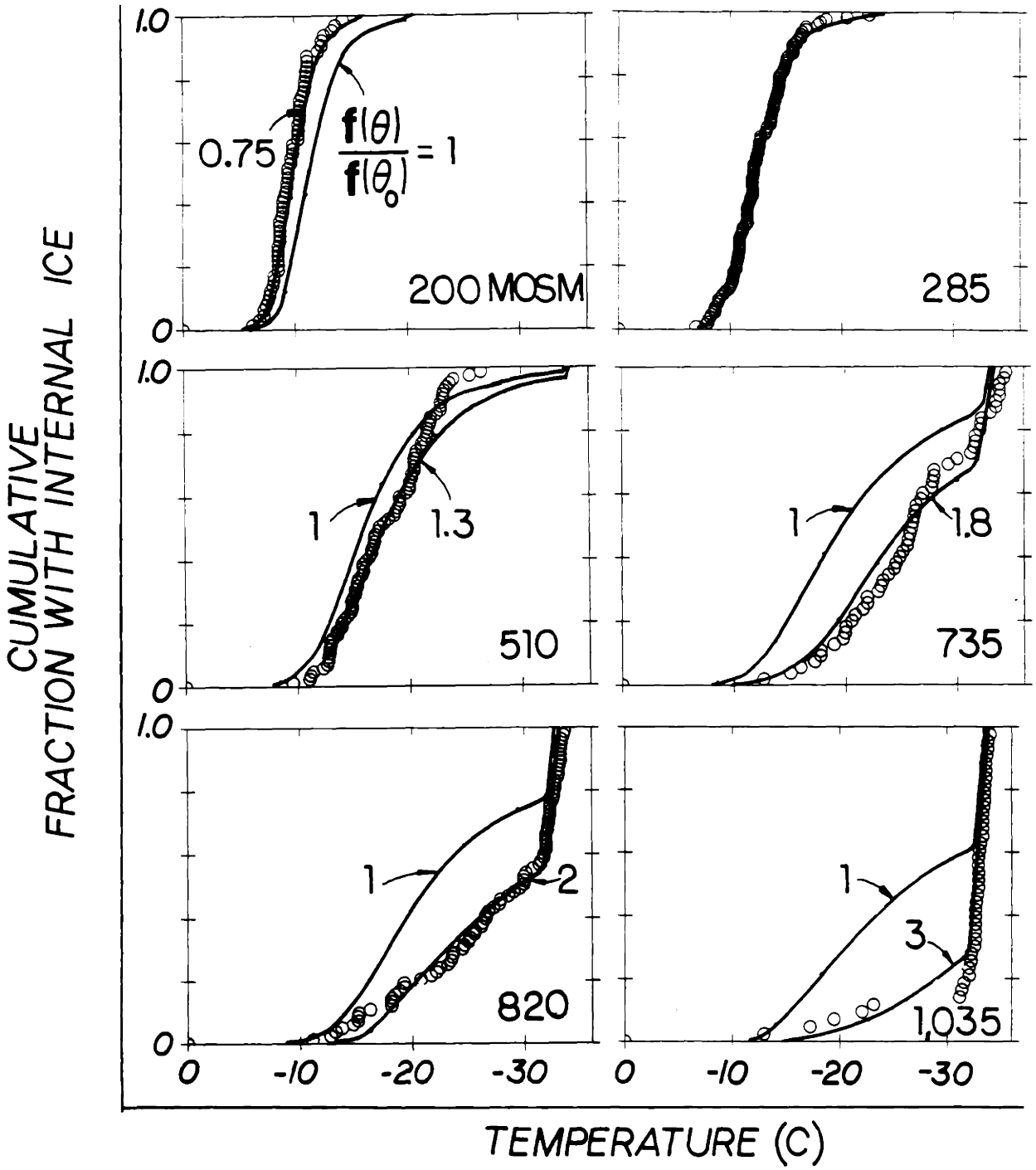

FIGURE.7.4. Cumulative fraction of mouse oocytes with intracellular ice formation vs. temperature as a function of $f(\theta)/f(\theta_o)$ in various concentrations of PBS+NaCl+BSA solutions: (a) 200 mosm; (b) 285 mosm; (c) 510 mosm; (d) 735 mosm; (e) 820 mosm; (f) 1,035 mosm.

effects of changing the electrolyte concentration were incorporated into our equations, the contact angle was always assumed to remain constant. Given the fact that the experiments were run at rapid rates to prevent water transport, the thermodynamic state of internal solution is fairly well defined in these experiments. One can, therefore, obtain a fairly accurate empirical relationship for concentration dependence of the contact angle from experimental results depicted in Fig.4.4. This will be the focus of this section.

The value of $f(\theta)/f(\theta_0)$ that is required to match the theory with data can be obtained by solving Eqs.(6.99)-(6.101) and (6.112) in concentrations ranging from 200 to 1,035 mosm as shown in Fig.7.4. The best value of $f(\theta)/f(\theta_0)$ can be evaluated for each concentration by fitting the data to the analytical solution. This would yield a series of values for $f(\theta)/f(\theta_0)$ in different concentrations. Since the value of $f(\theta_0)$ is constant and known from experiments in isotonic concentration, one can predict the value of the contact angle from $f(\theta)/f(\theta_0)$ using Eq.(6.68). The summary of such calculations is shown in Fig.7.5 which presents θ as a function of the solute mole fraction of the suspending solution. As can be seen from this figure, θ is a linear function of solute mole fraction and increases from approximately 32^o in 200 mosm to 47^o in 1,035 mosm.

A close look to the terms making up the contact angle is necessary at this point. The contact angle is defined as:

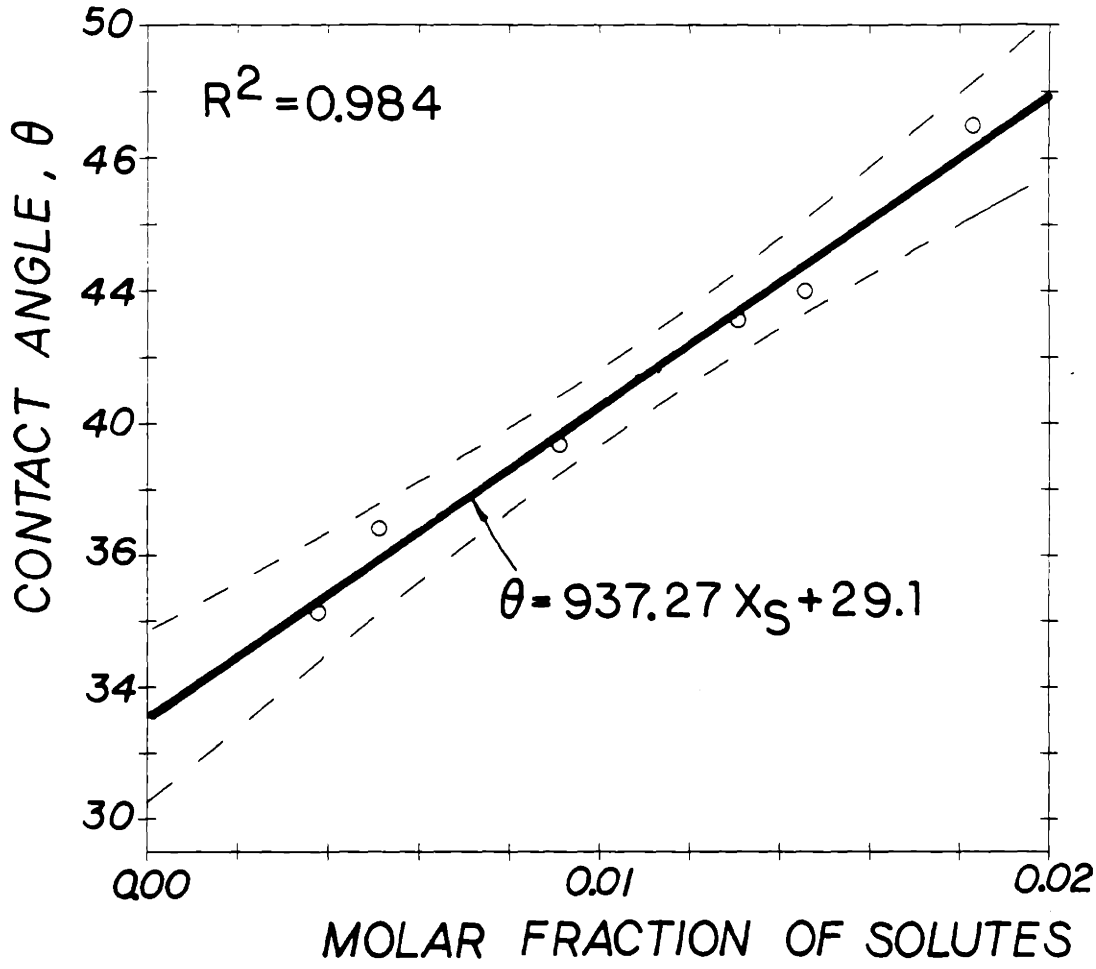

FIGURE.7.5. Variation of the contact angle for heterogeneous nucleation as a function of the molar fraction of solutes within the oocytes as determined from Fig.7.4. Dashed curves represent ±95% confidence intervals.

$$\cos \theta = \frac{\sigma^{\alpha S} - \sigma^{\beta S}}{\sigma^{\alpha\beta}} \qquad (7.6)$$

where $\sigma^{\alpha S}$, $\sigma^{\beta S}$ and $\sigma^{\alpha\beta}$ are the interfacial energies between solution-substrate, ice-substrate and ice-solution, respectively. The change in ice-solution interface energy is small in increasing concentration of electrolyte solutions as discussed in Chapter VI. Therefore, this cannot be the cause of changing the contact angle with dehydration of the oocytes. In addition, any increase in $\sigma^{\alpha\beta}$ with concentration will alter similarly the particle catalized nucleation which is not consistent with experimental observations (Fig.4.4 and Table 7.2). In contrast to $\sigma^{\alpha\beta}$, the two other terms, $\sigma^{\alpha S}$ and $\sigma^{\beta S}$, appearing in the numerator of Eq.(7.6), substrate being the plasma membrane, may change with dehydration (or concentration) without altering the particle catalyzed nucleation. Given the lack of knowledge concerning the contact angle between the plasma membrane and the ice, it is impossible to specify any quantitative reason to account for the observed change in Fig.7.5. Two qualitative speculations follow.

First, when the oocytes are frozen in hypertonic solutions, the hyperpolariztion of the plasma membrane is reduced compared to the hyperpolarization in isotonic solution as shown in Fig.5.9. The reduction in the hyperpolarization of the membrane may increase the contact angle as suggested from the experimental results.

Second, if the plasma membrane compression is assumed to take place in the form of a reduction of surface area per molecule, then this increased surface concentration produces a reduction in the surface free energy of the oocyte and therefore in surface tension (Williams & Takahashi 1987). This is also expected from the Gibbs surface energy equation. The changes in membrane surface tension with dehydration are worked out in detail by several investigators (see for example, Wolfe & Steponkus 1981). Williams and Takahashi (1987) suggested that in unfertilized sea-urchin eggs, exposure to hypertonic NaCl solutions results in a loss of surface tension associated with cell volume reduction. If this is the case than the contact angle in Eq.(7.6) may be altered. One can speculate on an endless number of alternatives to explain this alteration at the plasma membrane, however all of these speculations are very hypothetical at this point. In the rest of this study we will assume that the contact angle between the plasma membrane-ice-solution follows an empirical relationship determined from our experiments as shown in Fig.7.5.

The cumulative response of mouse oocytes can be calculated using Eq.(7.5) and the following relation for the contact angle between plasma membrane-ice

$$\theta = 937.27\ X_s + 29.096 \qquad (7.7)$$

as shown in Fig.7.5. Fig.7.6 shows the result of these calculations as described in detail in the previous sections. Heterogeneous nucleation

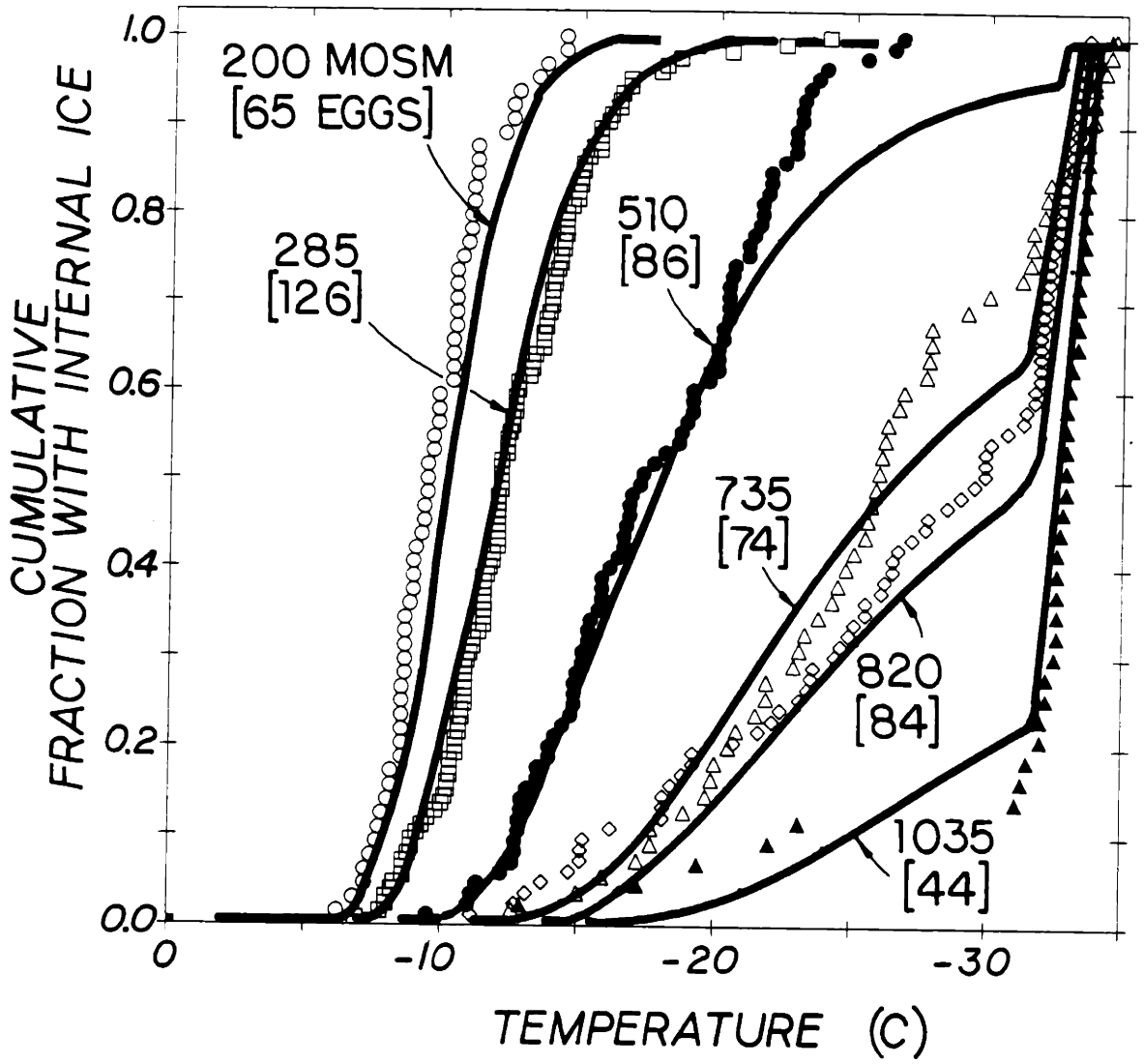

FIGURE.7.6. Theoretical and experimental cumulative fractions of mouse oocytes with intracellular ice as a function of temperature in various anisotonic solutions. Cooling rate was 120°C/min. Number of oocytes and concentrations used are represented on the curves.

in biological cells is described using a single parameter empirically determined from experiments, in addition to the parameters required to model the homogeneous nucleation kinetics. This is in agreement with classical nucleation theory that the nucleation catalytic potency of the substrate can be characterized by a single parameter, namely the contact angle, θ (Turnbull 1952a). Satisfactory agreement between theory and experiments (Fig.7.6) supports the validity of the heterogeneous nucleation theory as applied to biological cells.

Fig.7.7 represents the freezing temperature for a given percentage of internal ice formation (PIF) as a function of solute and macromolecule volume fraction as obtained from Fig.7.6. As the concentration of the suspending medium is increased, PIF_{10}, PIF_{50} and PIF_{90} curves approach to the T_{hom} curve, however, there is always a constant difference between PIF's and T_{hom}. This suggests that the plasma membrane catalyzed nucleation became less effective as the concentration of the cytoplasm was increased and the particle catalyzed nucleation became active. The theoretical predictions are in excellent agreement with the available experimental data by introducing Eq.(7.7) for the contact angle, θ, in Eqs.(6.99)-(6.101). As can be seen from this figure, the nucleation temperature is always above the estimated homogeneous nucleation temperature as discussed in the previous sections and tabulated in Table 7.3. Our theory predicts this behavior based on its two different nucleation catalysis mechanism. By increasing the concentration of the external solution and consequently dehydrating the

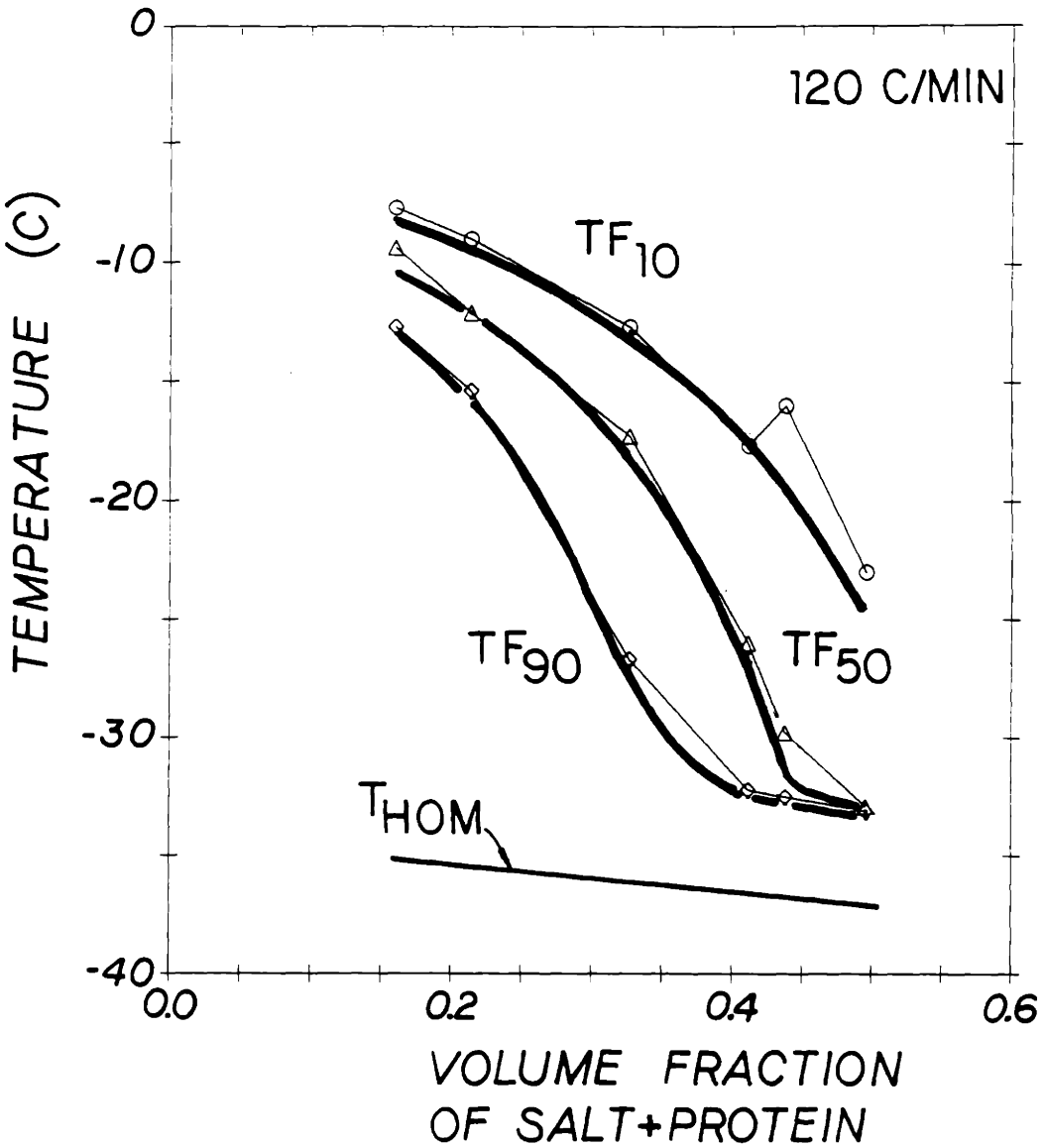

FIGURE.7.7. Theoretical and experimental freezing temperatures for 10, 50, and 90% of mouse oocytes to form intracellular ice. Homogeneous nucleation temperature is also shown (App.B). Volume fraction of salt and proteins is calculated as given by Eq.(6.87).

oocytes prior to the freezing, the plasma membrane (mechanism I) catalyzed nucleation mechanism is rendered ineffective through changes in θ such that the particle (mechanism II) catalyzed nucleation takes over to initiate the internal ice formation at a much faster kinetics. To the best of this author's knowledge, this is the first time in the literature that the results of experimental observations of intracellular ice formation could be explained by the effects of two different nucleation mechanisms based on the classical heterogeneous nucleation theory.

7.3. Sensitivity Analysis

It is, now, necessary to analyze the sensitivity of the two nucleation equations (Eqs.(6.99)-(6.101)) to various parameters to justify that the most likely parameter to change at the required order-of-magnitude to explain the experimental results in Fig.4.4 is the contact angle θ. The overall relationship for both nucleation mechanisms (Eqs.(6.99)-(6.101)) can be summarized as follows

$$I^s = \Omega_{het} \exp\{\kappa_{het}/\Delta T^2 T^3\} \qquad (7.8)$$
$$\Omega_{het} = \text{func}(\Omega_o, [f(\theta)]^{1/6}, 1/\eta, A_c)$$
$$\kappa_{het} = \text{func}(\kappa_o, f(\theta))$$

There are mainly 3 parameters that can introduce major error to the

solution of this equation. First, any error in the preexponential term due to Ω_o, $1/\eta$, A_c may change the nucleation kinetics. Second, any error in the exponential term due to κ_o may alter the theoretical predictions. Third, error in the term $f(\theta)$ appearing both in the preexponential and exponential terms, i.e. contact angle, may alter the nucleation kinetics as discussed in the last section. Since, Ω_o and κ_o include all the terms in isotonic conditions, they are constants. Therefore, only $f(\theta)$, $1/\eta$, and A_c may change with concentration.

Fig.(7.8) shows that the solution of the plasma membrane catalyzed nucleation equation (Eqs.(6.99)-(6.101), (6.112)) is sensitive to all of these parameters. However, there are certain qualitative differences in analytical predictions by varying these parameters. For the plasma membrane catalyzed nucleation, decreasing Ω^I_{het} decreases the nucleation probability as expected. In contrast, the nucleation probability is increased by decreasing κ^I_{het}. The effect of varying $f(\theta)$ is different because it appears both in preexponential and exponential terms. Its effect on the nucleation probability through the exponential term is stronger because it is the sixth power of the term appearing in the preexponential term. Nevertheless, increasing $f(\theta)$ decreases the nucleation probability through its effect on the exponential term while it decreases the preexponential term by $\{f(\theta)\}^{1/6}$. The combined effect is somewhere in between depending on the value of the parameter.

A similar sensitivity analysis can be done for nucleation mechanism

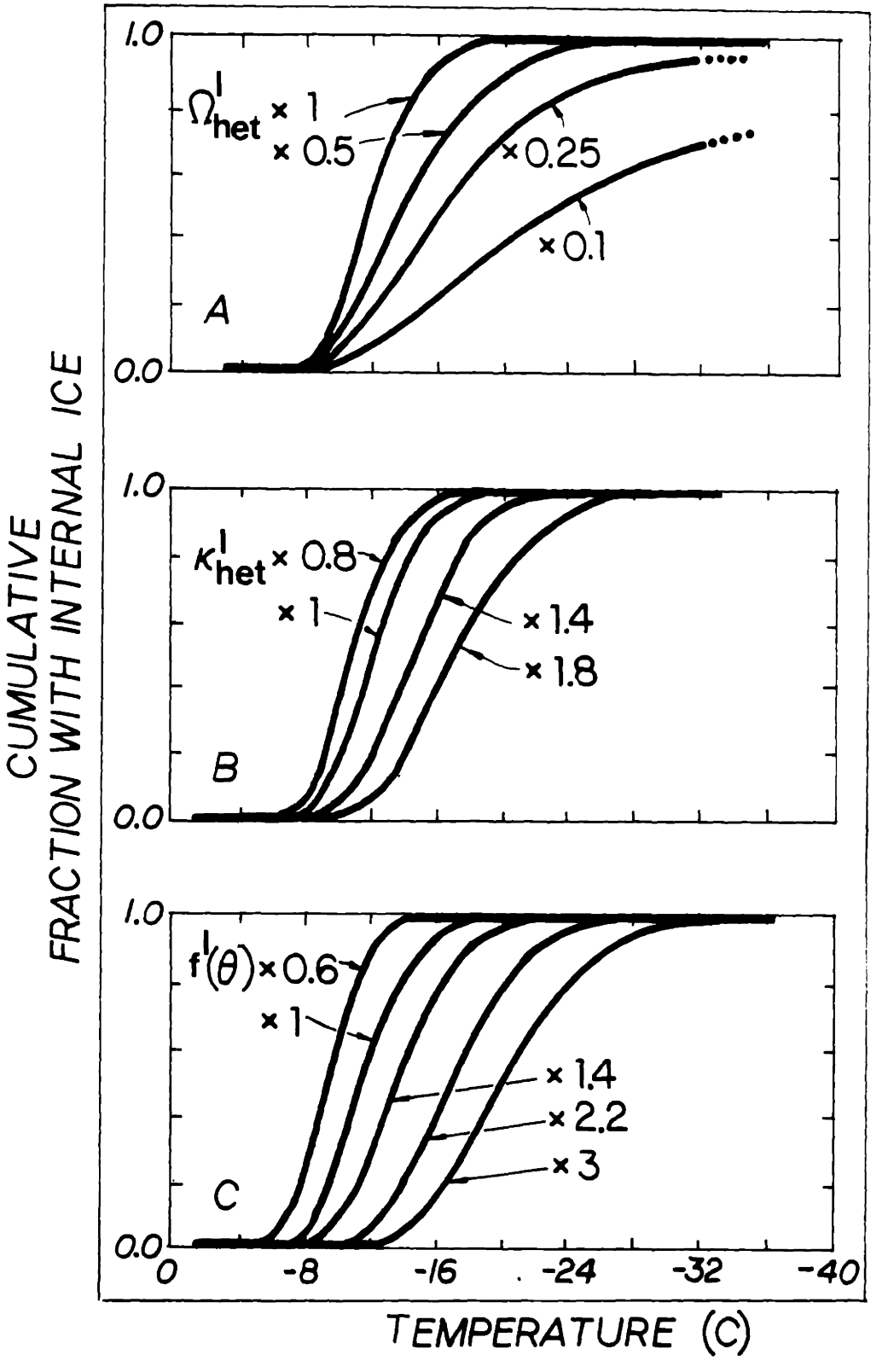

FIGURE.7.8. Effect of varying (a) Ω^I_{het}; (b) κ^I_{het}; and (c) $f^I(\theta)$ on the fraction of mouse oocytes with intracellular ice as a function of temperature when the catalytic surface is the plasma membrane.

II (particle catalyzed nucleation). As can be seen from Fig.(7.9) any slight change in the exponential or $f(\theta)$ term would alter the nucleation kinetics drastically. However, the nucleation kinetics is not a very strong function of Ω^{II}_{het}. The nucleation temperature could only be depressed 2°C by decreasing Ω^{II}_{het} by 1000.

Several very important conclusions can be drawn from these figures. First of all, experimental evidence in Fig.4.4 suggests that the nucleation mechanism II (particle catalyzed nucleation) is not altered by increasing the concentration (see also table 7.2). This means that any parameter that changes the plasma membrane catalyzed nucleation at the order of magnitude observed in Fig.4.4 should not change the particle catalyzed nucleation (or should change it only slightly). Therefore, the ignored concentration dependence of $\sigma^{\alpha\beta}$ could not be the reason for the discrepancy between the theory and the experiments.

Only parameters entering Ω^{I}_{het} may substantially alter the plasma membrane catalyzed nucleation while the change in particle catalized nucleation is small. There are two most likely sources of errors that can alter the value of Ω^{I}_{het} with concentration beside the contact angle as discussed above. These can be summarized as follows:

1) In the preexponential term, it is assumed that the number of water molecules in contact with the catalytic surface varies with the surface area of the oocytes. This is equivalent to assuming that the internal solution is dilute so that the number of solute molecules in contact with catalytic surface

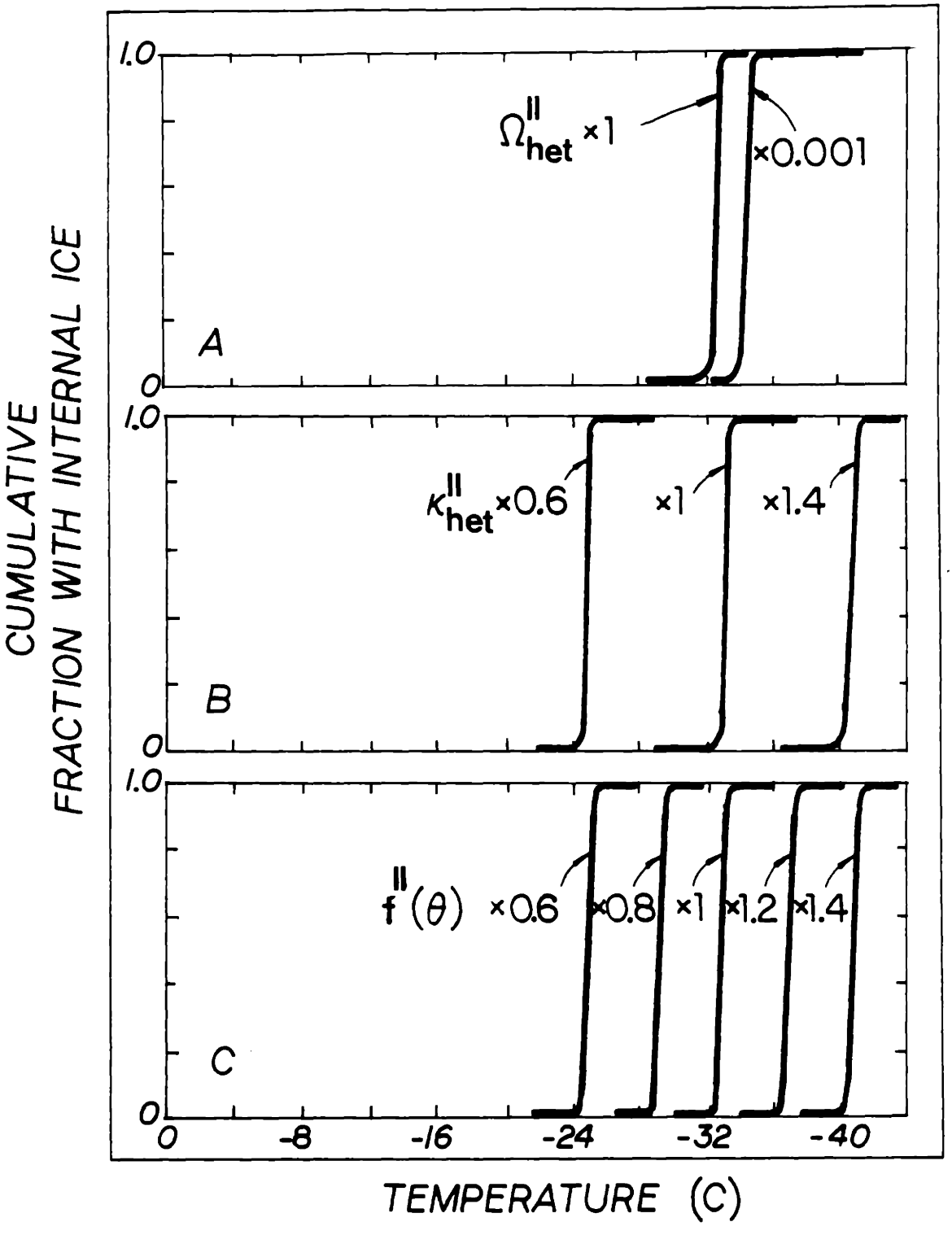

FIGURE.7.9. Effect of varying (a) Ω^{II}_{het}; (b) κ^{II}_{het}; and (c) $f^{II}(\theta)$ on the fraction of mouse oocytes with intracellular ice as a function of temperature when the catalytic surface is the supramolecular particles.

(Eq.(6.75)) can be ignored. The number of moles of solute inside the oocytes remains constant during dehydration. There are approximately $6x10^{-11}$ moles of solute at isotonic conditions (App.A). The number of moles of water in the oocytes is approximately $1.1x10^{-8}$ moles. When the oocytes are exposed to 1,035 mosm, the water volume is reduced approximately to 45% of the initial water content. Thus, the number of moles of water in the oocytes is decreased to $0.55x10^{-8}$. This value is still very large compared to $6x10^{-11}$ moles of solute. This means that the internal solution can be assumed to be dilute on a molar basis even in concentrations as high as 1,035 mosm.

ii) The error introduced in decoupling the temperature and concentration effects on the viscosity (see Chapter VI for a detailed derivation of viscosity equations) can be important. Unfortunately, we do not have a good estimation of this error since there are no experiments with combined temperature and concentration effects on the viscosity of solutions with a suspension of macromolecular particles. Our calculations showed that the preexponential term needs to be decreased by 5 times to fit the theory with experimental data in 1,035 mosm. This means that the relative viscosity of the cytoplasm to the viscosity of pure water (η/η_w) should increase by the same amount since it appears in the preexponential term. The relative viscosity (η/η_w) in 1,035 mosm solution can be estimated to be about 6 from Eq.(6.79). An increase by five times would yield a value of 30 for (η/η_w) which is an unexpectedly high value for cytoplasmic viscosity (Wojcieszyn et al. 1981; Mastro et al. 1984; Mastro & Keith 1984).

The order-of-magnitude analysis given above suggests that the most

likely parameter to effect the kinetics of ice formation at the required experimental magnitude (Fig.4.4) is the contact angle, θ as proposed in the previous section. A change from 32^{o} in 200 mosm to 47^{o} in 1,035 mosm seems to explain all of the experimental observations in Fig.4.4 based on a coupled two nucleation mechanisms with different kinetics. More experimental analysis is necessary to support the validity of the proposed empirical relationship in Eq.(7.7).

In the next chapter, the proposed intracellular ice formation theories based on the heterogeneous nucleation theory will be applied to other experimental conditions to further evaluate its validity.

CHAPTER VIII

COMPUTER SIMULATIONS
&
CORRELATION OF THE THEORETICAL MODEL WITH EXPERIMENTS

8.1. Introduction

In the previous chapter, the parameters describing the ice nucleation inside cells were determined using rapid freezing experiments in anisotonic solutions. It was suggested that there were two distinct mechanism of ice formation inside the cells. The first type ice nucleation mechanism occurs when the cells are exposed to the extracellular ice. The belief is that the plasma membrane becomes an active catalytic surface in the presence of the external ice. In the second instance, the formation of intracellular ice is catalyzed by the presence of intracellular proteins, macromolecules or organelles. A probabilistic model is used to combine these two distinct mechanisms of intracellular ice formation.

Now, the kinetic model for intracellular ice formation will be challenged with further experiments. The theoretical predictions based

on the kinetics model will be correlated with 3 different types of experimental observations: (1) freezing the cells in isotonic PBS+BSA solutions at different rates from 1°C/min to 120°C/min; (2) exposure of the oocytes to the external ice at constant subzero temperatures; and (3) a new two step rapid freezing protocol in 1,035 mosm solutions. In addition, computer simulations will be used to investigate the effect of the initial external undercooling prior to the freezing.

8.2. Experiments in Isotonic Solutions at Various Cooling Rates

The common approach in cryobiology is to determine the experimental cooling rate dependence of intracellular ice formation (Leibo et al. 1978; Scheiwe & Korber 1987; Myers et al. 1987b). This can be achieved by freezing oocytes in isotonic solutions at different cooling rates and obtaining the experimental kinetics of intracellular ice formation.

Kinetics of Intracellular Ice Formation. The procedures used were similar to the previous experiments in anisotonic solutions at 120°C/min. Briefly, the oocytes were frozen in isotonic PBS+BSA solutions. The initial seeding temperature for the external ice was kept roughly at -0.6°C. The final temperature of the cooling was -40°C. Results of such experiments are displayed in Fig.8.1(a). Theoretical predictions using the analytical model developed in this study are shown in Fig.8.1(b). Both theoretical and experimental results show that the

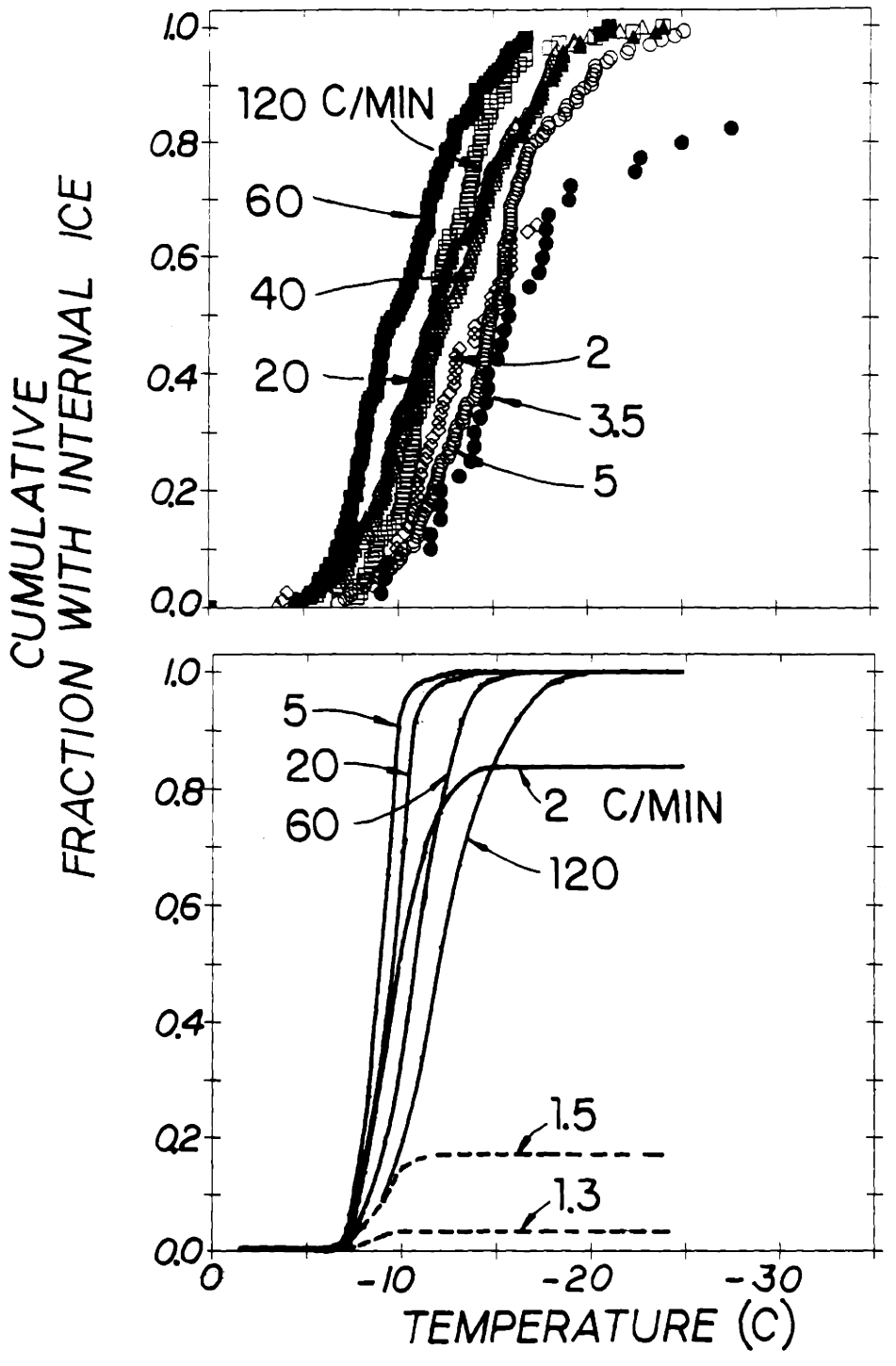

FIGURE.8.1. (a) Experimental and (b) theoretical cumulative fractions of mouse oocytes with intracellular ice formation as a function of temperature for various cooling rates in isotonic solutions. Cooling rates are indicated for each curve. Initial temperature was -0.615°C.

incidence of intracellular ice formation is strongly dependent on the cooling rate and the minimum temperature imposed. The number of oocytes containing internal ice is increased by increasing the cooling rate and/or by decreasing the minimum temperature imposed. Although, the correlation between theoretical and experimental results is satisfactory, the kinetics of the theoretical predictions does not match exactly with the experimental results.

There may be three major reasons for the discrepancy between theory and experiments:

(1) cell-to-cell variations: this has been discussed in length in Chapter V (see Fig.5.2). There is an appreciable amount of variation of the water permeability parameters. The deviation from the mean behavior occurs because of the distributed values of the permeability coefficients and, in all probably, ice nucleation parameters as well.

(2) concentration polarization effects: in the theory of nucleation kinetics, the effects of the concentration polarization of solutes behind the plasma membrane is neglected (Levin et al. 1977b). Accumulation of ions and solutes behind the plasma membrane occurrin$at slow cooling rates may influence the contact angle for heterogeneous nucleation on the plasma membrane.

(3) simplifying assumptions in the model: there are several assumptions in our model which may be the source of the discrepancy. Two of the critical assumptions are the empirical concentration dependence of the ice-solution

contact angle and prediction of the cytoplasmic viscosity. The merits of these assumptions are discussed in the last two chapters. Basic knowledge is necessary in order to fully understand the concentration dependence of these parameters.

The analysis can be fine-tuned to optimally fit the data by including the effects of the distributed biophysical parameters, concentration polarization, and/or assigning new empirical relations for the contact angle and viscosity. However, correlation of our model with further experiments to challenge its validity would be a more productive exercise. It is not justifiable to complicate the mathematics of the problem in order to improve the correlation between the experiments and the theory.

Intracellular Ice Formation as a Function of Cooling Rate. The data in Fig.8.1(a,b) can be plotted in a different format that is commonly used in cryobiology to indicate the incidence of intracellular ice formation as a function of the cooling rate as shown in Fig.8.2. This presentation of data does not include the dynamic nature of the physical system. A sharp demarcation zone is observed as a function of the cooling rate. The number of oocytes to contain internal ice increases from 0% at 1°C/min to 100% at 5°C/min as predicted from both experiments and theory. The agreement for intermediate rates is satisfactory. The sharp transition in the incidence of intracellular ice formation as a function of the cooling rate is typical of many cell types as shown in Fig.1.2 (Morris & McGrath 1981; Callow & McGrath 1985; Scheiwe & Korber 1987; McGrath et al. 1975; Cosman 1983).

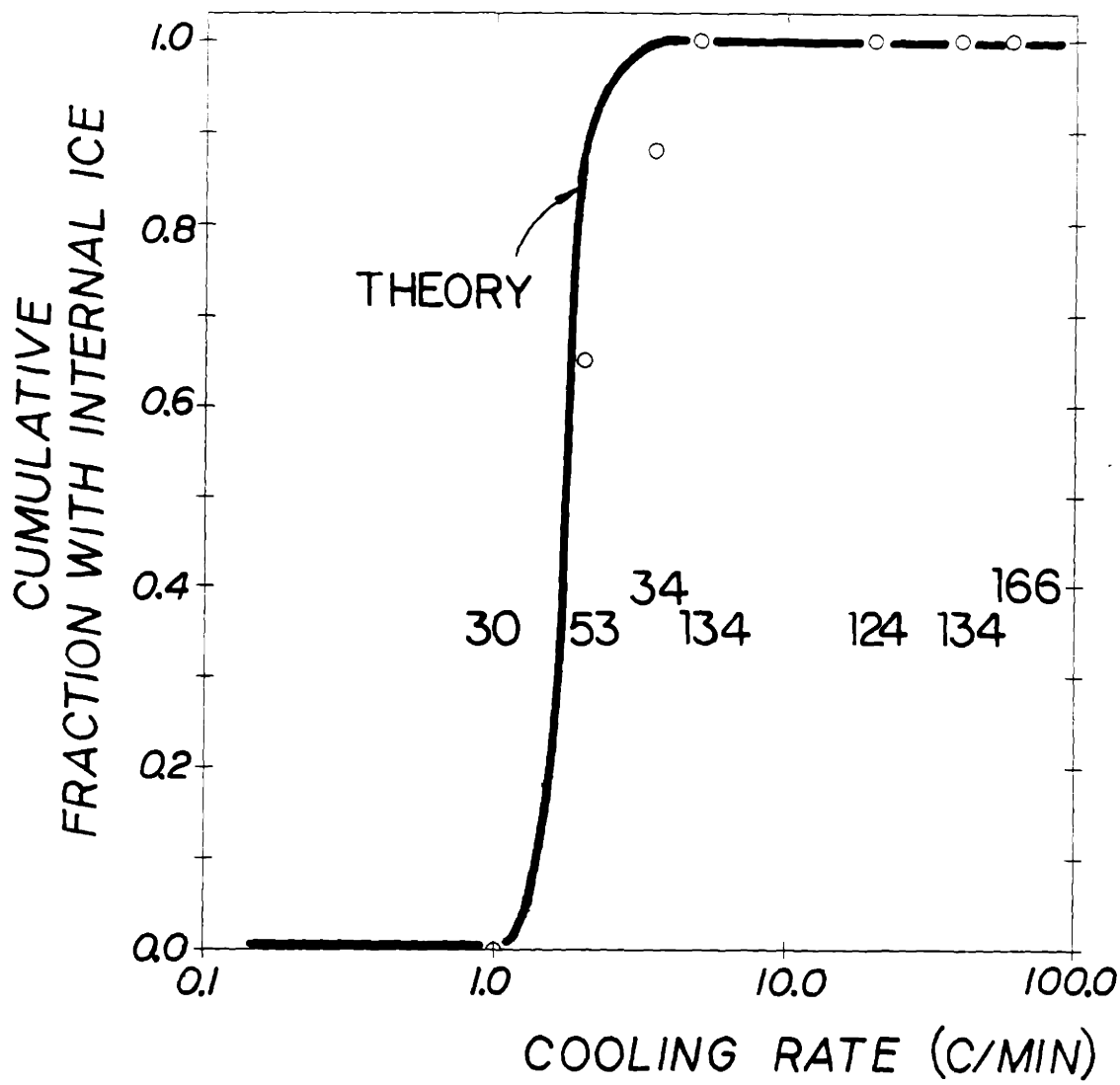

FIGURE.8.2. Experimental and theoretical cumulative fractions of mouse oocytes with intracellular ice formation as a function of cooling rate in isotonic solution. Numbers in brackets represent the number of oocytes pooled together from 5 to 10 sets of experiments. Extracellular ice was seeded at -0.615°C.

Crystallization Temperature as a Function of Cooling Rate. The temperature for 50% of the total number of oocytes to freeze internally (TF_{50}) as a function of the cooling rate can also be obtained from Fig.8.1. As can be seen from Fig.8.3 the kinetic model predictions are in good agreement with experiments. The overall mean freezing temperature for unprotected mouse oocytes over the whole cooling rate range is -12.5 ± 1.1°C. The experimental TF_{50} shows no statistical correlation with the cooling rate. The analytical model based on the heterogeneous nucleation theory predicts that TF_{50} averaged over all of the cooling rate range is -9.7 ± 1.7°C. Recently, Myers et al. 1987b determined the overall nucleation temperature of immature bovine oocytes frozen in TL-Hepes solution. Their result showed that the overall nucleation temperature of immature bovine oocytes was -13° and -14°C at 4 and 16°C/min, respectively. Similar results are obtained by Shabana & McGrath (1988) for unprotected hamster oocytes. They reported that the overall mean freezing temperature is approximately -13°C and is independent of the cooling rate. Results from unprotected two different type of oocytes, namely bovine and hamster oocytes, are in excellent agreement with our results. Fig.1.2 shows similar cooling rate independent mean freezing temperatures for other types of cells. The possibility of non-stochastic nucleation catalyzed by surface patches cannot be ruled out based on these results (Turnbull 1953).

In conclusion, there is no statistically significant dependence of

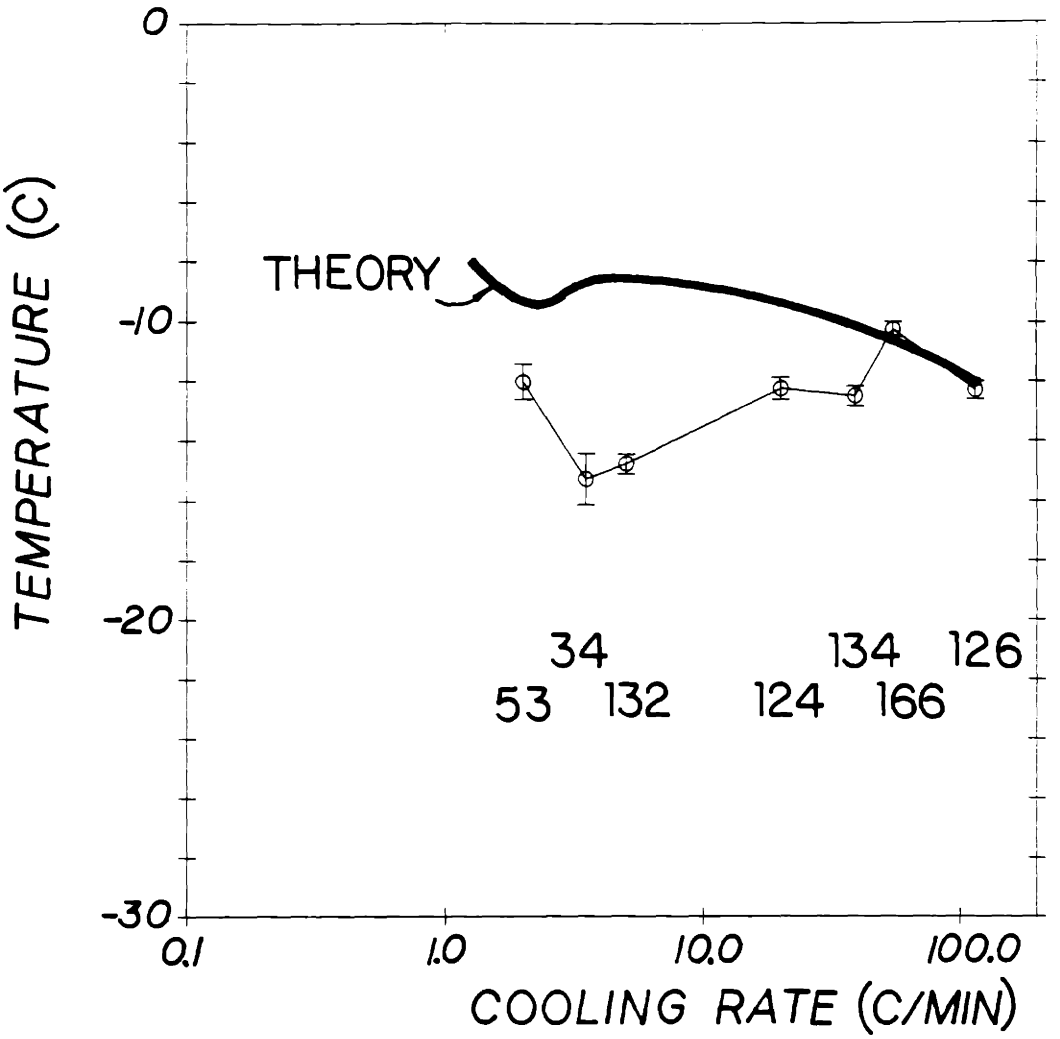

FIGURE.8.3. Experimental and theoretical temperatures for 50% of mouse oocytes to form intracellular ice as a function of cooling rate in isotonic solution. Numbers of oocytes from 5 to 10 sets of experiments pooled together are shown in brackets. Extracellular ice was seeded at -0.615^{o}C.

the mean nucleation temperature on the cooling rate as predicted from experiments or theory. It has always been confusing to have slight or no dependence of the mean freezing temperature on the cooling rate. Intuitively, the mean freezing temperature should be much lower at low cooling rates due to substantial water loss increasing the concentration of the internal solution and depressing the ice nucleation kinetics (see Figs.5.3 and 5.4). Instead experimental observation revealed almost a constant mean temperature for a large range of cooling rates. This was one of the major reasons to accept the hypothesis by Mazur (1963) that cells have a critical ice nucleation temperature at which the plasma membrane ceases to be a barrier to the external ice.

Although the cooling rate dependence of TF_{50} is negligible, the theoretical prediction shown in Fig.8.3 has a peculiar form quite different than a constant line that needs to be further emphasized. At high cooling rates (3.5 to 120^{o}C/min), TF_{50} decreases slightly by increasing the cooling rate as is expected from the classical nucleation theory. At low cooling rates (1 to 3.5^{o}C/min), there is a minimum at approximately 1.8^{o}C/min. The minimum TF_{50} is -9.2^{o}C at 1.8^{o}C/min and increases to -7.9^{o}C and -8.5^{o}C for both lower and higher cooling rates, respectively. The range of cooling rates that the observed minimum TF_{50} occurs corresponds to the transition zone as shown in Fig.8.2. This is because there is a competition between water efflux, ice nucleation kinetics and total number of oocytes frozen at a given cooling rate. The same behavior is seen in the experimental results as shown in

Fig.8.3. At the low cooling rate region corresponding to the sharp transition zone of Fig.8.2, the observed minimum is -15.3°C at 3.5°C/min and increases to -12.1°C and -14.8°C at 2 and 5°C/min, respectively. Experimental results from other studies (Morris & McGrath 1981; Scheiwe & Korber 1983; Scheiwe & Korber 1987; Shabana & McGrath 1988) showed similar qualitative behaviors. However, the number of the cells used in these studies are not adequate to draw any quantitative conclusion. Interestingly enough, the minimum temperature seen in these studies correspond well with the transition zone for critical cooling rates. It is important enough to mention these similarities between our theory and experimental findings, however, it is not quantifiable enough to justify further discussions.

In summary, the proposed kinetic model for intracellular ice formation is consistent with experimental findings. The fact that TF_{50} is not a strong function of the cooling rate as calculated from heterogeneous nucleation theory applied to biological cells is extremely important.

8.3. Experiments at Constant Temperatures in Isotonic Solutions

Kinetics of Intracellular Ice Formation. Experiments at constant temperatures in isotonic PBS+BSA solutions were performed to determine the kinetics of the intracellular ice formation as described in Chapter IV. Fig.8.4 shows the theoretical predictions of the kinetics model

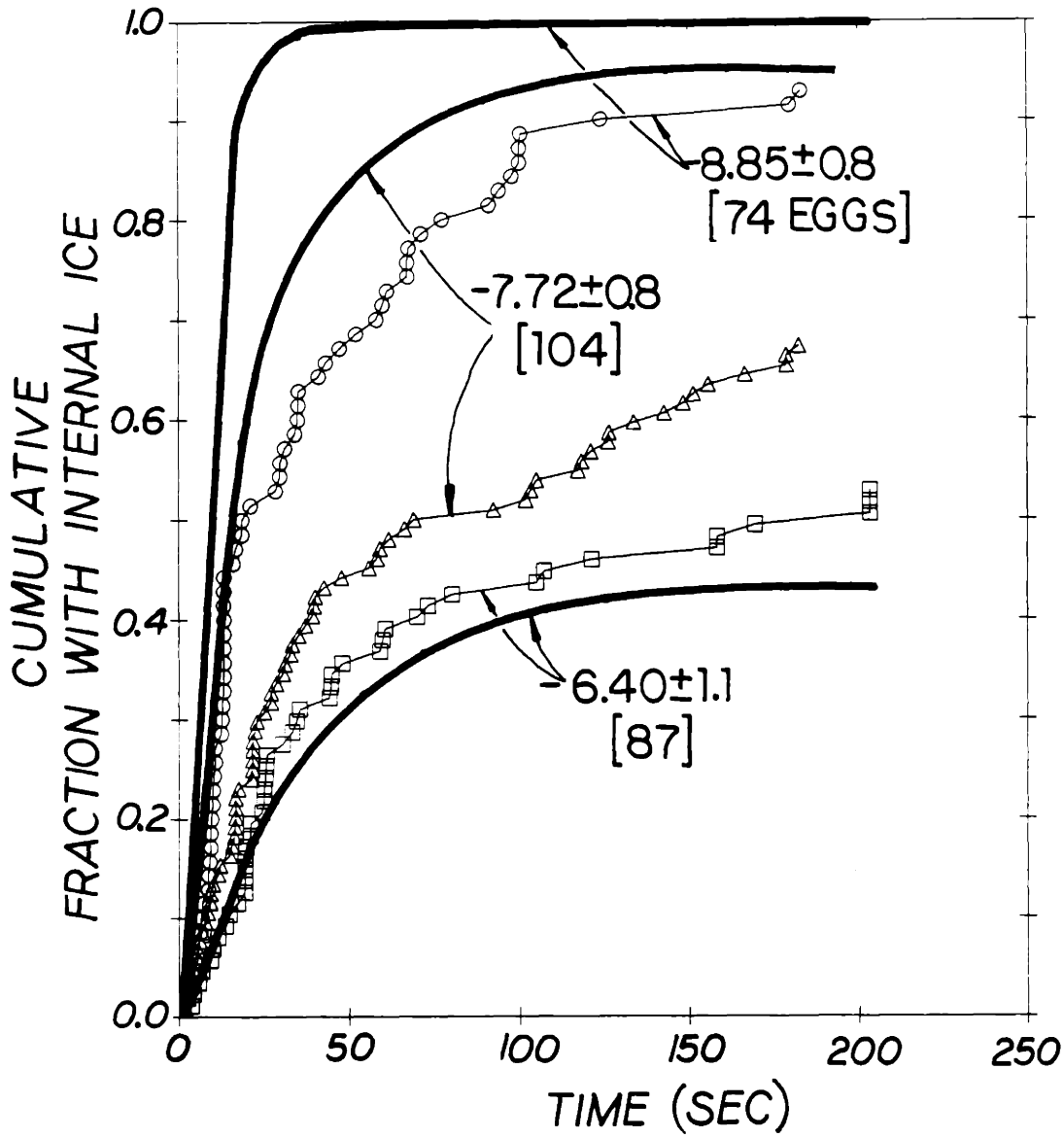

FIGURE.8.4. Experimental and theoretical cumulative fractions of mouse oocytes with intracellular ice formation as a function of time at different temperatures. Numbers in brackets represent the number of oocytes pooled together from 3 to 5 sets of experiments. Extracellular ice was seeded at -1°C prior to rapid drop of temperature to the desired constant temperature.

together with the experimental results. The qualitative agreement is good. Both theory and experiments display an increase in the incidence of intracellular ice formation with time. In addition, the kinetics of the intracellular ice formation becomes faster at exposures to lower constant temperatures. The disagreement between the theory and experiments becomes substantial at low temperatures. This may be due to the extensive rapid water transport at lower temperatures (Fig.5.5) as well as experimental difficulties associated with constant temperature experiments. Effects of concentration polarization and distributed biophysical properties may drastically alter the predictions as discussed in the previous section. The effects of concentration polarization on the contact angle between the plasma membrane-ice-solution as well as on the ice-solution interfacial energy may be especially important.

Probability of Intracellular Ice Formation as a Function of Temperature. Fig.8.4 can be displayed in a more conventional way. The total number of oocytes containing ice can be plotted as a function of the constant holding temperature by neglecting the kinetic effects. This is done in Fig.8.5. The theoretical predictions agree well with the experimental results. According to both theory and experiment, the number of oocytes nucleating intracellularly increases from less than 10% at $-6^{0}C$ to more than 90% at $-9^{o}C$. This transition zone between -6 to $-9^{o}C$ for critical temperatures is significantly different than the transition zone obtained from constant rate cooling experiments shown in

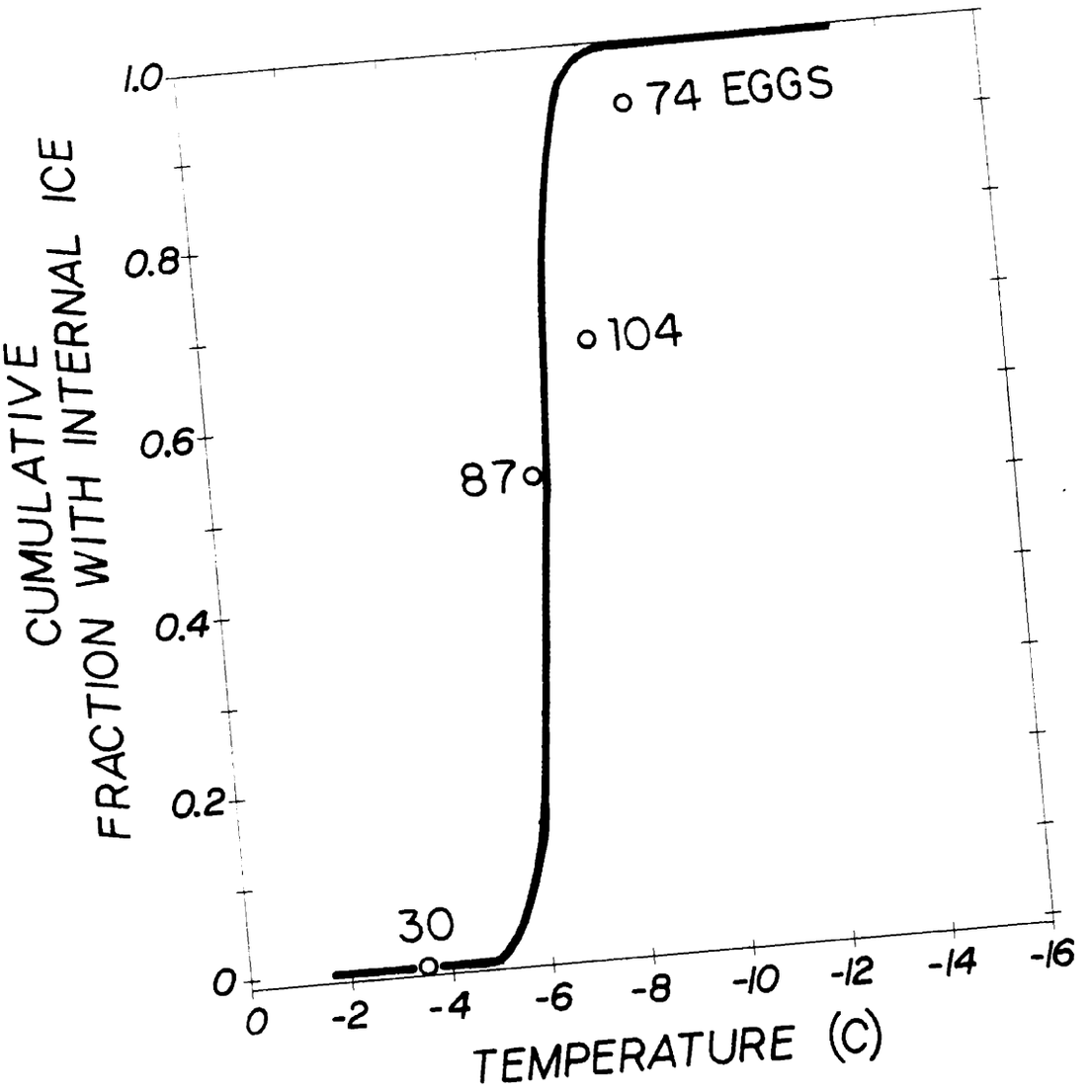

FIGURE.8.5. Experimental and theoretical cumulative fraction of mouse oocytes with intracellular ice formation as a function temperature. Oocytes were suspended in isotonic solution. Extracellular solution was seeded at -1°C prior to the rapid cooling to the desired constant temperature.

Fig.8.3. The kinetic model developed in this study accounts quantitatively for the differences observed in the nucleation temperatures between the constant cooling rate and constant temperature experiments. As it will be shown in the next chapter, the existing hypotheses of intracellular ice nucleation fail to account for this experimental observation.

8.4. Two-Step Rapid Freezing Protocol

The dramatic depression of the kinetics of intracellular ice formation by increasing the concentration of the cell-suspension solution from 285 to 1,035 mosm may have significant consequences from an applied cryobiological point of view. New optimum freezing protocols can be designed using the analytical model and the experimental observations obtained from this study. An optimum freezing protocol may be defined as the fastest possible protocol which would avoid intracellular ice formation. Such a protocol would obviously eliminate the damage caused by intracellular ice formation and minimize the damage due to exposure to high electrolyte concentrations. Non-linear cooling rates can also be used to achieve this goal. However, simpler procedures are more desirable from a practical point of view.

A two-step protocol with an intermediate dehydration period may be sufficient to minimize the freezing damage. Briefly, a two-step

protocol will have an initial cooling period to an intermediate temperature at which a holding phase is used to dehydrate the cells. The holding period is followed with the final cooling period. Two-step protocols have already been used for freezing of Chinese hamster culture cells in 5% (v/v) dimethylsulfoxide (McGann & Farrant 1976). The optimization of the protocol for culture cells by experimental trial and error showed that the intermediate temperature and the time of holding at that temperature are the crucial parameters determining the success of the protocol. In the rest of this section we will use our theoretical simulation to predict the best values for the intermediate holding temperature as well as the time for dehydration. These analytical results will then be tested by experiments using mouse oocytes.

The rationale to test a two-step freezing protocol in this study is three fold: (1) challenge our kinetics model with a complex freezing protocol to further verify its applicability; (2) emphasize the power of an analytical approach to freezing of cells; and (3) underline the principles of a new approach to oocyte freezing. The following constraints are applied in the design of the two-step freezing protocol:

PHASE I: initial rapid cooling will be at 120^{o}C/min since this rate is fast enough to impede any water transport from mouse oocytes thereby minimizing the damaging internal concentration increase during freezing. The optimum final temperature of the freezing will be determined from the analytical model. In addition, oocytes will be frozen in

1,035 mosm since this concentration is high enough to depress the nucleation kinetics without causing toxic or osmotic damage (Fig.2.7).

PHASE II: The second phase will be a holding period. The optimum time for the dehydration period will be determined from the analytical model. Our definition of the optimum dehydration time is to reach the osmotic equilibrium with 0% intracellular ice formation at the end of the dehydration period.

PHASE III: Second rapid cooling period will be down to -50°C at 120°C/min. The total incidence of ice formation at the end of the third phase is required to be less than 10%.

The final temperature of the initial cooling period and the dehydration time to reach osmotic equilibrium at this intermediate temperature will be determined from analytical simulations in order to optimize the two-step freezing protocol.

Analytical Predictions. The analytical model was used to obtain the kinetics of ice nucleation incidence for various intermediate temperatures. Fig.8.6 shows results of such calculations. For an intermediate temperature of -30°C, the fraction of oocytes with internal ice was 21% at the end of Phase I. This fraction increased to 98% after 3 minutes of dehydration. The fraction of oocytes with internal ice decreased by increased intermediate temperatures as shown in Fig.8.6. When the oocytes were cooled to -15°C at 120°C/min the fraction of oocytes with ice was 0%. During the 1 minute dehydration interval, the

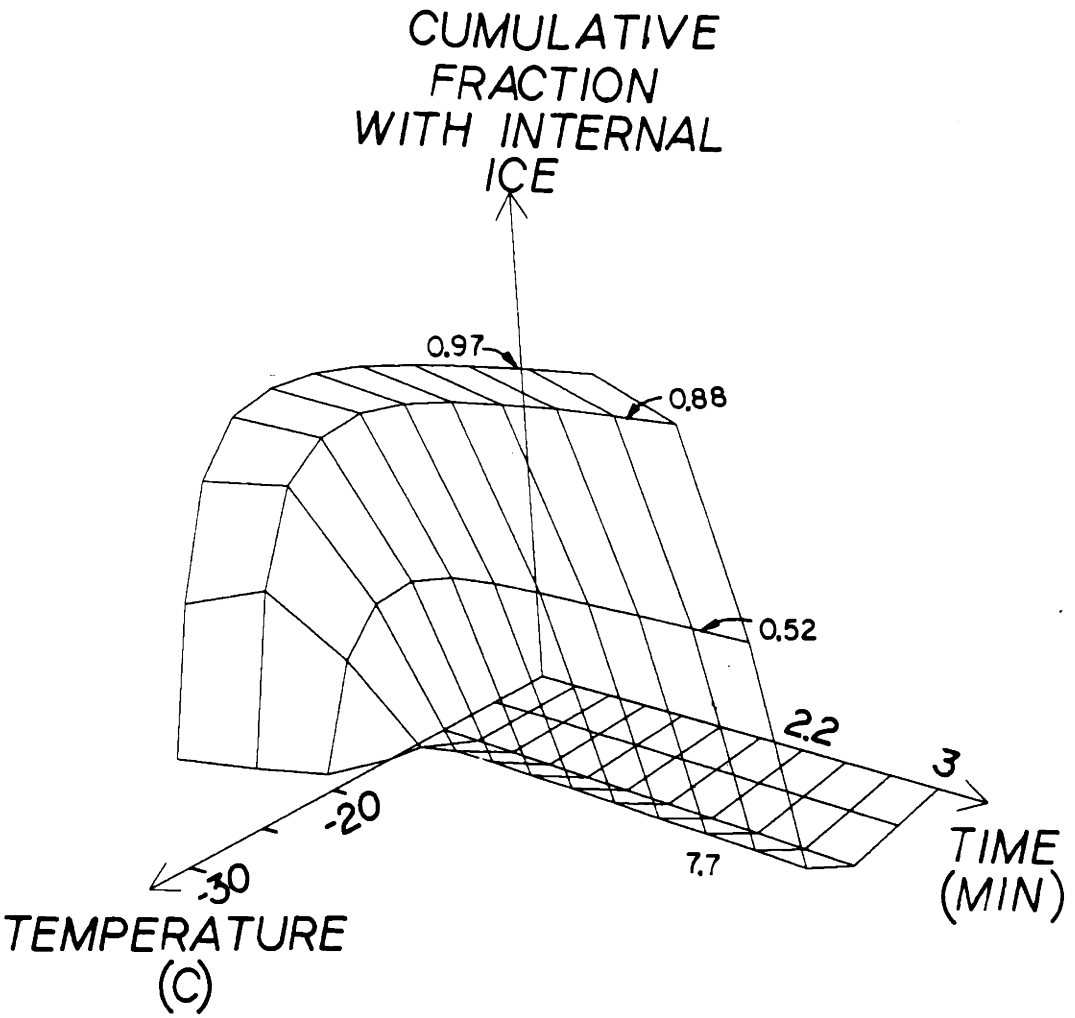

FIGURE.8.6. Fraction of mouse oocytes with intracellular ice formation as calculated form theoretical model for a two-step freezing protocol. Oocytes are cooled to an intermediate temperature and then hold at that temperature until they completely dehydrate. Oocytes are suspended in 1,035 mosm PBS+NaCl+BSA solution.

fraction of oocytes with ice increased to 8%. None of the remaining oocytes formed internal ice with subsequent cooling to -50°C at 120°C/min as predicted from the theoretical simulations. For intermediate temperatures higher than -15°C, the incidence of internal ice may be lowered to 0%. However, it was decided to have some of the oocytes form intracellular ice so that the theoretical predictions could be better verified. In summary, the following protocol is used: (1) freezing from -1 to -15°C at 120°C/min; (2) dehydration at -15°C for 3 minutes; and (3) subsequent freezing to -50°C at 120°C/min. The total fraction of oocytes forming intracellular ice ought to be 8% based on our theoretical calculations. The total time required for the whole protocol was less than 5 minutes. A conventional oocyte and/or embryo freezing protocol would take between 2 to 4 hours (Leibo 1977).

Experimental Verification of the Two-Step Protocol. In the first set of experiments, seven oocytes were cooled to -15°C at 120°C/min and then dehydrated at -15°C for 3 minutes. None of the oocyte showed intracellular ice formation. Oocytes were thawed after the dehydration without subsequent freezing to -50°C. All of the 7 oocytes showed morphological recovery. They responded osmotically after the external ice melted during thawing to 25°C. Oocytes were observed for 5 minutes at 25°C for any possible time dependent damage. No change in morphology was observed during the subsequent 5 minutes.

Fig.8.7 shows a sequence of micrographs from this experiment.

FIGURE.8.7. Sequence of micrograph illustrating the behavior of mouse oocytes cooled to -14.2°C at 120°C/min in 1,035 mosm. Oocytes were dehydrated at -14.2°C for 5 minutes and then brought back to 25°C at 250°C/min. None of the oocytes contained intracellular ice as shown in (a-d). (e,f) Oocytes were observed to be osmotically active after the temperature was back to 25°C. Scale shows 100 μm.

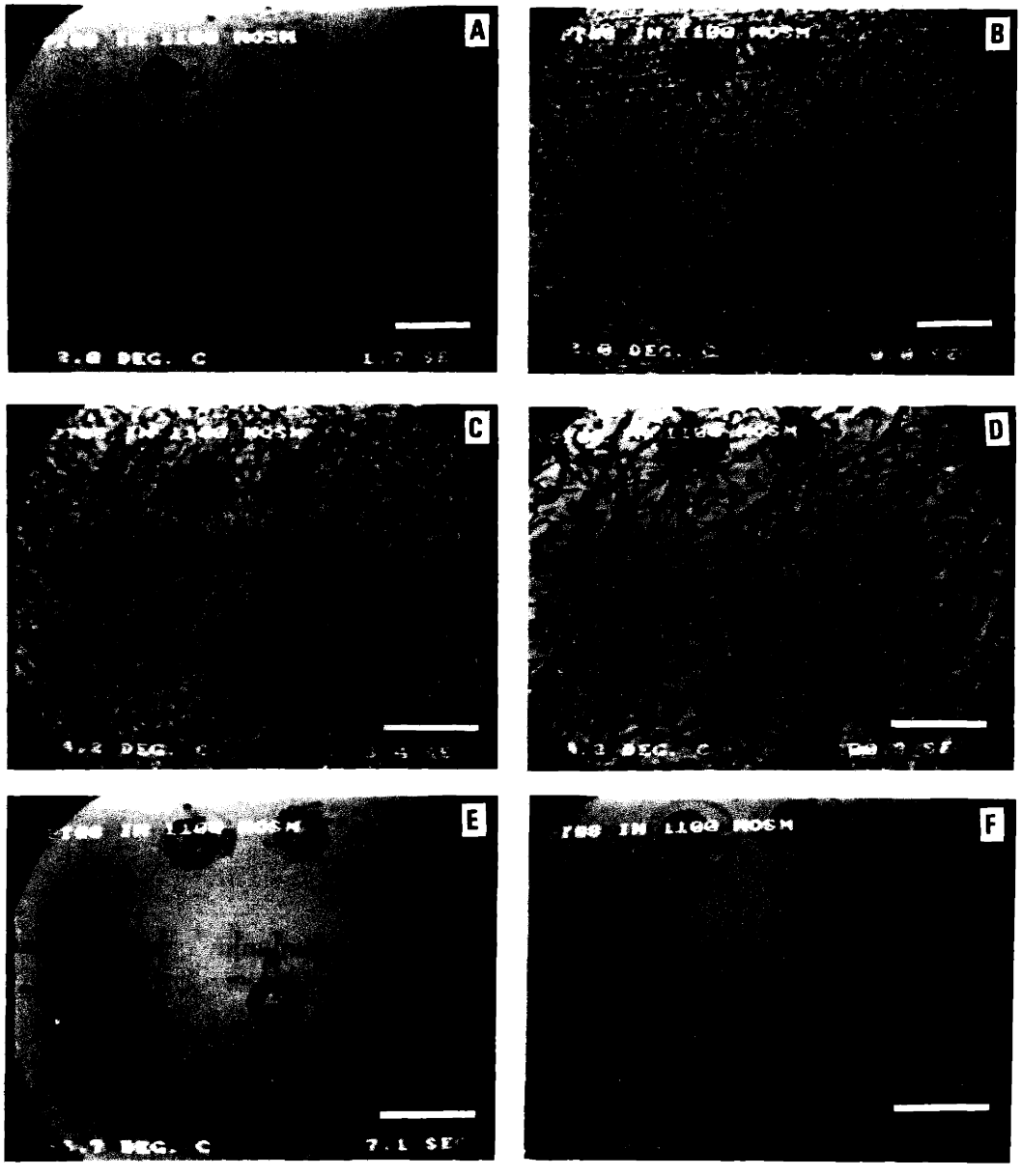

PLATE-8

Oocytes from this sequence show clear differences when compared to oocytes forming intracellular ice during freezing. Examples of damaged morphology from oocytes that formed ice during freezing are given in all of the micrographs in Chapter IV. The micrograph in Fig.4.15 shows 11 oocytes frozen at 2°C/min down to -40°C and then rapidly (250°C/min) warmed to 0°C before increasing the temperature to 25°C/min. As can be seen from the last two micrographs, immediately after the warming, all the oocytes that nucleated intracellularly showed damaged morphology while two oocytes that escaped from intracellular ice formation looked morphologically normal. However, both of those oocytes degenarated rapidly (less than 30 seconds) at 25°C. In contrast to slowly cooled oocytes, the rapidly cooled oocytes showed normal stable morphology after the temperature was brought back to 25°C for 5 minutes (Fig.8.7). The oocytes could not be recovered from the cryostage for further analysis of the viability.

In the next 4 sets of experiments, 40 oocytes were frozen following the two-step protocol optimized using theoretical simulations as mentioned above. Ten of these oocytes formed intracellular ice during freezing to -50°C. Twenty four of the 40 oocytes were morphologically normal after thawing to 25°C. Thus, twenty-five percent of the oocytes nucleated intracellularly as compared to 8% predicted from the theory. Eighty percent of the oocytes that did not contain ice during freezing showed normal morphology (Fig.8.8).

FIGURE.8.8. Sequence of micrographs illustrating the behavior of mouse oocytes cooled to -50°C in two steps. Oocytes were suspended in 1,035 mosm. Arrows indicate the oocytes with intracellular ice formation. (a) Prior to the seeding of the extracellular ice; (b) after cooling to -14.2°C at 120°C/min; (c) dehydration at -14.2°C for 5 minutes; (d) subsequent cooling to -50°C at 120°C/min; (e) warming back to 25°C at 250°C/min; and (f) 3 minutes later. Scale shows 100 μm.

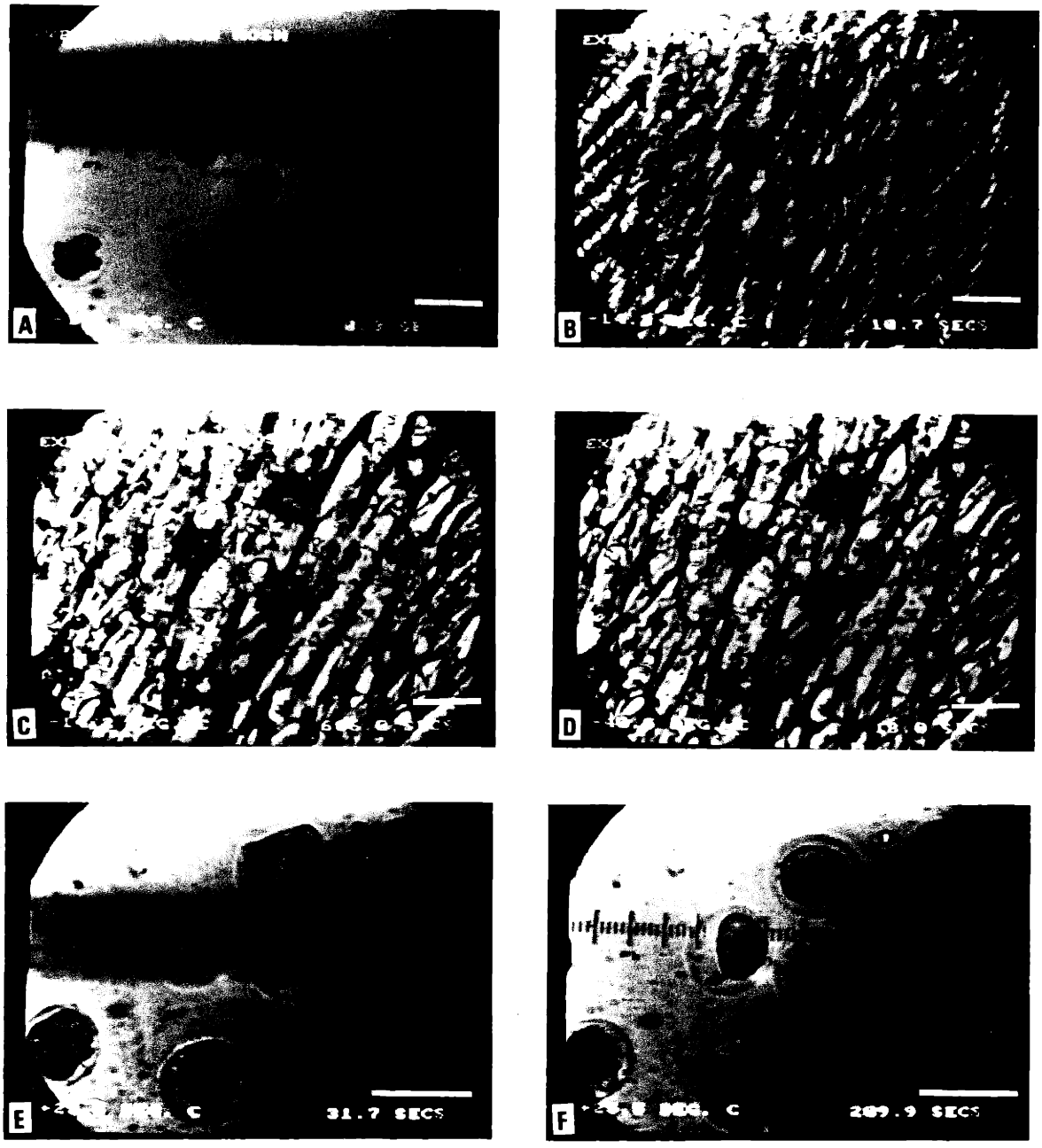

PLATE-9

The author acknowledges the fact that morphological viability does not mean much for most of the biological cells and especially for oocytes with very complex internal structure and biological functions. The point we would like to make is that the new kinetic model describing the formation of ice inside the mouse oocytes is a powerful tool to predict the freezing behavior of oocytes. Compared to the experimental trial and error type approach of McGann & Farrant (1976), the quantitative approach used here is much more effective. To the best of this authors knowledge, this was the first time that the unprotected mouse oocytes could be frozen down to -50^{o}C in less than 5 minutes with excellent morphological recovery. From morphological recovery to actual viability, there are many technical and biological issues to be addressed. A better experimental model with another type of cell may be necessary to address these issues since oocytes have very complex biological functions during fertilization and may be disturbed easily. In addition, there was no attempt to use cryoprotectants in this study. Hypertonic sodium chloride solution can be replaced with cryoprotective non-penetrating polymers to dehydrate the cells and to depress their internal ice nucleation kinetics.

8.5. Incidence of Internal Freezing: Dependence on Extracellular Undercooling.

The experimental and theoretical results stated above are with negligible extracellular undercooling. However, undercooling of the cell-suspending medium below the equilibrium freezing point (-0.53°C for PBS+BSA) is common in freezing studies. If extracellular undercooling occurs, a drastic decrease of the transition zone for critical cooling rates is observed (Fig.8.2). Diller (1975), Diller (1979), Schwartz & Diller (1984), and Cosman (1983) confirmed this behavior experimentally for various mammalian cells. In this section, a computational approach will be used to analyze the behavior of mouse oocytes as a function of the extracellular undercooling. Analytical results will be qualitatively compared to the experiments from other cells.

Equations describing the ice nucleation kinetics in mouse oocytes were solved using different initial conditions of the extracellular undercooling prior to the seeding of the ice in the suspending medium. Fig.8.9 shows the simulation results for a cooling rate of 1.5°C/min at initial undercoolings of 0, 3, and 6°C. The cumulative incidence of intracellular ice formation as well as the kinetics of ice nucleation are increased with increasing extracellular undercooling. The fraction of oocytes with internal ice is 18, 60, and 100% for external undercoolings of 0, 3, and 6°C, respectively. This is because more water is retained in oocytes when the initial external undercooling is

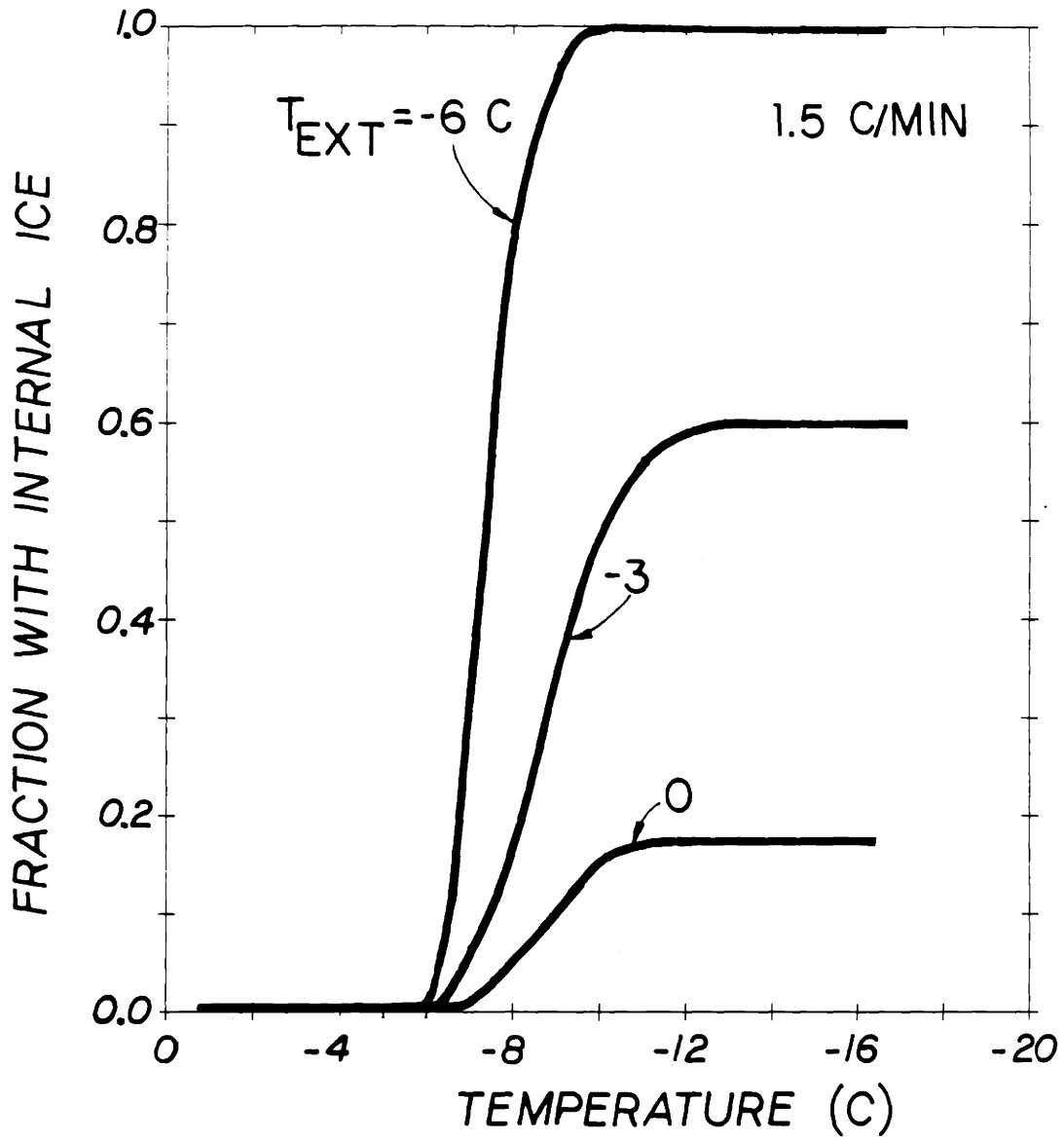

FIGURE.8.9. Cumulative fraction of mouse oocytes with intracellular ice formation as a function of temperature as calculated from the theoretical model. Extracellular seeding temperatures are shown for each curve. Oocytes are suspended in isotonic solution. Cooling rate is 1.5°C/min.

increased (Fig.5.5). The oocytes with more water content have higher likelihood of forming intracellular ice at a given temperature. Fig.8.10 shows the effect of the external undercooling on the cumulative behavior of the incidence of intracellular ice formation when the final cooling temperature is -40°C. This form of plotting the data ignores the kinetic effects shown in Fig.8.9. As can be seen from Fig.8.10, the fraction of mouse oocytes with internal ice increases with increasing the external undercooling and the cooling rate. The oocytes form intracellular ice irrespective of the cooling rate when the external undercooling exceeds 5.5°C according to the theory. At lower external undercoolings the fraction of ice formation inside the oocytes is decreased as expected. At rates higher than 3°C/min, oocytes contain ice irrespective of the amount of the external undercooling. These predictions are in excellent qualitative agreement with experimental studies from other mammalian cells (Diller 1975; Diller 1979; Schwartz & Diller 1984; Cosman 1983).

The analysis carried out in this section clearly demonstrates the importance of the external undercooling in a freezing protocol. Several degrees of centigrade change in the amount of the external undercooling may cause drastic differences in the freezing protocol. A careful control of the initial external undercooling prior to the initiation of the ice in the cell-suspending medium is crucial to the design of reliable freezing protocols.

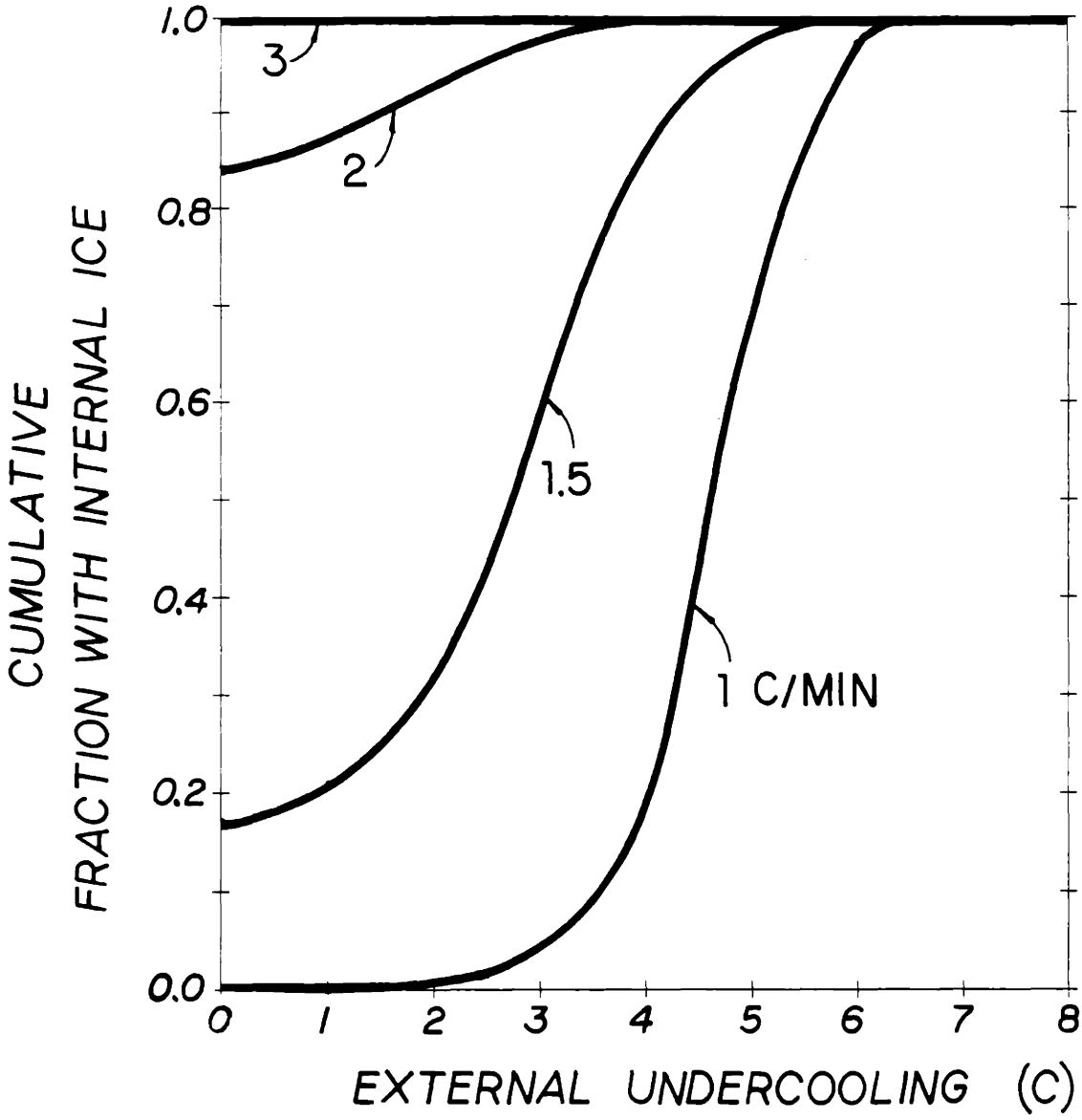

FIGURE.8.10. Cumulative fraction of intracellular ice formation as a function of external undercooling as calculated from the theoretical model. Cooling rates are indicated for each curve.

8.6. Conclusion

The theory developed in Chapter VI and the ice nucleation parameters determined in Chapter VII are used to predict the freezing behavior of the oocytes during various cooling regimes. Satisfactory agreement is obtained between the proposed theory and the experiments. The discrepancy between the model and the data increases with increased dehydration of the oocyte during freezing. The reason for this may be due to the incorrect values assigned to the plasma membrane-ice contact angle and/or to the viscosity, the distributed behavior of the oocytes, and the concentration polarization effects. On present evidence, the heterogeneous nucleation mechanism seems to be the most likely mechanism of intracellular ice nucleation. The fact that the cell's freezing behavior could be modelled using one single parameter (θ) describing the heterogeneous nucleation in addition to the parameters (Ω_o and κ_o) modelling the homogeneous nucleation supports the proposed hypothesis of internal ice formation.

CHAPTER IX

DISCUSSION OF EXISTING THEORIES FOR INTRACELLULAR ICE FORMATION

9.1. Introduction

The existing hypotheses of intracellular ice formation can now be discussed in the context of our heterogeneous nucleation theory. This will allow us to compare our theory with previous theories to further evaluate its applicability. It is important first to review the pertinent literature.

The study of ice formation within cells seems to begin with Goeppert's (1830, 1883) observations. The first mechanistic interpretation of experimental findings was by Muller-Thurgau (1886). He proposed that ice crystals formed intracellularly at rapid cooling rates whereas ice formed only in the intercellular spaces at slow cooling rates. Chambers & Hale (1932) proposed that the plasma membrane of the cell acts as a barrier against internal freezing in the presence of external ice based on direct microscopic investigation. In 1936, Levitt & Scarth suggested that the ice formed intracellularly at high cooling rates due to excessive undercooling of the cytoplasm. However,

cells escaped from internal ice formation at slow rates of cooling by excessive water efflux.

A quantitative interpretation of internal ice formation was not advanced until 1963. Mazur (1963, 1965) suggested that external ice can grow through aqueous pores (3 to 8 Å) in the membrane if the temperature is below a certain value (usually -5 to -15°C). This is due to the depression of the freezing temperature of water in small capillaries (Jackson & Chalmers 1958). According to Mazur, above a critical temperature (usually -5 to -15°C), external ice cannot penetrate inside cells because the plasma membrane acts as a mechanical barrier. However, the plasma membrane loses its effectiveness to prevent external ice to grow into cells below the critical temperature. The magnitude of the critical temperature corresponds to the equilibrium freezing temperature of water inside microscopic aqueous pores. The 'pore' theory suggested by Mazur in 1963 has been extensively used in the field.

Recently, some investigators suggested that internal ice formation may be due to membrane failure. Mechanical (Steponkus et al. 1983; Dowgert & Steponkus 1983; Scheiwe & Korber 1982a), electrical (Steponkus et al. 1984b), and thermal (Quinn 1985; Thom & Matthes 1988; Thom 1988) effects may account for the membrane damage during freezing. Once the plasma membrane is damaged by one of these effects than the external ice will be in direct contact with undercooled internal solution and ice can freely grow into cells.

In contrast to both 'pore' and 'membrane failure' hypotheses, Toscano et al. (1975) proposed that the internal ice formation in red blood cells can be caused by internal nucleators, namely hemoglobin, during freezing. They did not, however, rule out the possibility of external triggering. Later studies by Franks & co-workers (Franks et al. 1983; Mathias et al. 1984) showed that there are effective nucleators in many cells, however, they are only active at temperatures close to homogeneous nucleation temperature of the cytoplasm. Burke et al. (1975, 1976) have investigated some plant tissues and found that they do not contain heterogeneous nucleators.

In this study, we proposed a new mechanism to interpret ice formation within cells in the presence of external ice (Fig.9.1). According to our point of view, intracellular ice can nucleate by two distinct mechanisms within cells. First, ice can nucleate heterogeneously on the plasma membrane in the presence external ice. Our suggestion is that external ice may alter the plasma membrane to make it an energetically favorable substrate for ice nucleation. We call this type of nucleation 'plasma membrane catalyzed' nucleation. Second, cells would nucleate spontaneously at temperatures close to their homogeneous nucleation temperature (usually between -30 to -40^{o}C). The nucleation may be heterogeneous (if there are active internal nucleators) or homogeneous (if there are no internal nucleators for only very few cases). This is called 'particle catalyzed' nucleation. Both of these mechanisms are combined to predict the cumulative probability

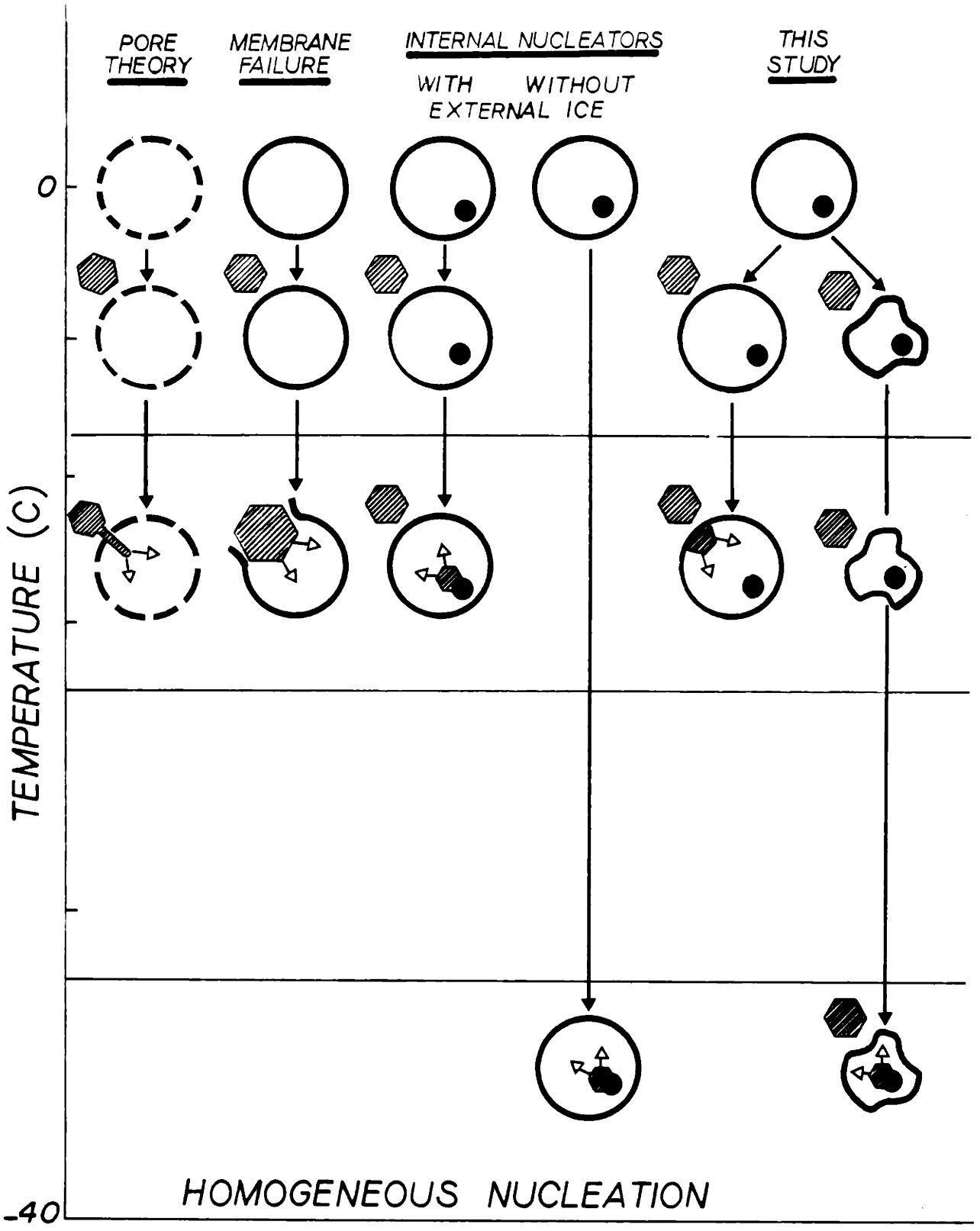

FIGURE.9.1. Schematic representation of existing and proposed mechanisms for intracellular ice formation within biological cells.

of internal ice formation (discussed in detail in Chapters VII & VIII). It is noteworthy to mention here that there seems to be a confusion in the cryobiology literature in the use of terms 'crystallization' and 'nucleation.' Both the pore and the membrane failure theories assume the growth of the extracellular ice into the cells, therefore, the temperature at which this happens should be called 'crystallization' temperature as opposed to 'ice nucleation' temperature.

9.2. Intracellular Ice Formation Through Aqueous Pores in the Plasma Membrane

In 1965, Mazur has suggested that the internal ice in the presence of the external ice is seeded by the extracellular ice through the cell membrane. He has proposed an explanation why the plasma membrane prevents the passage of ice crystals above a critical temperature (usually between -5 to -20°C) but permits their passage below the critical temperature, called T_{crt} in this study. According to his view, the depression of the melting point of small ice crystals with curved surfaces can account for the observed intracellular freezing temperature. If the surface of a liquid is very large compared to its volume, the freezing temperature of the liquid will be depressed (Jackson & Chalmers 1958). Therefore, small ice crystals can only be stable and pass through aqueous pores at temperatures below a critical temperature corresponding to the freezing temperature in pores. Mazur calculated the melting temperature of an ice crystal in microscopic pores using the Kelvin equation (Mazur 1965)

$$\Delta T = T_f - T_{crt} = \frac{2v^{\alpha} T_f \sigma^{\alpha\beta} \cos \theta}{r_c \Delta H_f} \qquad (9.1)$$

where θ is the contact angle between ice-solution (not ice-capillary as in this study), and r_c is the radius of the capillary. If, for example, $\theta = 80^{o}$, Eq.(9.1) would become

$$\Delta T \simeq 50 / r_c \qquad (9.2)$$

and the pore radius at -10°C would be 5 Å. A pore radius of 5 Å would agree with permeability studies done by Solomon (1968). Although some electron micrographs of cell membranes have been interpreted as indicative of the presence of fine aqueous pores (de Robertis et al. 1965), the existence and size of membrane pores are not incontestable (Shanes 1963). Each type of cell with different r_c and θ values would yield a similar relationship to Eq.(9.2) accounting for the variability in their observed intracellular freezing temperature. Obviously, such an approach do not take into consideration the kinetics of the intracellular ice formation as shown in Figs.4.5 and 4.14. The value of the critical temperature is usually called cytoplasm ice nucleation temperature (Mazur et al. 1984; Steponkus et al. 1983). The reservation for this term is mentioned in the previous section. In this study, T_{crt} will be called 'cytoplasm' freezing temperature and/or ice formation temperature.

As Mazur pointed out, Kelvin equation is only valid for macroscopic systems and its application for microscopic systems is questionable

(Viaud, 1972; Enustun et al. 1978). A pore of 5 Å in diameter would contain roughly 5 water molecules. In this type of a fine capillary, the thermodynamic relation of the Kelvin type used to calculate the equilibrium freezing temperature is not valid in the framework of thermodynamics. The growth of an organized crystalline surface through a microscopic pore of approximately 5 Å is also questionable. The dimensions of a unit cell of hexagonal ice composed of 6 water molecules are approximately 7.4 Å in height and 4.5 Å in edge length, therefore, only one hexagonal ice crystals can only inside a pore of radius 5 A. It is very difficult to envisage that a unit cell of ice can orient itself to grow through the pore. If one assumes that homogeneous nucleation takes place inside the capillary at -10°C, the radius of the critical cluster is approximately 40 Å. This is an order-of-magnitude larger than estimated pore size. In summary, it is very unlikely that ice can actually grow through pores of 3 to 8 Å in radius in the plasma membrane, after all the presence of pores in membranes is a speculation (Shanes 1963).

Although many theoretical concerns are listed above, correlation of the theory with experiments would probably be the best evaluation of the pore theory. Generally, the cytoplasm ice formation temperature (T_{crt}) in Eq.(9.1) is determined from freezing experiments similar to Fig.4.16 and the probability of intracellular ice formation (P) is assigned a value of zero when the degree of supercooling (ΔT) is $< 2^{o}C$ or when the fraction of water content (V_w/V_{wo}) is < 0.1 at T_{crt}. P is assigned a value of 1.0 when $\Delta T > 2^{o}C$ and $(V_w/V_{wo}) > 0.1$ at T_{crt}. These

assumptions are based on general experimental observations and are discussed in Mazur (1977). Many different values are assigned to these parameters in the literature (Mazur 1977; Mazur et al. 1984; Cosman 1983). There is no theoretical rational to choose one value of ΔT or (V_w/V_{wo}) over another one.

Consider an example using the above criteria for P for the mouse oocyte experiments in 285 mosm (Fig.4.14). The cytoplasm freezing temperature (T_{crt}) is approximately -12.5°C from Fig.4.16. Calculation of ΔT or (V_w/V_{wo}) to predict P is possible using the water transport model described in Chapter V (Fig.5.4). As can be seen from Fig.5.4, ΔT is $< 2^oC$ at -12.5°C for a cooling rate of approximately 1°C/min giving P = 0. In addition, ΔT is $> 2^oC$ at -12.5°C when the cooling rate exceeds 1.5°C/min yielding P = 1. Fig.9.2 shows this result compared to experimental data as well as our theoretical prediction based on heterogeneous nucleation theory. Mazur's theory predicts more or less the same range of transition cooling rates and can be assumed to be accurate given all the experimental uncertainties. It is important to mention here that P is not very sensitive to the values assigned for ΔT or (V_w/V_{wo}), whereas it is very sensitive to the value assigned for T_{crt} (see Mazur 1977; Mazur et al. 1984). This can be proven simply by performing the same exercise as above with different values of T_{crt}, ΔT, and (V_w/V_{wo}). To summarize, T_{crt} is obtained from constant cooling rate experiments (Fig.4.14 or 4.16), then combined with a criterion for P to predict the transition cooling rate in Fig.4.17. The result is shown in Fig.9.2. All of Figs.4.14, 4.16, 4.17, and 9.2 are actually from the

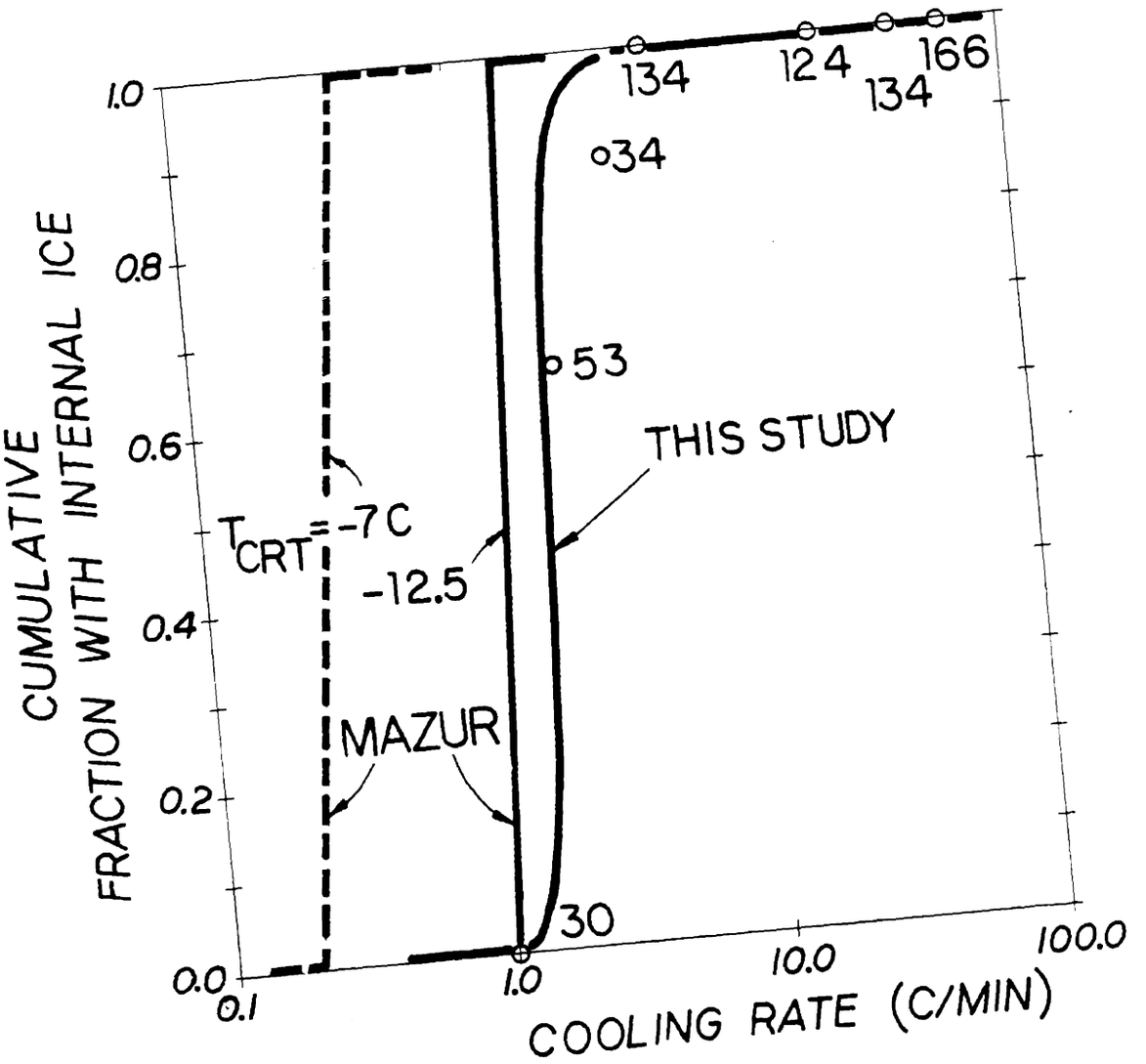

FIGURE.9.2. Cumulative fraction of mouse oocytes with intracellular ice formation as a function of cooling rate as obtained from Mazur's (1965) pore theory and this study. Oocytes were suspended in isotonic PBS solution. Numbers in brackets represent the numbers of oocytes used for each experimental condition.

same experiments. As mentioned above ΔT and (V_w/V_{wo}) do not affect the results significantly, therefore, one predicts Fig.9.2 from Fig.4.14 which are actually same experiments. Such an empirical approach might have been very helpful if one could predict P for different freezing protocols using a single value for T_{crt} as determined from Fig.4.14. However, T_{crt} varies depending on the experimental conditions. As discussed in Chapter VIII, the amount of external undercooling influences T_{crt} in such a way that larger undercoolings decreases T_{crt}. Mazur (1977) assigned different T_{crt} values for each different external undercooling to predict the probability of internal ice formation in red blood cell experiments. The validity of such an empirical approach is questionable.

Now, lets extend this exercise to constant temperature experiments as shown in Fig.4.19. The value of T_{crt} from constant temperature experiments is between -5 to -8°C (roughly -7°C) and it is somewhat higher than the one determined from cooling experiments (i.e. -12.5°C). If one uses -7°C instead of -12.5°C to predict P, the transition cooling rate in Fig.9.2 is shifted to higher temperatures as shown with dashed curve. The pore model cannot account for these experimental observations. Should -7°C from constant temperature experiments or -12.5°C from constant cooling rate experiments be used as the cytoplasm freezing temperature?

Another sets of experiments that the pore model can be tested against is rapid (120°C/min) cooling experiments in hypertonic solutions

as depicted in Fig.4.5. The value for T_{crt} temperature decreases from -12.5°C in 285 mosm to -32°C in 1,035 mosm. The reader should refer to Chapters IV and VIII for detailed discussion of these experiments. Similar results are also obtained for non-acclimated and acclimated plant protoplasts (Steponkus et al. 1983) when they are suspended in hypertonic solutions. Pore model cannot offer any explanation to this dramatic depression in the nucleation temperature (approximately 20°C). At 1,035 mosm, sixty four percent dehydration of the cell prior to freezing has taken place. One may argue that pores are getting smaller (!) by dehydration, however, this is not consistent with slow cooling rate experiments where dehydration exceeds 80% while T_{crt} is still assumed to be constant at -12.5°C. It is noteworthy here that P is assigned a value 1 at -12.5°C for 1.5°C/min according to Mazur's criterion of internal ice formation given above in which case (V_w/V_{wo}) is $< 20\%$ at the time of observable internal ice formation. In addition, at constant temperature cell dehydrates while T_{crt} is constant at -7°C. To summarize, somehow dehydrating cells prior to freezing depresses T_{crt} drastically (Fig.4.5), whereas dehydrating at constant subzero temperature increases T_{crt} (Fig.4.19) and dehydrating at constant cooling rate does not alter T_{crt} at all (Fig.4.14). The pore theory cannot account for these observations.

Given all the above theoretical and experimental considerations, it can be concluded that the pore model fails to explain the most simple experimental findings that are satisfactorily predicted using the heterogeneous nucleation theory developed in this study (see Chapters

VII and VIII).

9.3. Intracellular Ice Formation Due to Altered or Damaged Plasma Membrane

An alternative to the pore theory is the penetration of the external ice inside cells through damaged plasma membrane. According to this view, the seeding of the intracellular solution is the result of the failure of the plasma membrane. At a critical temperature, the plasma membrane breaks down and is no longer able to act as a barrier to external ice resulting in nucleation of the intracellular contents. Therefore, intracellular ice formation is the consequence of membrane failure rather than the cause as proposed by Mazur's pore theory. However, both pore and damaged membrane theories assume the growth of external ice into the liquid cytoplasm.

Although the cause of the membrane failure is not known, there are several speculations about what mechanism may be responsible for the membrane failure. Existing theories are: (1) mechanical, (2) electrical, and (3) thermal/chemical effects. The validity of these effects can be best verified by correlation with experimental findings. In this section, these hypotheses will be challenged with experimental observations discussed in Chapter IV for mouse oocytes, if necessary further evidence from other studies will be given.

Mechanical Failure of the Plasma Membrane. Steponkus et al. (1983) and Dowgert & Steponkus (1983) suggested that seeding of the intracellular solution is the result of the mechanical failure of the plasma membrane. The mechanical failure theory is consistent with the comment by Chambers & Hale (1932) that the critical temperature (T_{crt}) is the one at which the plasma membrane breaks down. The hypothesis of mechanical failure is based on Steponkus & his colleagues' extensive analysis of intracellular ice formation in nonacclimated and acclimated isolated protoplasts. A major distinction between the freezing behavior of nonacclimated and acclimated protoplasts is the temperature at which internal ice formation is observed. In nonacclimated protoplasts, internal ice formation occurs over a relatively narrow temperature range with a median -15°C, whereas in acclimated protoplasts, internal ice formation occurs over a broader temperature range with a median -42°C. Steponkus et al. (1983) and Dowgert & Steponkus (1983) have concluded that the decreased incidence of intracellular ice formation in acclimated protoplasts is due to an increase in the stability of the cell membrane, and the mechanical breakdown of the membrane should account for the difference in cytoplasmic freezing temperatures of nonacclimated and acclimated protoplasts. However, as can be seen from Fig.9.3, Steponkus and co-workers results can be explained based on our heterogeneous nucleation mechanisms catalyzed by the plasma membrane. The changes occurring in the plasma membrane during acclimation may be increasing the contact angle between the ice and the plasma membrane to shift the nucleation kinetics to lower temperatures. In addition, in

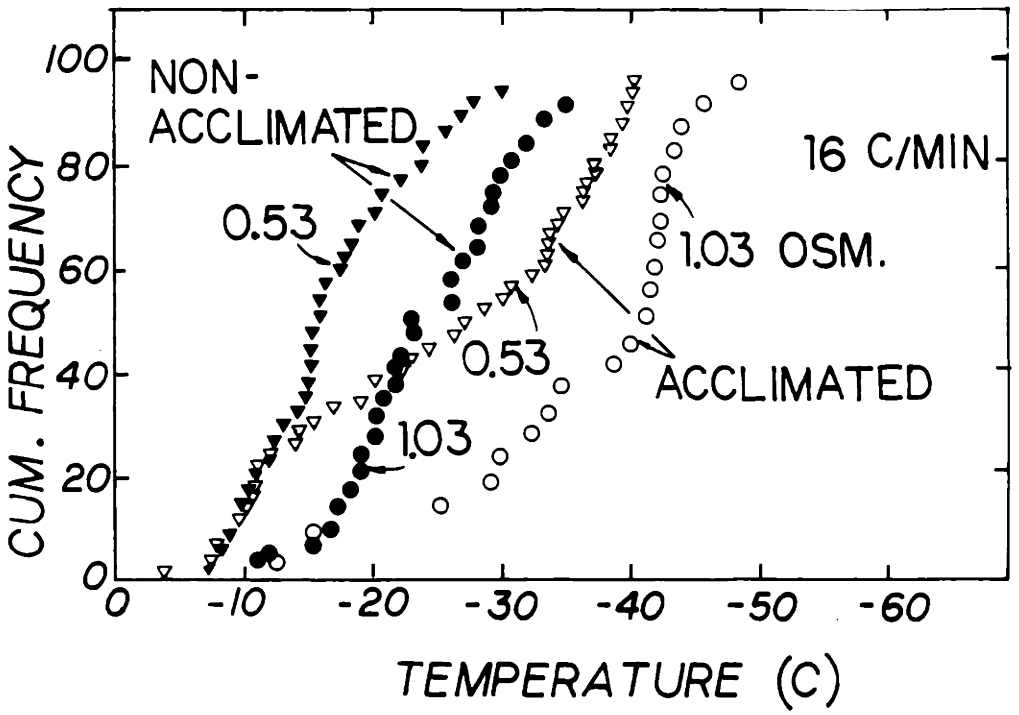

FIGURE.9.3. Cumulative frequency of intracellular ice formation as a function of the nucleation temperature for nonacclimated and acclimated protoplasts suspended in 0.53 and 1.03 osm $CaCl_2$+NaCl cooled at 16°C/min. At 16°C/min, the total number of nonacclimated protoplasts observed was n=33 for 0.53 osm, n=29 for 1.03 osm; for acclimated protoplasts, n=46 for 0.53 osm, n=25 for 1.03 osm. Isotonic solutions for nonacclimated and acclimated protoplats are 0.53 osm and 1.03 osm, respectively. (Redrawn from Dowgert & Steponkus 1983).

Fig.9.3 for acclimated protoplasts frozen in 1.03 mosm, there is a sudden increase in the nucleation kinetics at about -42°C. This is very similar to our results as shown in Fig.4.4 suggesting two distinct nucleation mechanisms for plant protoplasts as well.

Scheiwe & Korber (1982a) offered an explanation to the mechanism by which external ice may damage the cells mechanically. According to their view, at relatively high temperatures during freezing, the liquid interior of the cell allows the membrane to deform without harm. At lower temperatures, the intracellular solution becomes more viscous, consequently, deformation of the plasma membrane is hindered because of the increased work of deformation due to stiffer membrane. This may lead to some ductile fracture of the membrane so that the external ice contacts the intracellular solution. The only experimental confirmation given by these authors is their observation with mononuclear cell which nucleated at much lower temperatures than polymorphonuclear cells (Schiewe & Korber 1982a, 1982b, 1987). It is well known that PMC are very susceptible to the effects on the membrane of mechanical or osmotic forces and this difference in membrane characteristic may result in the difference observed for their freezing temperatures.

One can evaluate the mechanical failure theory using experiments with mouse oocytes from this study. First of all, the viscosity of the internal solution of the dehydrated cells (Fig.4.7 and 6.13) is much higher than non-dehydrated cells. In addition, dehydration in an electrolyte solution of NaCl would destabilize the plasma membrane due

to desorption of membrane components (Lovelock 1953a,b; McGrath 1977). Therefore, dehydrated oocytes prior to freezing (Fig.4.14) should be damaged much easier than oocytes in isotonic solutions, and consequently the freezing temperature of the cytoplasm should be higher. However, this conclusion contradicts with the experimental findings. The mean freezing temperature in 1,035 mosm is -32°C versus -12.5°C in 285 mosm. In addition, Mazur (1965) suggests that the mechanical failure of the membrane cannot account for internal ice formation because 50 to 100% of yeast cells can survive external ice formation without damage to membranes if the temperature remains above -10°C, or if cooling to lower temperatures is either slow (1°C/min) or very rapid (10^{+4}°C/min).

Recently, Tondorf et al. (1988) and Hendl et al. (1988) measured the adhesive interaction between ice-liposomes,and ice-mouse oocytes to investigate the possible importance of direct mechanical interactions between cells and ice, respectively. Significant adhesive interactions between ice and giant liposomes were observed. In contrast to giant liposomes, mouse oocytes did not show a significant adhesive interaction with external ice in isotonic conditions near 0°C suggesting that mechanical effects for mouse oocytes are negligible. Therefore, it is very unlikely that the mechanical membrane failure due to contact with external ice crystals can be the cause for the membrane damage resulting in internal ice formation, at least in mouse oocytes.

Electrical Effects. Steponkus et al. (1984b) has suggested the possible involvement of electrical transients that arises during freezing of the suspending medium resulting in membrane failure. It is important to first consider how such electrical transients arise.

Workman & Reynolds (1950) determined that the potential observed during the solidification of dilute aqueous solutions was due primarily to a preferential incorporation of one ionic species into the ice matrix. The excess of the ionic species incorporated into the ice lattice and the excess of counter-ions in the solution near the interface create an electric field in front of the interface. The electric field extends across the electric double layer in front of the interface.

The most important factor in determining the magnitude of the electrical potential produced during freezing is the velocity of the interface. At very slow interface velocities, there is enough time to reach chemical potential equilibrium by simple electrodiffusion so that the potential increase is very small. At higher rates, electrodiffusion lags behind the preferential incorporation of certain ions at the interface and as a result larger potentials are sustained. At very large rates of the interface, the potentials are smaller, probably due to the mixing currents in the solution, irregular interface geometries and incorporation of both kinds of ions.

Based on the above simplistic explanation of freezing potential, one can conceive that the plasma membrane may be damaged due to the electrical potentials in front of the ice interface as suggested by Steponkus et al. (1984b). Their result showed that freezing protoplast suspensions in 0.5M sorbitol to -10°C at rapid rates resulted in potentials of nearly 4V and survival was low (12%), whereas, during slow cooling to -4°C, no measurable potential occurred and the survival was high (60%). Based on this result, they suggested the possible contribution of electric potentials to the membrane failure leading to the formation of intracellular ice. However, neither direct cryomicroscopic observation of ice formation was done for the given experimental conditions nor the slow and rapid cooling rates were specified. Previous results by Dowgert & Steponkus (1983) showed that the mean intracellular nucleation temperature for nonacclimated protoplasts in 0.1M $CaCl_2$ + 0.15M NaCl solution was -15°C. Therefore, there is no a priori reason to believe that protoplasts in 0.5M sorbitol contained ice at rapid cooling to -10°C. It should also be kept in mind that the stage used for electrical studies (Steponkus et al. 1984b) is similar to unidirectional freezing stages (Rubinski & Ikeda 1984) and the solidification process is quite different than conventional freezing stages used in their previous studies (Dowgert & Steponkus 1983). The application of the results obtained from special purpose stages to conventional stages is questionable.

During a conventional freezing protocol, the extracellular solution is seeded at a certain undercooling (usually 2 to 3°C), external ice

grows and interface sweeps through the suspending medium. Cells are encapsulated in the ice matrix at the beginning of the cooling and there is no ice-solution interface that moves at a rapid rate during the subsequent cooling. One may suggest that there are electrical effects occurring while the interface first passes through the suspending medium and encapsulates cells at the beginning of the cooling protocol. If this is true, the external ice should enter the cell right at the beginning of the freezing protocol due to 3 reasons. First, the potential required to cause membrane breakdown increases strongly with decreased temperature (Coster and Zimmermann 1975; Zimmermann 1982). Therefore, it is more likely that the cell membrane failure can occur at higher temperatures at the start of the freezing protocol. Second, the damage kinetics is faster at higher temperatures favoring faster cell membrane breakdown at high temperatures at the beginning of external ice seeding than at lower temperatures. Third, ice is the best-known nucleator and it will grow through the membrane immediately after any damage occurs at the beginning of the freezing. There is no plausible reason to assume that the membrane is not damaged by external ice until a critical temperature (usually -5 to -15^{o}C) is reached.

Steponkus et al. (1984b) suggested the generation of a substantial electrical potential across the plasma membrane may not occur until the ice makes a close approach to the membrane at some point. However, their experimental potential recordings and recent analysis by Hubel et al. (1988) show that the freezing potential in front of the ice-solution interface would die out quickly due to electrodiffusion once the

interface comes to a stop or slows which is the case after the seeding of the external ice as discussed above. It is, therefore, very unlikely that there will be any electrical potential remaining to cause membrane breakdown when the intracellular nucleation occurs usually at -5 to -15°C. This is especially true for slow cooling rate experiments. For example, it would take more than 10 minutes to reach -12°C for oocytes cooled at 2°C/min after the start of the freezing at -1°C. This is enough time to reach equilibrium by electrodiffusion (Hubel et al. 1988).

The evidence given above indicates that the electrical component to membrane damage during freezing is probably not a major one, although some contribution to membrane damage is possible. As Steponkus et al. (1984b) suggests the role of electrical transients in intracellular ice formation can be only evaluated quantitatively if the electrical fields during freezing are characterized temporally and spatially with respect to the cell membrane.

Thermal Damage Mechanisms. Quinn (1985) proposed that lipid-phase separation of the cell membrane by cooling may cause damage to the membrane due to a series of phase transitions occurring in the membrane as a function of temperature. He also demonstrated that the damage does not occur until cells are reheated which excludes the possibility that gel transformations of the membrane can cause membrane failure resulting in intracellular ice formation. In addition, McGrath (1987) presented a

model that describes the mechanical failure of the plasma membrane due to thermal stresses resulting in lytic membrane tensions. He suggested that this type of damage may be important in cold shock. However, if thermal effects are a major factor in the formation of intracellular ice, internal ice should occur regardless of whether or not the suspension contains ice.

Thom & Matthes (1988) and Thom (1988) presented an experimental method to measure the mechanical deformability of red blood cell membranes as a function of temperature to measure the viscoelastic changes occurring in the cell membrane during cooling. Their results show a rapid increase with elestic modulus of the cell membrane with decreasing temperature. According to their measurements, red blood cell membrane cannot withstand deformations below -10^{o}C because it becomes nearly brittle. They suggest that small volume changes induce very high forces to the membrane resulting in the breakdown of a brittle membrane. They used electrical field force (up to 2,000 V/cm) to stretch cells at low temperatures to obtain their stress strain relation as a function of temperature. The author has reservations about this approach since externally applied electrical fields would destabilize the cell membrane and effect their viscoelastic properties, especially if the field strength is as high as 2,000 V/cm used in some of their experiments (Corda et al. 1982; Zimmermann 1982; Kotyk et al. 1988). In addition, they did not observe any effect of cryoprotectants to the stress-strain relation of the plasma membrane. Substitution of glycerol (2 M) had no influence on the mechanical behavior. Strong dependence of internal ice

nucleation temperature on cryoprotectant concentration is well-documented (Rall et al. 1983). Therefore, their results contradict with their conclusion.

9.4. Intracellular Ice Formation Caused by Internal Nucleators

Toscano et al. (1975) suggested that an alternative for internal freezing of cells might be the nucleators inside the undercooled cytoplasm triggering the nucleation of intracellular ice, although they did not rule out the possibility of external ice triggering the internal ice formation. Extensive study of red blood cells and hemoglobin in suspensions by Franks and co-workers (Franks et al. 1983; Mathias et al. 1984) showed that red blood cells nucleate at a temperature 0.5°C above the nucleation temperature of the suspending medium (approximately -40°C) in the absence of external ice. In addition, the nucleation temperature of aqueous hemoglobin, isolated from red blood cells, is substantially lower than that of water or the intact cytoplasm. Therefore, neither whole red blood cells nor suggested proteins, namely hemoglobin, can nucleate undercooled water between -5 to -15°C (Toscano et al. 1975). These nucleators are only effective at significantly lower temperatures than observed intracellular freezing temperatures in the presence of external ice. Hence, it continues to appear more likely that the seeding agent for the freezing of cytoplasm is the external ice by itself per se.

9.5. Conclusion

Various mechanisms of intracellular ice formation in biological cells are discussed. There is basically no quantitative theory at this point to predict the probability of ice formation in cells during a freezing protocol. It is also very interesting that membrane failure hypotheses never considered the possibility of ionic effects. As shown in Chapter V, the trans-membrane potential may be hyperpolarized due to transient ionic fluxes. It is very likely that the ionic effects can cause more hyperpolarization of the membrane potential than electrical transients. In addition, ionic effects are a function of the two-phase equilibrium diagram of the suspending medium. Therefore, they are more or less the same for results reported from different laboratories with different experimental techniques and equipments. On the other hand, electrical transients are function of the external variables such freezing stage design, temperature gradients, interface kinetics, etc. If one keeps in mind that there is a universality to the reported results, it may be more meaningful to correlate membrane failure with an equilibrium condition rather than very specific conditions. The investigation of ionic effcets should definetely be considered as the possible cause of membrane failure in the context of 'membrane failure' hypotheses of internal ice nucleation.

It is clear from the above discussion that there is extensive evidence against the 'pore', 'membrane failure', and 'internal

nucleators' mechanisms that are proposed as possible means of initiating internal freezing in biological cells. We remain convinced that intracellular ice formation, under conditions considered here, can be explained satisfactorily by our theory of two distinct heterogeneous nucleation mechanisms. Ionic, mechanical, electrical, and thermal effects due to the presence of external ice during freezing may all alter the plasma membrane to make it a good ice nucleator as discussed in the previous two chapters. Ionic effects seem to play a major role in internal ice formation, however, which consequence(s) of external ice is responsible for membrane alteration and internal ice formation will depend largely on the type of cell itself.

CHAPTER X

DISCUSSION & CONCLUSIONS

Overview

Theoretical and experimental analyses of intracellular ice nucleation in unprotected mouse oocytes revealed that there are two distinct mechanisms responsible for intracellular ice formation. Both of the mechanisms are heterogeneously catalyzed, however, the active nucleators are different. Depending on freezing conditions, the plasma membrane and/or supramolecular structures are effective in initiating the ice formation intracellularly. The two distinct nucleation mechanisms are called 'plasma membrane catalyzed' nucleation and 'particle catalyzed' nucleation depending on whether the active nucleator is the plasma membrane or supramolecular structures. Plasma membrane catalyzed nucleation is characterized by the contact angle between the ice-plasma membrane and particle catalyzed nucleation is described by the contact angle between the ice-particle and the radius of the particle as it should be expected from heterogeneous nucleation theory.

Plasma membrane catalyzed nucleation is active under usual freezing conditions (usually between -5 to -20°C) in isotonic solutions, whereas particle catalyzed nucleation is encountered at temperatures close to homogeneous nucleation temperature (usually between -30 to -40°C). Therefore, in most of the practical cases, cells nucleate by plasma membrane catalyzed nucleation before reaching the temperature range at which particle catalyzed nucleation is active. However, certain conditions, such as the absence of external ice or prefreeze dehydration, may depress the kinetics of plasma membrane catalyzed nucleation and particle catalyzed nucleation can be observed.

It is suggested that the external ice plays a major role in plasma membrane catalyzed nucleation. It is the effect of the external ice on the plasma membrane that makes the cell membrane a good ice nucleator. The presence of external ice was shown to have ionic, mechanical, electrical, and thermal effects on the plasma membrane. Especially the ionic effects are thought to alter the plasma membrane to render it an energetically favorable ice nucleator.

The theoretical nucleation model combines the plasma membrane and particle catalyzed nucleations. In addition, the model is coupled with the water transport model to predict the thermodynamic state of the cell cytoplasm. The cumulative incidence of internal ice formation for a given protocol can be estimated by solving the coupled water transport and ice nucleation models.

The analytical solution of the theoretical model requires the knowledge of certain biophysical parameters. These parameters are: (1) water permeability of the plasma membrane, L_{pg}; (2) activation energy of the water permeability, E_{Lp}; (3) preexponential nucleation factors (kinetic coefficients), Ω^{I}_{o} and Ω^{II}_{o} and (4) exponential factors (thermodynamic coefficients), κ^{I}_{o} and κ^{II}_{o}. Determination of these parameters require an extensive experimental analysis with precise temperature control.

Experimental Techniques

There are two important experimental issues that must be satisfied in order to analyze the ice nucleation kinetics in biological cells. First, the number of cells should be enough for reliable statistics and the viability tests should be accurate. Second, thermal gradients in the freezing stage should be minimized. The first requirement is achieved by using mouse oocytes. The second one is satisfied by a new isothermal stage design incorporating a sapphire plate onto the freezing stage. A discussion of these issues follow.

Mouse oocytes at metaphase II from hybrid (B6D2F1) mice were used for permeability and nucleation kinetics experiments. There were several advantages of using mouse oocytes: (1) in vitro fertilization of

eggs from inbred mice is a reliable viability test; (2) 20 to 30 eggs can be obtained from one animal; (3) their large size allows easier detection of internal ice formation; (4) a large number of freezing data is already accumulated on mouse oocytes.

In order to be able to use oocytes at metaphase II, it was necessary to determine the functionality of the eggs prior to experiments by in vitro fertilization. The overall fertilization rate was determined to be 90% (715/796) and the subsequent growth to blastocyst stage was 82% (583/715). A series of control experiments were performed to optimize in vitro fertilization conditions. The use of hyaluronidase to remove the cumulus mass may have adverse effects on the plasma membrane if not used appropriately. Our treatment with hyaluronidase had no statistically significant effect on fertilization and subsequent growth rates. The fertilization rate for hyaluronidase treated oocytes was 82% (302/368) and growth to blastocyst was 83% (250/301). It was concluded that oocytes were free of damage after treatment with hyaluronidase. There has also been some concern about the cold sensitivity of oocytes (Gracia et al. 1986), however very recent results with hybrid mice reports no effect of cold treatment at 15^{o}C on the viability of oocytes (Jackson & Kiessling 1988). We have also tested the effect of cooling oocytes to 0^{o}C before insemination. Cooling oocytes to 0^{o}C for 0, 15, 30, 60 or 150 minutes resulted in fertilization rates of 75%, 94%, 86%, 81%, and 87%, respectively, and blastocyst formation rates of 92%, 90%, 92%, 86%, and 85% for the 0, 15, 30 or 60 minute exposed groups,

respectively. There was also no indication of parthenogenic activation due to cold shock since oocytes cooled to 0°C for 0, 60 or 150 minutes and subsequently cultured without insemination cleaved to 2-cell stage at rates of 4%, 3% and 0%, respectively. These result confirm that oocytes are viable prior to experiments.

An 'isothermal' freezing stage was designed to minimize errors introduced by thermal gradients. This is an important forward step in experimental analysis of the ice formation in biological cells. Sapphire was employed to reduce gradients of the heating window. We have investigated the effect of sapphire thickness on the maximum thermal gradients across the window and have found 0.025 inch (0.64 mm) to be a good compromise between the competing requirements of reduced gradients and rapid thermal response. With the coolant stream temperature and flow rate adequately set, sample cooling rates of several hundred °C per minute have been achieved for temperatures as low as -60°C. Measured gradients for these flow conditions were in the range of 0.1°C per 10 millimeter at sample temperatures near 0°C.

Water Transport During Freezing

A model for the dehydration of unprotected cells subjected to freezing was presented in this study. The permeability at 0°C, L_{pg}, and the activation energy, E_{Lp}, of unfertilized mouse ova were determined

simultaneously by fitting experimentally measured volumes of ova to theoretically predicted volume/temperature curves using non-linear regression analysis. The mean value and standard deviation of L_{pg} were found to be 0.044 and 0.008 μm/min-atm and the mean value and standard deviation of E_{Lp} were found to be 13.3 and 2.5 kcal/mol. These results agree closely with Leibo's (1981) results obtained from suprazero temperature permeability experiments.

Results of this study indicate that there are a great deal of individual variations in permeability parameters. A distributed parameter approach was presented to model the probabilistic nature of permeability parameters. The properties whose distributions were required in analyzing water transport were surface area-to-volume, reference permeability and activation energy. The probability density functions of these properties were combined with the water transport model to predict the distribution of cell volume change as a function of temperature for a given cooling rate. Analysis has shown that the volume distribution becomes spread out at slow cooling rates due to the distributed biophysical parameters. Results agree well with the observed experimental volume curves. A very important conclusion of this analysis is that any study of ice nucleation at slow cooling rates will have a large experimental discrepancy because it is coupled with the distributed behavior of oocytes during freezing. However, at rapid rates, there will be no time for water transport and oocytes will remain constant at their initial volume (i.e. diameter). Since the initial

diameter distribution is narrow (79.1±4 μm), the undesired effects of the distributed response can be minimized. This analysis led to the conclusion that ice nucleation experiments should be performed at rapid rates to impede water transport and consequently distributed behavior. This should increase accuracy and reliability of ice nucleation experiments. Computer simulations suggest that there is only 8% and 3% water loss when oocytes cooled to -20°C at 40 and 120°C/min, respectively (Fig.5.3). It is decided to use 120°C/min for ice nucleation experiments to minimize the effect of water transport on the ice nucleation kinetics.

Theory of Intracellular Ice Nucleation During Freezing

The heterogeneous nucleation theory was modified to accommodate simultaneous temperature, volume and concentration changes occurring during freezing of biological cells. Many assumptions and approximations were used in the derivation of nucleation equations. This section contains a discussion of the critical assumptions and approximations.

The interface between the cluster (phase β) and solution (phase α) was treated as a conceptual 'dividing surface' of zero volume as proposed by Gibbs (1961) and interfacial free energy, σ, was assumed to be independent of size. The independence of interfacial free energy on

cluster size has been examined critically by many investigators and various theoretical relations for radius dependence of σ are suggested (Tolman 1949; Buff & Kirkwood 1950; Cahn & Hilliard 1958; Rasmussen et al. 1983; Jayaraman et al. 1986). The size dependence effect was determined to be significant for clusters containing less than 120 water molecules (see Fig.6.5). In the case of freezing oocytes, it was determined that the critical cluster contained approximately 1,000 water molecules at -20°C in 285 mosm PBS+BSA solution for a cooling rate of 120°C/min (Fig.6.6). For higher initial suspending solution concentrations, the critical cluster was larger. Therefore, the assumption of size independent interfacial free energy was justified for the system under study so that the ice nucleation in oocytes could be treated adequately in the framework of Gibb's thermodynamics.

In the preexponential term in Eq.(6.99), it is assumed that the number of water molecules in contact with the plasma membrane varies with the surface area of the oocyte when oocytes are dehydrated in hypertonic solutions prior to freezing. This assumption may introduce large errors if the internal milieu cannot be considered dilute for dehydrated oocytes. There are approximately 1.1×10^{-8} moles of water and 6×10^{-11} moles of solute in the cytoplasm. When oocytes are exposed to 1,035 mosm, the water content is decreased to 0.55×10^{-8} while the solute content remains the same. The number of moles of solutes for dehydrated oocytes is still very small compared to the number of moles of water, therefore, the cytoplasm can be considered dilute on a molar basis.

Although the cytoplasm of dehydrated oocytes can be treated as dilute on a molar basis, it is not dilute on a volume basis. Since transport processes are considered on a volume basis, they should be treated accordingly. Therefore, it is important to include dehydration effects in the calculation of activation energy for molecular transport. Based on Eyring's treatment of rate processes (Eyring 1935; Glasstone et al. 1941), the activation energy for molecular transport can be expressed as a function of the solution's viscosity by Eq.(6.76). The viscosity of cytoplasm can be estimated from the solute volume fraction assuming that the cytoplasm is a well mixed solution containing various ions and macromolecules. This kind of description of the cytoplasm is referred as the 'solution description.' The other extreme for cytoplasm modelling is the 'organized description' in which all the solutes and macromolecules are associated with cellular ultrastructures (Clegg 1984; Keith 1979). Aqueous compartments in between cellular ultrastructures are assumed to be pure water. According to the 'organized description' of the cytoplasm, the viscosity of the solution does not change with dehydration. Further experimental work is necessary to prove the validity of the 'organized description.' In this study, we preferred to use the conventional 'solution description' of the cytoplasm. The concentration (i.e. dehydration) dependence of the cytoplasm was obtained in a similar manner to the concentration of solutions containing suspension of rigid particles in a continuum as given by Eq.(6.79).

The viscosity of the intracellular milieu was also assumed to have the same temperature dependence as pure water. A power law temperature dependence of viscosity was used based on recent mode-coupling theories (Bengtzelius et al. 1984; Angell 1988). The agreement between experimental data available in the range of 0 to -20°C and theoretical formula (Eq.(6.89)) is satisfactory as shown in Fig.6.15.

The thermodynamic driving force for crystallization was calculated using recent experimental data for heat capacities of both ice and water. A new relation (Eq.6.94) was suggested and compared to other simpler relations. The error between this new relation and Hoffman's (1958) relation was shown to be less than 2%. Therefore, it was decided to use Hoffman's equation due to its simplicity. (Eq.(6.96)).

The experimentally observed variable is the probability of internal ice formation. Nucleation frequency is not amenable to direct experimental measurements. Therefore, it was necessary to relate the experimentally determined probability of the nucleation to nucleation frequency. It has been shown that the probability of nucleation could be related to the nucleation rate as given in Eqs.(6.110) and (6.111) based on the assumption that each cell has the same active nucleators with identical properties. The possible effects of individual behavior of cells was ignored due to lack of evidence from simpler systems such as the freezing of droplets.

The ice nucleation parameters, namely Ω_o and κ_o, were determined from experimental observations of the incidence of internal ice formation. This was done using the non-linear regression analysis to correlate theoretical ice nucleation model with experimental data. The results of such calculations are discussed in the next sections.

Plasma Membrane Catalyzed Intracellular Ice Nucleation

It has been speculated in this study that the internal ice formation in the presence of extracellular ice was catalyzed heterogeneously by the plasma membrane via the effects of the external ice. Ice nucleation experiments at a cooling rate of 120°C/min in 285 mosm PBS+BSA solutions can be used to determine the ice nucleation coefficients. Experiments showed that the fraction of oocytes with internal ice increased from 5% at -8°C to 95% at -18°C when oocytes cooled at 120°C/min in isotonic saline. Correlation of the theory with the experimental kinetics of fraction of oocytes frozen internally revealed the following ice nucleation parameters:

$$\begin{aligned} \Omega_o^I &= 3.56 \times 10^{+9} \quad (1/m^2\text{-s}) \\ \kappa_o^I &= 4.60 \times 10^{+8} \quad (K^5) \end{aligned} \tag{10.1}$$

where I refers to plasma membrane catalyzed nucleation. The contact angle between ice-plasma membrane from the exponential coefficient was

determined to be 35^{o}. The value of $f(\theta)$ was approximately 0.0228 as calculated from Eq.(6.68). This suggests that the free energy of formation for heterogeneous nucleation was decreased by a factor $f(\theta)$ compared to the free energy of formation for homogeneous nucleation. The contact angle in the absence of external ice is not known for mouse oocytes, however, it must be larger than 35^{o} since oocytes do not form internal ice in the absence of external ice. Therefore, the presence of external ice must be altering the plasma membrane in such a way that the cell membrane becomes an energetically favorable catalytic site for ice nucleation.

Since membranes are very dynamic structures responding to external perturbations, it has been proposed that the contact angle may be altered by ionic (hyperpolarization), electrical (hyperpolarization), mechanical (adhesion to ice, squeezing) and thermal (phase transition, viscoelasticity) effects of the external ice. The last three effects were analyzed in Chapter IV in the context of 'membrane failure' theories of internal ice formation. It has been shown that none of these four effects is enough to cause membrane failure, although they may alter the membrane. In addition, ionic effects were discussed in detail in Chapter V. The analysis of transient ionic fluxes due to the increased external ionic concentrations with the formation of extracellular ice has shown that the membrane was hyperpolarized from -15 mV at $0^{o}C$ to -80 mV at $-8^{o}C$ (Fig.5.8). It is suggested that many consequences of hyperpolarization such as increased membrane fluidity

and hydrophobicity, change in membrane surface potential and charge, and orientation polarization of proteins and lipids may account for the decreased θ in the presence of external ice.

Orientation polarization effects were calculated based on the Langevin factor. Results have shown that the fraction of integral membrane proteins with a dipole of 300 debye aligned with the electrical field increased from 16% prior to external ice formation at 0°C to 60% in the presence of external ice formation at -8°C. It is proposed that this degree of orientation of proteins and lipids may alter the hydrophobicity of the cell membrane due to the electrostatic effects on water molecules. These speculations are not unreasonable, however, they do not prove unequivocally the reason why θ decreased in the presence of external ice.

The 'membrane failure' hypotheses of internal ice formation considers mechanical, electrical, and thermal effects. Ionic effects are somehow ignored. Our analysis showed that ionic effects are most likely to be much more stronger than mechanical, electrical and thermal effects. To the best of this author's knowledge, this is the first time the possibility of the involvement of ionic effects in membrane failure is discussed in the context of intracellular ice formation.

The contact angle is a function of the interfacial energies between solution-membrane, solution-ice, and ice-membrane. For a complex

process such as freezing which involves simultaneous variations in temperature and concentration, the contact angle would not remain constant. Unfortunately, there are no means to estimate analytically the variation in contact angle during freezing. Instead, an experimental approach has been followed to determine the change in θ with dehydration. Oocytes were cooled at 120°C/min in the presence of external ice in different anisotonic solutions. The kinetics of internal ice nucleation dramatically slowed down with increasing concentration. The fraction of oocytes with internal ice was 50% at approximately -9, -12.5, -17, -26, -30, and -32.5°C in 200, 285, 510, 735, 820, and 1,035 mosm PBS+BSA solutions. An increase from 32° in 200 mosm to 47° in 1,035 mosm was enough to explain the depression in the kinetics of nucleation in hypertonic solutions. An empirical relationship for θ was determined from these experiments. It is suggested that the change in θ may be due to decreased surface tension of the cell membrane and/or decreased hyperpolarization during freezing in hypertonic solutions. However, this could not be proven from the present experiments. The agreement between theory and experiments is excellent using the empirical relationship for θ.

Particle Catalyzed Nucleation

An increase in the kinetics of intracellular ice nucleation was observed at approximately -31°C when oocytes are frozen in concentrations higher than 735 mosm. It is suggested that this shift in

nucleation kinetics is due to a change in the mechanism of nucleation. It is proposed that the rapid nucleation kinetics below -31°C was catalyzed by supramolecular particles within oocytes instead of the plasma membrane. The evidence supporting this proposal can be summarized as follows.

(1) The mechanism of rapid nucleation within cells below -31°C is assumed to be heterogeneous because the nucleation temperature (between -31 to -34°C) is always higher than the estimated homogeneous nucleation temperature of a saline droplet which has the same size and concentration as an oocyte (between -35.5 to -37.12°C). (2) In addition, the ice nucleation parameters are found to be

$$\begin{aligned} \Omega_o^{II} &= 1.84 \times 10^{+50} \quad (1/m^2\text{-s}) \\ \kappa_o^{II} &= 1.08 \times 10^{+12} \quad (K^5) \end{aligned} \tag{10.2}$$

where II refers to 'particle catalyzed' nucleation. Because the value of the preexponential factor is smaller than the estimated homogeneous nucleation factor, the heterogeneous nucleation is assumed to be most probable mechanism. (3) The values of the parameters correlated well with Franks et al.'s (1983) results on undercooled cells that favor supramolecular particle catalyzed nucleation. (4) Further insight to the mechanism of nucleation has been obtained by predicting the radius (R) of the catalytic particle and the contact angle (θ). Upper and lower limits for R and θ were found to be

$$15^0 < \theta < 80^o$$
$$10^{-7} < R < 4 \times 10^{-7} \quad (cm) \qquad (10.3)$$

These ranges of R and θ are reasonable for biological cells, however, the exact supramolecular particle could not be determined just based on these numbers.

Combined Nucleation Mechanism

The cumulative fraction of oocytes with intracellular ice during a freezing protocol was determined by combining plasma and particle catalyzed nucleation mechanisms (Eq.7.5). The combined mechanism was verified with freezing experiments in anisotonic solutions at 120°C/min. Excellent correlation between theory and experiments was obtained (Figs.7.6 and 7.7). Freezing experiments at slow rates and at constant temperatures have been used for further correlation of the theory with experiments.

Cooling rates between 2°C/min to 120°C/min were used to determine the kinetics of intracellular ice formation. Both theoretical and experimental results showed similar dependence of the nucleation kinetics as a function of the cooling rate. However, the kinetics of the theoretical predictions did not match exactly with the experimental results (Fig.8.1). Experimental uncertainties, cell-to-cell variations, concentration polarization effects, and simplifying assumptions in the model are proposed to account for the discrepancy.

The incidence of internal ice formation as a function of the cooling rate showed a sharp demarcation zone (Fig.8.2). The number of oocytes containing internal ice increased from 0% at 1°C/min to 100% at 5°C/min as predicted from both experiments and theory. The agreement for intermediate rates was satisfactory as well.

One of the most universally established experimental result in cryomicroscopy is the insensitivity of the mean intracellular nucleation temperature to the cooling rate. For a wide range of cooling rates, cells of various types have demonstrated a critical temperature at which they form internal ice irrespective of their undercooling, water content, and concentration. This critical temperature is used as a biophysical parameter at which external ice grows into cells either through pores or damaged membrane (Mazur 1965, Steponkus et al. 1983). Therefore, any proposed mechanism of ice nucleation within cells must be consistent with this experimental finding. The temperature at which fifty percent of oocytes contained ice as a function of cooling rate was determined to be approximately -12.5°C±1.7°C and -9.7±1.1°C for mouse oocytes from experiments and theory, respectively (Fig.8.3). Due to the complex mass and heat transfer processes occurring during freezing, the heterogeneous nucleation theory predicts that TF_{50} is insensitive to cooling rate. The author believes that this is one of the most critical tests to evaluate the validity of the theory proposed. An unresolved dilemma since the beginning of modern cryomicroscopy (Diller & Cravalho

1970) is quantitatively predicted using the kinetics model developed in this study.

Although, the theoretical prediction revealed an average of -9.7°C for TF_{50}, the theoretical prediction had a peculiar form quite different than a constant line. At cooling rates between 3.5 to 120°C/min, TF_{50} decreased slightly by increasing the cooling rate. At low cooling rates between 1 to 3.5°C/min, there was a minimum at approximately 1.8°C/min. The minimum TF_{50} was -9.2°C at 1.8°C/min and increased to -7.9°C and -8.5°C for both lower and higher cooling rates, respectively. The range of cooling rates at the observed minimum corresponded to the demarcation zone for the fraction of oocytes with internal ice increasing from 0% to 100%. Interestingly enough, the minimum temperature seen in most of the experimental studies (Schiewe & Korber 1983; schiewe & Korber 1988; Shabana & McGrath 1988) corresponds to the demarcation zone of cooling rates (Fig.1.2). However, the number of cells used in these studies were not large enough to draw any further quantitative conclusions.

Experiments at constant temperatures in isotonic solutions have been correlated with theoretical predictions. The qualitative agreement of the kinetics of nucleation is good, however, the quantitative theory does not match with the experiments (Fig.8.4). Both theory and experiments displayed an increase in the incidence of intracellular ice formation with time exposure to external ice. The correlation of the theory was shown to be excellent (Fig.8.5) when the incidence of

intracellular ice nucleation was plotted as a function of temperature after reaching steady-state (i.e. no more oocytes nucleated as a function of time at a given temperature.) The incidence of internal ice formation increased from 0% to 100% when the temperature was decreased approximately from -3.5°C and -4°C to -10°C and -8°C as observed form experiments and theory, respectively.

An overall analysis of the data and theory showed a satisfactory correlation based on the discussion above. Further test of the theory was performed by optimizing a two-step freezing protocol. The two-step cooling protocol in 1,035 mosm had an initial cooling period at 120°C/min after seeding of the external ice to an intermediate temperature at which a holding period was used to dehydrate oocytes. The holding period was followed with a second cooling period at 120°C/min down to -50°C. The intermediate holding temperature and time as determined from the analytical model was -15°C and 5 minutes to yield an overall of 8% intracellular ice formation, respectively. Forty oocytes were frozen following the two-step protocol (Fig.8.6). Ten of these oocytes formed intracellular ice when frozen to -50°C yielding a 25% intracellular nucleation compared to 8% from the theoretical prediction. Twenty-four of the 30 oocytes (80%) without internal ice formation was morphologically normal after thawing. To the best of the author's knowledge, this is the first time in literature oocytes could be frozen down to -50°C and brought back to 25°C in less than 5 minutes with 60% (24/40) overall viability. There is no reliable technology

today for oocyte freezing. However, the available ones take 3 to 4 hours freezing time at rates ranging from 0.35 to 1°C/min in various cryoprotectants (1.5 to 2 M). Since, the objective of this study has been to analyze the kinetics of ice nucleation we have not attempted to optimize our freezing technique to be able to obtain viable oocytes.

The effect of extracellular undercooling at the beginning of the freezing has demonstrated a dramatic effect on the incidence of intracellular nucleation. A drastic increase in the fraction of cells with internal ice was observed when increasing the external undercoolings prior to the seeding of the external solution (Diller, 1975; Diller 1979; Cosman 1983; Schwartz & Diller 1984). Analytical predictions using the theoretical model proposed in this study showed similar dependence of the incidence of oocytes with internal ice on the external undercoolings (Fig.8.10). The fraction of oocytes with internal ice was determined to be 18, 60, and 100% for external undercoolings of 0, 3, and 6°C, respectively. No experiments were conducted to verify these analytical predictions.

Critique of Existing Mechanisms of Intracellular Ice Formation

The existing hypotheses of internal ice formation are discussed in the context of our heterogeneous nucleation theory.

Mazur's (1965) suggestion of external ice penetrating through pores (3 to 8 A !) across the plasma membrane ('pore theory') has been tested against experimental results from this study. According to the pore theory, there is a critical temperature, T_{crt}, below which external ice can go through the pores. It has been revealed that pore theory could not account for the following experimental observations:

- the difference in T_{crt} from constant cooling rate and constant temperature experiments: T_{crt} from constant cooling rate experiments were found to be roughly -12.5°C (Fig.8.3), whereas T_{crt} from constant temperature experiments were determined to be -7°C (Fig.8.5).

- depression of the mean nucleation temperature in hypertonic solutions: T_{crt} depressed from -12.5°C when suspended in 285 mosm to -32.9°C when suspended in 1,035 mosm (Fig.7.7).

- kinetics of ice nucleation: T_{crt} is treated as a biophysical parameter at which all cells nucleate, the kinetics of the ice nucleation is completely ignored in pore theory.

An alternative theory to pore theory is the penetration of the external ice inside cells through damaged plasma membrane. At critical temperatures, the cell membrane breakdowns and is no longer able to act as a barrier to external ice resulting in nucleation of internal contents. There have been suggestions in the cryobiology literature that mechanical, electrical and thermal effects of freezing may cause

the cell membrane to fail.

The mechanical damage hypothesis was shown as unable to explain results with mouse oocytes in hypertonic solutions. In addition, it has been discussed that Steponkus et al.'s (1983) results with nonacclimated and acclimated protoplasts can be adequately explained using the theory proposed in this study. According to our point of view, cold acclimation alters the surface and physical characteristics of the cell membrane which makes it a poor ice nucleator, and depresses the internal ice nucleation kinetics. Extensive experimental evidence on changes occurring during acclimation of the cell membrane for plant protoplasts are already shown by Steponkus et al. (1983). The dramatic alteration in the internal ice nucleation characteristics of acclimated cells has been a long-standing unresolved issue in the science of cryobiology. Now, we propose a new interpretation of the results, further experimentation can only verify the hypothesis.

A definite statement with respect to the contribution of electrical effects could not be made, however, enough theoretical and experimental evidence are shown that electrical transients cannot cause membrane failure at the observed temperature range (usually -5 to -15^{o}C) during freezing:

- ice-solution interface grows fast enough to produce electrical transients only at the beginning of the freezing protocol after the seeding of the external ice (Steponkus et al. 1984; Hubel et al. 1988).

- the membrane breakdown voltage is increased with decreased temperature (Coster & Zimmermann 1975; Zimmermann 1982).

- the relaxation of the electrical transients is very rapid (Steponkus et al. 1984; hubel et al. 1988).

- the relaxation time for possible pores opened in the membrane is very rapid (Zimmermann 1982; Weaver et al. 1986).

In addition, it is shown that ionic effects are much more important than electrical transients. The trans-membrane potential of mouse oocytes is estimated to hyperpolarize from approximately -15 mV at $0^{o}C$ prior to freezing to -80 mV at $-8^{o}C$ after the formation of external ice. This is the first time that ionic effects are discussed as a possible means of altering or damaging the cell membrane during freezing.

The discussion of thermal effects during freezing cannot cause membrane failure to cause internal ice formation was also presented. If thermal effects are a major factor in the formation of internal ice, internal ice should occur regardless of whether or not the suspension contains ice.

Toscano et al.'s (1975) proposal that the formation of internal ice (between -5 to $-15^{o}C$) catalyzed heterogeneously by internal nucleators in red blood cells (RBC) in the presence of external ice is assumed to be insufficient based on Franks et al.'s (1983) recent undercooling experiments with RBC. Frank's et al. (1983) has shown that neither

whole RBC nor hemoglobin (only internal structure in RBC) could nucleate undercooled water between -5 to -15°C.

Based on the above discussion, it is suggested that there is extensive evidence against the 'pore', 'membrane failure', and 'internal nucleators' mechanisms that have been proposed to explain the formation of internal ice in biological cells.

Outlook

It was the purpose of this study to analyze quantitatively intracellular ice formation using cryomicroscopy. A mechanism of intracellular ice formation is described based on the heterogeneous nucleation theory. The mathematical formulation of the intracellular ice nucleation using heterogeneous nucleation theory leads to a theoretical model which is shown to correlate favorably with experimental observations. For the first time in the literature, incidence of intracellular ice formation could be predicted based on a theoretical model. The model is not without its own limitations. Further quantitative knowledge of what happens to the cell membrane as a consequence of the presence of external ice will lead to better understanding of the mechanisms of intracellular ice nucleation and modifications of the theory. A better knowledge of the complex ionic, electrical, mechanical, thermal changes occurring during freezing of

biological cells with a strong emphasis on the biology of cell membranes is fundamental to the study of ice formation within cells.

Suggestion for Future Research

Future research to contribute to the understanding of the mechanism of intracellular ice formation can be made in experimental and theoretical areas.

Experimental advancements can be focused on either applied or basic aspects of the intracellular ice formation. Applied research can be done to design optimum freezing protocols for mouse oocytes based on the data obtained in this study. Improvement of the freezing stage is an essential part of this research so that the oocytes can be recovered from the freezing stage after a freeze-thaw protocol. In the basic aspects, experimental setups can be developed to investigate the effects of external ice on artificial membranes and liposomes. Application of this theory to non-acclimated and acclimated protoplasts may be an important test to verify the validity of the proposed theory.

Theoretical model of ice nucleation inside cells can also be improved. Some of the simplifying assumptions in the derivation of the equations can be reconsidered. Theoretical models of the effects of the external on the plasma membrane is another possible area of research to ameliore the theory proposed in this study.

APPENDIX A

CALCULATION OF THE SALT+PROTEIN VOLUME FRACTION

1) Calculate the solute moles of hydrated pseudo-binary water-salt-protein mixture inside the mouse eggs, n_s,

$$v_s n_s = \pi_i^o V_c(1 - V_b) \rho_w = 6\times10^{-11} \text{ moles}$$

(v_s = 2, dissociation constant; π_i^o = 285 mosm/lt H_2O, isotonic osmolality;; $V_c = \pi D^3/6$ (m^3), initial cell volume; ρ_w = 1000 kg/m^3, density of water).

2) Calculate the moles of protein in the egg, n_p,

$$n_p = m_{DRY} / mw_p = 0.71\times10^{-12} \text{ moles}$$

(m_{DRY} = 31.97 mμg, total dry mass of the egg (Abramczuk and Sawicki, 1974); mw_p ~ 45,000, molecular weight of proteins (Adair and Adair, 1938; Edsall, 1953).

3) Calculate the number of moles of a fictititious solution species, n_m, present within the cell

$$n_m = n_p + v_s n_s = 6.07 \times 10^{-11} \text{ moles.}$$

4) Calculated hydrated apparent molar volume of salts in the egg, v_s^h,

$$v_s^h = v_s + v_w = v_{KCl} + v_w = 45.5 \text{ cm}^3/\text{mol}$$

(v_s = 27.5 cm^3/mol, unhydrated molar volume of salts (i.e. KCl since [KCl] >> [NaCl], Powers and Tupper, 1975; Biggers et al., 1977); v_w = 28 cm^3/mol, molar volume of water).

5) Calculate hydrated apparent molar volume of the egg interior based on a weighted average of the values for protein and salt, v_m^h,

$$v_m^h = (n_s v_s^h + n_p v_p^h) / n_m = 841 \text{ cm}^3/\text{mol}$$

($v_p^h = 7 \times 10^4$ cm^3/mol, hydrated apparent molar volume of proteins (Levin, 1976a)).

6) Calculate the hydration number for proteins, h_p,

$$h_p = (mw/mp)\ (\rho_p/\rho_w)\ (v_p/v_w) = 1{,}515 \text{ mol } H_2O/\text{mol protein}$$

((mw/mp) = 0.4 gH_2O/g protein (Adair and Adair, 1938), gram water per gram protein; ρ

ρ_p = 1.4 , protein density, $v_p = 5 \times 10^4$, unhydrated molar volume of

proteins (Adair and Adair, 1938)).

7) Calculate the average hydration number for salt-protein, h_m,

$$h_m = (h_s n_s + h_p n_p)/ n_m = 18.21 \text{ mol } H_2O/\text{mol protein}$$

8) Calculate the total water mass within the egg, mw,

$$mw = mp\ (1 - r)/r$$

(r = 0.15, dry mass as ratio of wet mass (Loewenstein and Cohen, 1964; Abramczuk and Sawicki, 1974)).

9) Calculate the total number of bound water molecules, n_w^B, within the egg

$$n_w^B = h_m n_m = 0.1\text{x}10^{-8} \text{ moles}$$

10) Calculate the total water moles within the cell, n_w,

$$n_w = mw/(\rho_w \upsilon_w) \simeq 1.1\text{x}10^{-8} \text{ moles}$$

11) Calculate the total number of free water molecules, n_w^F,

$$n_w^F = n_w - n_w^B \simeq 1.00\text{x}10^{-8} \text{ moles}$$

12) Find the solute volume fraction, ϕ_m,

$$\phi_m = h_m \upsilon_m^h / (n_w^F \upsilon_w + n_m \upsilon_m^h) = 0.22\ (22\%)$$

APPENDIX B

CALCULATION OF THE HOMOGENEOUS NUCLEATION TEMPERATURE

The homogeneous nucleation temperature of mouse oocytes can be calculated based on the assumption that the cytoplasm has the same ice nucleation characteristics as an electrolyte droplet of equivalent size and concentration (Rall et al. 1983). Therefore, the homogeneous nucleation temperature of an oocyte will depend on its size and concentration.

Wood & Walton (1970) has determined that a tenfold increase in the droplet diameter increases the homogeneous nucleation temperature (T_{hom}) by 2°C. In addition, Thomas & Staveley (1952), and Mossop (1955) have reported that T_{hom} of a 1 μm water droplet is -39°C. By combining these two informations, one can obtain the homogeneous nucleation temperature for water droplets of a given size. The depression of the homogeneous nucleation temperature due to electrolyte content can also be estimated from the simple relationship between the freezing temperature and the osmolality. By introducing the effects of both the size and the concentration, the homogeneous nucleation temperature of an oocyte can be estimated from the information given above.

APPENDIX C

MOLARITY VS. TEMPERATURE

The relationship between the molarity and the temperature is determined from the Handbook of Physics & Chemistry (Weast 1973). A third order polynomial is used for the correlation. The figure below shows the result of the curve fit.

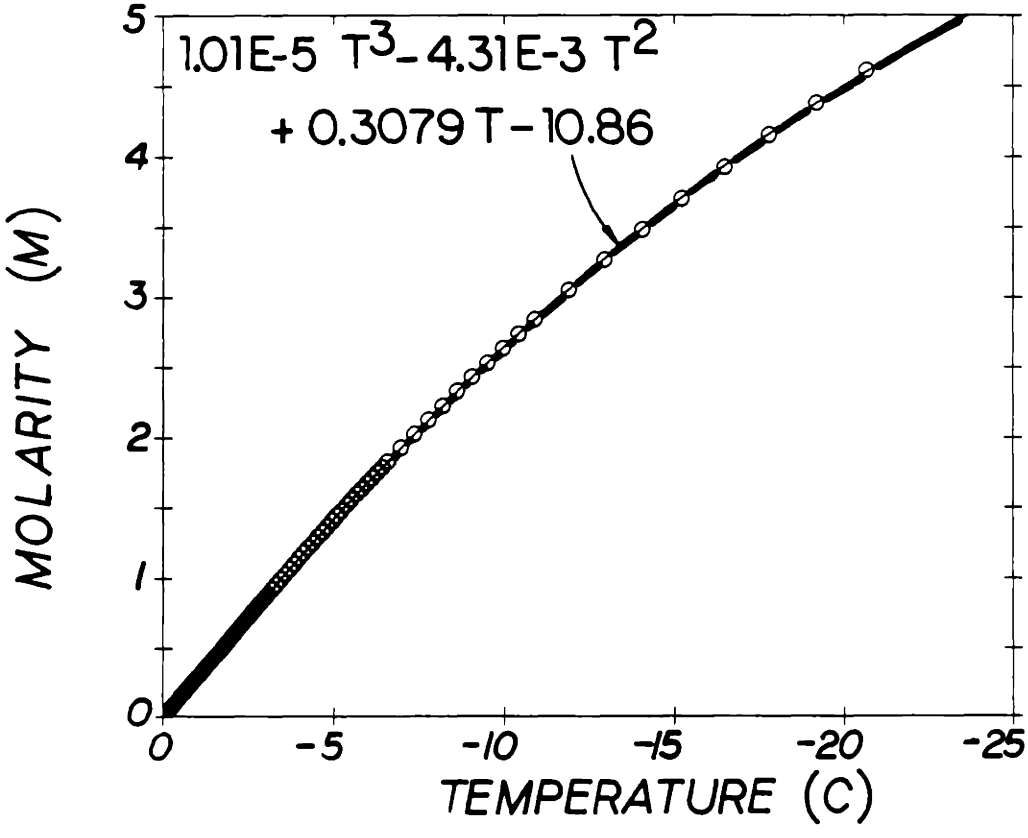

REFERENCES

Abramczuk, J., and Sawicki, W. Variation in dry mass and volume of nonfertilized oocytes and blastomeres of 1-, 2- and 4-celled mouse embryos. J.Exp.Zool. 188, 25-34 (1974).

Adair, G.S., and Adair, M.E. The densities of protein crystals and the hydration of proteins. Proc.R.Soc.Lond.Ser.B..Biol.Sci. 120, 422-446 (1938).

Adamson, A.W. "Physical Chemistry of Surfaces," Interscience Publishers, New York, 1960.

Amory, D.E., and Rouxhet, P.G. Surface properties of Saccharomyces cerevisiae and Saccharomyces carlsbergensis: chemical composition, electrostatic charge and hydrophobicity. Biochim.Biophys.Acta 938, 61-70 (1988).

Angell, C.A. Approaching the limits. Nature 331, 206-207 (1988).

Angell, C.A., Shuppert, J., and Tucker, J.C. Anomalous properties of supercooled water. Heat capacity, expansivity, and proton magnetic resonance chemical shift from 0 to -38°. J.Phys.Chem. 77, 3092-3099 (1973).

Antonow, G. Sur la tension superficielle a la limite de deux couches. J.Chem.Phys. 5, 372-385 (1907).

Arakelyan, V.B., Arakelyan, S.B., Avakyan, Ts.M., and Aslanyan, V.M. Electrostatic effects on transport of water across bilayer lipid membranes. Biofizika 30, 170-171 (1985).

Armant, R.D., Kaplan, H.A., and Lennarz, W.J. Fibronectin and laminin promote in vitro attachment and outgrowth of blastocyst. Dev.Biol. 116: 519-523, 1986.

Asahina, E. Intracellular freezing and frost resistance in egg-cells of the sea-urchin. Nature 191, 1263-1265 (1961).

Asahina, E. Frost injury in living cells. Nature 196, 445-446 (1962).

Asahina, E., Shimada, K., and Hisada, Y. A stable state of frozen protoplasm with invisible intracellular ice crystals obtained by rapid cooling. Exp.Cell Res. 59, 349-358 (1970).

Barthakur, N., and Maybank, J. Anomalous behavior of some amino-acids as ice nucleators. Nature 200, 866-868 (1963)

Becker, R. Die keimbildung bei der ausscheidung in metallishen mischkristallen. Ann.Physik. 32, 128-140 (1938).

Becker, R., and Doring, W. Kinetishe behandlung der keimbildung in ubersattigten dampfen. Ann.Phys. 24, 719-752 (1935).

Bengtzelius, U., and Sjolander, A. Dynamics of supercooled liquids and the glass transition. J.Phys. C17, 5915-5934 (1984).

Bevington, P.R. "Data Reduction and the Error Analysis for the Physical Sciences," McGraw-Hill, New York, 1959.

Biggers, J.D. New observations on the nutrition of the mammalian oocyte and the preimplantation embryo. In "The Biology of Blastocyst" (R.J. Blandau, Ed.), pp. 319-327, Univ. of Chicago Press, 1971.

Biggers, J.D., Borland, R.M., and Powers, R.D. Transport mechanisms in the preimplantation mammalian embryo. In "The Freezing of Mammalian Embryos" (K. Elliott and J. Whelan, Eds.), Ciba Foundation Symposium, pp.129-153. Elsevier, New York, 1977.

Blakely, J.M. Thermodynamics of surfaces and interfaces. In " Encyclopedia of Materials Science and Engineering" (M.B. Bever, Ed.) pp. 4962-4967. Pergamon, 1986.

Blum, R.M., and Forster, R.E. The water permeability of erythrocytes. Biochem.Biophys.Acta 203, 410-423 (1970).

Brinster, R.L., and Biggers, J.D. In-vitro fertilization of mouse ova within explanted fallopian tube. J. Reprod.Fertil. 10, 277-279 (1965).

Brown, R.H. Membrane surface charge: discrete and uniform modelling. Progr.Biophys.Molec.Biol. 28, 343-370 (1974).

Buckle, E.R. Studies on the freezing of pure liquids II. The kinetics of homogeneous nucleation in supercooled liquids. Proc.R.Soc. A261, 189-196 (1961).

Buff, F.P. Spherical interface. II. Molecular theory. J.Chem.Phys. 23, 419-427 (1955).

Buff, F.P., and Kirkwood, J.G. Remarks on the surface tension of small droplets. J.Chem.Phys. 18, 991 (1950).

Burke, M.J., George, M.F., and Bryant, R.G. Water in plant tissues and frost hardiness. In "Water Relations of Foods" (R.B. Duckworth, ed.). pp.111-135. Academic Press, New YOrk, 1975.

Burke, M.J., Gusta, L.V., Quamme, H.A., Weiser, C.J., and Li, P.H. Freezing and injury in plants. Annu.Rev.Plant Physiol. 27, 507-528 (1976).

Burns, J.R., and Turnbull, D. Kinetics of crystal nucleation in molten isostatic polypropylene. J.App.Phys. 37, 4021-4026 (1966).

Cahn, J.W., and Hilliard, J.E. Free energy of a non-uniform system. I. Interfacial free energy. J.Chem.Phys. 28, 258-267 (1958).

Cahn, J.W., and Hilliard, J.E. Free energy of a non-uniform system. II. Thermodynamic basis. J.Chem.Phys. 30, 1121-1124 (1959).

Callow, R.A., and McGrath, J.J. Thermodynamic modelling and cryomicroscopy of cell-size, unilamellar, and paucilamellar liposomes. Cryobiology 22, 251-267 (1985).

Carte, A.E. The freezing of water droplets. Proc. of the Phys.Soc. 69, 1028-1037 (1956).

Carte, A.E. Probability of freezing. Proc.Phys.Soc. 73, 324 (1959).

Chalmers, B. How water freezes. Scien.Amer. 200, 114-122 (1959).

Chambers, R., and Hale, H.P. The formation of ice in protoplasm. Proc.R.Soc.Lon. Ser.B. 110, 336-352 (1936).

Chang, M.C. Fertilization of rabbit ova in vitro. Nature 193, 466, (1959).

Chapman, D.L., A contribution to the theory of electrocapillarity. Phil.Mag. 25, 475-481 (1913).

Christian, J.W. The classical theory of nucleation. In "The Theory of Transformations in Metals and Alloys" (J.W. Christian, Ed.), Part 1, pp. 418-475. Pergamon Press, New York, 1975.

Clegg, J.S. Prperties and metabolism of the aqueous cytoplasm and its boundaries. Am.J.Physiol. 246, R133-R151 (184).

Cooper, W.A. A possible mechanism for contact nucleation. J.Atmos.Sci. 31, 1832-1837 (1974).

Corda, D., Pasternak, C., and Shinitzky, M. Increase in lipid microviscosity of unilamellar vesicles upon the creation of transmembrane potential. J. Membrane Biol. 65, 235-242 (1982).

Cormia, R.L., Price, F.P., and Turnbull. Kinetics of crystal nucleation in polyethylene. J.Chem.Phys. 37, 1333-1340 (1962).

Cosman, M.D., Effect of Cooling Rate and Supercooling on the Formation of Ice in a Cell Population, Ph.D. Thesis, Dept. of Mechanical Engn., Massachusetts Institute of Technology, 1983.

Cosman, M.D., and Cravalho, E.G. Optimal cooling protocols for cryopreservation of individual cells, Cryobiology 15, 704-705 (1978).

Cosman, M.D., Cravalho, E.G., and Huggins, C.E., An electronic cryomicroscope temperature controller, Cryobiology 16: 613, 1979.

Cosman, M.D., Cravalho, E.G., and Huggins, C.E., A cryomicroscope data acquisition system: design and performance, Cryobiology 19: 663, 1982.

Cosman, M.D., Toner, M., Kandel, J., and Cravalho, E.G. An integrated cryomicroscopy system, Cryo-Letters, in press.

Coster, H.G.L., and Zimmermann, U. The mechanism of electrical breakdown in the membranes of Valonia utricularis. J.Membrane Biol. 22, 73-90 (1975).

Defay, R. Etude thermodynamique de la tension superficielle; affinite et vitesse d'adsorption. Bull.Classe.Sci. Acad.Roy.Belg. 16, 1249-1263 (1930).

Defay, R., and Sanfield, A. Chaleur de fusion de la glace en presence d'une solution aqueuse de sel. Bull.Soc.Chim.Belg. 68, 295-302 (1959).

DeNordwall, H.J., and Staveley, L.A.K. Further studies of the supercooling of drops of some molecular liquids, J.Chem.Soc. 224-227 (1954).

DePena, R.G., Iribarne, J.V., and Achaval, E.M. The freezing of supercooled droplets of electrolyte solutions. J.Atmos.Sci. 19, 302-308 (1962).

DeRobertis, E.D.P., Nowinski, W.W., and Saez, F.A. "Cell Biology." W.B. Saunders Company, Philedelphia-London, 1965.

Deryaguin, B.V. General theory of nucleation. I. Theory of homogeneous condensation upon moderate supersaturation. J.Colloid Sci. 38, 517-522 (1972).

Dietz, T.E., Diller, K.R., and Aggarwal, J.K., Automated computer evaluation of time-varying cryomicroscopical images, Cryobiology 21: 200-208, 1984.

Diller, K.R. Intracellular freezing: effect of extracellular supercooling. Cryobiology 12, 480-485 (1975).

Diller, K.R. Intracellular freezing of glycerolized red cells. Cryobiology 16, 123-131 (1979).

Diller, K.R., Quantitative low temperature optical microscopy of biological systems, J.Microsc. 126: 9-28, 1981.

Diller, K.R., and Cravalho, E.G., A cryomicroscope for the study of freezing and thawing processes in biological cells, Cryobiology 7: 191-199, 1970.

Diller, K.R., and Bradley, D.A. Measurement of the water permeability of single human granulocytes on a microscopic stopped-flow mixing system. Trans.ASME J.Biomed.Eng. 106, 384-393 (1984).

Diller, K.R., Cravalho, E.G., and Huggins, C.E. Intracellular freezing in biomaterials. Cryobiology 9, 429-440 (1972).

Dowgert, M.F., and Steponkus, P.L. Effect of cold acclimation on intracellular ice formation in isolated protoplasts. Plant Physiol. 72, 978-988 (1983).

Dufour, L., and Defay, R. "Thermodynamics of Clouds," Academic Press, New York, 1963.

Dunning, W.J. General and theoretical introduction. In "Nucleation" (A.C. Zettlemoyer, ed.), pp. 1-67, Marcel Dekker, New York, 1969.

Edsall, J.T. The size, shape and hydration of protein molecules. In "The Proteins" (H. Neurath and K. Bailey, eds.), Vol.1, Part B, pp.549-726. Academic Press, New York, 1953.

Edwards, G.R., and Evans, L.F. Effect of surface charge on ice nucleation by silver iodide. Trans.Faraday Soc. 58, 627-634 (1962).

Einstein, A. Eine neue bestimmung der moleku-dimensionen. Ann.Physik 19, 289-306 (1906).

Einstein, A. Eine neue bestimmung der moleku-dimensionen (correction). Ann.Physik 54, 591 (1911).

Enustun, B.V., Senturk, H.S., and Yurdakul, O. Capillary freezing and melting. J.Coll.Int.Scien. 65, 509-516 (1978).

Eyring, H. The activated complex in chemical reactions. J.Chem.Phys. 3, 107-115 (1935).

Farkas, L. Keimbildungsgeschwindigkeit in ubersattigen dampfen, Z.Phys.Chem. A125, 236-242 (1927).

Fernandez, R., and Barduhn, A.J. The growth rate of ice crystals. Desalination 3, 330-342 (1967).

Fletcher, N.H. Size effect in heterogeneous nucleation. J.Chem.Phys. 29, 572-576 (1958).

Fletcher, N.H. Entropy effect in ice crystal nucleation. J.Chem Phys. 30, 1476-1482 (1959).

Fletcher, N.H. Nucleation and growth of ice crystals upon crystalline substrates. Aust.J.Phys. 13, 408-419 (1960).

Fletcher, N.H. Nucleation by crystalline particles. J.Chem.Phys. 38, 237-240 (1963).

Fletcher, N.H. "The Physics of Rain Clouds," 3th edition, Cambridge University Press, 1969.

Fletcher, N.H. "The Chemical Physics of Ice," Cambridge University Press, 1970.

Franks, F., and Bray, M. Mechanism of ice nucleation in undercooled plant cells. Cryo-Letters 1, 221-226 (1980).

Franks, F., Mathias, S.F., and Trafford, K. The nucleation of ice in undercooled water and aqueous polymer solutions. Colloids and Surfaces 11, 275-285 (1984).

Franks, F., Mathias, S.F., Galfre, P., Webster, D., and Brown, D. Ice nucleation and freezing in undercooled cells. Cryobiology 20, 298-309 (1983).

Frenkel, J. "Kinetic Theory of Liquids," Dover, New York, 1955.

Frumento, A.S. The electrical effects of an ionic pump. J.Theor.Biol. 9, 253-262 (1965).

Fukuta, N. Ice nucleation by metaldehyde. Nature 199, 475-476 (1963).

Fukuta, N. A study of the mechanism of contact ice nucleation. J.Atmos.Sci. 32, 1597-1603 (1975a).

Fukuta, N. Comments on "a possible mechanism for contact nucleation." J.Atmos.Sci. 32, 2371-2375 (1975b).

Fukuta, N., and Mason, B.J. Epitaxial growth of ice on organic crystals. J.Phys.Chem.Solids 24, 715-718 (1963).

Fulcher, G.S., J.Am.Chem.Soc. 8, 339, (1925).

Geduldig, D. Analysis of membrane permeability coefficient ratios and internal ion concentrations from a constant field equation. J.Theor.Biol. 19, 67-78 (1968).

Gibbs, J.W. "J.W. Gibbs, The Scientific Papers," Vol. 1, Dover, New York, 1961.

Glasstone, S., Laidler, K.J., and Eyring, H. "The Theory of Rate Processes," McGraw Hill, New York, 1941.

Goeppert, H.R. Uber die warme-entwickelung in den pflanzen, deren gefrieren und die schutzmittel gegen das selbe. Max and Comp., Berlin (1830). (Original not seen, cited in Steponkus et al. 1983).

Goeppert, H.R. Uber das gefrieren, enfrieren der pflanzen und schutzmitte dagegen, 1-87. Altes und neues (1883). (Original not seen, cited in Steponkus et al. 1983).

Gokhale, N.R., and Goold, J. Droplet freezing by surface nucleation. J.Appl.Met. 7, 870-874 (1968).

Gokhale, N.R., and Lewinter, O. Microcinematographic studies of contact nucleation. J.Appl.Met. 10,469-473 (1971)

Gokhale, N.R., and Spengler, J.D. Freezing of freely suspended supercooled water drops by contact nucleation. J.Appl.Met. 11, 157-160 (1972)

Goldman, D.E. Potential, impedance, and rectification in membranes. J.Gen.Physiol. 27, 37-60 (1943).

Gouy, G. Sur la fonction electrocapillaire. Ann.Phys. (Series 9) 7, 129-184 (1917).

Grahame, D.C. The electrical double layer and the theory of electrocapillarity. Chem.Rev. 41, 441-501 (1947).

Hallett, J. The temperature dependence of the viscosity of supercooled water. Proc.Phys.Soc. 82, 1046-1050 (1963).

Hardy, S.C. A grain boundary groove measurement of the surface tension between ice and water. Phil.Mag. 35, 471-487 (1977).

Hardy, S.C., and Coriell, S.R. Morphological stability and the ice-water interfacial energy. J.Crys.Growth. 3, 569-573 (1968).

Head, R.B. Steroids as ice nucleators. Nature 191, 1058-1059 (1961).

Head, R.B. Ice nucleation by α-phenazine. Nature 196, 736-738 (1962).

Hendl, A., McGrath, J.J., and Olien, C.R. On the adhesive interaction between ice and the mouse oocyte. cryo-Letters 8, 334-345 (1987).

Hobbs, P.V. "Ice Physics," Oxford University Press, England, 1974.

Hodgkin, A.L., and Katz, B. The effect of sodium ions on the electrical activity of the giant axon of the squid. J.Physiol. 108, 37-77 (1949).

Hoffer, T.E. A laboratory investigation of droplet freezing. J.Meteorology 18, 766-778 (1961).

Hoffman, J.D. Thermodynamic driving force in nucleation and growth processes. J.Chem.Phys. 29, 1192-1193 (1958).

Hollomon, J.H., and Turnbull, D. Nucleation. "Progress in Metal Physics" (B. Chalmers, Ed.), Vol. 4, pp. 333-388. Pergamon Press, London, 1953.

Hosler, C.L. On the crystallization of supercooled clouds. J.Met. 8, 326-331 (1951).

Hua, T.C., Cravalho, E.G., and Jiang, L. The temperature difference across the cell membrane during freezing and its effect on water transport. Cryo-Letters 3, 255-264 (1982).

Hubel, A., Toner, M., and Cravalho, E.G., Isothermal nucleation stage and its applications in the freezing of biological cells, in "Network Thermodynamics, Heat and Mass Transfer in Biotechnology", ed. K.R. Diller, ASME BED-Vol.5, HTD-Vol.90: 67-71, 1987.

Hubel, A., Korber, C., Cravalho, E.G., and Rau, G. Transient electrical potentials measured during the unidirectional freezing of $NaCl/H_2O$ solutions. J.Crystal Growth 87, 69-78 (1988).

Jackson, K.A., and Chalmers, B. Freezing of liquids in porous media with special reference to frost heave in soils. J.App.Phys. 29, 1178-1181 (1958).

Jackson, K.V., and Kiessling, A.A. Fertilization and cleavage of mouse oocytes exposed to the conditions of human oocyte retrieval for in vitro fertilization. J.Fert.Ster., in press.

Jayaraman, D., Subramanian, C., Dhanasekaran, R., and Ramasamy, P. Kinetics process of homogeneous nucleation incorporating the effect of curvature. J.Cryst.Growth 79, 997-1000 (1986).

Jones, D.R.H. The measurement of solid-liquid interfacial energies from the shapes of grain-boundary grooves. Phil.Mag. 27, 569-584 (1973).

Kantrowitz, A. Nucleation in very rapid vapor expansions. J.Chem.Phys. 19, 1097-1100 (1951)

Karasz, F.E., Champion, W.M., and Halsey, G.D. The growth of ice layers on the surfaces of anatase and silver iodide. J.phys.Chem. 60, 376-378 (1956)

Katchalsky, A., and Curran, P.F. "Nonequilibrium Thermodynamics in Biophysics," Harvard University Press, Cambridge, MA, 1981.

Keith, A.D. "The Aqueous Cytoplasm," pp. 183-194, Dekker, New York, 1979.

Kelton, K.F., Greer, A.L., and Thompson, C.V. Transient nucleation in condensed systems. J.Chem.Phys. 79, 6261-6276 (1983).

Ketcham, W.M., and Hobbs, P.V. An experimental determination of the surface energies of ice. Phil.Mag. 19, 1161-1173 (1969).

Keynes, R.D., and Lewis, P.R. The resting exchange of radioactive potassium in crab nerve. J.Physiol. 113, 73-98 (1951).

Koeing, F.O. On the thermodynamic relation between surface tension and curvature. J.Chem.Phys. 18, 449-459 (1950).

Korber, Ch., Englich, S., Schwindke, P., Scheiwe, M.W., Rau, G., Hubel, A., and Cravalho, E.G., Low temperature light microscopy and its application to study freezing in aqueous solutions and biological cell suspensions, J.Microsc. 141: 263-276, 1986.

Korber, C. Phenomena at the advancing ice-liquid interface: solutes, particles and biological cells. Quar.Rev.Biophys. 21, 229-298 (1988).

Korson, L., Drost-Hansen, W., and Millero, F. Viscosity of water at various temperatures. J.Phys.Chem. 73, 34-39 (1969).

Kotler, G., and Tarhis, L.A. On the dendiritic growth of pure materials. J.Crys.Growth 3-4, 603-610 (1968).

Kotyk, A., Janacek, K., and Koryta, J. "Biophysical Chemistry of Membrane Functions," John Wiley & Sons, New York, 1988.

Kourosh, S., and Diller, K.R. A unidirectional temperature gradient stage for solidification studies in aqueous solutions. J.Microsc. 135, 39-48 (1984).

Koutsky, J.A., Walton, A.G., and Baer, E. Nucleation of polymer droplets. J.Appl.Phys. 38, 1832-1839 (1967).

Langham, E.J., and Mason, B.J. The heterogeneous and homogeneous nucleation of supercooled water. Proc.Roy.Soc.(London) Ser.A 247, 493-504 (1958).

Leibo, S.P. Fundamental cryobiology of mouse ova and embryos. In "The Freezing of Mammalian Embryos" (K. Elliot and J. Whelan, Eds.) Ciba Foundation Symposium, pp.69-92. Elsevier, New York, 1977.

Leibo, S.P. Water permeability and its activation energy of fertilized and unfertilized mouse ova. J.Memb.Biol. 53, 179-188 (1980).

Leibo, S.P., McGrath, J.J., and Cravalho, E.G. Microscopic observations of intracellular ice formation in unfertilized mouse ova as a function of cooling rate. Cryobiology 15, 257-271 (1978).

Leibo, S.P., Farrant, J., Mazur, P., Hanna, M.G., and Smith, L.H. Effcets of freezing on morrow stem cell suspensions: interactions of cooling and warming rates in the presence of PVP, sucrose, or glycerol. Cryobiology 6, 315-332 (1970).

Levin, R.L. Kinetics of Water Transport in Biomaterials During Freezing. Sc.D. Thesis, Dept. of Mechanical Engineering, MIT, Cambridge, Mass., 1976.

Levin, R.L., Cravalho, E.G., and Huggins, C.E. Effect of hydration on the water content of human erythrocytes. Biophys.J. 16, 1411-1426 (1976a).

Levin, R.L., Cravalho, E.G., and Huggins, C.E.. A membrane model describing the effect of temperature on the water conductivity of erythrocyte membranes at subzero temperatures. Cryobiology 13, 419-429 (1976b).

Levin, R.L., Cravalho, E.G., and Huggins, C.E. Effect of solution non-ideality on erythrocyte volume regulation. Biochem.Biophys.Acta 465, 179-190 (1977a).

Levin, R.L., Cravalho, E.G., and Huggins, C.E. The concentration polarization effect in frozen erythrocytes. Trans.ASME J.Biomech.Eng., 65-73 (1977b).

Levin, R.L., Cravalho, E.G., and Huggins, C.E. Water transport in a cluster of closely packed erythrocytes at subzero temperatures. Cryobiology 14, 549-558 (1977c).

Levin, R.L., Cravalho, E.G., and Huggins, C.E. The concentration polarization effect in a multicomponent electrolyte solution-The human erytrocyte. J.Theor.Biol. 71, 225-254 (1978).

Levin, R.L., Ushiyama, M., and Cravalho, E.G. Water permeability of yeast cells at sub-zero temperatures. J.Membrane Biol. 46, 91-124

(1979).

Levine, J. Statistical explanation of spontaneous freezing of water droplets. Natl. Advisory Committee for Aeronautics, NACA Technical Note 2234, 1950.

Levitt, J., and Scarth, G.W. Frost-hardening studies with living cells. II. Permeability in relation to frost resistance and seasonal cycle. Can.J.Res. C14, 285-305 (1936).

Lindow, S.E. The role of bacterial ice nucleation in frost injury to plants. Ann.Rev.Phytopathol. 21, 363-384 (1983).

Ling, G.N. Hydration of macromolecules. In "Water and Aqueous Solutions: Structure, Thermodynamics and Transport Processes" (R.A. Horme, Ed.), pp.663-700. Wiley Interscience, New York, 1972.

Loewenstein, J.E., and Cohen, A. Dry mass, lipid content and protein content of the intact and zona-free mouse ovum. J.Embyol.Exp.Morph. 12, 113-121 (1964).

Lothe, J., and Pound, G.M. Reconsiderations of nucleation theory. J.Chem.Phys. 36, 2080-2085 (1962).

Lovelock, J.E. The haemolysis of human red blood cells by freezing and thawing. Biochim.Biophys.Acta 10, 414-426 (1953a)

Lovelock, J.E. The mechanism of the protective action of glycerol against haemolysis by freezing and thawing. Biochim.Biophys.Acta 11, 28-36 (1953b).

Mansoori, G.A. Kinetics of water loss from cells at subzero centigrade temperatures. Cryobiology 12, 34-45 (1975).

Marquant, D.W. An Algorithm of least square estimation of nonlinear parameters. J.Soc.Ind.App.Math. 11, 431-441 (1963).

Mastro, A.M., and Keith, A.D. Diffusion in the aqueous compartment. J.Cell Biology 99, 180s-187s (1984).

Mastroianni, Jr.L., and Biggers, J.D. "Fertilization and Embryonic Development In Vitro." Plenum Press, NY 1981.

Mathias, S.F., Franks, F., and Trafford, K. Nucleation and growth of ice in deeply undercooled erythrocytes. Cryobiology 21, 123-132 (1984).

Mazur, P. Kinetics of water loss from cells at subzero temperatures and likelihood of intracellular freezing. J.Gen.Physiol. 47, 347-369 (1963).

Mazur, P. The role of the cell membrane in the freezing of yeast and other single cells. Ann. NY Acad.Sci. 125, 658-676 (1965).

Mazur, P. The role of intracellular freezing in the death of cells cooled at supraoptimal rates. Cryobiology 14, 251-272 (1977).

Mazur, P. Freezing of living cells: mechanisms and implications. Am.J.Physiol. 143, C125-C142 (1984).

Mazur, P., and Schmidt, J. Interactions of cooling velocity, temperature, and warming velocity on the survival of frozen and thawed yeast. Cryobiology 5, 1-17 (1968).

Mazur, P., and Rigopoulos, N. Contributions of unfrozen fraction and salt concentration to the survival of slowly frozen human erythrocytes: influence of warming rate. Cryobiology 20, 274-289 (1983).

Mazur, P., and Cole, K.W. Influence of cell concentration on the contribution of unfrozen fraction and salt concentration to the survival of slowly frozen human erythrocytes. Cryobiology 22, 509-536 (1985).

Mazur, P., Leibo, S.P., and Chu, E.H.Y. A two-factor hypothesis of freezing injury-evidence from Chinese hamster tissue culture cells. Exp.Cell Res. 71, 345-355 (1972).

Mazur, P., Rall, W.F., and Rigopoulos, N. Relative contributions of the fraction of unfrozen water and salt concentration to the survival of slowly frozen human erythrocytes. Biophys.J. 36, 653-675 (1981).

Mazur, P., Rall, W.F., and Leibo, S.P. Kinetics of water loss and the likelihood of intracellular freezing in mouse ova. Cell Biophys. 6, 197-213 (1984).

Mazur, P., Farrant, J., Leibo, S.P., and Chu, E.H.Y. Survival of hamster tissue culture cells after freezing and thawing; interactions between protective solutes and cooling and warming rates. Cryobiology 6, 1-9 (1969).

Mazur, P., Leibo, S.P., Farrant, J., Chu, E.H.Y., Hanna, M.G., and Smith, L.H. Interactions of cooling rate, warming rate and protective additive on the survival of frozen mammalian cells. In "The Frozen Cell" (G.E.W. Wolstenholme and M. O'Connor, eds.).pp. 69-85. J.A. Churchill, London, 1970.

McGann, L.E., A versatile microcomputer-based temperature and cooling/warming rate controller, Cryobiology 16: 97-100, 1979.

McGann, L.E., and Farrant, J. Survival of tissue culture cells frozen by

a two-step procedure to -196°C. I. Holding temperature and time. Cryobiology 13, 261-268 (1976).

McGann, L.E., Turner, A.R., Allalunis, M.J., and Turc, J.-M. Cryopreservation of human peripheral blood stem cells: optimal cooling and warming conditions. Cryobiology 18, 469-472 (1981).

McGrath, J.J., The dynamics of freezing and thawing mammalian cells: the HeLa cell, M.S. Thesis, Dept. of Mechanical Engineering, Massachusetts Institute of Technology, 1974.

McGrath, J.J. The kinetics and dynamics of human erythrocyte freeze-thaw damage at sub-optimal cooling rates. Ph.D. Thesis, Dept. of Mechanical Engineering, Massachusetts Institute of Technology, 1977.

McGrath, J.J. A microscope diffusion chamber for the determination of the equilibrium and non-equilibrium osmotic response of individual cells. J.Microsc. 139, 249-263 (1985).

McGrath, J.J. Cold shock: thermoelastic stress in chilled biological membranes. In "Network Thermodynamics, Heat and Mass transfer in Biotechnology", (K.R. Diller, ed.), ASME BED-Vol.5, HTD-Vol.90: 67-78 (1988).

McGrath, J.J., Cravalho, E.G., and Huggins, C.E., An experimental comparison of intracellular ice formation and freeze-thaw survival of HeLa S-3 cells, Cryobiology 12, 540-550, 1975.

Meryman, H.T. Modified model for the mechanism of freezing injury in erythrocytes. Nature 218, 333-336 (1968).

Meryman, H.T. Freezing injury and its prevention in living cells. Annu.Rev.Biophys. 3, 341-363 (1974).

Miller, R.H., and Mazur, P. Survival of frozen-thawed human red cells as a function of cooling and warming velocities. Cryobiology 13, 404-414 (1976).

Miralles, A., Garcia, L.J., Soto, R.M., Martinez, C., Garcia, A., and Vila, L.L. Thermal shock in mouse oocytes. Cryobiology 24, 586 (1987).

Molisch, H. Untersuchungen uber das erfrieren der pflanzen. Jeana (1897). (Original not seen, cited in Steponkus et al. 1983).

Morris, G.J., and McGrath, J.J. Intracellular ice nucleation and gas bubble formation in spirogyra. Cryo-Letters 2, 341-352 (1981).

Mossop, S.C. The freezing of supercooled water. Proc.Phys.Soc.London Sec.B 68, 193-208 (1955).

Muller-Thurgau, H. Uber das gefrieren und erfrieren der pflanzen, II. Theile. Landw.Jahrb.Landwirsch 15, 453-610 (1886). (Original not seen, cited in Steponkus et al. 1983).

Myers, S.P., Lynch, D.V., Pitt, R.E., and Steponkus, P.L. Cryobehavior of drosophila embryos. Cryobiology 24, 549 (1987a).

Myers, S.P., Lin, T.-T., Pitt, R.E., and Steponkus, P.L. Cryobehavior of immature bovine oocytes. Cryo-Letters 8, 260-275 (1987b).

Niwa, K., Imai, H., Kim, C.I., and Iritani, A. Fertilization in vitro of hamster and mouse eggs in a chemically defined medium. J.Reprod.Fert. 58, 109-114 (1980).

Novikov, A.N., Tkachenko, S.I., Stribul, T.F., and Ryandin, V.F. Possibility of using exponential cooling regimes in cryopreservation of biological specimens. Biophysics 30, 1136-1139 (1985).

Ohki, S., and Ohshima, H. Donnan potential and surface potential of a charged membrane and effect of ion binding on the potential profile. In "Electrical Double Layers in Biology" (M. Blank, ed.), pp. 1-16. Plenum Press, New York, 1986.

Ohki, S. Membrane potential of squid axon. In "Electrical Double Layers in Biology" (M. Blank, ed.), pp. 103-118. Plenum Press, New York, 1986.

Orrico, M. Water Permeability of Mouse Ova and Predicted Osmotic Behavior During Freezing. M.S. Thesis, Dept. of Mechanical Engineering, Massachusetts Institute of Technology, Cambridge, MA, 1988.

Orrico, M., Toner, M., and Cravalho, E.G. Experimental distribution of permeability parameters of mouse ova and their behavior during freezing. Cryobiology 25, 562 (1988).

Oxtoby, D.W. Nucleation of crystals from the melt. In "Dynamic Aspects of Structural Change in Liquids and Glasses" (C.A. Angell and M. Goldstein, Eds.), Vol. 484, pp.27-39. Annals of the New York Academy of Sciences, 1986.

Papanek, T.H. The Water Permeability of the Human Erythrocyte in the Temperature Range +25°C to -10°C. Ph.D. Thesis, Dept.of Mechanical Engineering, Massachusetts Institute of Technology, Cambridge, MA, 1978.

Pegg, D.E., and Diaper, M.P. On the mechanism of injury to slowly frozen erythrocytes. Biophys.J. 54, 471-488 (1988).

Pethig, R. "Dielectric and Electronic Properties of Biological Materials," John Wiley & Sons, New York, 1979.

Pethig, R. Ion, electron, and proton transport in membranes: a review of the physical processes involved. In "Modern Bioelectrochemistry" (F. Gutmann and H. Keyzer, eds.) pp. 199-239. Plenum Press, New York, 1986.

Pitter, R.L., and Pruppacher, H.R. A wind tunnel investigation of freezing of small water droplets falling at terminal velocity in air. Quart.J.Roy.Meteor.Soc. 99, 540-550 (1973).

Polge, C., Smith, A.U., and Parkes, A. Revival of spermatozoa after vitrification and dehydration at low temperatures. Nature 164, 666-668 (1949).

Porsche, A.M., Korber, C., Englich, S., Hartmann, U., and Rau, G. Determination of the permeability of human lymphocytes with a microscope diffusion chamber. Cryobiology 23, 302-316 (1986).

Power, B.A., and Power, R.F. Some amino acids as ice nucleators. Nature 194, 1170-1171 (1962).

Powers, R.D., and Tupper, J.T. Some electrophysiological and permeability properties of the mouse egg. Dev.Biol. 38, 320-331 (1974).

Powers, R.D., and Tupper, J.T. Ion transport and permeability in the mouse egg. Expt.Cell.Reserch 91, 413-421 (1975).

Powers, R.D., and Tupper, J.T. Developmental changes in membrane transport and permeability in the early mouse embryo. Dev.Biol. 56, 306-315 (1977).

Prigogine, I., and Defay, R. "Chemical Thermodynamics," Longmans, Green, New York, 1954.

Pruppacher, H.R. Some relations between the supercooling and the structure of aqueous solutions. J.Chem.Phys. 39, 1586-1594 (1963).

Pruppacher, H.R., and Neiburger, J. The effect of water soluble sustances on the supercooling of water drops. J.Atmos.Sci. 20, 376 (1963).

Pruppacher, H.R., and Klett, J.D. "Microphysics of Clouds and Precipitation," D. Reidel Publishing Company, Boston, 1978.

Pushkar, N.S., Itkin, Y.A., Bronstein, V.L., Gordiyenko, E.A., and Kozmin, Y.V. On the problem of dehydration and intracellular crystallization during freezing of cell suspensions. Cryobiology

13, 147-152 (1976).

Quinn, P. A lipid phase separation model of low-temperature damage to biological membranes. Cryobiology 22, 128-146 (1985).

Rall, W.F., Mazur, P., and McGrath, J.J. Depression of the ice-nucleation temperature of rapidly cooled mouse embryos by glycerol and dimethyl sulfoxide. Biophys.J. 41, 1-12 (1983).

Rapatz, G., and Luyet, B. Effects of cooling rates on the preservation of erythrocytes in frozen blood containing various protective agents. Biodynamica 9, 333-350 (1965).

Rasmussen, D.H. Energetics of homogeneous nucleation. J.Cryst.Growth 56, 45-55 (1982).

Rasmussen, D.H., and MacKenzie, A.P. Effect of solute on ice-solution interfacial free energy; calculation from measured homogeneous nucleation temperatures. In "Water Structure at the Water-Polymer Interface" (H.H.G. Jellinek, Ed.), pp.126-145. Plenum Press, New York, 1972.

Rasmussen, D.H., and MacKenzie, A.P. Clustering in supercooled water.J.Chem.Phys. 59, 5003-5013 (1973).

Rasmussen, D.H., Macaulay, M.N., and MacKenzie, A.P. Supercooling and nucleation of ice in single cells. Crtobiology 12, 328-339 (1975).

Rasmussen, D.H., Applebly, M.R., Leedom, G.L., and Babu, S.V. Homogeneous nucleation kinetics. J.Cryst.Growth 64, 229-238 (1983).

Reischel, M.T., and Vali, G. Freezing nucleation in aqueous electrolytes. Tellus 27, 414-426 (1975).

Rich, G.I., Sha'afi, R.I., Ramualdez, A., and Solomon, A. Effect of osmolality on the hydraulic permeability coefficient of red cells. J.Gen.Physiol. 52, 941-954 (1968).

Robinson, R.A., and Stokes, R.H. "Electrolyte Solutions," 2nd edition, Butterworth, London, 1959.

Rubinski, B., and Ikeda, M. A cryomicroscope using directional solidification for the controlled freezing of biological materials. Cryobiology 21, 480-485 (1984).

Rule, G.S., Law, P., Kruuv, J., and Lepock, J.R. Water permeability of mammalian cells as a function of temperature in the presence of dymethylsulfoxide: correlation with the state of the membrane lipids. J.Cell.Physiol. 103, 407-416 (1980).

Sakai, A., and Yoshida, S. Survival of plant tissue at super-low temperature. VI. Effcets of cooling and rewarming rates on survival. Plant Physiol. 42, 1695-1701 (1967).

Sax, R.J., and Goldsmith, P. Nucleation of water drops by Brownian contact with AgI and other aerosols. Quart.J.Roy.Meteor.Soc. 98, 60-72 (1972)

Schaefer, V.J., Formation of ice crystals in ordinary and nuclei-free air. Ind.Eng.Chem. 44, 1300-1304 (1952).

Scheiwe, M.W., and Korber, C. Formation and melting of intracellular ice in lymphocytes. Cryo-Letters 3, 265-274 (1982a).

Scheiwe, M.W., and Korber, C. Formation and melting of intracellular ice in granulocytes. Cryo-Letters 3, 275-284 (1982b).

Scheiwe, M.W., and Korber, Ch., Thermally defined cryomicroscopy and some applications on human leukocytes, J.Microsc. 126: 29-44 (1982c).

Scheiwe, M.W., and Korber, Ch., Basic investigations on the freezing of human lymphocytes, Cryobiology 20: 257-273 (1983).

Scheiwe, M.W., and Korber, Ch., Thermally defined cryomicroscopy and thermodynamic analysis in lymphocyte freezing, Cryobiology 21: 93-105 (1984).

Scheiwe, M.W., and Korber, C. Quantitative cryomicroscopic analysis of intracellular freezing of granulocytes without cryoadditive. Cryobiology 24, 473-483 (1987).

Schwartz, G.J., and Diller, K.R. Parameters affecting the osmotic behavior of cells during freezing and thawing: human granulocytes. Cryo-Letters 2, 359-372 (1981).

Schwartz, G.J., and Diller, K.R., Design and fabrication of a simple, versatile cryomicroscopy stage, Cryobiology 19: 529-538, 1982.

Schwartz, G.J., and Diller, K.R., Osmotic response of individual cells during freezing I. Experimental volume measurements , Cryobiology 20: 61-77 (1983a).

Schwartz, G.J., and Diller, K.R., Osmotic response of individual cells during freezing II. Membrane permeability analysis, Cryobiology 20: 542-552 (1983b).

Schwartz, G.J., and Diller, K.R. Analysis of the water permeability of human granulocytes at subzero temperatures in the presence of extracellular ice. Trans.ASME J.Biomech.Eng. 105, 360-366 (1983c).

Schwartz, G.J., and Diller, K.R. Intracellular freezing of human granulocytes. Cryobiology 21, 654-660 (1984).

Shabana, M., and McGrath, J.J. Cryomicroscope investigation and thermodynamic modelling of the freezing of unfertilized hamster ova. Cryobiology 25, 338-354 (1988).

Shah, S.J., Diller, K.R., and Aggarwal, S.J., A personal computer-based temperature control system for cryomicroscopy, Cryobiology 24: 163-168, 1987.

Shanes, A.M. Membrane permeability: monolayer relationships. Science 140: 824-25 (1963).

Silvares, O.M. A thermodynamic model of water and ion transport across the membrane during freezing and thawing: the human erythrocyte. Ph.D. Thesis, Dept. Mech. Eng., Massachusetts Institute of Technology, 1974.

Silvares, O.M., Cravalho, E.G., Toscano, W.M., and Huggins, C.E. The thermodynamics of water transport from biological cells during freezing. Trans.ASME J.Heat Transfer 97, 582-588 (1975).

Solomon, A.K. Characterization of biological membranes by equivalent pores. J.Gen.Physiol. 51, 335S-364S (1968).

Steponkus, P.L., and Weist, S.C. Plasma membrane alterations following cold acclimation and freezing. In "Plant Cold Hardiness and Freezing Stress" (P.H. Li and A. Sakai, Eds.) pp.75-91. New York, Academic, 1978.

Steponkus, P.L., and Dowgert, M.F. Gas bubble formation during intracellular ice formation. Cryo-Letters 2, 42-47 (1981).

Steponkus, P.L., Dowgert, M.F., and Gordon-Kamm, J. Destabilization of the plasma membrane of isolated plant protoplasts during a freeze-thaw cycle: the influence of cold acclimation. Cryobiology 20, 448-465 (1983).

Steponkus, P.L., Dowgert, M.F., Ferguson, J.R., and Levin, R.L., Cryomicroscopy of isolated plant protoplasts, Cryobiology 21: 209-233, 1984a.

Steponkus, P.L., Stout, D.G., Wolfe, J., and Lovelace, R.V.E. Freeze-induced electrical transients and cryoinjury. Cryo-Letters 5, 343-348 (1984b).

Stusnick, E., and Hurst, R.P. Numerical determination of membrane permeability analysis. J.Theor.Biol. 37, 261-271 (1972).

Sundquist, B.E., and Oriani, R.A. Homogeneous nucleation in a miscibility gap system. A critical test of nucleation test. J.Chem.Phys. 36, 2604-2615 (1962).

Taborek, P., Kleiman, R.N., and Bishop, D.J. Power-law behavior in the viscosity of supercooled liquids. Phys.Rev.B. 34, 1835-1840 (1986).

Terwilliger, T.C. and Solomon, A.K. Osmotic water permeability of human red cells. J.Gen.Physiol. 77, 549-570 (1981).

Thijssen, H.A.C, Vorstman, M.A.G., and Roels, J.A. Heterogeneous nucleation of ice in water and aqueous solutions. J.Crys.Growth 3, 355-359 (1968).

Thom, F. Deformation of the cell membrane at low temperatures II: elastical deformability of the erythrocyte membrane. Cryo-Letters 9, 308-315 (1988).

Thom, F., and Matthes, G. Deformation of the cell membrane at low temperatures I: a cryomicroscopical technique. Cryo-Letters 9, 300-307 (1988).

Thomas, D.G., and Staveley, L.A.K. A study of the supercooling of drops of some molecular liquids. J.Chem.Soc. 4569-4577 (1952).

Thompson, C.V., and Spaepen, F. On the approximation of the free energy change on crystallization. Acta.Metallurgica 27, 1855-1859 (1979).

Tondorf, S., McGrath, J.J., and Olien, C.R. On the adhesive interaction between ice and cell-size liposomes. Cryo-Letters 8, 322-333 (1987).

Toner, M. The Water Permeability of Bovine Embryos at Suprazero Temperatures and Their Predicted Freezing Behavior. M.S. Thesis. Dept. of Mechanical Engineering, Massachusetts Institute of Technology, Cambridge, MA, 1985.

Tolman, R.C. The effect of droplet size on surface tension. J.Chem.Phys. 17, 33-337 (1949).

Toscano, W.M., Cravalho, E.G., Silvares, O.M., and Huggins, C.E. The thermodynamics of intracellular nucleation in the freezing of erythrocytes. Trans.ASME 97(3), 326-332 (1975).

Turnbull, D. Transient nucleation. Amer.Inst.Min.Met.Engrs. T.P. 2365, Metals.Tech., 774-783 (1948).

Turnbull, D., and Fisher, J.C. Rate of nucleation in condensed systems. J.Chem.Phys. 17, 71-73 (1949).

Turnbull, D. Kinetics of heterogeneous nucleation. J.Chem.Phys. 18, 198-203 (1950a).

Turnbull, D. Isothermal rate of solidification of small droplets of mercury and tin. J.Chem.Phys. 18, 768-769 (1950b)

Turnbull, D. Correlation of liquid-solid interfacial energies calculated from supercooling of small droplets. J.Chem.Phys. 18, 769 (1950c)

Turnbull, D. Formation of crystal nuclei in liquid metals. J.App.Phys. 21, 1022-1027 (1950d).

Turnbull, D. Kinetics of solidification of supercooled liquid mercury droplets. J.Chem.Phys. 20, 411-424 (1952).

Turnbull, D. Theory of catalysis of nucleation by surface patches. Acta Metal. 1, 8-14 (1953).

Turnbull, D. Phase changes. In "Solid State Physics" (F. Seitz and D. Turnbull, Eds.), Vol. 3, pp. 225-306. Academic Press, New York, 1956.

Turnbull, D. Free volume model of the liquid state. in "Liquids: Structure, Properties, Solid Interactions" (T.J. Hughel, Ed.), pp.6-24,Elsevier, New York, 1965a.

Turnbull, D. The undercooling of liquids. Scientific American 212, 38-46 (1965b)

Turnbull, D. Undercoolability and the exposure of metastable structures. In "undercooled Alloy Phases" (E.W. Collins and C.C. Koch, Eds.), Proceedings of the 1986 Hume-Rothery Memorial Symposium, pp. 3-22, Annual Meeting of TMS-AIME, 1986.

Turnbull, D., and Vonnegut, B. Nucleation catalysis. Ind.Eng.Chem. 44, 1292-1298 (1952).

Turnbull, D., and Cormia, R.L. Kinetics of crystal nucleation in some normal alkane liquids. J.Chem.Phys. 34, 820, (1961).

Uhlmann, D.R., and Chalmers, B. The energetics of nucleation. Ind.Engnr.Chem. 57, 19-31 (1965).

Uzu, Y., and Sano, I. On the freezing of the droplets of aqueous solutions. J.Meteo.Soc.Japan 43, 290-292 (1965)

Vali, G., and Stansbury, E.J. Time dependent characteristics of the heterogeneous nucleation of ice. Can.J.Phys. 44, 477-502 (1966).

Vand, V. Viscosity of solutions and suspensions. J.Phys.Chem. 52, 277-

299 (1947).

Viaud, P.R. Freezing of the water content of porous membranes. Cryobiology 9, 233-239 (1972).

Vogel, H. Das temperatur-abhangigkeitsgesetz der viskositat von flussigkeiten. Phys.Z. 22, 645-646 (1921).

Volmer, M., and Weber, A. Keimbildung in ubersattigten gebilden, Z.Physik.Chem. A119, 277-301 (1926).

Volmer, M. Uber keimbildung und keimwirkung als spezialfalle der heterogenen katalyse. Z.Electrochem. 35, 555-561 (1929).

Volmer, M. "Kinetik der Phasenbildung," Vol. 4, Steinkopf, Dresden, 1939.

Vonnegut, B. The nucleation of ice formation by silver iodide. J.appl.Phys. 18, 593-595 (1947).

Walton, A.G. Nucleation in liquids and solutions. In "Nucleation" (A.C. Zettlemoyer, Ed.), pp.225-307. Marcel Dekker, New York, 1969.

Weast, R.C. "Handbook of Chemistry and Physics," 54th edition, CRC Press, 1973.

Weaver, J.C., Powell, K.T., and Mintzer, R.A. The electrical capacitance of bilayer membranes the contribution of transient aqueous pores. Bioelectro.Bioenerg. 12, 393-404 (1984).

Weyl, W.A. The surface of glasses as affected by heavy metal ions. Trans.Soc.Glass Tech. 32, 247-259 (1949).

Williams, R.J., and Takahashi, T. The role of osmotic stress and surface energy in freezing injury of sea urchin eggs. Comp.Biochem. Physiol. 73A, 621-626 (1982).

Williams, R.J., and Takahashi, T. An oil drop method for detecting interfacial energy changes in osmotically stressed sea urchin eggs. Cryobiology 21, 684-685 (1984).

Wojcieszyn, J.W., Schlegel, R.A., Wu, En-S., and Jacobson, K.A. Diffusion of injected macromolecules within the cytoplasm of living cells. Proc.Natl.Acad.Sci. USA 78, 4407-4410 (1981).

Wolfe, J., and Steponkus, P.L. The stress-strain relation of the plasma membrane of isolated plant protoplasts. Biochim.Biophys.Acta 643, 663-668 (1981).

Wood, G.R., and Walton, A.G. Kinetics of ice nucleation from water and

electrolyte solutions. Res. and Dev. Progr. Rep. No. 500, Office of Saline Water (U.S. Dept. of the Interior, Washington, D.C., 1969.

Wood, G.R., and Walton, A.G. Homogeneous nucleation kinetics of ice from water. J.App.Phys. 41, 3027-3036 (1970).

Woodruff, D.P. "Solid-Liquid Interface," Cambridge University Press, Cambridge, 1973.

Workman, E.J., and Reynolds, S.E. Electrical phenomena occuring during the freezing of dilute aqueous solutions and their possible relationship to thunderstorm electricity. Phys.Rev. 78, 254 (1950).

Yanagimachi, R., and Chang, M.C. Fertilization of hamster eggs in vitro. Nature 200, 281-282 (1963).

Yanagimachi, R., and Chang, M.C. In Vitro fertlization of hamster ova. J.Exp.Zool. 156, 361-376 (1964).

Zeldovich, J.B. Acta Physicochim. URSS 18, 17 (1943).

Zettlemoyer, A.C., Tcheurekdjian, N., and Chessick, J.J. Surface properties of silver iodide. Nature 192, 653 (1961).

Zettlemoyer, A.C., Tcheurekdjian, N., and Hosler, C.L. Ice nucleation by hydrophobic substrates. J.Appl.Math.Phys. 14, 496-502 (1963).

Zimmermann, U. Electric field-mediated fusion and related electrical phenomena. Biochim.Biophys.Acta 694, 227-277 (1982).